DETERMINATION OF THE OPTIMUM GEOFOAM GEOMETRY FOR SHALLOWLY BURIED FLEXIBLE PIPE BY FINITE ELEMENT ANALYSES

A THESIS SUBMITTED TO
THE GRADUATE SCHOOL OF NATURAL AND APPLIED SCIENCES
OF
MIDDLE EAST TECHNICAL UNIVERSITY

BY

YAVUZHAN KEFCİ

IN PARTIAL FULFILLMENT OF THE REQUIREMENTS
FOR
THE DEGREE OF MASTER OF SCIENCE
IN
CIVIL ENGINEERING

DECEMBER 2020

Approval of the thesis:

DETERMINATION OF THE OPTIMUM GEOFOAM GEOMETRY FOR SHALLOWLY BURIED FLEXIBLE PIPE BY FINITE ELEMENT ANALYSES

submitted by **YAVUZHAN KEFCİ** in partial fulfillment of the requirements for the degree of **Master of Science** i**n Civil Engineering, Middle East Technical University** by,

Prof. Dr. Halil Kalıpçılar
Dean, Graduate School of **Natural and Applied Sciences** _____

Prof. Dr. Ahmet Türer
Head of the Department, **Civil Engineering** _____

Assoc. Prof. Dr. Nejan Huvaj Sarıhan
Supervisor, **Civil Engineering Dept., METU** _____

Examining Committee Members:

Prof. Dr. Bahadır Sadık Bakır
Civil Engineering Dept., METU _____

Assoc. Prof. Dr. Nejan Huvaj Sarıhan
Civil Engineering Dept., METU _____

Prof. Dr. Erdal Çokça
Civil Engineering Dept., METU _____

Assoc. Prof. Dr. Nabi Kartal Toker
Civil Engineering Dept., METU _____

Prof. Dr. Taha Taşkıran
Civil Engineering Dept., Ankara Yıldırım Beyazıt University _____

Date: 28.12.2020

I hereby declare that all information in this document has been obtained and presented in accordance with academic rules and ethical conduct. I also declare that, as required by these rules and conduct, I have fully cited and referenced all material and results that are not original to this work.

Name, Surname : Yavuzhan Kefci

Signature :

ABSTRACT

DETERMINATION OF THE OPTIMUM GEOFOAM GEOMETRY FOR SHALLOWLY BURIED FLEXIBLE PIPE BY FINITE ELEMENT ANALYSES

Kefci, Yavuzhan
Master of Science, Civil Engineering
Supervisor : Assoc. Prof. Dr. Nejan Huvaj Sarıhan

December 2020, 179 pages

Buried pipes are subjected to various loading conditions such as embankment loads, traffic loads etc. and in order to protect the buried pipes, the induced trench method and compressible inclusions are used. Expanded polystyrene (EPS) geofoam is one of the most advantageous compressible material that is used for protection of buried pipes. In the literature, researchers generally focused on the protection of rigid culverts and pipes, and there has been only limited amount of research on the protection of buried flexible pipes, which have limits of pipe deformation in their service life. This study aims to define the optimum EPS geometry that would be placed on top of the shallowly buried flexible pipe, via finite element method using PLAXIS 2D software. Firstly, a verification study is conducted with the results of an extensively-instrumented laboratory model test from the literature. Then, the verified numerical model is used to investigate the effects of the EPS geofoam's geometrical properties such as optimum width and thickness in addition to its location and density with more than 120 numerical analyses. Besides, in the case of using two layers of EPS, the effects of EPS layers' location and their spacing is examined with numerical analyses. For the protection

of flexible pipes with the help of EPS geofoam, the varying improvement ratios (22% and 84% improvement in pipe deflection) are achieved using different density, location and geometry of the EPS geofoam. For the 30-cm pipe diameter, under uniform embankment loading conditions at the ground surface, by considering cost / performance criteria, it is recommended that (i) EPS should be located right above the pipe crown, (ii) width of EPS geofoam is suggested as 1 x diameter of pipe (D), (iii) EPS geofoam thickness is suggested as 5 cm (D/6) to mobilize the positive arching fully, (iv) more compressible EPS should be preferred (in this study EPS-10 having 10 kg/m^3 nominal density) without exceeding the yield strength of the EPS. The literature review presented in this study will be an up-to-date resource for the researchers, and the results of the study will contribute to the more effective design of the protection systems of shallowly buried flexible pipes by imperfect trench method with EPS geofoam.

Keywords: Shallowly Buried Flexible Pipe, Plaxis 2D, EPS Geofoam, Soil Arching, Imperfect Trench Method

ÖZ

SIĞ GÖMÜLÜ ESNEK BORULAR ÜZERİNDE TEŞKİL EDİLECEK OPTİMUM GEOFOAM GEOMETRİSİNİN SONLU ELEMANLAR ANALİZLERİ İLE BELİRLENMESİ

Kefci, Yavuzhan
Yüksek Lisans, İnşaat Mühendisliği
Tez Yöneticisi: Doç. Dr. Nejan Huvaj Sarıhan

Aralık 2020, 179 sayfa

Gömülü borular, dolgu yükleri, trafik yükleri vb. çeşitli yükleme koşullarına maruz kalırlar ve gömülü boruları korumak için yapay hendek metodu ve sıkıştırılabilir yatak malzemeleri kullanılır. Genleştirilmiş polistiren (EPS) köpük gömülü boruların korunması için kullanılan en avantajlı sıkıştırılabilir malzemelerden biridir. Literatürde, araştırmacılar genel olarak rijit menfez ve boruların korunması üzerine yoğunlaşmışlardır ve bu sebeple hizmet ömürleri boyunca deformasyon limitleri olan gömülü esnek boruların korunması ile ilgili sınırlı sayıda araştırma yapılmıştır. Bu çalışma, PLAXIS 2D yazılımı kullanılarak sonlu elemanlar yöntemi ile sığ gömülü esnek bir boru üzerine yerleştirilecek EPS köpük malzemesinin optimum geometrisinin belirlenmesini amaçlamaktadır. İlk olarak, literatürden elde edilen ve detaylı aletsel gözlem yapılmış laboratuvar deney sonuçları ile nümerik modelin doğrulaması yapılmıştır. Daha sonra, doğrulaması yapılan nümerik model, 120'den fazla analiz ile optimum EPS köpük genişliği ve kalınlığı gibi geometrik özelliklerin yanı sıra EPS köpük malzemesinin boru üzerindeki lokasyonu ve yoğunluğunun etkisini araştırmada kullanılmıştır. Esnek boruların EPS köpük yardımıyla korunması için, EPS köpük yoğunluğu, geometrisi ve lokasyonuna bağlı

olarak boru esnemelerinde 22-84% arasında değişen iyileşme oranları elde edilmiştir. 30 cm çapında ve yüzeyden düzgün yayılı yükleme koşulları altında maliyet / performans kriterleri gözetilerek (i) EPS köpük boru tacının hemen üzerine yerleştirilmelidir, (ii) EPS genişliği 1 x boru çapı (D) olarak önerilmektedir, (iii) EPS kalınlığı pozitif zemin kemerlenmesinin tamamen oluşması için 5 cm (D/6) olarak önerilmektedir, (iv) EPS'in yenilmeyeceği şekilde mümkün olan en sıkışabilir EPS tercih edilmelidir (bu çalışmada EPS-10, anma yoğunluğu 10 kg/m^3). Bu çalışma kapsamında özetlenen literatür taraması sonuçları araştırmacılar için güncel bir kaynak olacaktır ve bu çalışmanın sonuçları, sığ gömülü esnek boruların EPS köpük kullanılarak yapay hendek metoduyla korunmasını konu edinen sistemlerin daha efektif tasarlanmasına katkı sağlayacaktır.

Anahtar Kelimeler: Sığ Gömülü Esnek Boru, Plaxis 2D, EPS Köpük, Zemin Kemerlenmesi, Yapay Hendek Yöntemi

Dedicated to my family

ACKNOWLEDGMENTS

I would like to express my deepest gratitude, respect and appreciation to my advisor, Assoc. Prof. Dr. Nejan Huvaj Sarıhan, for her understanding, patience, guidance, and, most importantly, valuable time having spared to me through graduate studies and thesis period.

I would like to thank each of the esteemed members of the thesis jury for their interest in this thesis topic and for their unique time, especially during the COVID-19 epidemic that embraced the world in 2020.

I am very grateful to dear members of the Civil Engineering Department of the Middle East Technical University for their contribution and enlightening to me.

I would also like to state my deepest appreciation to Ece Dilan Asma, a wonderful classmate and colleague, for her valuable and unconditional help during the graduate period.

TABLE OF CONTENTS

LIST OF TABLES

LIST OF FIGURES

LIST OF ABBREVIATIONS

2D	2-Dimensional
3D	3-Dimensional
AASHTO	Standard Specifications for Highway Bridges
ACPA	American Concrete Pipe Association
ASCE	American Society of Civil Engineers
ASTM	American Society for Testing and Materials
CD	Consolidated-Drained
CFCDRBC	China Fundamental Code for Design on Railway Bridges and Culverts
CGCDHBC	China General Code for Design of Highway Bridges and Culverts
CPPA	Corrugated Polyethylene Pipe Association
EPS	Expanded Polystyrene
ETI	Embedded Trench Installation (Method)
EVA	Ethylene Vinyl Acetate
FEM	Finite element Method
GAF	Gu Anguan Formula
HDPE	High Density Polyethylene
HSS	Hollow Structural Section
ITI	Imperfect (Induced) Trench Method
MEPM	Marston’s earth pressure method
NCHRP	National Cooperative Highway Research Program
PVC	Polyvinyl Chloride
TS EN ISO	Turkish Standards
TUCM	Terzaghi’s underground cavern method
UC	Unconfined Compression
USA	United States of America
USCS	Unified Soil Classification System

LIST OF SYMBOLS

$\mathbf{A}$	Cross section area
$\mathbf{A_{pipe}}$	Area of smooth pipe per unit length
$\mathbf{c'}$	Effective cohesion of soil
$\mathbf{C_c}$	Coefficient of curvature
$\mathbf{C_u}$	Coefficient of uniformity
$\mathbf{D}$	Diameter of pipe
$\mathbf{D_{10}}$	Effective particle size
$\mathbf{D_{50}}$	Average particle size
$\mathbf{D_r}$	Relative density of soil
$\mathbf{E}$	Modulus of elasticity
$\mathbf{E_1}$	Elastic modulus of EPS geofoam at initial part
$\mathbf{E_{50}^{ref}}$	Secant stiffness in standard drained triaxial test
$\mathbf{EA}$	Normal stiffness
$\mathbf{EI}$	Bending stiffness
$\mathbf{e_{max}}$	Maximum void ratio
$\mathbf{e_{min}}$	Minimum void ratio
$\mathbf{E_{oed}^{ref}}$	Tangent stiffness for primary oedometer loading
$\mathbf{E_{ur}^{ref}}$	Unloading/reloading stiffness
$\mathbf{G_s}$	Specific gravity
$\mathbf{I}$	Moment of inertia
$\mathbf{I_{HDPE}}$	Moment of inertia of HDPE pipe
$\mathbf{K_0}$	Lateral earth pressure coefficient
$\mathbf{m}$	Stress dependent stiffness according to power law
$\mathbf{P^{ref}}$	Reference stress
$\mathbf{R_{inter}}$	Interface strength reduction factor
$\mathbf{t_{smooth}}$	Thickness of smooth pipe
$\mathbf{U_x}$	Maximum horizontal deformations at the pipe wall
$\mathbf{U_y}$	Maximum vertical deformations at the pipe wall
$\mathbf{w}$	Weight of pipe
$\boldsymbol{\psi}$	Angle of dilatancy
$\boldsymbol{\Phi'}$	Angle of internal friction
$\boldsymbol{\mu}$	Interface friction coefficient

γ'_{dry}	Dry unit weight of soil
δ	Interface friction angle
δ_B	Settlement at the base of pipe
δ_W	Settlement at the 35 cm wedge of pipe springline
$\Delta x/2$	Horizontal deflection
Δy	Vertical deflection
ε_1	Axial strain
ε_v	Volumetric strain
μ_p	Peak interface friction coefficient
ρ_{EPS}	Density of EPS geofoam
σ_1	Axial stress
υ	Poisson's ratio
Φ'_R	Residual interface friction angle

CHAPTER 1

INTRODUCTION

Buried pipes are generally used to transport a substance, generally fluid in the form of either liquid or gas and rarely in a solid-state, from one point to one another. As well as highway, railway and airway transportation, pipeline transportation has regulations on design.

At the very beginning, pipes are subcategorized into two as rigid pipes and flexible pipes by considering deformation behavior. The deformation behavior of the pipe is not only affected by the material properties of the pipe itself but also affected by environmental conditions like soil properties surrounding it. Briefly, it is a relationship between pipe stiffness and soil stiffness, which is hard to determine and statically indeterminate (Moser & Folkman, 2008). According to Moser and Folkman (2008), a pipe that does not show structural distress, at the moment it deflects at least 2 percent, is called a flexible pipe; others can be called rigid.

Although the load-carrying capacity of rigid pipe obtained from parallel-plate load test or three-edged load test (Figure 1.1) is higher, the flexible pipe can carry much more load than that of rigid pipe in the buried condition with the help of soil arching mechanism and increasing passive side support (Figure 1.2). About allowable deflection for flexible pipes, some researchers (Janson & Molin, 1981; Rogers et al., 1995; Schluter & Shade, 1999) found that the performance limit is between 20-30% deflections, a general agreement for allowable deflection limit is 5% (American Lifelines Alliance, 2005; Moser & Folkman, 2008) with a factor of safety of four and 2% for flexible pipe with a rigid coating (ASCE, 2009).

Not only the load-carrying capacity, taking into account the deflection limitation, but also other advantages of flexible pipes play an important role in the choice of flexible pipe. Those are (Uni-Bell, 2013);

- Excellent protection against corrosion and chemical attack
- Lightweight material
- Watertight joints
- Abrasion and wear resistance
- High impact strength
- Superior hydraulic efficiency
- Has no adverse effect on water quality
- Good thermal insulations
- Comparatively flame resistant
- Low cost

Briefly, flexible pipes, generally made of PVC or HDPE, are sustainable pipes with respect to steel, iron and concrete rigid pipes.

a) UTest (2020) b) Söylemez (2017)

Figure 1.1. a) Three-edge load test and b) parallel-plate load test

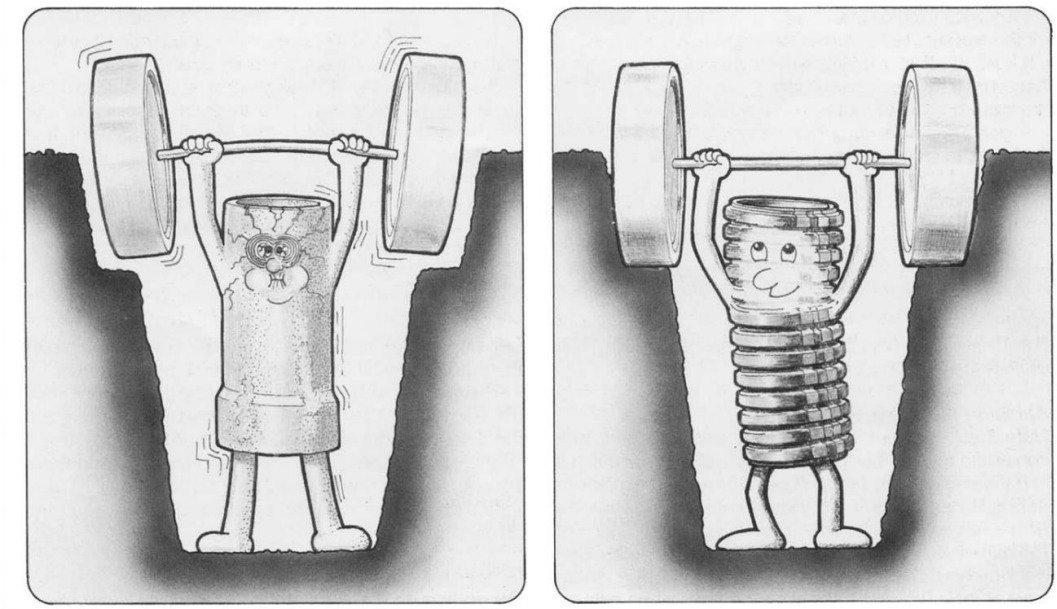

Figure 1.2. Rigid pipe versus flexible pipe [taken from Järvenkylä (1989)]

For these reasons, the importance and usage of flexible pipes are getting increasing. There are some performance limit criteria for flexible pipes (ASCE, 2009; Moser & Folkman, 2008; Uni-Bell, 2013). Those are;

- Stress performance limit
- Fatigue performance limit
- Reverse curvature performance limit
- Longitudinal bending
- Ring buckling
- Localized profile buckling
- Wall crushing
- Hoop and flexural strains

By considering the aforementioned performance limit criteria, although the 5% deformation criterion is generally met, in some special cases, it may be necessary to reduce the forces acting on the wall of shallowly buried flexible pipes. For this case, the trend of using the imperfect trench installation (ITI) or embedded trench installation (ETI), by placing compressible soft zone above or circumference of

flexible pipe, to improve the deformation behavior of shallowly buried flexible pipes emerge as it is in the case of rigid pipes.

1.1 Problem Statement

In order to create soft compressible inclusion for induced trench installation, different kind of materials have been used in literature like leaves (Spangler, 1958), cardboards (Edgar et al., 1989), straw-bale (Larsen & Hendrickson, 1962; McAffee & Valsangkar, 2004) wood-chips and sawdust (McAffee & Valsangkar, 2004; Parker et al., 2008), tire-soil mixtures (Jean & Long, 1990; Mahgoub & El Naggar, 2019; Moghaddas Tafreshi et al., 2012; Ni et al., 2018) and EPS geofoam (Akınay, 2017; Anil et al., 2015; Kang et al., 2007b; Meguid & Ahmed, 2020; Söylemez, 2017; Sun et al., 2005; Witthoeft & Kim, 2016).

Horvath (1997) and Vaslestad (1993) states that it is difficult to determine stress-strain behavior properly of the aforementioned materials except for EPS geofoam since they are non-fabricated, mostly organic and non-homogeneous. Additionally, Vaslestad (1993) states that organic materials have a tendency to dissolution when they are buried, and they are susceptible to bio-degradability. At this time, cases of occurrence of additional distress have been reported on culverts due to the dissolution of organic materials (Krizek et al., 1971; Rude, 1978). Krizek et al. (1971) also reported that instead of using organic material, with unpredictable stiffness, as soft inclusion, it is better to use loose soil, although it is not as effective as soft organic inclusions in reducing load.

Contrary to the above mentioned, EPS geofoam has the strength and deformation properties specified by the standards since it is produced in the factory. Besides, it is highly resistant to chemical attacks and is not biodegradable. Unlike the materials above, it is a homogeneous and durable material. It is very easy to transport and use in construction due to its lightweight property. In addition to all

these, it is fire resistant and has a high thermal insulation feature. Considering all these, its usage in the induced trench installation method is increasing day by day.

After a comprehensive literature review, it has been observed that there are only a few studies on the improvement of deformation behavior of shallowly buried flexible pipes with EPS geofoam as soft inclusion. Kang et al. (2007a) propose optimum soft zone geometry for embedded trench installation as a result of numerical analysis for deeply buried flexible PVC pipe. However, these numerical analyses were not verified with full-scale laboratory tests. Söylemez (2017) conducted laboratory tests on shallowly buried flexible PVC pipe improved with EPS geofoam. In his research, Söylemez investigated the effect of density, location, thickness, width and multiple layers. However, the study of Söylemez was carried out under circular loading conditions in order to reflect the loading of the truck tire. Additionally, the study of Söylemez has imperfection about digital instrumentation and results are difficult to be verified with a numerical model since the only output is vertical deformations. Akınay (2017) conducted full-scale laboratory tests on improving the behavior of buried HDPE pipe by using EPS geofoam with comprehensive instrumentation for monitoring the behavior of the test pipe and soil surrounding. In his study, Akınay investigated five different EPS geofoam combinations around the pipe, which are above the pipe, below the pipe, above and below the pipe, 90° semi-saddle at the lower and upper boundary of the pipe and complete wrapping of pipe with EPS geofoam called embedded trench installation. Results of experiments reveal that by considering cost efficiency and performance, placing of single EPS geofoam layer above the HDPE pipe offers the best solution. However, in the study of Akınay, optimization of that single EPS geofoam layer was not done.

By considering drawbacks of creating a compressible zone with EPS geofoam in geometry called embedded trench installation (wrapping the pipe as suggested by (Akınay, 2017; Kang et al., 2007a)), the followings are noted;

- EPS is relatively expensive so that geometry (quantity) should be optimized

- Need to be fabricated in the form of pipe (diameter) by considering bedding thickness
- Embedded trench installation is time-consuming with respect to imperfect trench installation

In order to overcome this gap in Akınay's work, it is decided to verify a numerical model with laboratory tests of Akınay and then conduct parametric numerical analyses for the determination of the optimum compressible inclusion geometry for imperfect trench installation on the shallowly buried flexible pipes.

1.2 Research Objectives

This study aims to determine the optimum EPS geofoam geometry for imperfect trench installation on the shallowly buried flexible pipes.

1- To determine the optimum EPS geofoam location, width and thickness above the flexible pipe.
2- To determine the effect of EPS geofoam density on the behavior of flexible pipe.
3- To determine the necessity of the second EPS geofoam layer above the first EPS geofoam layer.
4- To show that whether the Plaxis 2D finite element program can successfully model the behavior of flexible pipe improved with EPS geofoam by using the appropriate constitutive model for EPS, soil and flexible pipe.
5- To show that EPS geofoam material can be successfully modeled in small strain finite element numerical model with the linear elastic material model by directly using unconfined compression (UC) test results obtained from laboratory experiments or literature.
6- To provide a comprehensive database for the literature, including almost results of 128 numerical analyses in both graphical and tabular form.

1.3 Scope

This study investigates the optimum imperfect trench geometry, by using finite element analysis (FEM), to be created using EPS geofoam on shallowly buried flexible pipes. In Chapter 2, the literature review is presented. Methodology and the details of the numerical modeling are presented in Chapter 3. Verification of the numerical modeling is done in Chapter 4 by using existing laboratory experiment's results from the literature. In Chapter 5, parametric study is done in order to investigate the effect of the location, thickness, density and width of the compressible zone together with effect of using two layers with different thicknesses and spacing between two consecutive compressible zones. In Chapter 6, results of the numerical analyses are summarized. In the conclusion part, limitations of the study are given and future studies are recommended.

CHAPTER 2

LITERATURE REVIEW

A pipe is classified as rigid or flexible based on its relative stiffness with respect to the elastic medium that has been embedded (Mcgrath, 1999). Moser and Folkman (2008) define that flexible pipes can deflect at least 2% with any permanent deformation, and rigid pipes do not provide this criterion. Steel and plastic (PVC, HDPE, etc.) pipes are usually stated as flexible and concrete pipes as rigid. There are also semi-rigid pipes, which are flexible pipes coated with rigid coatings. The classification of the pipe must be considered carefully by the designer since the behavior and performance of the pipe would be affected either it is flexible or rigid. The strength against wall stresses caused by internal pressure and external loading is usually important for rigid pipes, whereas, for flexible pipes, the stiffness should be considered to resist deformation (ovalization) and buckling (Figure 2.1). For flexible pipes, the allowable deformation is reported as 0.05D-0.075D (American Lifelines Alliance, 2005; CPPA, 2006; NCHRP, 1999; Spangler, 1941)

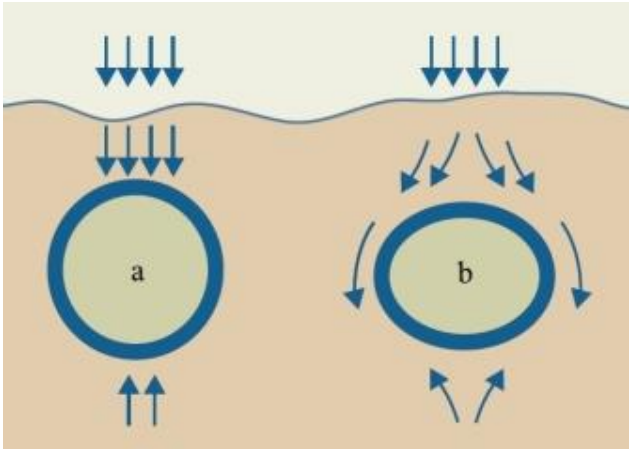

Figure 2.1. Deflection of (a) rigid pipe and (b) flexible pipe
(taken from: https://www.krahmisr.com/hdpepipes.htm)

The load distribution on pipes depends on many criterions such as height of the fill, fill material and installation method as well as the relative stiffness of pipe and surrounding soil (Vaslestad et al., 2011). The pioneer study on calculation of earth loads on buried pipes from Marston and Anderson (1913) defines two types of external loadings. The first loading condition is obtained by digging of a narrow trench in undisturbed soil and called as "trench (conduit) installation" (Figure 2.2a). In trench condition, the settlement of backfill and pipe creates frictional forces on the walls of the trench. The frictional force creates a reduction of the vertical load caused by the weight of the backfill. The second loading condition was called as "embankment installation". It is described as "positive projecting conduit" if the top of the pipe is above the natural ground surface (Figure 2.2b). The "negative projecting conduit" is founded in a trench and backfilled up to the embankment level (Figure 2.2c).

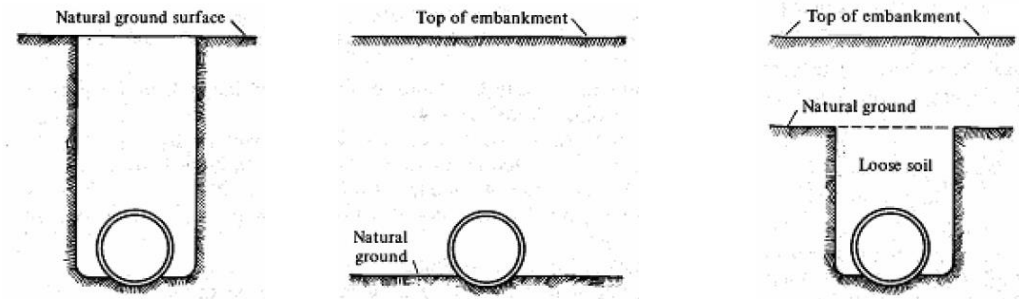

a) Trench installation

b) Embankment installation (positive projection)

c) Embankment installation (negative projection)

Figure 2.2. Installation conditions of pipes [taken from Kang (2007)]

In positive projecting conduits, two separate cases are defined as shown in Figure 2.3 below. In Figure 2.3a, under overburden pressure, a rigid pipe is expected to have less deformation than the adjacent soil due to its stiffness. On the contrary, in Figure 2.3b, the flexible pipe and backfill material would have more deformation than the adjacent soil medium. The differences in settlements would cause shear forces between the soil column above the pipe and adjacent soil medium. In flexible pipes, shear forces created by the differential settlement are directed

upward on the walls of the compressible zone. In other words, the forces created in soil resisted maintaining the original position of soil block above the pipe against a settlement. So, the flexible pipe will experience a vertical load that is lower than the weight of the soil column above due to upward shear forces. This behavior is called positive (or active) soil arching (Figure 2.4a). In rigid pipes, the differential settlement causes downward movement of adjacent soil and creates a greater vertical load compare to the weight of the soil column above, and it is called negative (or passive) soil arching (Figure 2.4b). It was reported that (Al-Naddaf et al., 2019; Terzaghi, 1943) the positive soil arching can be mobilized with small deformations. However, Han (2015) reported that the elastic modulus of the soil must be at least 100 times higher than the pipe in order to have sufficient relative displacement.

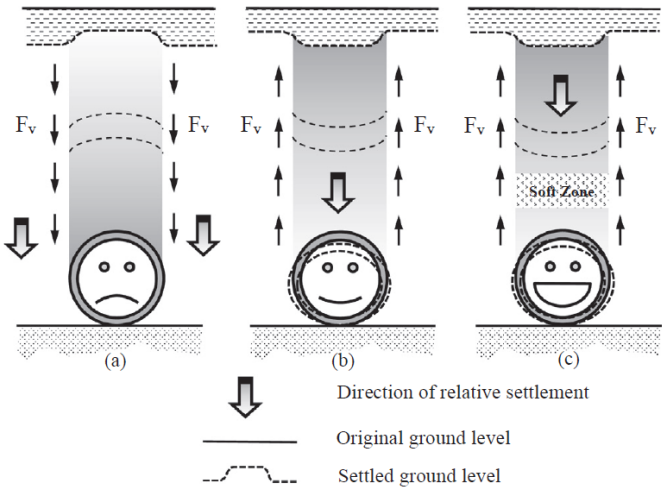

Figure 2.3. Load distribution on (a) rigid pipe under embankment, (b) flexible pipe in embankment installation, (c) rigid/flexible pipe in ITI [taken from Kang (2019)]

The benefits of loading condition of the "trench condition" can be utilized where the "positive projecting conduit" is required to implement by the imperfect (induced) trench installation (ITI) (Marston, 1922). The pipe is placed on the natural ground and the regular compacted embankment fill is done on the sides of the pipe. A compressible inclusion is placed on top of the pipe and embankment fill is completed. Thus, a trench condition is created in an embankment installation is

achieved since the soil prism above the pipe would be settled more compare to the adjacent soil. Due to the differential settlement, the frictional forces directing upward contributes to the reduction of vertical loads on the pipe (Figure 2.3c).

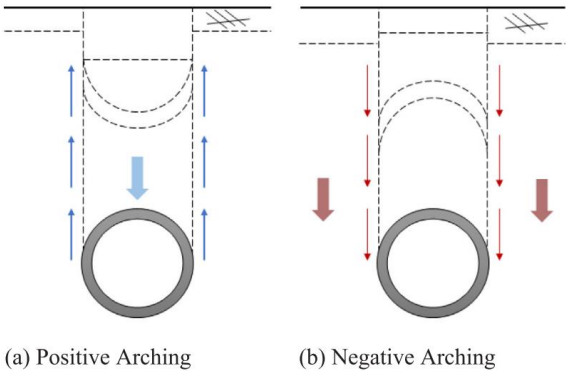

Figure 2.4. Types of arching effects [taken from Kang et al. (2020)]

In recent studies, it is claimed that the imperfect trench method (Kang et al., 2020; Santos et al., 2020) does not mitigate the earth pressure at the sidewalls and the bottom of the structures. Therefore, the pipe is suggested to encapsulate by the compressible inclusion and this method is described as embedded trench installation (Figure 2.5).

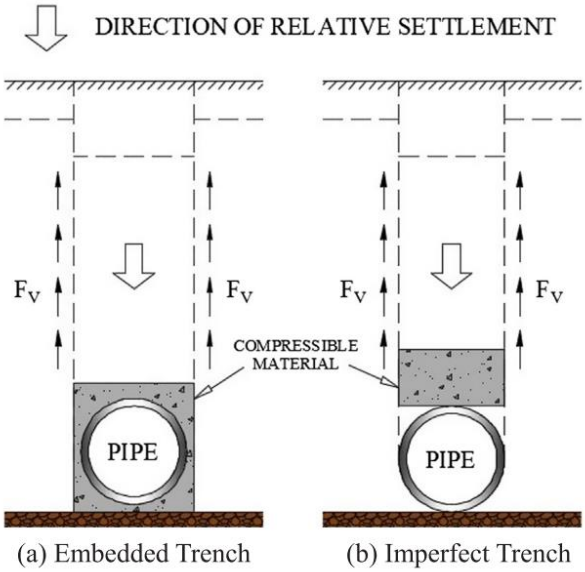

Figure 2.5. ETI and ITI implementations [taken from Santos et al. (2020)]

A very detailed literature review has been done within the scope of this study including both rigid and flexible pipes protected with the creation of trench methods. The results of the literature review are presented in detail below in order to create a solid background about previous studies and earnings.

2.1 Studies Using Various Materials as Soft Inclusion in Trench Installation Methods on Rigid Culverts and Pipes

Kim and Yoo (2005) presented both linear and nonlinear finite element analysis to investigate the load distribution on deeply buried rigid box culverts implemented with the imperfect trench method. The numerical models were validated with an example by Katona and Vittes (1982). The concrete box culvert was analyzed for different geometric configurations of the loose material zone and backfill materials. The elastic modulus of loose material was in the range of 4.79 kPa to 47.9 kPa. The culvert had the dimensions of 2.44 m x 2.44 m, and the thickness of both wall and slab was 305 mm. The width of the loose material zone was varied between 1.0w and 2.5w, as w denotes the culvert width. Similarly, the effect of height of the loose material zone (h) and spacing to the top of the culvert (h') were investigated between 0.75 m to 4.5 m and 0 to 2.44 m, respectively.

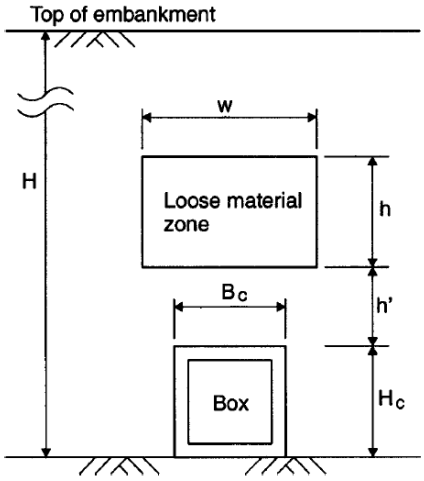

Figure 2.6. Geometric configuration and notation of numerical model of Kim & Yoo (2005)

The authors concluded that the load reduction factor could be as high as 85% depending on the elastic modulus of the soft inclusion and geometry. The load reduction rates regarding different elastic modulus of lightweight material with varying h/Hc and w/Bc ratios were also examined and the best results were obtained with the lowest E value. The load reduction rates with varying loose material zone width were tabulated in Table 2.1. It can be seen that a loose material zone with a width larger than 1.5w did not contribute significantly.

Table 2.1 Rate of load reduction regarding different width of the loose material zone

Modulus of lightweight material	Width of back fill layer, w/B_c			
	1.0	1.5	2.0	2.5
47.9 kPa (100 ksf)	32.8	41.1	39.1	36.7
23.9 kPa (50 ksf)	43.6	58.6	57.0	54.3
4.79 kPa (10 ksf)	56.9	83.7	85.3	84.8

In a similar fashion, as the thickness of the loose material zone (h) exceeds 1.5 times of culvert height ($1.5H_c$), no significant contribution was observed (Figure 2.7a). Besides, the most efficient load reduction rates have been obtained by placing the loose material on top of the culvert. As the spacing between the loose material zone and the culvert increased, contributions to the load reduction were diminished (Figure 2.7b).

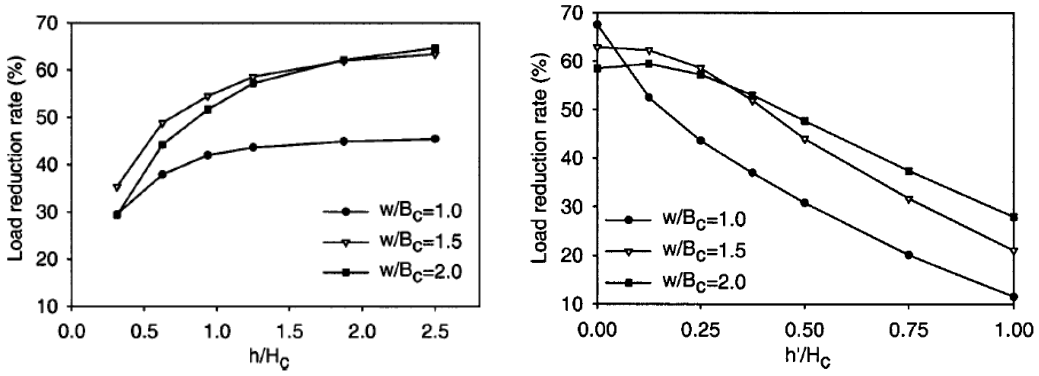

a) Effect of thickness of the loose material zone

b) Effect of the location of the loose material zone

Figure 2.7. Results of numerical analysis of Kim & Yoo (2005)

Kang et al. (2007b) proposed the optimum geometry of soft zone for the deeply buried concrete pipes implemented with induced trench method. The width, height, and the distance from the top of the pipe to the bottom of the soft zone were adjusted with parametric studies with over 1000 cases in order to obtain the most effective combination to reduce earth pressure. In the analysis, the elastic modulus of the soft zone was varying between 345 kPa to 2756 kPa, since the E values for geofoam and bales of hay had been presented as like by McAffee and Valsangkar (2004). It was stated that implementation of the soft zone only at the crown of the pipe causes higher lateral earth pressures due to redistribution of the load from the crown to the sides. Moreover, in the case of embankment installation (no soft zone), stress concentration at the invert of the pipe was not observed; however, in the case of imperfect trench installation, a considerable amount of stress concentration was observed at the pipe invert. In order to prevent the significant pressure increase observed on the sidewalls and invert, the most effective geometry for reducing earth pressure was designated as Figure 2.8b, whereas in practice, Figure 2.8c had been implemented traditionally (Kim & Yoo, 2005)

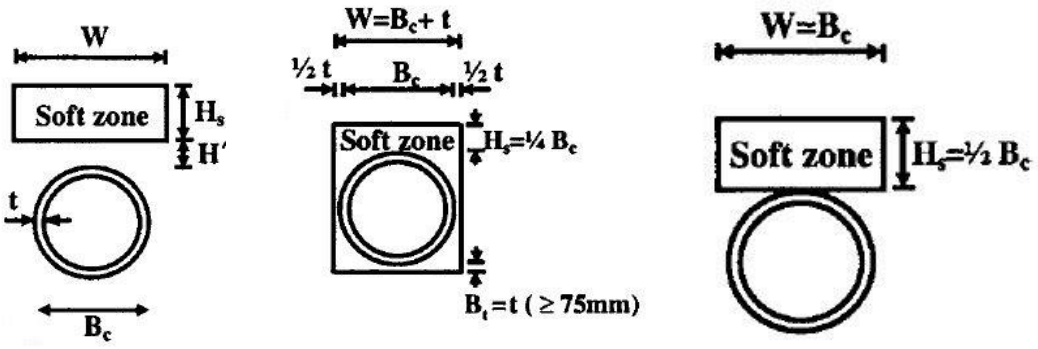

a) Notation b) Proposed geometry c) Traditional geometry

Figure 2.8. Applications of trench geometries (Kang et al., 2007b)

The analyses showed that Poisson's ratio and the ratio of the height of fill to the outside diameter of pipe did not have a significant impact on the load reduction rates. However, the modulus of elasticity of compressible inclusion was found as an effective factor. Different elastic modulus values were introduced to the proposed geometry (Figure 2.8b) and found that the load reduction rate increased by softer materials (Figure 2.9).

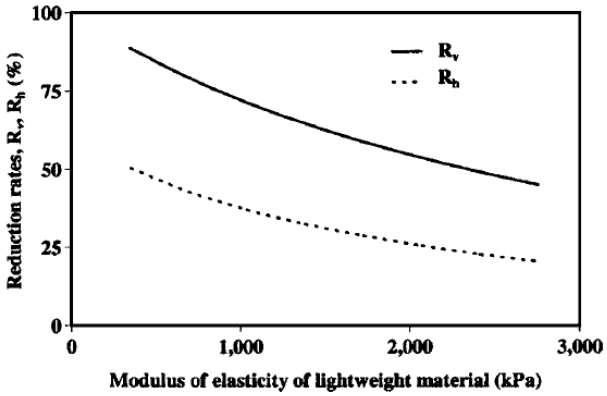

Figure 2.9. Effect of modulus of elasticity on load reduction rates

Kang et al. (2008a) also studied the optimum geometry of soft zone for the deeply buried relatively flexible corrugated steel pipes implemented with induced trench method. The soft zone geometry was proposed as Figure 2.10b by numerical parametric analyses with similar methods and material parameters of Kang et al.

(2007b). The authors conclude that reduction factor for wall stresses is 0.69 for the proposed geometry. Besides, some predictor equations on maximum earth pressures on pipe walls, deflections, and arching factor reduction rates have been obtained as a function of the modulus of elasticity of soft zone and the slenderness ratio of pipe.

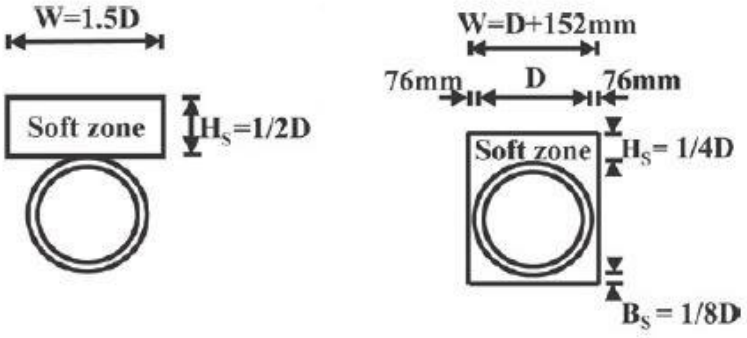

a) Traditional geometry b) Proposed geometry

Figure 2.10. Applications of trench geometries (Kang, Parker, & Yoo, 2008)

Kang et al. (2008b) investigated the forces developed by earth pressures acting on the walls of the buried rigid box culvert, with special attention given to the frictional forces acting on the sidewalls in the case of installation of the imperfect trench method. Previously, the study of the Kim & Yoo (2005) revealed that implementation of the imperfect trench installation significantly increases the contact pressure of the culvert bottom due to the increase in the frictional force near sidewalls of the culvert. Kang et al. (2008a) pointed out that in the case of implementation of ITI, the effect of frictional forces governs the design. This effect of frictional forces can be improved with the help of ETI. For this purpose, finite element analyses were conducted in order to provide the optimum geometry of the soft zone to reduce the earth loads. Similar to the studies of Kang et al. (2008a), the modulus of elasticity of soft zone varied between 345 kPa to 2756 kPa, that corresponds to the E values of geofoam and bales of hay presented by McAffee and Valsangkar (2004). The numerical analyses of embankment installation without

soft zone were performed with different combinations of foundation conditions (yielding or unyielding), interface conditions and side fill treatments. According to the results, the obtained load value at the bottom of the culvert always exceeds the total earth load and dead load of the structure, due to the downward frictional force on the sidewalls. The frictional force was found as 7%-19% and 25-30% of the total vertical load at the bottom, for compacted and uncompacted side fills, respectively. The traditional soft zone geometry for the implementation of the imperfect trench method (Figure 2.11c) led to the development of significant frictional forces on sidewalls, although it was effective for the reduction of vertical earth load. The frictional forces create 77-79% and 80-81% of the total vertical load, for the uncompacted and compacted side fills, respectively. So, the optimum geometry was proposed as Figure 2.11b to reduce the sidewall shear and vertical load at the bottom, as well as minimizing the volume of material for cost purposes.

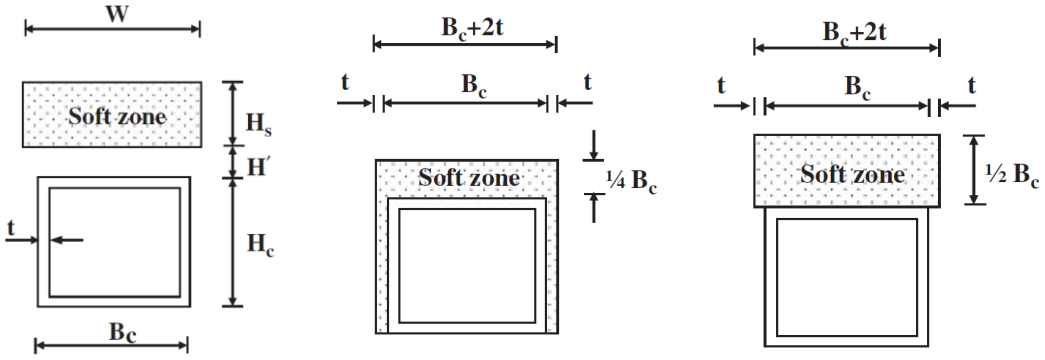

a) Notation b) Proposed ETI geometry c) Traditional geometry

Figure 2.11. Trench applications (Kang, Parker, Kang, et al., 2008)

Parker et al. (2008) evaluated the installation of imperfect trench installation on rigid concrete pipe (Figure 2.12), with an outer diameter of 375 cm and the inner diameter of 300 cm, with both field tests and numerical analysis. The burial depth for the concrete pipe was 19.4 m. As a soft inclusion, sawdust was used with a Young's modulus of 185 kPa, Poisson's ratio of 0.3 and unit weight of 265 kg/m^3. Dimensions of the soft zone were 275 cm in height and 400 cm in width. At the

end of the construction, vertical stress on the concrete pipe was measured as 16% - 24% of overburden pressure, whereas horizontal stresses measured at the pipe springline was between 33% - 45% of overburden stress. Researchers revealed that due to the inclusion of soft zone above the rigid pipe, soil pressures were redistributed from the crown and concentrated around springline. Horizontal stresses measured at the pipe springlines were reported to be significantly higher than stresses at the pipe crown. Researchers also adopted a numerical model, FLAC, to the same field observations and investigated settlements and stresses inside the embankment. It was concluded that vertical stress calculated at the bottom of the concrete pipe was 50% higher than that of the vertical stress at the pipe crown so that vertical stress governed the design.

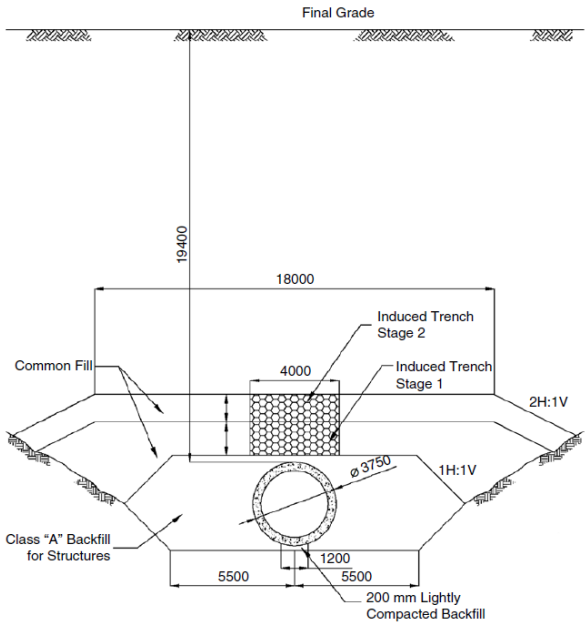

Figure 2.12. Installation of the imperfect trench application (Parker et al., 2008)

McAffee and Valsangkar (2005) instrumented a newly constructed rigid culvert in New Brunswick, which was designed according to the induced trench method, to evaluate the earth pressure values and settlement amount over the discussion about the suspension of induced trench installation since it was found difficult to construct by ACPA. In the field test, the culvert had an inside diameter of 0.9 m

and 75 m in length. It was placed at the base of the embankment with a height of 11.5 meters. The compressible inclusion was selected as sawdust and its dimensions were 1D of width and 0.5D in height, as D states for the outside diameter of the pipe. The backfill was granular material. The field data have been collected during two year period after embankment construction by the instrumentation made with nine pressure cells, 16 settlement plates and two dial gauges. At the end of embankment construction, the vertical earth pressure at the crown of the pipe was measured as 0.24-0.39 of the overburden pressure. The horizontal earth pressure on the wall of the pipe was 0.44-0.51 times the overburden pressure at mid-height of the pipe. It was reported that the vertical earth pressure was found significantly lower compared to Marston's formula (0.7 of overburden) whereas the horizontal earth pressure was obtained higher than expected. It was concluded that the load is redistributed from the crown to the sides and creates higher horizontal stress at walls.

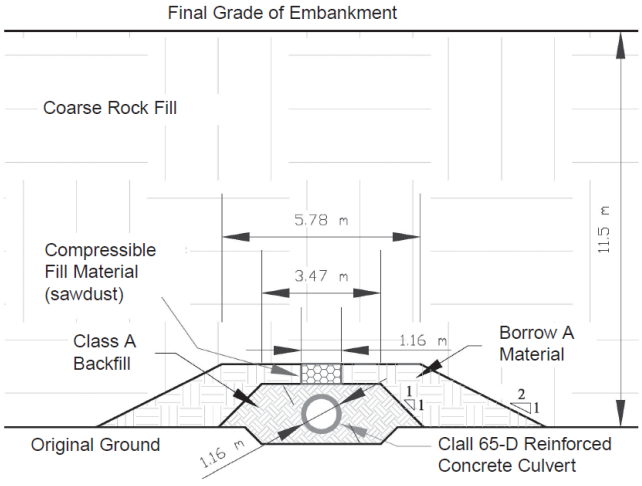

Figure 2.13. Details of the induced trench application of McAffee and Valsangkar (2005)

2.2 Studies Using EPS Geofoam as Soft Inclusion in Trench Installation Methods on Rigid Culverts and Pipes

The obtained results of McAffee and Valsangkar (2005) were compared with centrifuge testing (Figure 2.14) and numerical modeling by McAffee and Valsangkar (2008) for the purpose of investigating the H/B ratio (height of compressible zone divided by culvert width) and thickness of the compressible layer. The centrifuge testing was objected to reflect the effect of embankment height to culvert width ratio instead of simulating the exact field model. The compressible inclusion was selected as EPS geofoam to simulate sawdust usage on the field. It was reported by researchers that measured vertical stress on the top of the culvert was 1.16 times higher than overburden pressure. When a compressible zone with a width of 1D and height of 0.5D is induced, vertical pressure at the top of the culvert is reduced to 0.24 of the overburden pressure. Results up to this point were concluded as compatible with field results. If the thickness of the compressible zone decreased to half (0.25D), then vertical stress acting at the top of the culvert reduced to 0.38 of the overburden pressure. For the horizontal pressures, it was concluded that in the case of no compressible zone, 0.45 times of the overburden pressure acted on the culvert sidewalls. However, an increase in the horizontal pressures of 0.47 and 0.49 times of the overburden pressures was measured for the case of induced trench installation with a thickness of 0.5D and 0.25D, respectively. When the width of the compressible layer, for the case of a thickness of 0.5D, is 1.5D, a significant amount of reduction in horizontal stress, which is 0.39 times the overburden pressure, was measured. One important conclusion is the more uniform pressures can be observed on the walls of the culvert if the width of the compressible zone increased to 1.5D. Additionally, the numerical models had performed with the finite difference method with the help of FLAC. The vertical pressure calculated at the crown and walls were 0.62 and 0.45 of the overburden pressure, respectively. Researchers pointed out that pressure distribution over the full culvert width can be considered by the numerical model,

which shows that after pressure distribution, average vertical pressures are higher than that of horizontal pressures so that design is governed by vertical pressures. It was concluded that Marston's theory supplies sufficient safety for induced trench design for a single culvert.

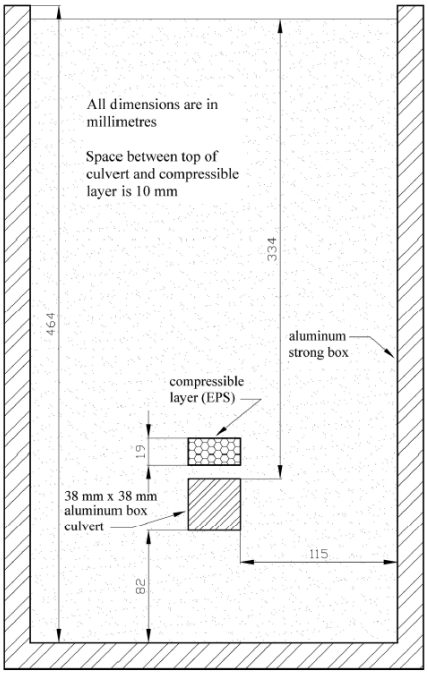

Figure 2.14. Details of the induced trench application of McAffe and Valsangkar (2005)

Okabayashi et al. (1994) investigated the effect of flexible (compressible) material to reduce vertical earth pressure on rigid culverts by centrifuge testing for 14 different cases. The cases were created by altering the width and position of the flexible material. The testing apparatus had a maximum acceleration of 200g and an effective radius of 1.50 meters. Experiments were conducted under maximum gravitational acceleration of 80g with an increment of 10g per step. The flexible material used in the experiments was Expanded Polystrol and it had performed elastic behavior up to 10% strain then fallen on the plastic range. It was found that flexible material made a significant contribution to reducing the vertical earth pressure. The effect of width was not found significant, whereas the best result was

obtained as the flexible material that has the same width as culvert and placed at right above the structure. In the study, the arching mechanism was observed by the photoelastic experimental methods for both positive projection and induced trench methods.

Sun et al. (2005) investigated the reduction of vertical stress by EPS geofoam on buried rigid highway culvert constructed in Kentucky using the finite difference method via FLAC. The cast-in-place culvert had 2.7 m inner width and 2.4 m inner height. The thickness of walls, ceiling and bottom slab were 0.3 m, 0.64 m and 0.66 m, respectively (Figure 2.15). The total length of the culvert was 112.8 meters. Two different EPS dimensions have been implemented on the in-situ experiment model with three different sections under 16.5 m high embankment. In the first section, the width of EPS was the same as the culvert and it had a thickness of 60 cm (2 feet). In the second section, the width was 1.5 times the culvert and its thickness was the same as the former. On both sections, EPS was placed directly on top of the culvert. The last section was for reference measurements and had no EPS. The sections were instrumented with pressure cells and strain gauges.

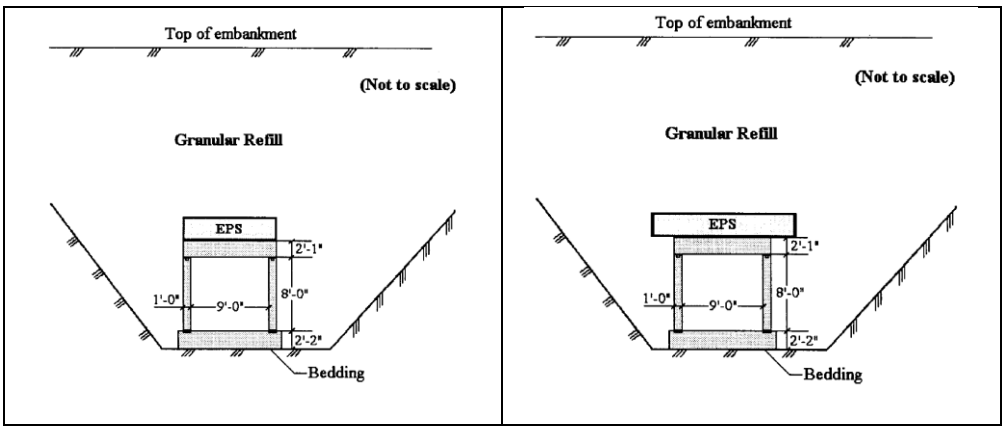

Figure 2.15. Dimensions of culvert and EPS on the in-situ experiment of Sun et al. (2005)

The 2D numerical model has been calibrated with the data obtained from the in-situ model. EPS material was modeled as a linear elastic material. According to the

results of numerical models (Figure 2.16), stresses acting at the top and bottom of the culvert walls reduced to 28% and 42% of the case in which no EPS geofoam was implemented. It was reported that the wider geofoam application did not contribute significantly to vertical stress reduction. Besides, the maximum stress acting on the side walls was found as 184% of the reference test value for EPS width is the same as the culvert width. It was measured as 163% of the reference test value for EPS width is 1.5 of culvert width. These findings were evaluated as lower than the required design values, although maximum stress acting on the sidewalls were obtained higher due to the implementation of EPS. Researchers concluded that change in the moments acting on the sidewalls of the culvert was insignificant whether EPS is implemented or not. Stresses acting on the sidewalls of the culvert, however, increased dramatically in the case of EPS implementation above the culvert. Increasing the width of EPS from one times the width of the culvert to 1.5 times of the culvert width was not so effective.

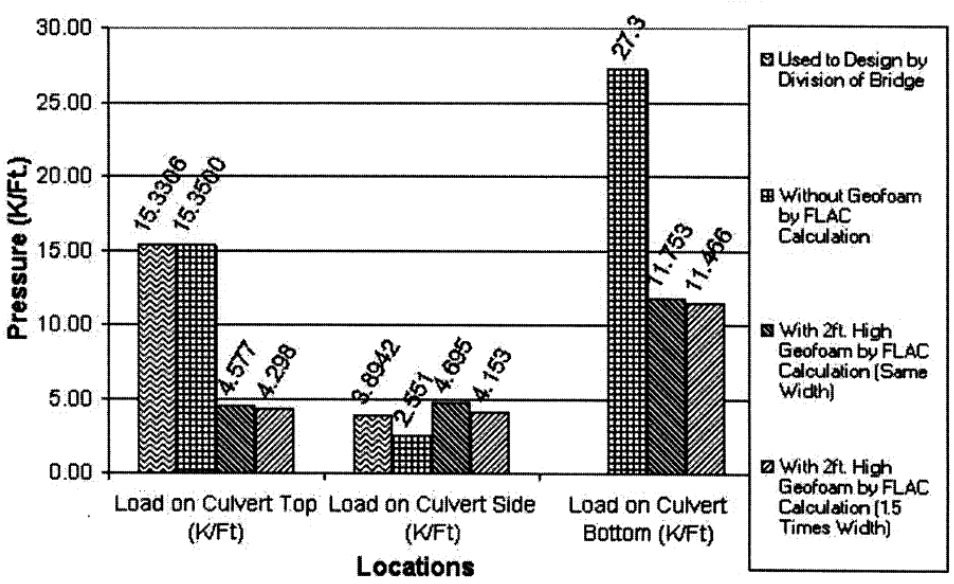

Figure 2.16. Dimensions of culvert and EPS on the in-situ experiment of Sun et al. (2005)

The optimum geometry of EPS geofoam has been investigated by Kim et al. (2010) with model and full-scale tests for reduction of earth pressures. In tests, both the

single layer and the double layer of EPS configuration have been investigated with no EPS condition to compare the results. Burial depths for model and full-scale tests are 8D and 2.5D, respectively. The objective of model tests was to examine the effect of EPS width and spacing of layers in the case of double EPS configuration. In the tests, a steel pipe with a diameter of 10 cm was placed in a soil bin with dimensions of 140 cm x 100 cm x 90 cm. The corrugated steel pipe laid on the ground of the test bin so sand fill above the pipe was 80 cm. The EPS was chosen with a thickness of 5 cm and a density of 15 kg/m^3, and backfill material selected as poorly graded (SP) silica sand. In order to take measurements, each section was instrumented with three earth pressure cells, five settlement plates, two steel plates and two deformation rods. In total, nine different sections were examined. The full-scale model tests (Figure 2.17) were performed with a steel pipe with a diameter of 1 m and a thickness of 2 mm. The fill material on site was well-graded sand (GW) and EPS density was selected as the same with model tests. The dimensions of EPS were 1 m in width, 1.8 m in length and 0.1 m thick. In order to take measurements, each section was instrumented with three earth pressure cells, five settlement plates, two steel plates and two deformation rods.

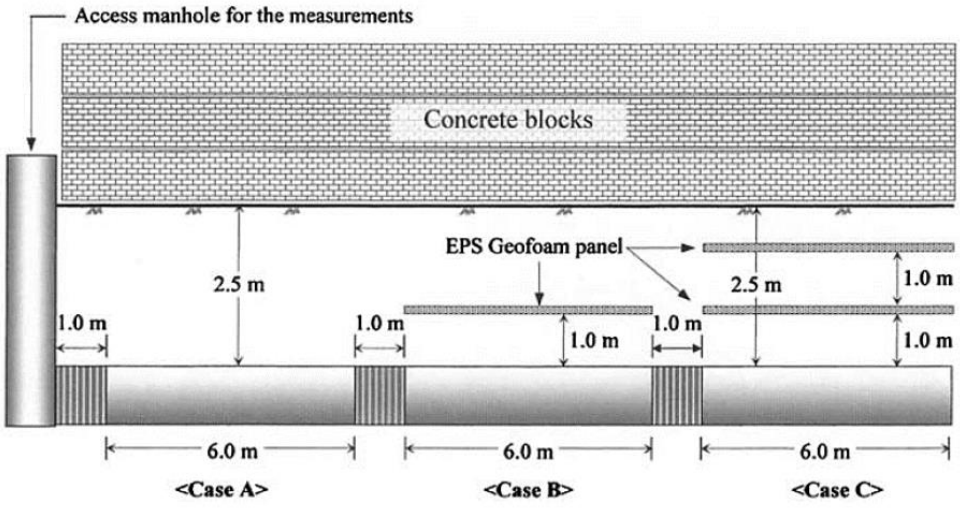

Figure 2.17. The configuration of full-scale model tests of Kim et al. (2010)

It was concluded that the width of EPS should not exceed 1.5 times of pipe diameter since it has no contribution to the reduction of earth pressures. Moreover, a larger width than the optimum one diminishes the arching effect. According to the model test results, the vertical stress values decreased by 73% when a single EPS geofoam layer was placed on the pipe, while the vertical stress values decreased by 71% when a 5 cm thick double row EPS geofoam was placed. Optimum spacing between two consecutive EPS geofoam for the case of using double geofoam was determined as one pipe diameter (1D). After this point, the effect of inclusion of the second EPS layer diminished. Considering the case of installing EPS geofoam with the same width, placing double layer EPS geofoam with a gap of one pipe diameter between them was more successful in reducing stress on the pipe. In full-scale tests, the reduction in the vertical pressure was measured as 31% and 36% for the cases of placing single EPS geofoam and double EPS geofoam, respectively. However, horizontal pressure reduction for single and double layer was found as 5% and 37%, respectively.

McGuigan and Valsangkar (2010) investigated centrifuge testing and numerical modeling of earth pressures on rigid box culverts implemented by the induced trench method. The foundation conditions and geometry of the compressible zone have also been studied. The centrifuge testing was done in two sets as the culvert settled on the either unyielding or yielding foundation. For both sets, positive projecting (no compressible inclusion) and induced trench method were modeled with several configurations. The centrifuge testing was done by using 1.6 m radius geotechnical centrifuge and 38 mm x 38 mm x 195 m aluminum model box culvert. Although the modulus of elasticity of aluminum was higher than the concrete, the results would be more conservative since less arching effect occurred. The backfill material was selected as uniform sand and the compressible material was EPS geofoam. The unyielding foundation condition was created by settled the culvert directly on the centrifuge box with a fill height of 162 mm. The culvert box settled on a sand bed of 38 mm thick for the yielding foundation conditions (Figure 2.18), and the fill height was 152 mm. The EPS material was placed 4 mm above the top

of the culvert. The tests were performed under 70g, so that the dimensions would correspond to 2.66 m box culvert under a fill height of 11.34 m and 10.64 m. The EPS material was 0.3 m away from the top of the culvert. The width of the EPS was equal to the width of the culvert and its thickness was selected as 0.66 of its height. The earth pressures on the top and bottom of the culvert as well as the side walls were measured with transducers. In order to perform further parametric studies, finite difference analyses with FLAC were performed. The backfill material was modeled with the Mohr-Coulomb model and EPS was modeled as a linearly elastic material with an elasticity modulus of 700 kPa and a density of 10.5 kg/m^3. The centrifuge tests were modeled with FLAC and results were compared in Table 2.2 and Table 2.3 for unyielding and yielding foundation conditions, respectively.

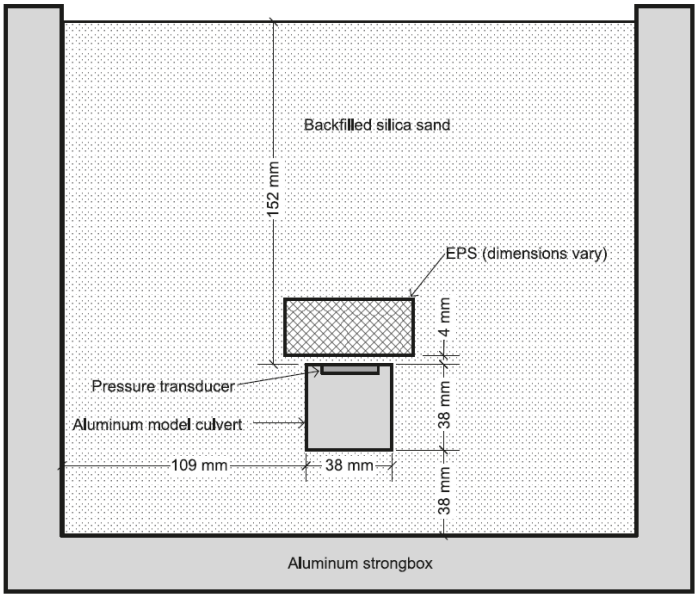

Figure 2.18. Dimensions and setup for centrifuge test box of McGuigan and Valsangkar (2010)

Table 2.2 Comparison of centrifuge testing and FLAC models of McGuigan and Valsangkar (2010) for unyielding foundation condition

Compressible zone		Earth pressure on top[a]			Lateral earth pressure on sides[b]			Contact pressure on base[c]
Width	Thickness	Centrifuge[d]	FLAC	Diff (%)	Centrifuge[d]	FLAC	Diff (%)	FLAC
—	—	1.20	1.35	12	0.30	0.38	27	1.50
$1.0B_c$	$1.0H_c$	0.26	0.25	4	0.38	0.46	21	0.78
$1.25B_c$	$1.0H_c$	0.28	0.25	11	0.38	0.47	24	0.73
$1.5B_c$	$1.0H_c$	0.25	0.27	8	—	0.45	—	0.70
$1.0B_c$	$0.25H_c$	0.31	0.42	35	—	0.41	—	0.90
$1.0B_c$	$0.5H_c$	0.28	0.31	11	—	0.44	—	0.82
$1.0B_c$	$0.66H_c$	0.27	0.28	4	—	0.45	—	0.80
$1.0B_c$	$0.75H_c$	0.28	0.27	4	—	0.45	—	0.79

Table 2.3 Comparison of centrifuge testing and FLAC models of McGuigan and Valsangkar (2010) for yielding foundation condition

Compressible zone		Earth pressure on top[a]			Lateral earth pressure on sides[b]			Contact pressure on base[c]		
Width	Thickness	Centrifuge	FLAC	Diff (%)	Centrifuge	FLAC	Diff (%)	Centrifuge	FLAC	Diff (%)
—	—	1.33	1.21	9	0.43	0.43	0	1.13	1.09	4
$1.0B_c$	$0.66H_c$	0.24	0.25	4	0.46	0.48	4	0.75	0.75	0
$1.5B_c$	$0.66H_c$	0.27	0.28	4	0.47	0.47	0	0.71	0.70	1
$2.0B_c$	$0.66H_c$	0.31	0.35	13	0.43	0.48	12	0.70	0.68	3
$1.5B_c$	$1.0H_c$	0.28	0.27	4	—	0.49	—	0.64	0.68	6

According to model test, vertical earth pressure acting on the top of the culvert, lateral pressure on the side at mid-height and contact pressure on the base of the culvert were reported to be 32%, 42% and 79% of overburden pressure for unyielding foundation case; however 28%, 47% and 73% of overburden pressure for yielding foundation case, respectively. The concern about the increase in the contact pressure at the base of the culvert proposed by Kang et al. (2008b) in the case of installation of imperfect trench installation was verified by this study. The authors conclude that the confirmed increase in contact pressure at the bottom of the culvert was due to the development of net downward frictional forces acting along the sidewalls of the culvert. However, researchers concluded that a significant amount of reduction at the contact pressure was observed in the case of ITI with respect to positive embankment construction case and ITI was still recommended as a viable design option for box culverts. Additionally, since the difference of results of numerical analysis and centrifuge tests were less than 15% and 5% for unyielding and yielding foundation cases, respectively, the parametric

studies for the different width and thickness of EPS were also studied. The optimum geometry of EPS has been defined as having a width of 1.2 times the culvert outer width with the thickness of 0.5 times its height and placed 0.3 m above the culvert.

McGuigan and Valsangkar (2011) also investigated twin box culverts with centrifuge testing and numerical models with similar setup and methods to the study of McGuigan and Valsangkar (2010). The study focused on the effect of spacing between culverts and the geometry of EPS above them. Three sets of centrifuge testing were conducted and their results were utilized for the calibration of FLAC models. The parametric numerical studies were performed to evaluate the effect of culvert spacing and geometry of EPS with a prototype model, as seen in Figure 2.19.

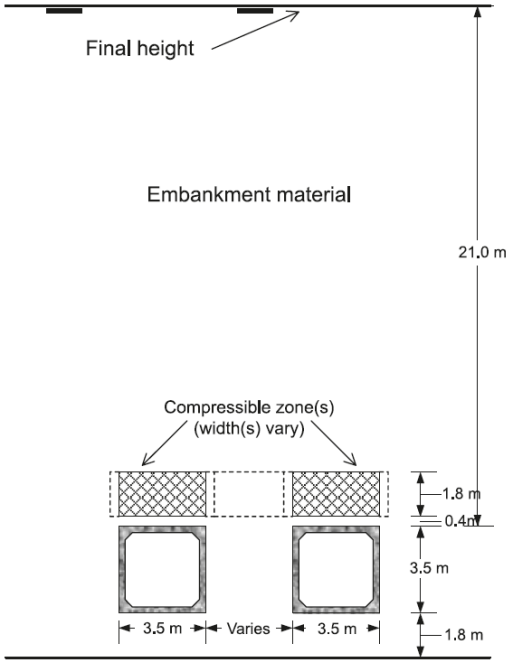

Figure 2.19. Geometry of prototype for parametric study configuration (Mcguigan & Valsangkar, 2011)

In order to evaluate the culvert spacing, analyses for the spacing of 0.5B, 1.0B and 1.5B were performed, as B denotes the width of the culvert. Besides, the geometry of EPS was configured in four different ways for varying widths. The first two configurations are composed of two zones (one zone for one culvert) with a width of 1.0B and 1.2B. The other two configurations have one zone with a width of 2.0B+s and 2.2B+s, as s denotes for culvert spacing. The results showed that in the case of positive projecting, the lowest earth pressures were obtained as the spacing was equal to 0.5B. As the spacing increased, the earth pressure values approached the single culvert case. For the induced trench conditions, the preferred EPS width varied with culvert spacing as 2.0B+s for the spacing of 0.5B and 1.0B, whereas two individual compressible zones of 1.2B for the spacing of 1.5B. It was reported that the induced trench conditions resulted in lower contact pressure comparing to the positive projection case. Also, for twin culverts induced with a single compressible zone, the contact pressures calculated at the bottom were asymmetrical because the downward shear forces on the outer walls were much greater than on the inner walls. For the 0.5Bc and 1.0Bc culvert spacing, approximately 30% higher base pressures were calculated at the outer edges of the culvert due to the aforementioned asymmetric loading. In any case, it was concluded that the induced trench installation method reduced calculated pressures on the box culvert. Researchers recommended using numerical modeling techniques in order to investigate resultant bending moments and pressures on box culverts for changing compressible zones and culvert geometries since numerical models reflected actual findings of the centrifuge test.

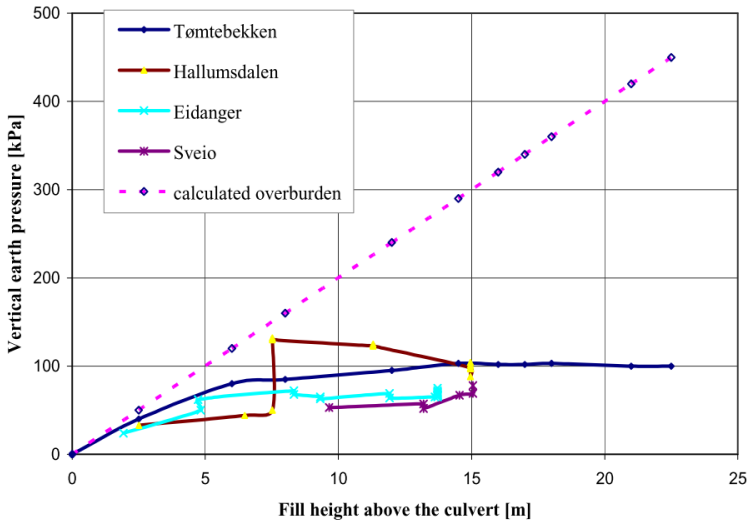

Figure 2.20. Comparison of measured versus calculated vertical pressures acting on the field tests of Vaslestad et al. (2011)

Vaslestad et al. (2011) have observed EPS geofoam blocks over buried rigid structures at four different instrumented field test sites for about 20 years. Three of the structures were concrete pipes with an inner diameter of 1.4 m to 1.6 m, and one of them was of a culvert with an outer width of 2 m. The study shared only the deformations and vertical earth pressure since horizontal earth pressure was not under the scope. The structures were instrumented with earth pressure cells and settlement tubes. On three of the fields, granular backfill material and on one of them, cohesive backfill material was used over EPS geofoam blocks. The overburden depth on pipes was varied between 10.8 m to 22 m (Figure 2.21). The EPS geofoam was selected with a density of 20 kg/m^3 and the compressive strength of 100 kPa. The long term observations resulted in that the compression of EPS geofoam material was ranged between 28-38% for granular fill and 54% for cohesive fill. Besides, it was observed that the deformation of EPS geofoam occurred in the construction phase, and no increase in pressure or deformation amount has occurred on pipes in the long term. The graph in Figure 2.20 compares the calculated and measured vertical pressures for varying overburden depths. As shown, the vertical stress affecting the culvert crown at the end of approximately 20 years has been measured as 23-25% and 45% of the overburden pressure in the

case of granular backfill and cohesive backfill, respectively. This clearly indicates the importance of the compaction of backfill for granular materials. It was found that the granular backfills were more effective for the reduction of the vertical earth pressure compared to the cohesive one.

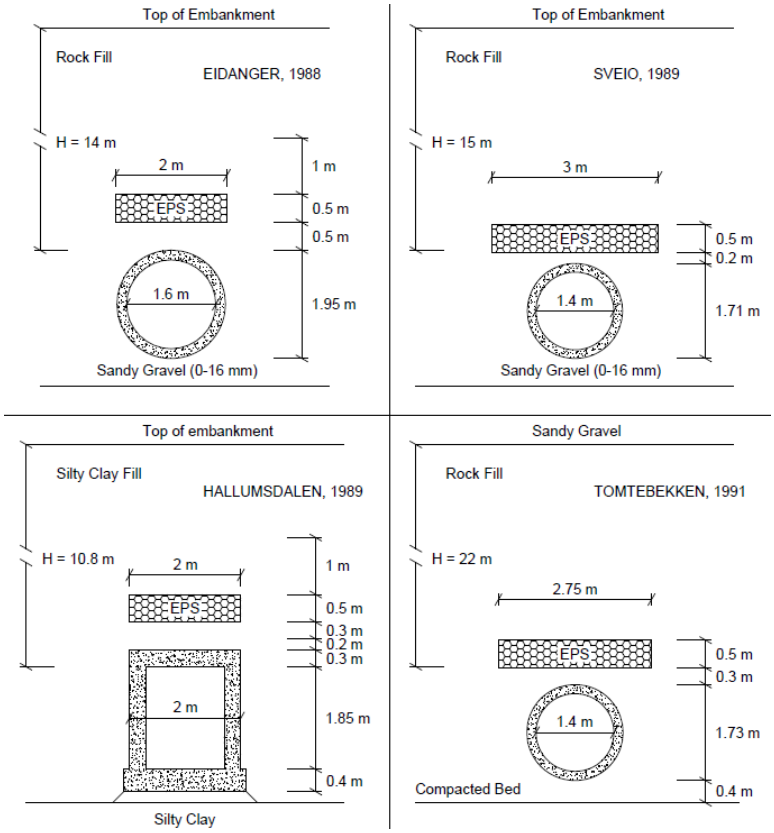

Figure 2.21. Placement of field installations of Vaslestad et al. (2011) [taken from Akınay (2017)]

Witthoeft and Kim (2016) investigated on optimum geometry of EPS geofoam over a steel pipe with a numerical model by using a finite-difference model called FLAC. The calibration of models was made with model tests done by Kim et al. (2010) and obtained results compared with finding presented in the mentioned study. EPS material was modeled as linear elastic material properties since EPS material did not enter the plastic range. The optimization of EPS geometry under the conditions of varying soil type and surcharge load, were done and the double layer EPS case was also investigated with numerical analyses. It was stated that the

optimization should satisfy the uniformity of stress around the pipe to overcome ovaling deformation (Figure 2.22). Therefore, the researchers aimed to have vertical stress at the crown of the pipe as low as possible with an acceptable ratio of horizontal stress to vertical stress ($0.9 \leq \sigma_{h,springline}/\sigma_{v,crown} \leq 1.1$).

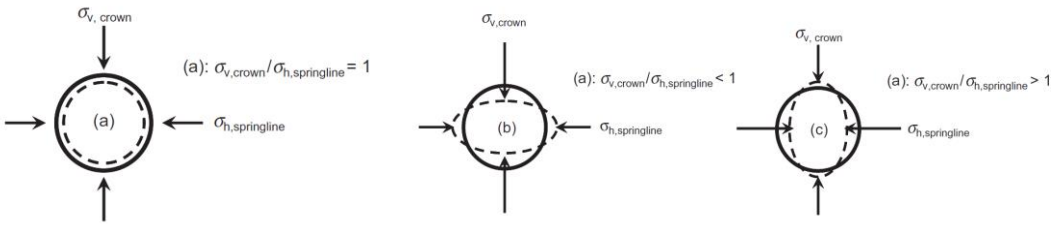

a) b) c)

Figure 2.22. Possible pipe deformations; (a) uniform stress around pipe, (b) larger vertical stress compared to horizontal stress, (c) larger horizontal stress compared to vertical stress [taken from Witthoeft & Kim (2016)]

The results of numerical analyses showed that the optimal width of geofoam is approximately 1.5D and thickness is considered as 5 cm and researchers highlighted that thickness of 5 cm should not be exceeded. Besides, double panel configuration was not evaluated since it did not satisfy the optimization criteria mentioned before. It was concluded that the upper EPS geofoam layer should have placed below the plane of equal settlement in order to create additional settlement so that arching could occur.

Meguid et al. (2017) studied the differences by laboratory tests between wrapping the rigid culvert (ETI) with EPS geofoam and placement on top of the rigid culvert (ITI), as well as the case of no EPS. These three different cases were examined with laboratory tests. Three reference tests were conducted together with two sets of ETI and ITI combinations of geofoam. The laboratory tests had been conducted in a soil chamber (1.4 m x 1.2 m x 0.45 m) with steel hollow structural section (HSS) with dimensions of 0.25 m x 0.25 m x 0.435 m and instrumented with tactile sensing pads placed on top, side and bottom walls. Dry sandy gravel was used as backfill material. Two different EPS configurations were studied (Figure 2.23).

Firstly, the conventional imperfect trench method with soft zone placed directly on top of the structure, and secondly, the structure covered with the soft zone. The pressure measurements over the culverts under 140 kPa surcharge loading were obtained.

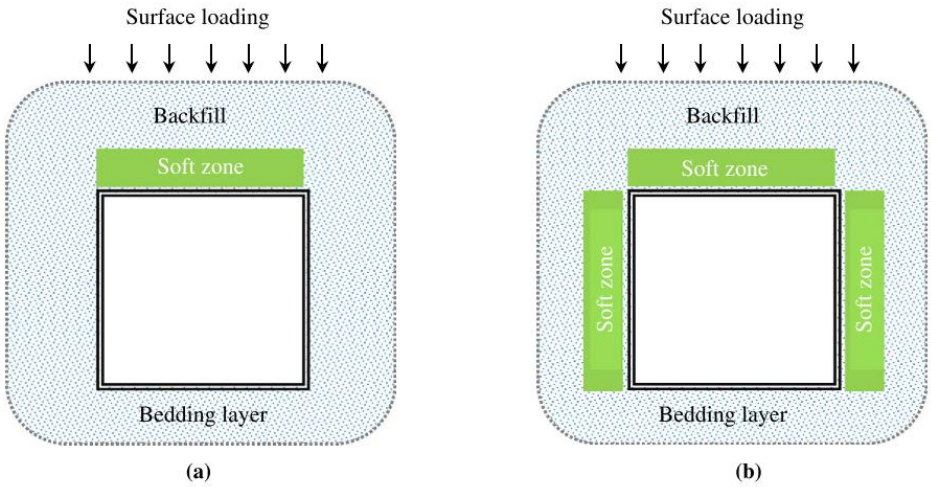

Figure 2.23. EPS configurations used in the study of Meguid et al. (2017)

Three different EPS densities have been evaluated regarding soil arching and stresses occurred in backfill by numerical modeling. As well as the EPS density, the maximum height of backfill which can be carried within design strain limitations are studied. The two dimensional finite element models by ABAQUS has been validated with laboratory test results which belongs to reference test (without EPS geofoam) and ETI configurations performed with EPS-15 and EPS-22.

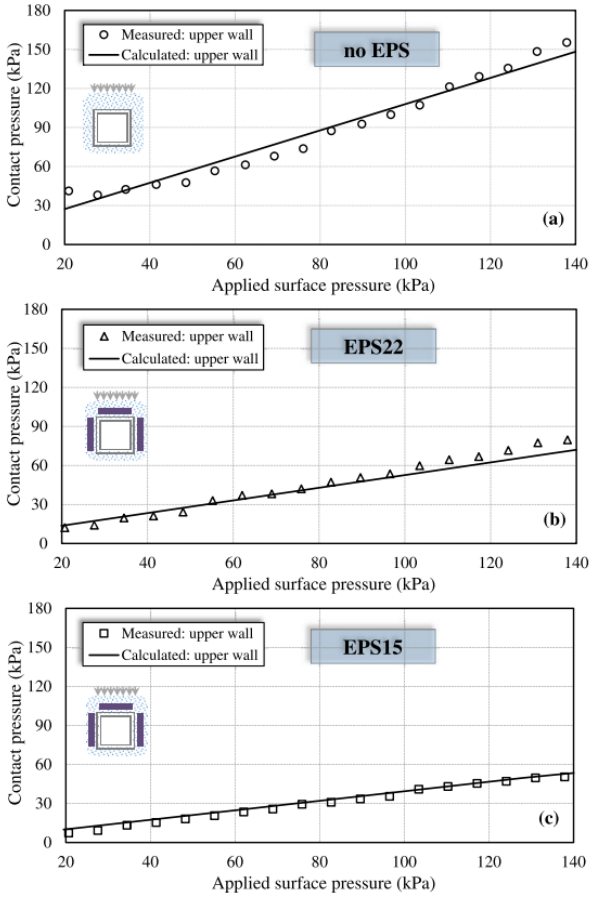

Figure 2.24. EPS configurations used in the study of Meguid et al. (2017)

After validation, the role of EPS geofoam density and configuration on earth pressure distribution on the walls of the structure was studied. The experiments showed that the stress experienced by crown and walls reduced by 64% and 70% with U-shaped EPS-15 geofoam. Researchers highlighted that introduction of ITI increases the pressures on the culvert wall. Therefore, depending on the stress, additional EPS geofoam could be induced near culvert walls and EPS density should be selected by considering strain, therefore stress on EPS geofoam.

Ma et al. (2019) studied the performance of single and multilayer EPS geofoam for load reduction on both rigid and flexible pipes with laboratory model tests by using PVC and steel pipes. The pipe had an outer diameter of 110 mm with a wall thickness of 3.2 mm. The pipe was placed in a box of 800 mm x 400 mm x 500 mm

(width x length and height) with the backfill material as sand. The width of EPS geofoam was designated as 1.5D, which equals 165 mm (Figure 2.25). The model was instrumented with 15 earth pressure cells. The density of EPS used in the study was 18 kg/m^3 (EPS-18) and the relative density of the sand was 95% with 8% water content.

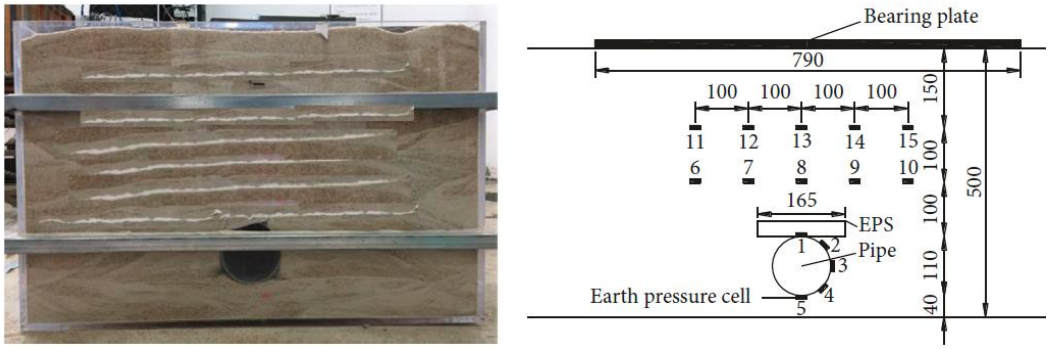

Figure 2.25. Laboratory model of Ma et al. (2019)

Different EPS thickness and number of layers were modeled and the configurations were given as Table 2.4. The model was loaded by steel bearing plate (790 mm x 400 mm x 14 mm) to simulate different overburden thicknesses.

Table 2.4 Laboratory model test configurations of Ma et al. (2019)

Scheme	Pipe material	Load-reducing material	Thickness of EPS, C (cm)	Layer spacing of EPS, Z (cm)	Number of EPS layers, N	EPS width, B (cm)
1	Steel pipe	—	—	—	0	—
2	Steel pipe	EPS	1	—	1	16.5
3	Steel pipe	EPS	2	—	1	16.5
4	Steel pipe	EPS	3	—	1	16.5
5	Steel pipe	EPS	4	—	1	16.5
6	Steel pipe	EPS	2	5	2	16.5
7	PVC pipe	—	—	—	0	—
8	PVC pipe	EPS	1	—	1	16.5
9	PVC pipe	EPS	2	—	1	16.5
10	PVC pipe	EPS	3	—	1	16.5
11	PVC pipe	EPS	4	—	1	16.5

According to the findings of the tests, the increase in EPS thickness has a significant effect on load reduction up to a certain level, and then remains constant. Besides, a double layer of EPS with the same total thickness as one layer EPS has been found to be more effective than the single layer. As usual, in case of low

overburden thickness, the flexible pipe can deform elastically and creates soil arching itself without any requirement of soft inclusion. Under high overburden thickness, the usage of EPS at the crown of the flexible pipes can help for load reduction and safe design. The researchers also reported that the earth pressure at the pipe crown shows a nonlinear change with increasing fill height since the load is distributed inside the backfill. Therefore, a nonlinear earth pressure formula was presented and its coefficients were obtained from the nonlinear regression analysis of data obtained from model tests. The results were compared with some well-established formulas (Figure 2.26) and the test results and found that the presented formula had the closest finding for the earth pressure measured at the crown of test models.

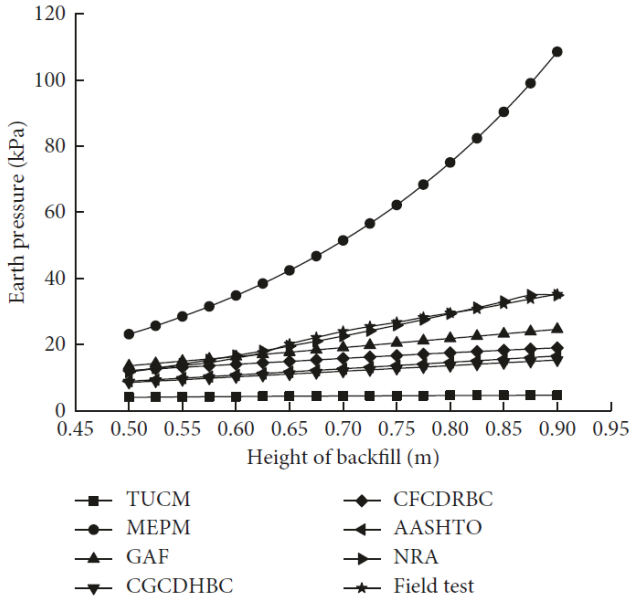

Figure 2.26. Comparison of earth pressures (Ma et al., 2019)

TUCM – Terzaghi's underground cavern method
MEPM – Marston's earth pressure method
GAF – Gu Anguan formula
CGCDHBC - China General Code for Design of Highway Bridges and Culverts
CFCDRBC - China Fundamental Code for Design on Railway Bridges and Culverts
AASHTO - Standard Specifications for Highway Bridges

Traditional 2D models with plane strain approach were not found sufficient to show the longitudinal behavior and reduction of horizontal earth pressure by Kang (2019). Therefore, 3D finite element models were developed and validated with the field studies of Parker et al. (2008). The models were developed on ABAQUS with Duncan-Selig soil models. The geometry of models was prepared in accordance with the field experiment sections and had a length of 60 m. Material properties of Parker's field experiment were used to define concrete, soil and soft zone material. Then, numerical analyses were investigated to show the effects of (a) incremental loading due to staged construction, (b) backfill material properties, (c) stiffness of the soft zone material, (d) imperfections of the soft zone and (e) loosening of side fills. Table 2.5 shows that with softer EPS material, the reduction of earth pressures was more significant. According to analysis results, the study claimed that the imperfect trench method was not sufficient in the reduction of pressure experienced by the bottom part of the pipe due to additional shear forces created by stress transfer in adjacent soil from top to bottom. Besides, it was clear that 2D approaches underestimate the reductions in horizontal pressure and successfully captures the vertical arching factors. In order to examine the longitudinal behavior of the buried pipe that burial depth is comparatively high and will be located on sloping land, it has been revealed that it is necessary to make 3D numerical models. The importance of backfill material properties and installation methodologies were highlighted again after Vaslestad (2011). It was concluded with the help of 3D numerical analysis, in the imperfect trench method, loosening in the side fill results in higher longitudinal stresses associated with bending moments.

Table 2.5 Reduction rate of earth pressures regarding different backfill soil and EPS properties

Arching factor	Modulus of elasticity of EPS Geofoam, E kPa (psi)	2-D FE analyses (2)	3-D FE analyses (D = 3.8 m)				
			SW90	SW80	ML90	ML80	Average
Vertical	345 (50)	86%	94%	91%	79%	64%	82%
Arching	689 (100)	78%	87%	82%	63%	43%	69%
Factor	1378 (200)	63%	76%	67%	41%	21%	51%
(VAF)	2756 (400)	42%	58%	46%	18%	5%	32%
Horizontal	345 (50)	48%	84%	82%	70%	58%	73%
Arching	689 (100)	42%	74%	69%	53%	37%	58%
Factor	1378 (200)	32%	59%	51%	32%	16%	39%
(HAF)	2756 (400)	18%	38%	28%	11%	2%	20%

Al-Naddaf et al. (2019) has conducted seven scaled laboratory tests (Figure 2.27); one test is without geofoam called reference test and the remaining six tests with EPS geofoam inclusion above the culvert, in order to investigate the effect of EPS geofoam stiffness and thickness on the distribution of vertical stress under static and cyclic loadings on above the rigid rectangular culvert made of concrete. The test soil used in the laboratory experiments is poorly graded, SP with respect to ASTM D2487-11 (2011), Kansas River sand with a relative density of D_r=75% and two different densities of EPS geofoams, EPS-12 and EPS-15 namely, are used in the experiments in order to study the effect of stiffness of soft inclusion. Also, two different thicknesses of geofoam were used in the experiments with t=0.2xB and t=0.4xB. Researchers reported that negative soil arching developed in the case of reference test and vertical soil pressure affected above the rigid culvert is 13% more than that of overburden pressure. Under static loading of 130 kPa, it is concluded that vertical soil pressure on rigid culvert is 37% more than the case without culvert. Inclusion of EPS geofoam reduced vertical stress above the culvert by a factor of 31% and 45% for EPS-15 and EPS-12, respectively. Softer inclusion reduced vertical stress more. However, contrary to general opinion, thinner EPS provided better improvement. Studies on cyclic loading showed that the soil

arching effect due to compressible geofoam was minimized, and stiffness of geofoam did not affect the reduction of vertical pressure.

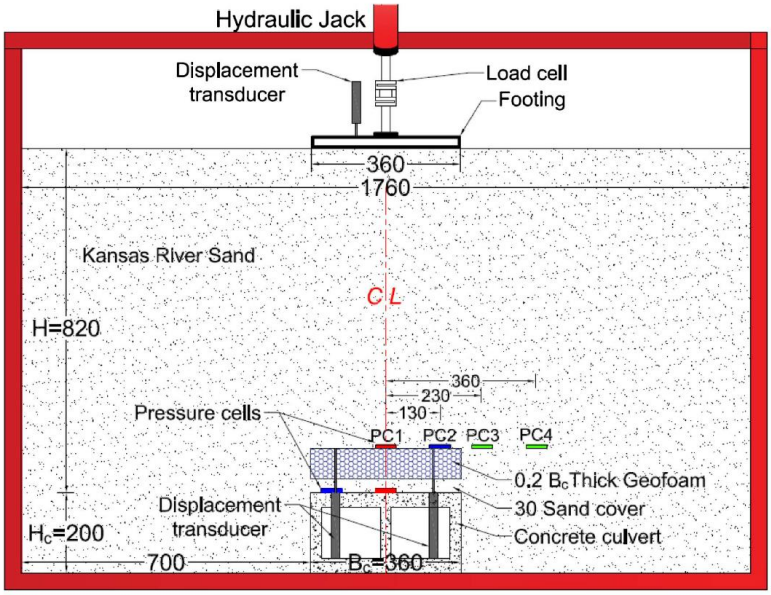

Figure 2.27. Scaled laboratory model of Al-Naddaf et al. (2019)

Santos et al. (2020) investigated the effects of the installation of the embedded trench and imperfect trench around a semi-flexible corrugated-steel arch pipe with numerical methods by using the finite element program ABAQUS. Different geometry combinations of EPS geofoam (EPS-15), pipe thickness and diameters were used in the study (Figure 2.28). Although the pipe used in the study was called by the researcher semi-flexible, which means deformation behavior is between somehow rigid and flexible pipes, relative settlement of the embankment soil was higher than that of corrugated steel pipe since having high stiffness, therefore; behavior of the pipe can be called as rigid when buried. The result of the study revealed that the height of the compressible material (H) plays an important role in reducing earth pressure, stress and deflections around the arch of the pipe, whereas the width of the compressible material did not significantly affect the behavior of the arch. The only variance was obtained in the stress at the springline of the pipe when the width of the compressible material increased. It was

concluded that while the stiffness of the steel pipe increased, a larger reduction in the earth pressure, stress and deflections were obtained around the arch of the pipe. As expected, it was reported that ITI method provided a better reduction in stress and deflections around the crown of the pipe; however, ETI method provided a better reduction in the soil stress around the pipe springline.

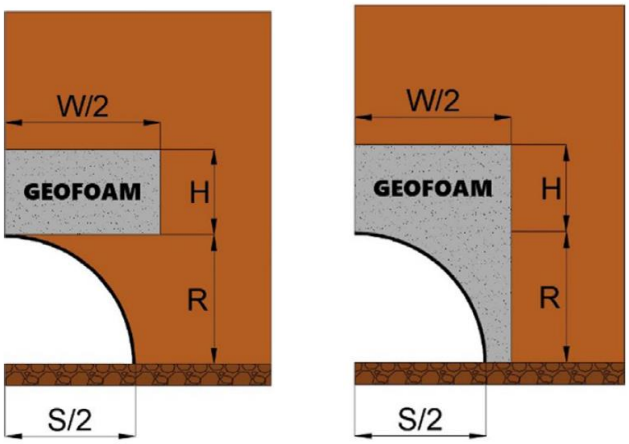

a) ITI b) ETI

Figure 2.28. Configuration of EPS geofoam placement for ITI and ETI methods [taken from Santos et al. (2020)]

In the study of Kang et al. (2020), the experimental and numerical studies about the embedded trench method and imperfect trench method on concrete arch structures were done upon the discussion of the increase in the contact pressure under the box culverts in the case of imperfect trench installation proposed by Kang et al. (2007b; 2008b) and verified with centrifuge models by McGuigan and Valsangkar (2010). The authors claim that this study is the first in-depth study of the literature in this area, which is the application of the ETI methods to the concrete arch structures. It was obvious that ITI reduces the contact pressure but to a limit and ETI was recommended for this situation. The embedded trench method was described as the pipe is entirely encapsulated by the compressible inclusion. The concrete arch structure constructed on the field had a width of 2 m, height of 1.5 m and length of 8 m, and it was instrumented with earth pressure gauges. The 6 m of backfilling

was done with 2 m increments. The three of the test sections were implemented on the same arch structure as shown in Figure 2.29.

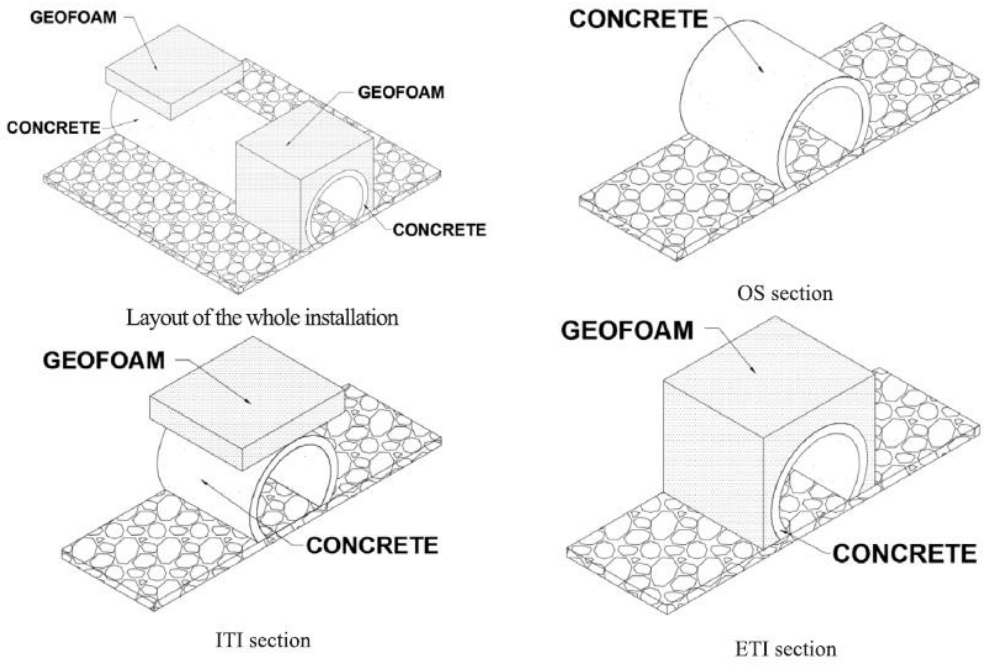

Figure 2.29. Field experiment setup (Kang et al., 2020)

The field tests were modeled by using the finite element program, ABAQUS, with non-linear soil models and the results were validated. In the models, both imperfect trench installation and embedded trench installation were implemented. Besides, earth pressures on culvert were calculated by semi-theoretical approach (AASHTO, 2014) and found as overestimated vertical earth pressures. It was reported that the earth pressure found in the field experiment and numerical studies deviated less than 10%. It was observed that as the fill height increase, the difference diminishes since the effect of EPS was more significant under higher pressures. It was reported that vertical earth pressure acting on the crown of the culvert reduced by at least 65% for both ITI and ETI method. By nature, rigid circular pipes are more convenient to create uniformly distributed arching than arch structures used in this study. Therefore, in order to protect the sides and bottom of the culverts, ETI method was recommended by the authors instead of ITI. However, in the study, the

improvement ratio for bottom contact pressure was not given for the case of both ITI and ETI method.

2.3 Studies Using EPS Geofoam as Soft Inclusion in Trench Installation Methods on Flexible Pipes

Since flexible pipes can deflect at least 2% without showing any permanent deformation, this behavior of flexible pipes results in positive soil arching itself. Therefore, there is limited number of studies in the literature about improving flexible pipes by imperfect trench installation by EPS geofoam.

Kang et al. (2007b), one of the pioneer studies about flexible pipe protected by imperfect trench installation by using EPS geofoam, has investigated the optimum compressible zone geometry for deeply buried corrugated flexible PVC pipe by using more than 1000 finite element analysis. The pipe used in the analysis has a diameter of 76 cm and burial depth is 12.2 m; however, in the numerical model, the soil medium above the pipe is modeled for the height of 3.25D and surface stress is applied (Figure 2.30). Numerical models are also validated with field test results on flexible pipes (Sargand, Hazen, et al., 2001; Sargand, Masada, et al., 2001). As a result of the parametric study, the following soft zone geometry is proposed (Figure 2.30). Researchers reported that the reduction rate of arching could reach up to 92% with the help of the imperfect trench installation while maximum wall stress reduced by 85% with the proposed geometry.

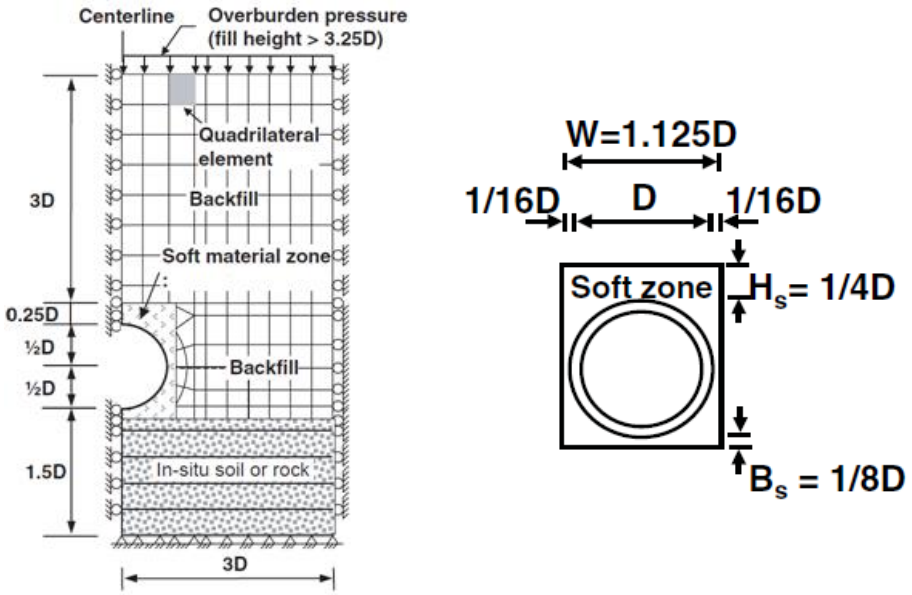

a) Numerical model b) Proposed soft zone geometry

Figure 2.30. A general overview of numerical model and soft zone geometry [taken from Kang et al. (2007a)]

Söylemez (2017) investigated the improvement of EPS geofoam located above the flexible PVC pipe in 1:1 scaled laboratory experiments. The test box used in the study has base dimensions of 100 cm x 100 cm and a height of 60 cm (Figure 2.31). Test soil was poorly graded sand with a relative density of 85%. Surface stress is applied with the help of the 26 cm diameter circular rigid plate in order to represent truck tire pressure defined in AASHTO. The flexible PVC pipe used in the experiment has an outer diameter of 200 mm with a length of 90 cm. The burial depth was 30 cm and less throughout 15 full-scale laboratory experiments. PVC pipe equipped with digital data acquisition system inside the pipe in order to measure horizontal and vertical deformation of the pipe. The main purpose of the study is to investigate whether there is an improvement after placement of EPS geofoam above the flexible pipe and if it was, what these factors are. For this purpose, the effect of EPS density, thickness, width and location were investigated. Moreover, the effect of distance between the two EPS geofoam layer was also included in the experiments. With the purpose of comparing the effect of

improvement, Söylemez also conducted two laboratory experiments without EPS geofoam.

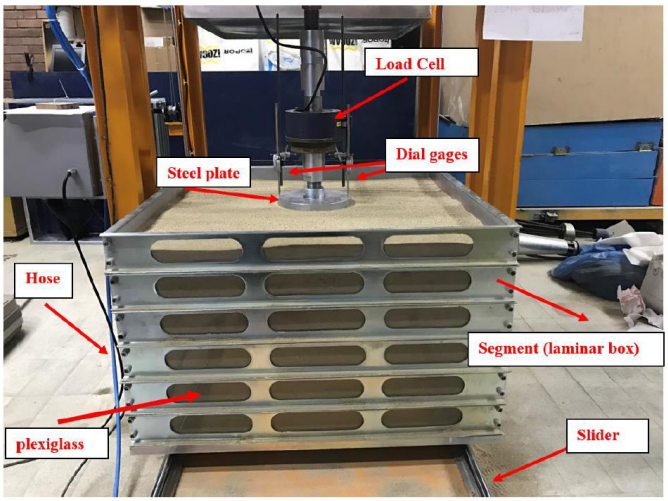

Figure 2.31. Experiment facility of Söylemez (2017)

After all, Söylemez concluded that the inclusion of EPS geofoam improved the pipe deformations to a point at which geofoam yields. After yielding the geofoam, deformations were suddenly increased and worse than that of no geofoam case. Improvement of geofoam inclusion is reduced the pipe deformations by a factor of 2 to 3. In addition, Söylemez reported that using geofoam with lower density improves pipe deformations more. However, since the low-density geofoam will yield earlier under high stresses, the amount of improvement might be low compared to the higher density geofoam. For this reason, the researcher emphasizes the importance of determining the compressive strength of geofoam and the load on it, especially for those who will follow the method of protecting shallowly buried flexible pipes with EPS geofoam. Stating that the effect of EPS geofoam width and the necessity of using double row EPS geofoam on pipe deformations are negligible, the researcher stated that using thicker geofoam will improve the pipe behavior more positively. However, a clear result could not be demonstrated due to the different EPS geofoam densities used in these experiments. Finally, the author stated that the geofoam material placed closer to the crown of the pipe

would reach the yield load later and therefore protect the pipe up to higher stress values. The work of Söylemez (2017) is very important because it is the only study that has reached the yielding stress among the studies in which shallowly buried flexible pipes are taken to protect with the imperfect trench method by using EPS geofoam as soft inclusion.

Kılıç and Akınay (2019) conducted full-scale laboratory tests on flexible HDPE pipe protected by imperfect trench method by using EPS-10 (10 kg/m^3) geofoam as soft inclusion. The test facility occurs with corrugated-lined HDPE pipe with a nominal diameter of 300 mm and actual ring stiffness of 8.8 kPa, angular medium-grained poorly graded silica sand with two different relative density of D_r=25% and D_r=40% for upper and lower sand, is instrumented comprehensively, can be called as best in the literature so far with earth pressure cells, potentiometric displacement sensors and settlement plates.

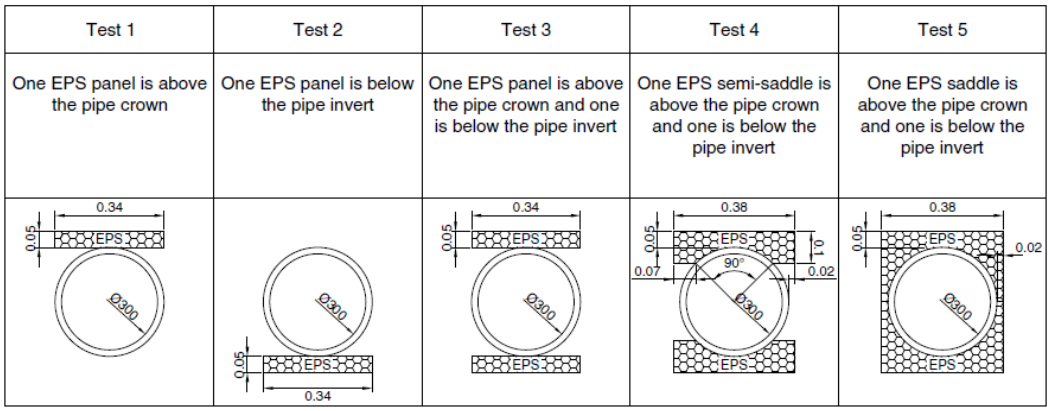

Figure 2.32. EPS geofoam configurations of Kılıç and Akınay (2019)

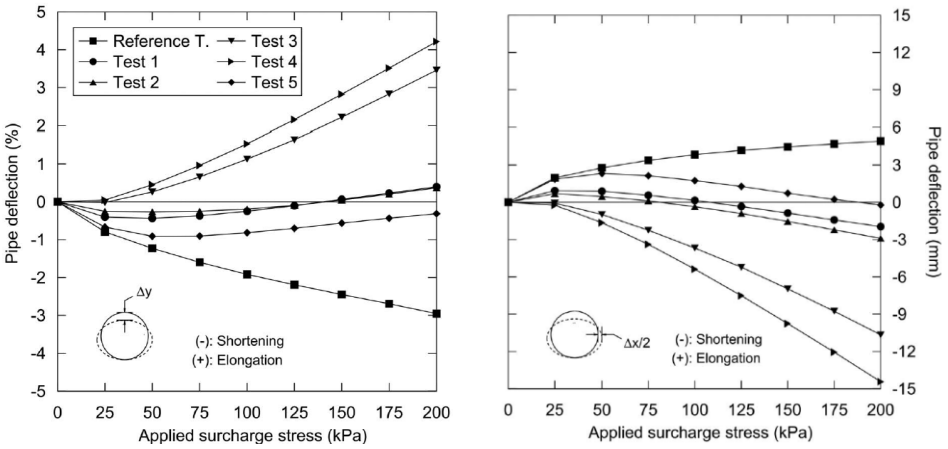

a) Vertical pipe deflections b) Horizontal pipe deflections

Figure 2.33. Comparison of vertical and horizontal deflections [taken from Kılıç and Akınay (2019)]

Five different EPS geofoam geometry combinations were tested for induced trench application together with a no-geofoam configuration called the reference test in order to make it possible to compare (Figure 2.32). Regardless of the soft inclusion geometry, positive soil arching developed and deformation behavior of the HDPE pipe is improved. Minimum EPS inclusion as the volume is Test-1 configuration and vertical stress reduced by 70% even one single EPS geofoam layer induced. Researchers concluded that the inclusion of EPS geofoam with a thickness of D/6 and width of D above the pipe provides the best improvement by considering cost-efficiency. The test results of this configuration showed that the vertical and horizontal stresses experienced by the pipe were reduced up to 76% and 65%, respectively. Besides, the vertical and horizontal deflections were 87% and 60% less, respectively, under the applied surface surcharge stress of 200 kPa (Figure 2.33). In addition, it was reported that horizontal and vertical pipe deflections are on the order of zero up to surcharge pressure of 100 kPa – 125 kPa.

Meguid and Ahmed (2020) evaluated the response of flexible pipes with a small diameter under repeated loading with laboratory experiments. The experiments have been performed with a high-density PVC pipe with a diameter of 0.15 m and

the wall thickness was 1 cm. It was instrumented with pressure sensing sheets. The pipe was placed in a chamber by 1.4 m x 0.45 m x 1.0 m and the spacing between chamber walls and pipe was 4D, as D denotes pipe diameter. The dimensions of chamber and pipe placement are selected in such a way that 2D loading conditions can be created. The backfill material was selected as dry sandy gravel. The EPS-22 geofoam material with a thickness of 0.5D was used. Besides, in order to reduce the friction effect on the walls of the chamber, a grease layer was used. The cyclic loading was applied at a rate of displacement of 1.3 mm/min with a steel plate that has the dimensions of 45 cm x 10 cm, and at its maximum applied pressure was 140 kPa. The overall test setup is shown in Figure 2.34. The laboratory test results showed that the vertical earth pressure at the crown was decreased from 84 kPa to 12 kPa with EPS inclusion, whereas at sidewalls, the earth pressure reduction was less significant. The result of this study shows that the deformation of shallowly buried flexible pipes under cyclic loads can be improved by EPS geofoam.

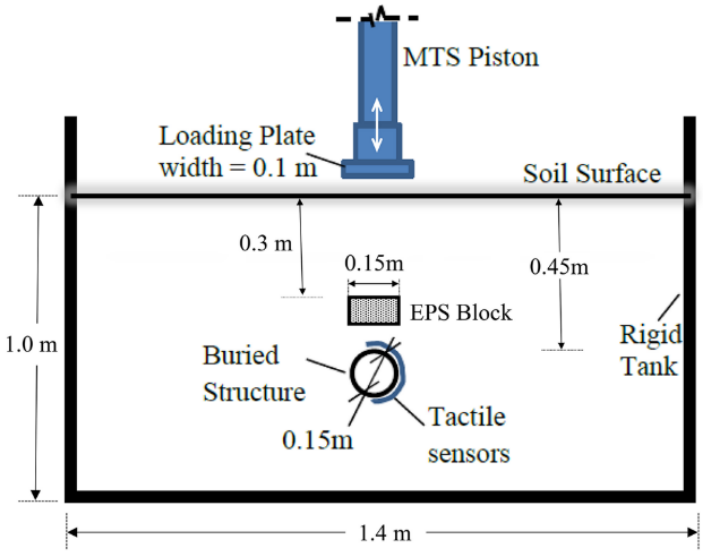

Figure 2.34. Laboratory test setup (Meguid & Ahmed, 2020)

CHAPTER 3

METHODOLOGY AND NUMERICAL MODELING

3.1 Laboratory Experiment of Akınay

In his doctoral (Ph.D.) dissertation, Akınay (2017) investigated the effects of using compressible bed material on buried flexible pipe behavior with the help of a 1:1 scale experiment setup in the geotechnical laboratory of Yıldız Technical University. In addition to laboratory tests, numerical methods by using finite element analysis are also used to investigate the effect of the inclusion of compressible bed material on the flexible pipe behavior.

In the study, five different compressible zone geometry configurations were studied to investigate the behavior of deformable pipe. EPS geofoam was used as compressible bed material in two different densities since one of the purposes of the study was the determination of the effect of density of compressible bed material on the pipe behavior.

In order to measure the soil stresses and ground settlements, the soil in the test facility was instrumented with pressure cells and settlement plates. In addition, to measure the deflection of the test pipe together with strains, potentiometric displacement sensors and biaxial strain gauges were also placed on the test pipe. Details about the test facility setup and test materials are presented below.

3.1.1 Test Facility

The test setup of Akınay consists of two main components that are test box and loading system (Figure 3.1). The test box has dimensions of 1.5m x 1.5m x 1.5m with three walls are 10 mm of steel and one wall is 30 mm thick Plexiglas. The

walls of the test box were supported by steel profile belts and counterforts in order to limit the outward movement of test box walls. The loading system is made up of two hydraulic pistons connected with a rigid steel ram with a total capacity of 50 tons.

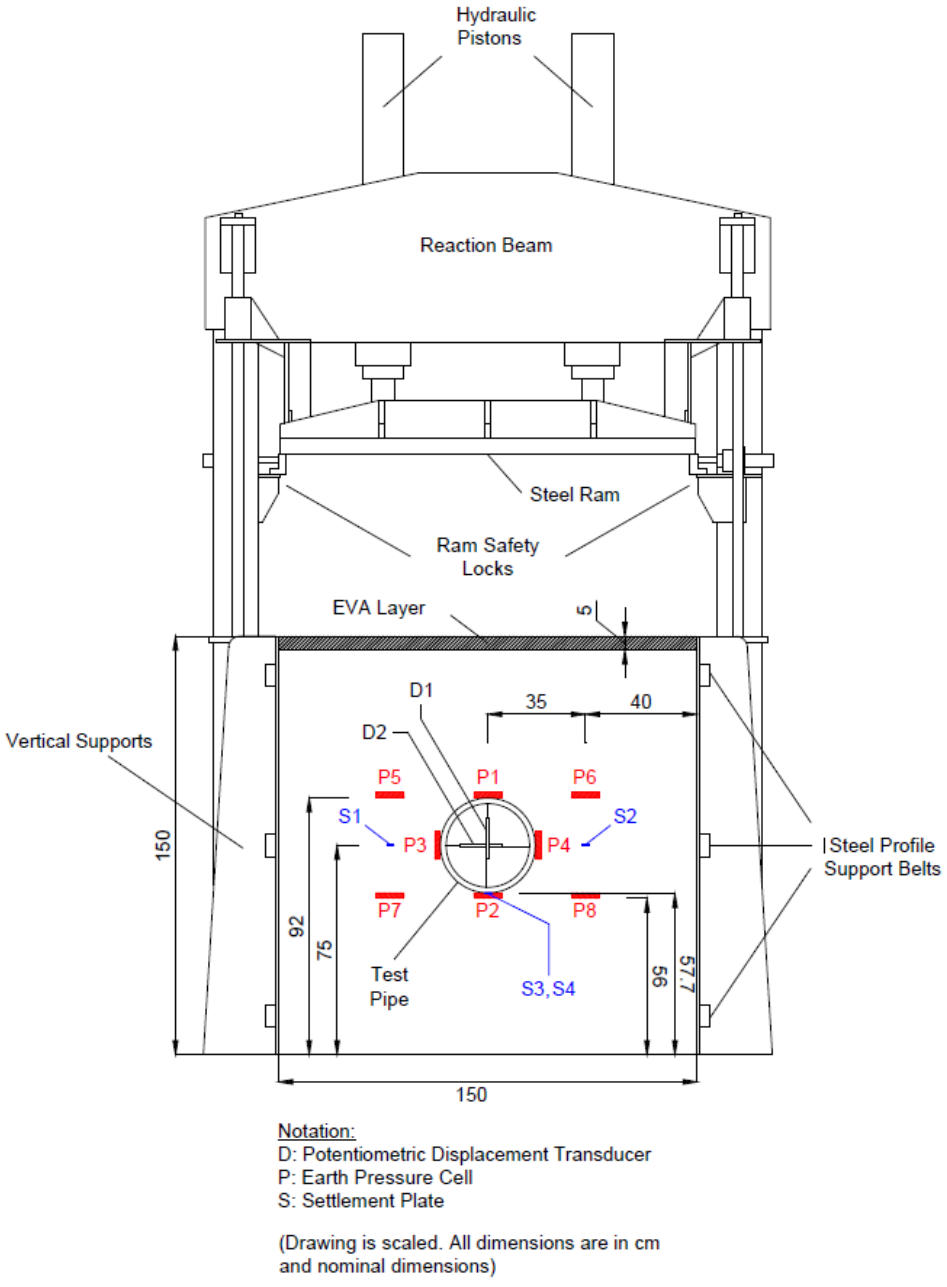

Figure 3.1. Test Facility [taken from Akınay (2017)]

In order to achieve uniform vertical loading, 5 cm thick ethylene vinyl acetate (EVA), by considering its linear elastic stress-strain behavior together with high compressibility, was placed between the soil surface and the rigid loading plate. Two 0.08 mm thick polyethylene sheets lubricated with Dow Corning Molykote 44 High-Temperature Bearing Grease-Medium were placed in order to minimize the interface friction between the wall of the test tank and soil medium. Moreover, in order to prevent sand grains from embedding to polyethylene sheets, 150 g/m^2 of non-woven geotextile and 2 mm thick HDPE geomembrane were placed between polyethylene sheets and sand medium.

3.1.2 Test Materials

3.1.2.1 Test Soil

The soil used in the study is defined as poorly graded, angular, medium-grained silica sand. According to the unified soil classification system (USCS), the soil class is SP. Index parameters of test sand are summarized in Table 3.1 below.

Table 3.1 Index properties of test sand

Specific gravity (G_s)	2.65
Coefficient of uniformity, (C_u)	2.57
Coefficient of curvature, (C_c)	0.92
USCS	SP
Maximum dry weight, (kN/m^3)	17.3
Minimum dry weight, (kN/m^3)	14.4
Maximum void ratio (e_{max})	0.81
Minimum void ratio (e_{min})	0.50
Average particle size (D_{50}) (mm)	0.76
Effective particle size (D_{10}) (mm)	0.35

During laboratory tests, the test sand was placed as loose as possible and in dry condition. Therefore, by using direct and indirect methods, the dry unit weight of test sand above the pipe invert was determined as 15 kN/m^3, which corresponds to the relative density of 25%. During test preparation, in order to set up the test pipe and necessary measurement devices, one person stepped in the test box, and therefore test sand was subjected to a bodyweight of personnel so that test soil under pipe invert determined to be consolidated under body weight. Due to this reason, the dry unit weight of test sand beneath the test pipe invert was determined as15.5 kN/m^{3,} which corresponds to a relative density of 40%.

Under confining pressures of 50 kPa, 100 kPa and 200 kPa, triaxial compression tests (Consolidated-drained, CD) tests were performed to determine shear strength parameters of test sand. During test, the shear rate was 0.95% strain per minute (≈1%). According to test results, internal friction angle of 30° and 35° were found for relative densities of 25% and 40%, respectively. In the test, a small amount of cohesion value was determined for both densities, however, neglected for practical reasons.

3.1.2.2 Test Pipe

In the test, a lined corrugated wall HDPE (high-density polyethylene) pipe was used as a flexible pipe. The nominal diameter of the test pipe was 300 mm (Ø300). Although the catalog value of nominal stiffness value of 8 kPa stated, the actual nominal stiffness value was determined as 8.8 kPa with respect to the standard of Thermoplastic pipes - determination of ring stiffness (TS EN ISO 9969). The moment of inertia and area of the pipe wall are determined as 488.6 mm^4/mm and 7.22 mm^2/mm per unit length, respectively.

The test pipe was placed in the test tank in 3 pieces of 49 centimeters in length in order to place instrumentation devices into the pipe. After placement, pipe joints

are linked up with butt-welding. The section of the HDPE wall is presented in Figure 3.2.

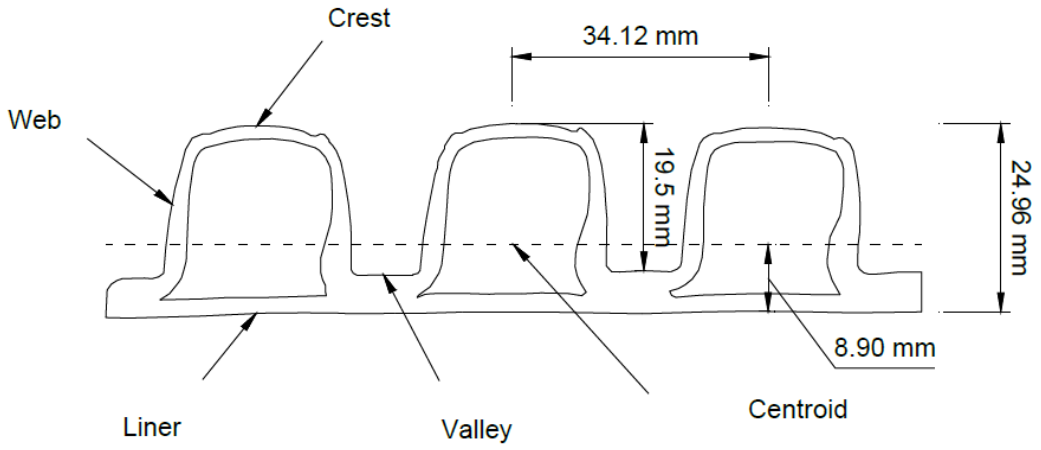

Figure 3.2. Section of HDPE wall [taken from Akınay (2017)

3.1.2.3 EPS Geofoam

Two different densities of EPS geofoam, which are EPS-10 and EPS-15 with nominal densities of 10 kg/m^3 and 15 kg/m^3 were used in the test as compressible bed material. In order to determine the engineering properties of EPS geofoam, unconfined compression (UC) tests were conducted on cylindrical EPS samples. The shear rate in the experiment was 1% strain per minute. The diameter and height of the samples were 50 mm. In order to measure the volumetric strain values, unconfined compression tests were carried out in a triaxial pressure vessel. The change in the volume of water inside the triaxial cell is assumed to be theoretically equal to the change in the volume of the EPS sample. By considering this theoretical assumption, the volume change of the test sample in dry conditions was measured indirectly. During the experiment, pore pressure drainage valves were switched to the open position in order to provide free air (gas) inside the EPS specimen to dissipate freely. This test procedure is similar to defined in the literature (Atmatzidis et al., 2001; Wong & Leo, 2006).

Axial stress, σ_1 (kN/m^2) – axial strain, ε_1 (%) and volumetric strain, ε_υ (%) – axial strain, ε_1 (%) graph obtained at the end of the unconfined compression test are presented in Figure 3.3 and Figure 3.4 for EPS-10 and EPS-15, respectively.

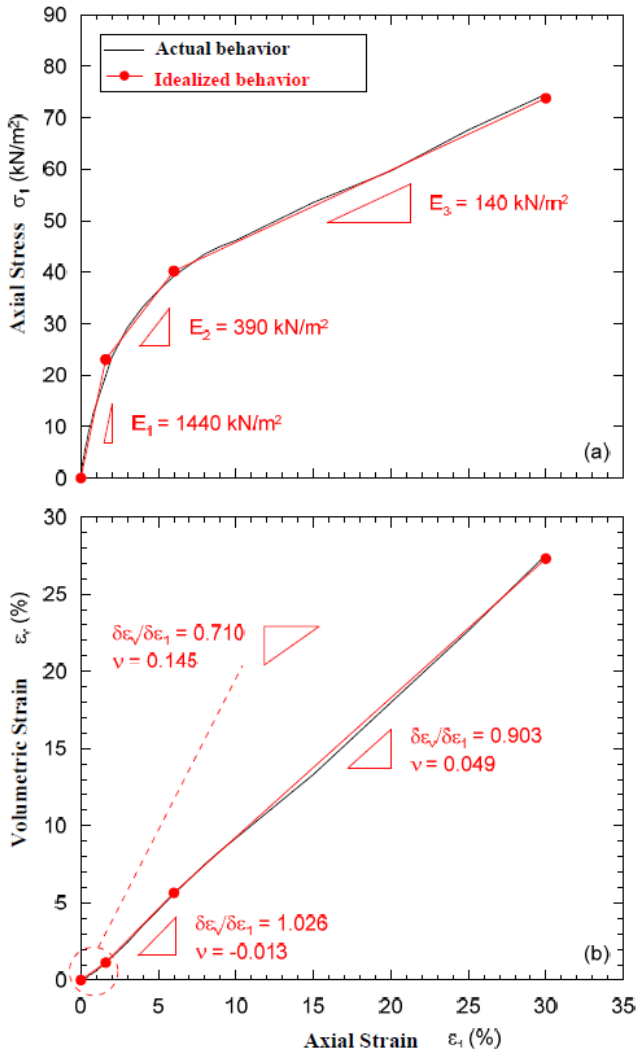

Figure 3.3. Stress-strain behavior of EPS-10 a) Axial strain – axial stress b) Axial strain – volumetric – strain [taken from Akınay (2017)]

3.2 Numerical Modeling

Laboratory experiments are time-consuming and costly. With the help of today's developing technology, computer programs can model physical behaviors in real life with high precision and accuracy, so-called successfully. In this study,

laboratory experiments that take a long time and require high costs were modeled with the 2D finite element program, Plaxis 2D (Brinkgreve et al., 2019b). Within the scope of this study, the numerical model that will work with the two-dimensional finite element method has been calibrated, reflecting the laboratory experiments conducted by Akınay in order to perform parametric studies. The results were compared with the laboratory test results and it was concluded that the models are valid. Details of the numerical model are explained in detail in the following chapters.

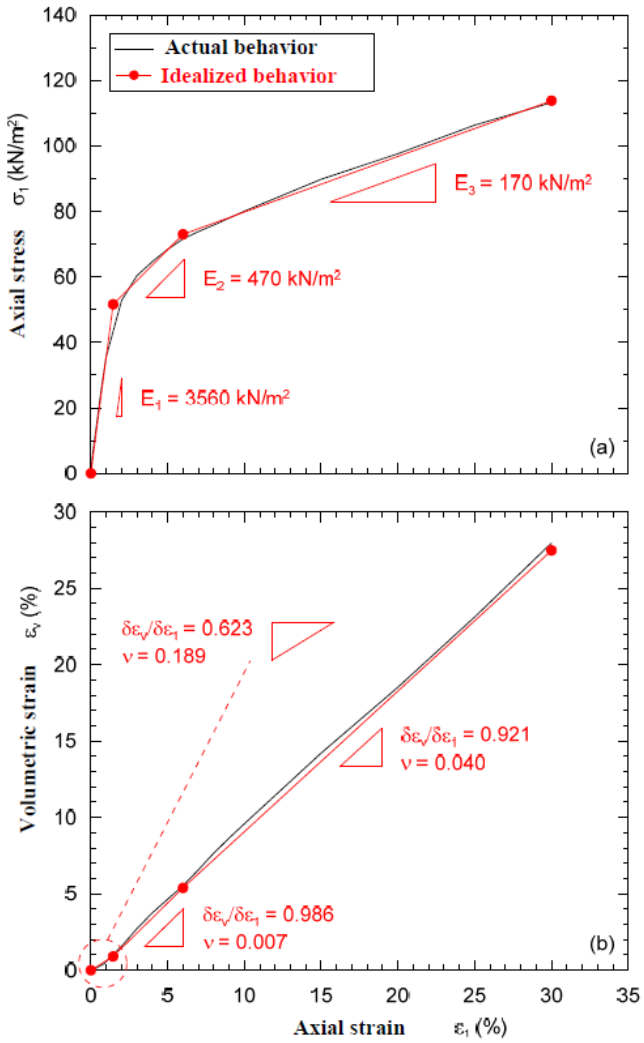

Figure 3.4. Stress-strain behavior of EPS-15 a) Axial strain – axial stress b) Axial strain – volumetric – strain [taken from Akınay (2017)]

3.2.1 General Geometry of the Numerical Model

3.2.1.1 Model Size

When the experimental setup is examined geometrically, it is observed that the test system is symmetrical with respect to the vertical axis (Figure 3.1). Additionally, according to test results obtained in the laboratory (Akınay, 2017), the settlement values observed in the test soil are symmetrical on both sides of the pipe. Also, it has been stated by Akınay that, in almost all experiments conducted within the scope of the study, it was observed that the pipe wall strains are almost symmetrical with respect to the vertical pipe axis. In the light of these data, it was decided to create the numerical model as half geometry, symmetrical with respect to the vertical pipe axis. Since analysis time is directly proportional to the number of elements; therefore, model size, modeling half geometry will significantly reduce analysis time. The base geometry of the numerical model is given in Figure 3.5.

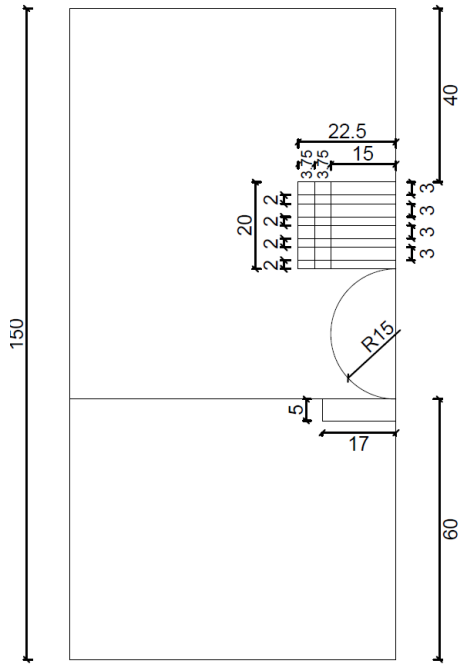

Figure 3.5. Base geometry of the numerical model

3.2.1.2 Boundary Conditions

The nominal boundaries of the test tank are directly modeled in the program. Since the external walls of the test tank are supported by rigid steel belts and girders, only vertical deformations are allowed for tank walls and horizontal deformations are restricted. In the same way, since strains and deformations of pipe walls are symmetrical with respect to the vertical axis, the intersection of pipe and symmetry axis is fixed in the horizontal direction and only vertical deformations are allowed. In Figure 3.6, boundary conditions defined in the numerical model are given.

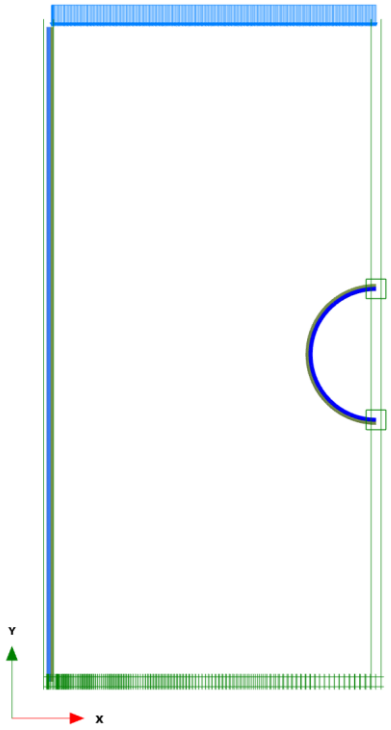

Figure 3.6. Boundary conditions of the numerical model

3.2.1.3 Initial Conditions and Staged Construction

Since the numerical model will be calibrated with laboratory test results, care has been taken to ensure compliance with laboratory tests while defining the initial conditions and staged construction conditions in the program.

For the initial phase, the calculation type was selected as “gravity loading” so that stress field equilibrium is satisfied for the generation of initial stresses for the case of non-horizontal soil layers. K0 procedure is recommended for the only situation that horizontal surface and all other soil layers are parallel to the surface together with phreatic level (Brinkgreve et al., 2019b). In the laboratory test, potentiometric displacement sensors and earth pressure sensors were settled to zero just before applying surface loading. This means readings were recorded after the application of surcharge stress. For this reason, in the program, filling of test tank with test soil, placement of the HDPE pipe and EPS geofoam stages were not modeled. Additionally, in the numerical analysis, the “reset displacement to zero” check-box activated under the numerical control parameters menu in the first construction stage following the initial phase. Except from the first construction stage following the initial phase, default parameters assigned by the program were used for deformation control parameters and numerical control parameters.

Surface pressure was modeled by using the “line load” option in Plaxis from 0 kPa to a maximum load of 200 kPa as staged construction. Since laboratory test results are recorded for loading of 25 kPa and its multiplies, at least eight construction stages were defined.

3.2.2 Input Parameters

3.2.2.1 Test Soil

In his doctoral study, Akınay (2017) prepared an experiment set (reference test) without EPS geofoam and HDPE pipe by filling the test tank only with test sand and followed standard test procedure. He was waited for half an hour by loading 25 kPa and its multiples until it reached a loading of 200 kPa. With the help of earth pressure sensors and settlement plates, Akınay obtained vertical and horizontal effective stress increase inside the test sand together with the settlement of soil. The layout of earth pressure sensors and settlement plates is shown in Figure 3.7.

The strength and deformation properties defined in the Plaxis 2D are determined with the help of back-calculation from the reference test and results of consolidated-drained triaxial compression test on test sand.

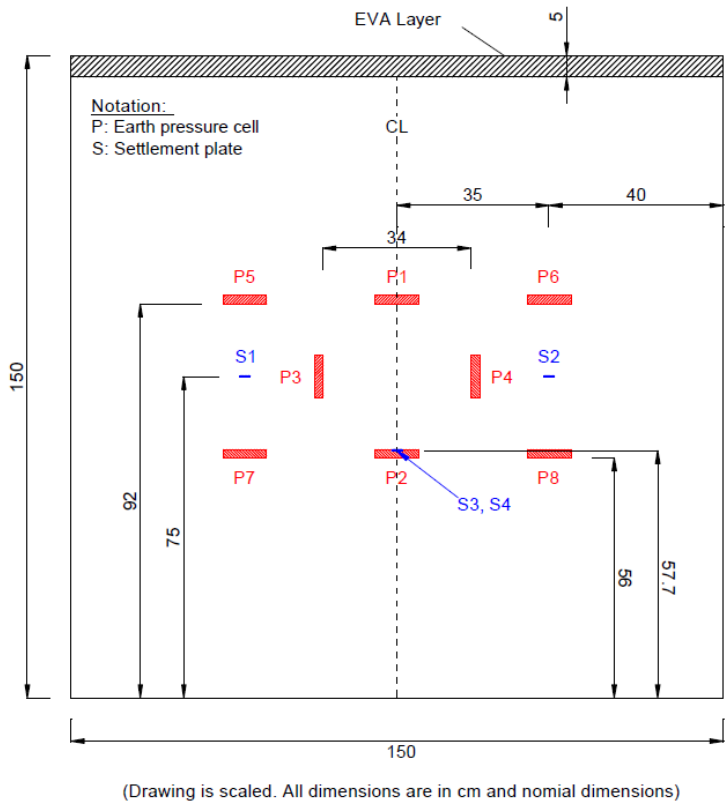

Figure 3.7. The layout of earth pressure sensors and settlement plates in laboratory test with no pipe and EPS geofoam [taken from Akınay (2017)]

The test sand is divided into two, namely, as upper sand and lower sand with respect to relative density value of D_r=25% and D_r=40%, respectively. According to triaxial compression test results, internal friction angle of $\Phi' \approx 30°$ and $\Phi' \approx 35°$ were found for relative densities of D_r=25% and D_r=40%, respectively. In addition to laboratory tests, internal friction angles of upper and lower sands were correlated with the help of data obtained from earth pressure cells in the reference test without the HDPE pipe.

The lateral earth pressure coefficient, "K_0" is calculated by using horizontal earth pressures determined by P3 and P4 cells (Figure 3.7) divided by effective vertical stress at rest situation. Also, with the help of Jaky's formula (1944), internal friction angles of test sand were correlated with equation (3.1)

$$K_0 = 1 - \sin \emptyset \tag{3.1}$$

In the test, a small amount of cohesion value was determined for both densities, however, neglected for practical reasons since it was thought that cohesion values were appeared to be depending on experimental conditions. Though, it is recommended by the material manual of the program that a very small amount of cohesion value should be defined in Plaxis 2D in order to eliminate complications (Brinkgreve et al., 2019a). For this reason, c'=0.1 kPa was assigned to both upper and lower sand. Since a positive value of cohesion is defined in the program, in order to eliminate the development of tensile strength, the "tension cut off" option is used.

Upper and lower sand was modeled in the program by using the "Hardening soil" model. The stiffness modulus value of the lower sand was determined by laboratory experiments. In contrast, the stiffness value for the upper sand was determined by the back analysis method with the help of the reference test without the HDPE test. Stiffness parameters of material properties are left as default. The strength and deformation properties of test sand defined in Plaxis 2D is summarized in Table 3.2

3.2.2.2 HDPE Pipe

Thermoplastic lined-corrugated wall HDPE pipe was modeled as a linear elastic plate element in Plaxis 2D. Although the HDPE pipe used in the laboratory test is a lined-corrugated wall pipe, it can only be modeled as a smooth plate element in the numerical model. Therefore, the moment of inertia of the HDPE pipe obtained from the laboratory test is converted to an equivalent value for the smooth pipe so

that moment of inertia of smooth pipe and therefore bending stiffness can be calculated to enter the numerical model. The moment of inertia of HDPE pipe from the laboratory test was given as $I_{HDPE} = 4.886 \times 10^{-7}\ m^4/m$ by Akınay (2017).

Table 3.2 Parameters for the hardening soil model [taken from Akınay (2017)]

Parameter	Value		
	Upper Sand		Lower Sand
Loading (kPa)	≤ 25	≥ 25	0 – 200
Angle of internal friction, Φ' (°)	30	30	35
Angle of dilatancy, ψ (°)	0	0	5
c' (kPa)	0.1	0.1	0.1
γ'_{dry} (kN/m^3)	15	15	15.5
Reference stress, P^{ref} (kPa)	100	100	100
Stress dependent stiffness according to power law, m	0.5	0.5	0.5
Secant stiffness in standard drained triaxial test, E_{50}^{ref} (MPa)	7.5	10	60
Tangent stiffness for primary oedometer loading, E_{oed}^{ref} (MPa)	7.5	10	60
Unloading/reloading stiffness, E_{ur}^{ref} (MPa)	22.5	30	180

$$I_{HDPE} = \frac{(1) \times {t_{smooth}}^3}{12} = 4.886 \times 10^{-7}\ m^4/m \qquad (3.2)$$

From equation (3.2), the thickness of the smooth pipe (t_{smooth}) is calculated as $1.803 \times 10^{-2}\ m$ therefore area of smooth pipe per unit length is calculated as $A_{Pipe} = 1.803 \times 10^{-2}\ m^2/m$.

Pipe parameters of linear elastic plate elements in the numerical model are summarized in Table 3.3 per unit length.

Table 3.3 HDPE pipe parameters for linear elastic plate element [taken from Akınay (2017)]

Parameter	Value
Moment of inertia, I (m^4/m)	4.886×10^{-7}
Cross section area, A (m^2)	1.803×10^{-2}
Modulus of Elasticity, E (kPa)	390000
Poisson's ratio, υ	0.46
Weight of pipe, w (kN/m/m)	0
Bending stiffness, EI (kN.m^2/m)	1.906×10^{-1}
Normal stiffness, EA (kN/m)	7032

3.2.2.3 Interface

In almost all projects where EPS geofoam material is used, geofoam blocks are in contact with various construction materials such as steel, wood, concrete, geosynthetics and soil. This results in a combined composite structure, called interface, that is exposed to axial and shear stresses together. Therefore, successful design and evaluation of these composite structures require a thorough understanding of interface shear characteristics of geofoam under a combination of normal and shear stresses.

3.2.2.3.1 Sand - EPS Geofoam Interface

Miki (1996) studied the interface shear properties of sand / geofoam (EPS-20) by direct shear tests. It is reported that the thicker bedding sand results in a smaller interface friction factor. If the bedding sand layer was thinner than 35 mm, the

interface friction factor was obtained as nearly 0.7. If the bedding sand layer is thicker than 35 mm, the interface friction factor was 0.55.

The interface friction angle between sand and geofoam was governed by the internal friction angle of sand, according to Negussey (1997). It results from the embedded sand grains in the geofoam block, so the sliding occurs on the sand/sand interface.

Negussey et al. (2001) studied soil / geofoam interface friction regarding different internal friction angle of the soils. The silica sand and geofoam block used in the tests have two different densities with an interface area of 100 mm x 100 mm. Sand / geofoam and sand / sand interfaces have been investigated and the sand / geofoam interface developed a slightly higher interface friction factor. The average friction factors for sand/geofoam and sand / sand interfaces were obtained as 0.85 (≈40°) and 0.68 (≈34°), respectively. Shear stress vs. applied normal pressure graph can be seen in Figure 3.8.

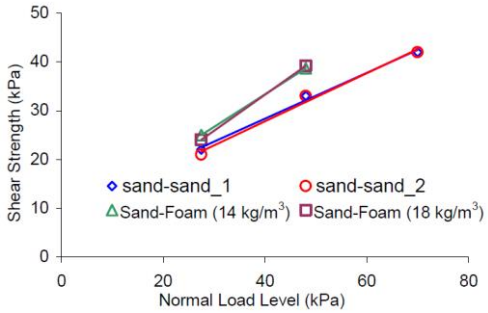

Figure 3.8. Normal stress (kPa) vs. shear strength (kPa)
[taken from Negussey et al. (2001)]

The interface shear resistance between EPS-20 geofoam / soil (i.e. sand, gravel and laboratory-made clay) was investigated by direct shear apparatus in the study of Atmatzidis et al. (2001). The mechanical and index properties of test soils were tabulated in Table 3.4. It was reported that for relatively low-stress ranges, the behavior of interface shear is purely frictional to a certain extent, then purely adhesional behavior has been observed.

Table 3.4 Material parameters for Atmatzidis et al. (2001)

Interface			Void Ratio	c_u/Φ		Particle Size (mm)		
						Type	min	max
Geofoam	vs	Sand	0.65	46	degree	Sub-Angular	0.60	0.85
Geofoam	vs	Clay	1.1	14	kPa	-	-	-
Geofoam	vs	Gravel	0.72	49	degree	Angular	4.75	9.52

Additionally, the effect of the density of EPS geofoam was examined with EPS-15, EPS-20 and EPS-30. The interface friction angle of 38.5° was reported for EPS geofoam / sand interface in any case. Direct shear test results are presented in Figure 3.9 and tabulated in Table 3.5.

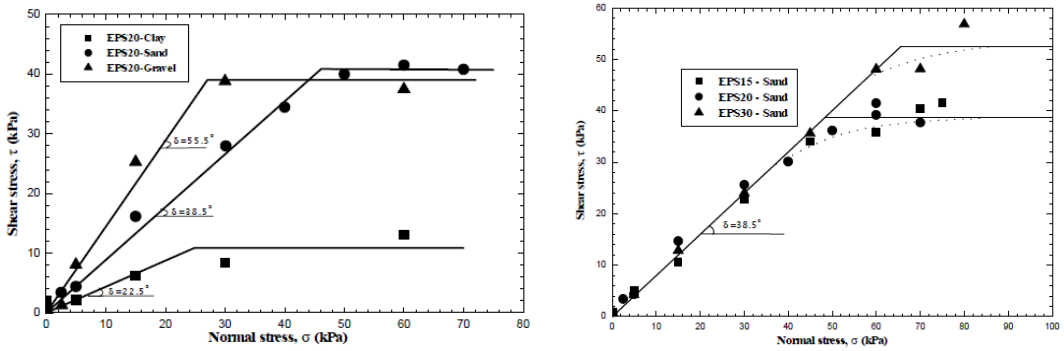

(a) Soil – EPS geofoam (b) Sand – EPS geofoam

Figure 3.9. Applied normal stress (kPa) vs. shear stress (kPa)

Xenaki and Athanasopoulos (2001) studied interface shear behavior of sand / EPS geofoam for EPS-10 and EPS-20. The effect of geofoam density, applied normal stress, void ratio, size and shape of the sand particles were investigated with a direct shear box that has an interface area of 100 mm x 100 mm. The normal stress vs. shear stress curve developed a nonlinear pattern in the sand / geofoam interface behavior and three subgroups were categorized as the phases of this curve (Figure 3.10). The interface friction behavior can be classified as frictional for lower normal stress values, whereas adhesional behavior was reported for higher values

of normal stress. The apparent interface friction angle of sand/geofoam is equal to the interface friction angle of sand/sand in the case of frictional behavior. As the adhesion increases, the apparent interface friction angle decreases and the mobilized adhesion would be equal to the shear resistance of EPS monoblock at the ultimate state.

Table 3.5 Direct shear test results of Atmatzidis et al. (2001)

Interface			Shear Rate (mm/min)	Number of Test	Density (kg/m^3)	Interface Friction δ (°)	μ
Geofoam	vs	Clay	1	5	20	22.5	0.41
Geofoam	vs	Sand		8	20	38.5	0.8
Geofoam	vs	Gravel		6	20	55.5	1.46
Geofoam	vs	Sand		8	15	38.5	0.8
Geofoam	vs	Sand		9	20	38.5	0.8
Geofoam	vs	Sand		8	30	38.5	0.8

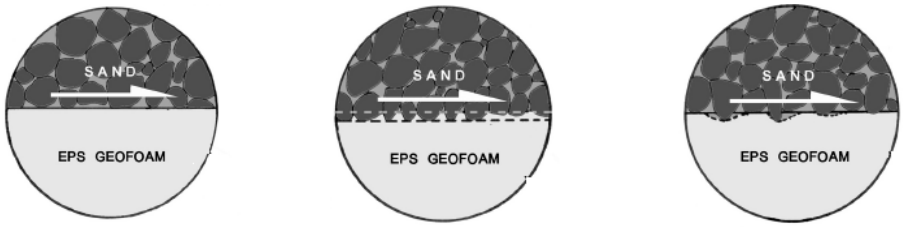

(a) Purely frictional (b) Purely adhesional (c) Adhesional-frictional

Figure 3.10. Interaction phases at EPS geofoam/sand
[taken from Xenaki & Athanasopoulos (2001)]

In the light of current literature, reported interface friction angle values are higher than that of interface friction angle of test sand itself used in Akınay's study. For this reason, no interface was assigned between sand and EPS geofoam in the numerical model and the interface between sand and EPS geofoam was evaluated as rigid.

3.2.2.3.2 Sand – Wall Interface

In order to reduce the interface friction between the test sand and test box wall, improvements have been made by Akınay on the wall with the methods suggested by Tognon (1999). Improvement details are described in the chapter "3.1.1 Test Facility". As a result of improvements, it was evaluated that interface friction between sand and wall decreased to a value of 5°, which is approximately one six times lower than that of interface friction angle of upper and lower sand, $\Phi' \approx 30°$ and $\Phi' \approx 35°$, respectively. Eventually, interface strength reduction factor (R_{inter}) is assigned as 0.17 in numerical model with hardening soil model properties.

3.2.2.3.3 Sand – HDPE Interface

Martin et al. (1984) investigated Ottawa sand – HDPE interface friction by using modified direct shear test apparatus under normal stresses of 13.8 – 103.5 kPa. Researchers reported that the interface friction angle between Ottawa sand – HDPE is $\delta=18°$; however, they did not specify at what displacement.

Saxena and Wong (1984) used direct shear test apparatus in order to examine interface friction between Ottawa sand and HDPE under normal stresses 69 – 207 kPa and a value of $\delta=19.8°$ was reported.

William and Houlihan (1987) used a large direct shear box to examine the Ottawa sand – HDPE interface under normal stresses of 3.5 – 69 kPa. They reported a value of $\delta=19.8°$ for relatively low normal stresses.

Negussey et al. (1989) investigated interface friction between HDPE geomembrane and Ottowa sand by using a ring shear test apparatus. The sand used in the experiment has a residual interface friction angle of (Φ'_R) 30.5° and peak and residual interface friction angle between sand – HDPE were 17.6° and 15°, respectively.

O’Rourke (1990) investigated the Ottawa sand – HDPE pipe interface under normal stresses of 3.5 – 69 kPa and a value of δ=19.1° was reported.

Vaid and Rinne (1995) investigated interface friction between HDPE and two types of sand, which are rounded (Φ'_{cv}=29) and angular (Φ'_{cv}=33), using the ring shear apparatus. Researchers reported that the interface friction coefficient value increases with increasing angularity. Peak interface friction coefficient (μ_p) value of 0.4 and 0.65 were reported for rounded and angular sand, respectively.

Bhatia and Kasturi (1996) investigated interface friction between HDPE geomembrane and uniform fine sand by using a large direct shear box. The sand used in the experiment has an interface friction angle of (Φ') 30.5° and peak and residual interface friction angle between sand – HDPE were found as 23.3° and 21.1°, respectively.

By considering the angularity of test sand used in Akınay’s study, interface friction angle predicted to be δ=20° and HDPE pipe surrounded by upper sand which has interface friction angle of Φ'=30°; therefore interface strength reduction factor (R_{inter}) is assigned as 0.67 in numerical model with hardening soil model properties.

3.2.2.4 Tank Wall

The walls of the test box are modeled with linear elastic plate elements in the numerical model. Boundary conditions assigned in the numerical model of tank wall are explained in chapter “3.2.1.2 Boundary Conditions (page 57)” in detail. In the numerical model, the thickness of the steel tank wall is accepted to be 5 cm with an elasticity modulus of 200 GPa. Since outward movements of tank walls are restricted and only vertical deformations are allowed, assigned thickness and elasticity modulus values are only indicative so that a tank wall can be modeled with reasonable parameters. In Table 3.6, parameters for linear elastic tank wall are summarized.

Table 3.6 Tank wall parameters assigned in numerical model
[taken from Akınay (2017)]

Parameter	Value
Material type	Elastic
Elasticity modulus, E (GPa)	200
Cross section area of tank wall per meter, A (m^2)	0.05
Moment of inertia of tank wall per meter, I (m^4/m)	1.042×10^{-5}
Axial stiffness of tank wall per meter, EA (kN/m)	10^7
Bending stiffness of tank wall per meter, EI (kN.m^2/m)	2083
Poisson's ratio	0.3
Weight of tank wall per meter (kN/m/m)	0

3.2.2.5 EPS Geofoam

In literature, EPS geofoam was modeled by using various kinds of material models in different numerical programs by researchers. The studies using EPS geofoam material in numerical models in the literature and the details of these studies are summarized in Table 3.7

In the scope of this study, geofoam will be used as soft compressible material subjected to static loading only. Therefore, only deformation characteristics of EPS geofoam are involved in the study. Failure of EPS geofoam, strength characteristics and unloading properties are out of the scope of this study. For this reason, EPS geofoam is modeled as a linear elastic material property that only requires elastic modulus and Poisson's ratio as input together with unit weight.

Table 3.7 Studies using EPS geofoam in numerical model

Study	Numerical Program	2D/3D	Material Type	EPS Density
Sun et al., 2005	FLAC	2D	Linear Elastic	EPS-20
Padade & Mandal, 2012	PLAXIS	2D	Mohr-Coulomb	EPS-15 EPS-20 EPS-22 EPS-30
AbdelSalam et al., 2015	PLAXIS	2D	Hardening Soil	EPS-20
Anil et al., 2015	ABAQUS	3D	Linear Elastic-Plastic	EPS-30
Witthoeft & Kim, 2016	FLAC	2D	Strain hardening/softening	EPS-15
Beju & Mandal, 2017a	PLAXIS	3D	Mohr-Coulomb	-
Akınay, 2017	PLAXIS	2D	Linear elastic	EPS-10 EPS-15
Kang et al., 2020	ABAQUS	2D	Planar Deformable	EPS-15

3.2.2.5.1 EPS-10 and EPS-15

Elastic modulus and Poisson's ratio were determined by using a load-deformation curve obtained from laboratory test results of unconfined compression tests done by Akınay (2017). In Figure 3.3 and Figure 3.4, the stress-strain curve of EPS geofoam was given for EPS-10 and EPS-15, respectively.

In order to idealize the material behavior, a three-piece linear elastic material model has been fitted by Akınay to the laboratory test results. In Table 3.8, idealized linear elastic material properties of EPS-10 and EPS-15 geofoams are tabulated.

Table 3.8 Idealized linear elastic material properties of EPS-10 and EPS-15 geofoams

Idealization	EPS-10			EPS-15		
	ε_1 (%)	**E (kN/m^2)**	**υ**	**ε_1 (%)**	**E (kN/m^2)**	**υ**
1st Part	0 - 1.60	1440	0.145	0 - 1.45	3560	0.189
2nd Part	1.60 - 6.0	390	0	1.45 - 6.0	470	0.007
3rd Part	6.0 - 30.0	140	0.049	6.0 - 30.0	170	0.04

3.2.2.5.2 EPS-20

Unconfined compression test results on EPS geofoam show that sample shape and dimensions are effective on the behavior of the stress-strain curve (Hazarika, 2006). Because of this reason, in order to provide consistency with stress-strain curves of EPS-10 and EPS-15 taken from the study of Akınay, a comprehensive literature review was made for the purpose of determining stress-strain curves of EPS-20 geofoam that is consistent with the study of Akınay. (Atmatzidis et al., 2001; Beju & Mandal, 2017b; Birhan & Negussey, 2014; Chun et al., 2004; Hazarika, 2006; Neto & Bueno, 2012; Padade & Mandal, 2012; Wong & Leo, 2006)

Hazarika conducted unconfined compression tests on EPS geofoam samples (loading rate: 9.0% strain/minute) with the following geometrical properties; (dimensions are width, length and height for cube samples, respectively)

- 50 mm × 50 mm × 50 mm
- 100 mm × 100 mm × 100 mm
- 50 mm × 50 mm × 100 mm
- 100 mm × 100 mm × 50 mm
- Φ=50 mm; H=100 mm

Within the scope of this study, unconfined compression test results presented by Hazarika on circular EPS-20 samples are selected. In Figure 3.11, the axial strain (%) – compressive stress (kPa) curve obtained from the study of Hazarika is presented.

According to the results of the experiments made on the samples except for the circular sample, the plastic strain part showed linear behavior. However, in circular samples (shown with up-side-down triangular), after approximately 15% strain, the linear behavior began to deteriorate. The reason lies behind this might be the height to diameter ratio. Wong and Leo (2006) stated that during the unconfined compression test, sprain was observed on samples whose height to diameter ratio is two. For this reason, for the elastic modulus of plastic strain part of circular EPS-20 samples, linear part started from 6% strain and ended at approximately 15% strain extended and it is accepted to be linear up to 30% strain.

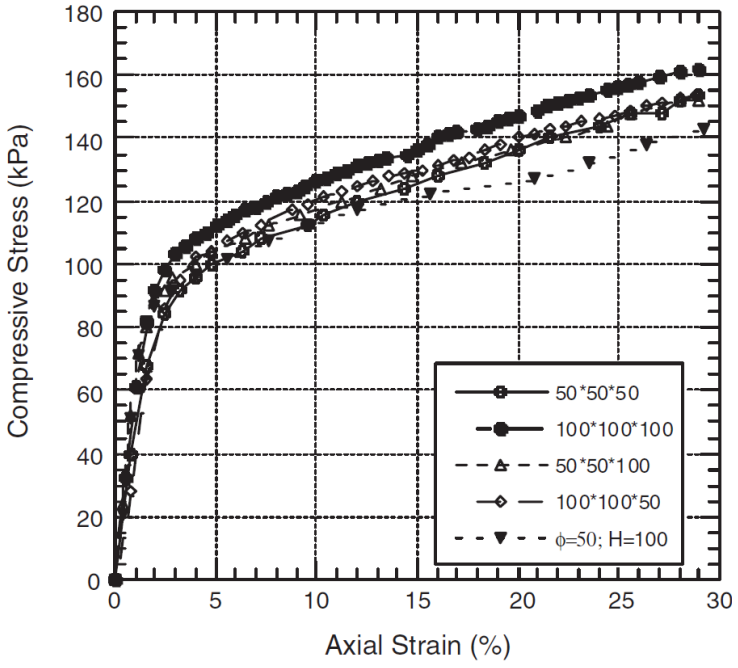

Figure 3.11. Axial strain (%) – compressive stress (kPa) [taken from Hazarika (2006)]

In order to idealize the material behavior, three-piece linear elastic material model has been fitted to the laboratory test results of the circular EPS-20 sample. Idealized linear elastic material properties of EPS-20 geofoam are tabulated in Table 3.9.

Table 3.9 Idealized linear elastic material properties of EPS-20

Idealization	**EPS-20**		
	ε_1 (%)	**E (kN/m^2)**	**υ**
1st Part	0 - 1.35	6000	0.125
2nd Part	1.35 - 6.0	535	0
3rd Part	6.0 - 30.0	220	0.05

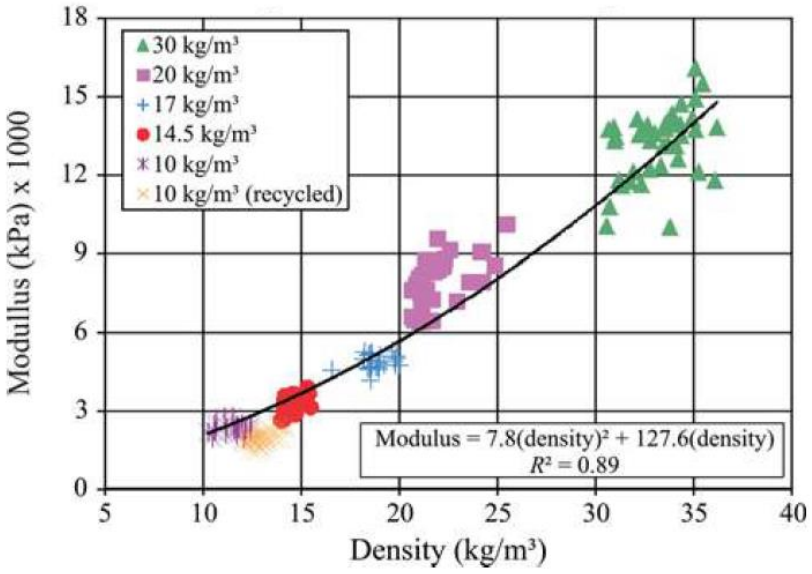

Figure 3.12. Tangent modulus of elastic phase [taken from Neto & Bueno (2012)]

Neto and Bueno (2012) collected approximately 350 compression test results in the literature published by different researchers and plotted initial tangent modulus versus density. From Figure 3.12, it can be indicated that the initial tangent modulus of EPS-20 geofoam is about 6000 kPa, which is compatible with the results of Hazarika. Also, after a detailed literature review, Stark et al. (2004)

plotted initial tangent modulus values versus density values (Figure 3.13) reported in the literature and proposed an equation;

$$E_1 = 450 \times \rho_{EPS} - 3000 \quad (3.3)$$

Where;

E_1= Elastic modulus of EPS geofoam at initial part (kPa)

ρ_{EPS}= Density of EPS geofoam (kg/m^3)

Then, the elastic modulus of EPS-20 geofoam at initial part estimated by using equation (3.3)

$$E_1 = 450 \times 20 - 3000 = 6000\ kPa$$

which is quite compatible with the laboratory test result of Hazarika.

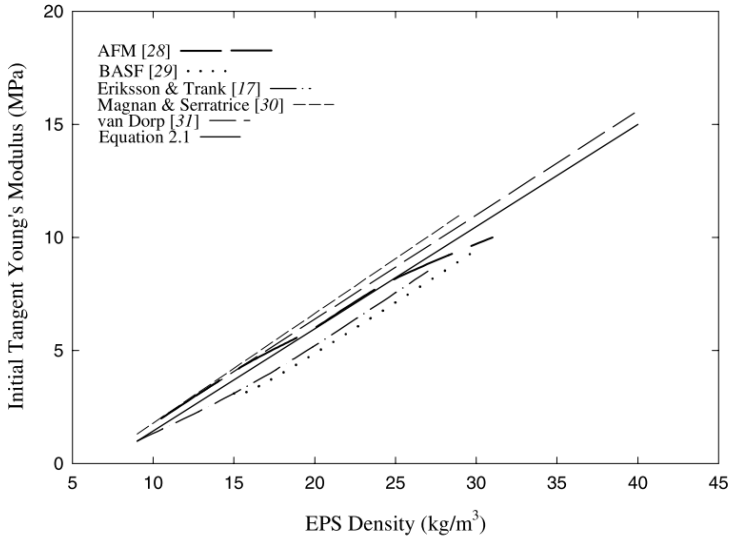

Figure 3.13. EPS geofoam density (kg/m^3) versus E_1 (kPa)
[taken from Stark et al. (2004)]

Stark et al. (2004) and Wong and Leo (2006) state that Poisson's ratio of EPS geofoam is very small positive value within the elastic range and over the plastic region suddenly decreases to virtually zero or negative value. Stark et al. (2004) shares obtained Poisson's ratio values for EPS-20 geofoam as υ=0.12 for initial elastic part and υ=0.03 for beyond.

All the same, for more accurate estimation of Poisson's ratio at the initial elastic part, Stark et al. (2004) and Padade and Mandal (2012) recommend using formula (3.4) given by EDO (1993) where ρ is EPS density in kg/m^3.

$$\upsilon = 0.0056 \times \rho + 0.0024 \tag{3.4}$$

As a result, linear elastic material properties assigned for EPS-20 geofoam are summarized in Table 3.9 and after a comprehensive literature review, assigned parameters are quite compatible with the literature.

3.2.3 Mesh Properties and Effect of Mesh Density

Plaxis 2D allows the user to select mesh elements as quadratic 6-node or 4th order 15 node triangular elements (Brinkgreve et al., 2019b). Execution of the mesh generation process is automatically done in the program. However, it does not always mean that the best useful mesh generation would be created by the program automatically. For this reason, the program allows users to refine finite element mesh globally or locally so that users can examine the output of mesh generation and will be able to modify mesh density if necessary.

During the parametric study, the location, width and thickness of geofoam will change. It is possible that finite element mesh may change every time geometry changes. In order to overcome this issue, a base geometry was created at the beginning of the analyses. This base geometry is created in a way so that it allows the creation of every possible EPS geofoam placement combination. (Figure 3.14) By doing this, in all analyses, the same mesh network will be used.

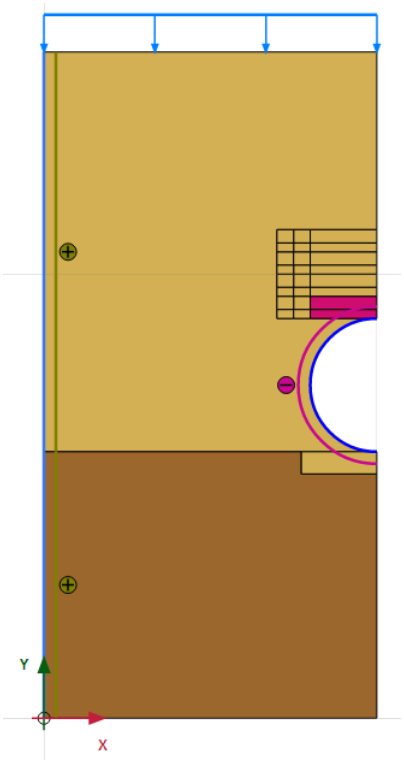

Figure 3.14. General overview of numerical model for mesh convergence analysis

Local or global refinements are defined in the program as “coarseness factor” which states that higher coarseness factor yields to coarse mesh, lower coarseness factor yields to finer mesh density oppositely. In this study, in order to obtain strain values more precisely, the coarseness factor for geofoam locations is decreased to a value of 0.35 from the default value. (1.0 for default) Since the inner side of the pipe will be excavated, therefore coarseness factor of 8.0 is assigned to the pipe element so that coarser mesh density will occur with respect to default mesh. Coarseness factor of 0.25 for the wall of test box (left border) and line load base are assigned by the program by default for structural borders. (Figure 3.15)

The analysis sensitivity and analysis time are related with the number of elements used in the numerical model. For this reason, the number of elements in the numerical model should be chosen carefully. Because using a less than necessary amount of element may cause wrong results, choosing more than the necessary amount of element will extend analysis time unnecessarily. A well-defined balance

should be established. In order to overcome this issue, mesh convergence analyses have been conducted before starting the parametric study.

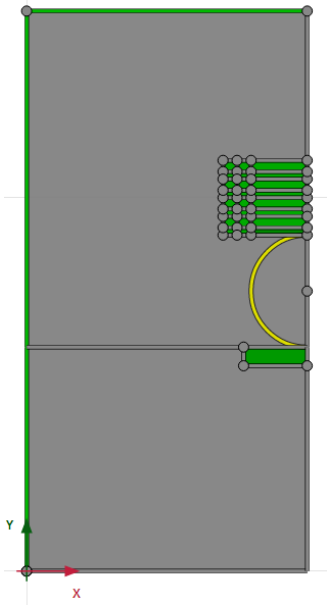

Figure 3.15. Local coarseness for base geometry

For the mesh convergence analyses, the combination where EPS-15 geofoam of 5 cm thickness and 30 cm width is placed directly on the pipe crown is taken into account under 100 kPa surface pressure. Material parameters for EPS-15 geofoam are the same as proposed by Akınay (2017). A general overview of the numerical model is given in Figure 3.14.

3.2.3.1 Mesh Convergence Analysis

A general overview of very coarse, coarse and medium mesh densities are given in Figure 3.16 together with fine and very fine mesh densities in Figure 3.17, respectively. Local coarseness factors are like as shown in Figure 3.15 above.

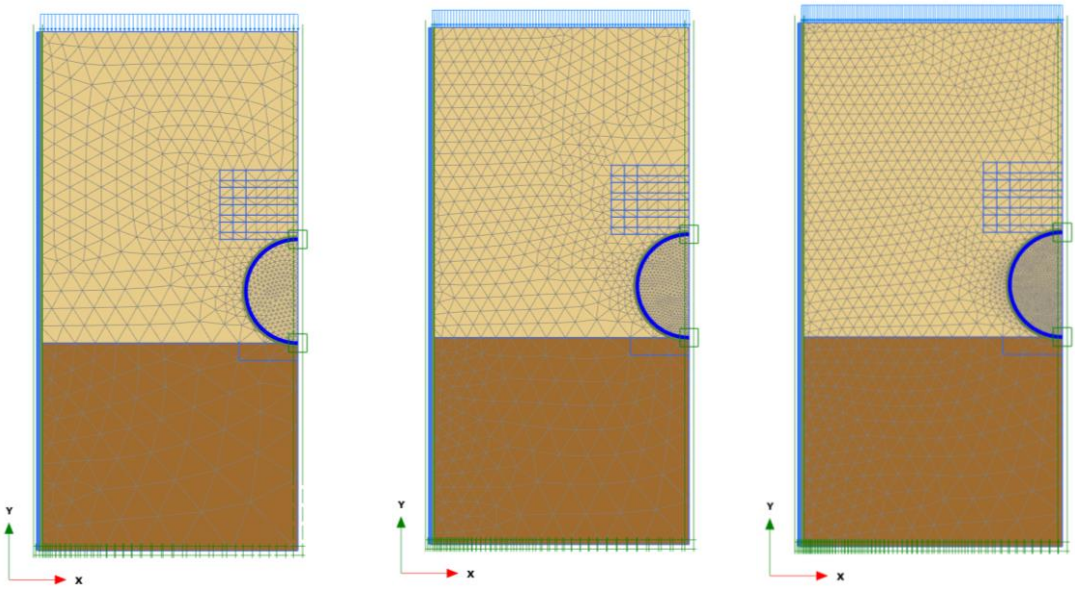

a) b) c)

Figure 3.16. Finite element meshes for a) very coarse mesh density b) coarse mesh density c) medium mesh density

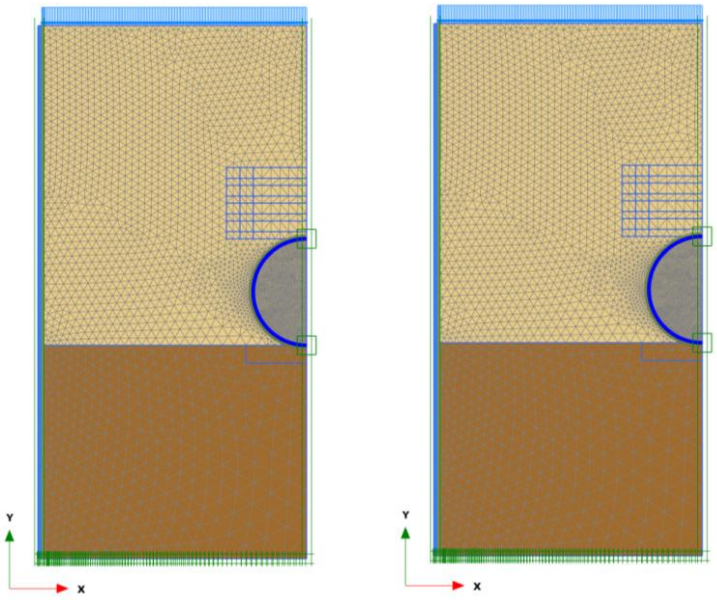

a) b)

Figure 3.17. Finite element meshes for a) fine mesh density b) very fine mesh density

The quantitative output of analysis time, element dimensions, number of elements, number of nodes and maximum horizontal (u_x) and vertical (u_y) deformations at the pipe wall are tabulated in Table 3.10 below.

Table 3.10 Quantitative outputs for different mesh densities

Mesh Density	Analysis Time	Relative Element Size (Element Dimensions)	Number of Element	Number of Nodes	u_x (mm)	u_y (mm)
Very Coarse	1 Minute	2 (0.201 m)	1367	11413	0.990	2.394
Coarse	2 Minutes	1.333 (0.134 m)	2444	20251	0.916	2.241
Medium	3 Minutes	1.0 (0.101 m)	4050	33327	0.878	2.165
Fine	5 Minutes	0.667 (0.067 m)	8805	71821	0.844	2.091
Very Fine	8 Minutes	0.5 (0.05 m)	15130	122877	0.822	2.047

Although the analysis time of very fine mesh density is relatively longer than other mesh densities, considering the results of mesh convergence analysis, very fine mesh density was selected for the parametric-numerical finite element analyses in the scope of this study.

CHAPTER 4

VERIFICATION OF THE NUMERICAL MODEL

In this section, the numerical model to be used for parametric analysis within the scope of the thesis will be verified with the laboratory experiment results made by Akınay (2017).

Verification will be made by using two different linear elastic material parameter sets which are bilinear elastic and trilinear elastic for EPS geofoam.

Akınay conducted laboratory tests in order to investigate effect of geometry of EPS geofoam as soft inclusion in five different combinations (Figure 4.1). However, the aim of this study is to examine the geometric variations of configuration-1, one of the configurations studied by Akınay. Therefore, numerical verification is only done for configuration of Test-1.

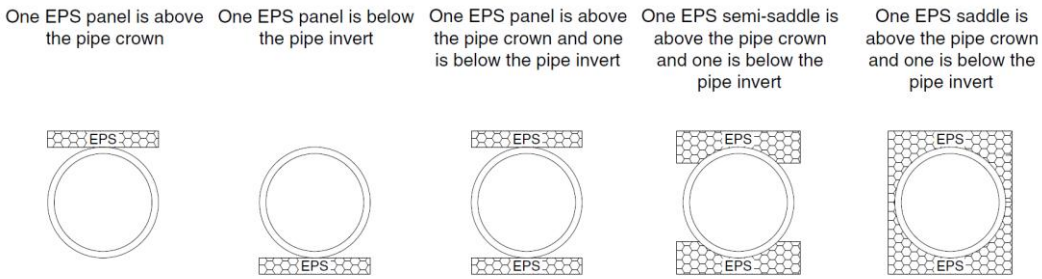

Figure 4.1. Pipe – EPS geofoam combinations from laboratory test [taken from Kılıç & Akınay (2019)]

4.1 Verification of the Reference Test

In order to show the validity of the numerical model, the results of the laboratory test without geofoam by Akınay were tried to be obtained by numerical model. In Figure 4.2, general overview of numerical model is given.

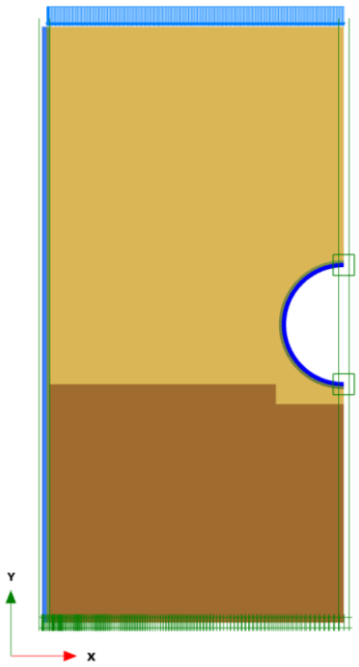

Figure 4.2. General overview of numerical model of reference test

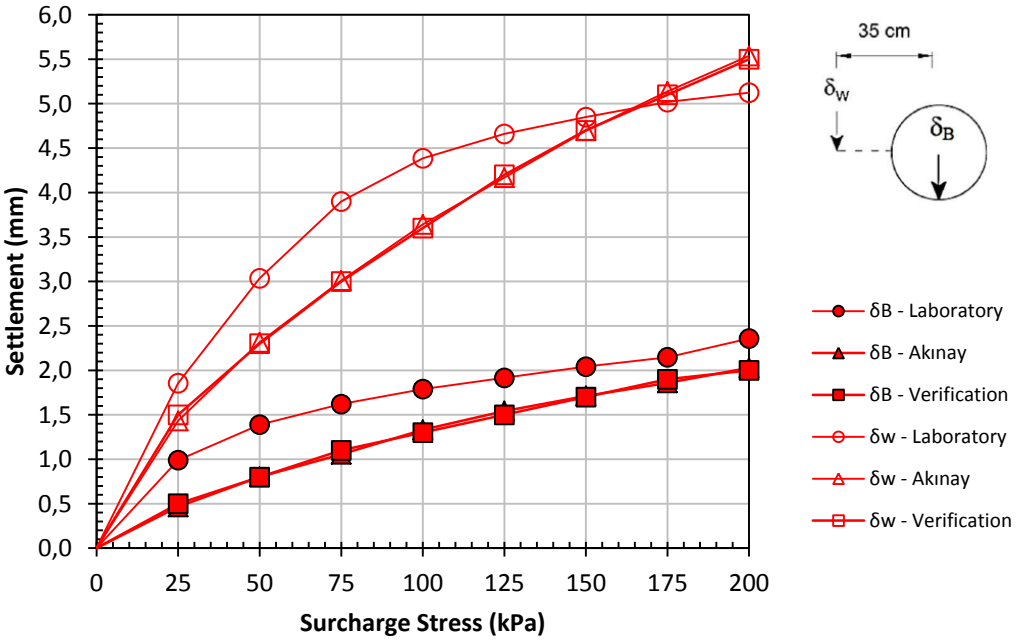

Figure 4.3. Comparison of settlements

During the laboratory tests, Akınay measured the settlements on locations which are 35 cm left and 35 cm right sides of pipe springline with the help of S1 and S2 settlement plates, respectively (Figure 3.7) together with settlement at the pipe base. Comparison of settlements, at the wedge of pipe springline and the pipe base, obtained from Akınay's laboratory test, numerical model of Akınay and verification of numerical model established in the scope of this study are given in Figure 4.3 where;

- δ_W is settlement at the 35 cm wedge of pipe springline (mm)
- δ_B is settlement at the base of pipe (mm)
- Circular points represent settlements obtained from laboratory tests
- Triangular points represent settlements obtained from numerical model of Akınay
- Rectangular points represent settlements obtained from verification model

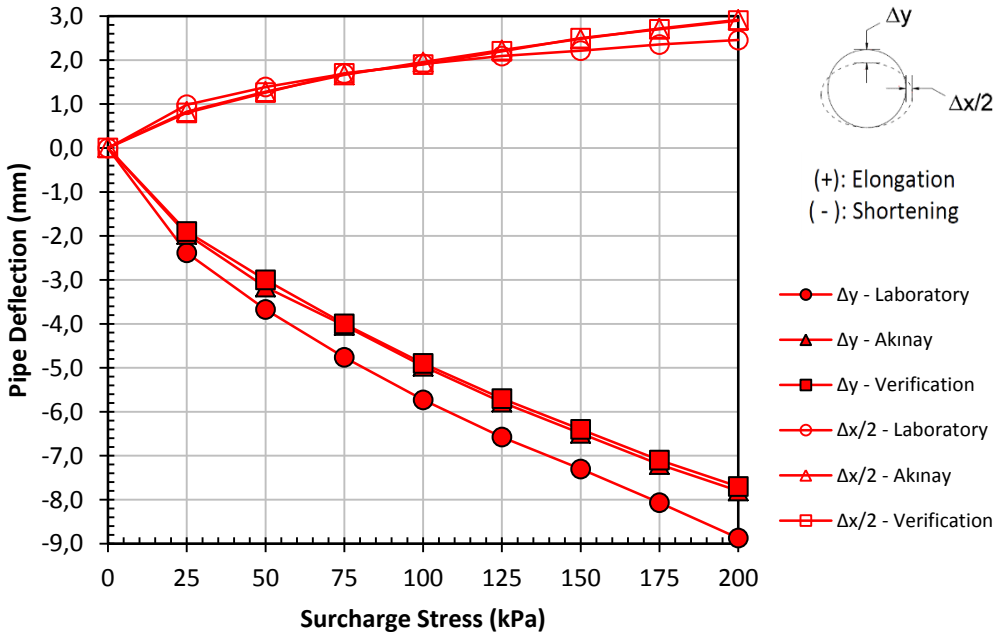

Figure 4.4. Comparison of deflections

During the laboratory tests, Akınay measured the vertical and horizontal pipe deflections in midlength of the HDPE pipe with the help of potentiometric

displacement transducers (Figure 3.7). Comparison of vertical and horizontal pipe deflections, at the midlength of the pipe, obtained from Akınay's laboratory test, numerical model of Akınay and verification of numerical model established in the scope of this study are given in Figure 4.4 where;

- Δy ($\Delta y=\Delta y_1- \Delta y_2$) is vertical deflection (mm) (Figure 4.5)
- $\Delta x/2$ is horizontal deflection (mm)
  (positive (+) and negative (-) values denotes elongation and shortening, respectively)
- Circular points represent deflections obtained from laboratory tests
- Triangular points represent deflections obtained from numerical model of Akınay
- Rectangular points represent deflections obtained from verification model

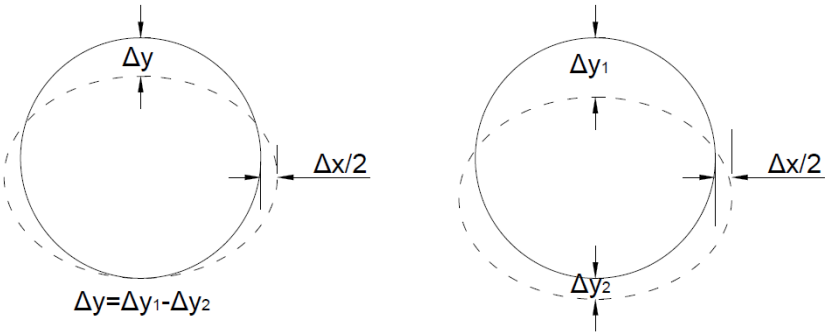

a) Idealized notation b) Actual notation

Figure 4.5. Definition of vertical and horizontal deflections

According to comparison of settlements and deformations presented in Figure 4.3 and Figure 4.4, numerical model (Plaxis 2D) established in the scope of this study successfully models the behavior of test soil and pipe in the case of without EPS geofoam. Numerical model of Akınay and verification model give almost same results which means model are in a good conformity.

4.2 Verification of Configuration-1

Verification has been made to show the validity of the numerical model in the case where EPS-10 and EPS-15 geofoam are placed on the crown of HDPE pipe (configuration-1, Figure 4.1). The numerical model was verified by both the bilinear elastic parameters suggested by Akınay and the trilinear elastic material parameters obtained by idealization of the unconfined compression test result. The values obtained from the numerical (validation) model were compared with the values obtained from Akınay's laboratory test results and numerical models. A general overview of the numerical model is given in Figure 4.6.

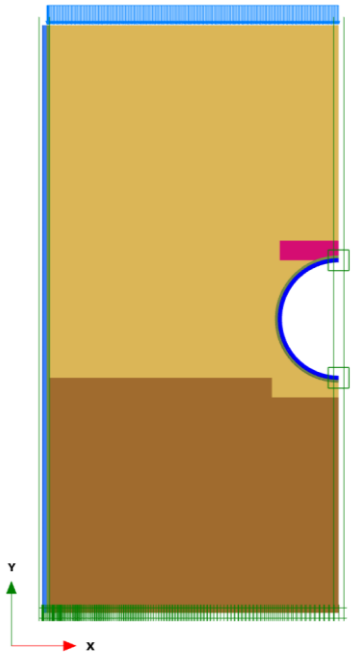

Figure 4.6. General overview of numerical model for configuration-1

4.2.1 Bilinear Elastic Material Parameter

In the laboratory tests made by the Akınay, there was EPS geofoam at the base of the pipe in all configurations except configuration of Test-1 (Figure 4.1). During the tests, settlements just above and below the EPS geofoam located under the

pipe's base elevation were measured with the help of S3 and S4 settlement plates (Figure 3.7). The vertical strain amount of EPS geofoam material was calculated with the help of the differences in the settlements measured at the upper and lower elevations of EPS geofoam material. From the stress-strain graphs obtained with unconfined compression test in the laboratory, the secant modulus value corresponding to the relevant strain value was read. Following the same methodology, a numerical model was created by updating the secant modulus value corresponding to each loading stage (25 kPa and its multiples) and the material properties in the related loading stage (staged construction) program. Briefly, Akınay makes back-calculations to capture the strain values obtained from full scale laboratory tests while determining these material properties in numerical model. Bilinear elastic material parameters were taken from Akınay (2017) and summarized in Table 4.1 below.

The numeric analysis results made by using the parameters idealized by Akınay are presented in Figure 4.7, Figure 4.8, Figure 4.9 and Figure 4.10 together with the laboratory test results and the results obtained from the numerical model of Akınay in order to verification. It should be remembered that, Akınay ignores the deformation on EPS geofoam takes place during filling of test tank with sand and takes into account only deformations after surface loading started.

Table 4.1 Back-calculated bilinear elastic material properties
[taken from Akınay (2017)]

Surface Pressure (kN/m^2)	EPS-10		EPS-15	
	E (kN/m^2)	υ	E (kN/m^2)	υ
0 - 25	430	0.049	960	0.022
25 - 200	140	0.049	170	0.040

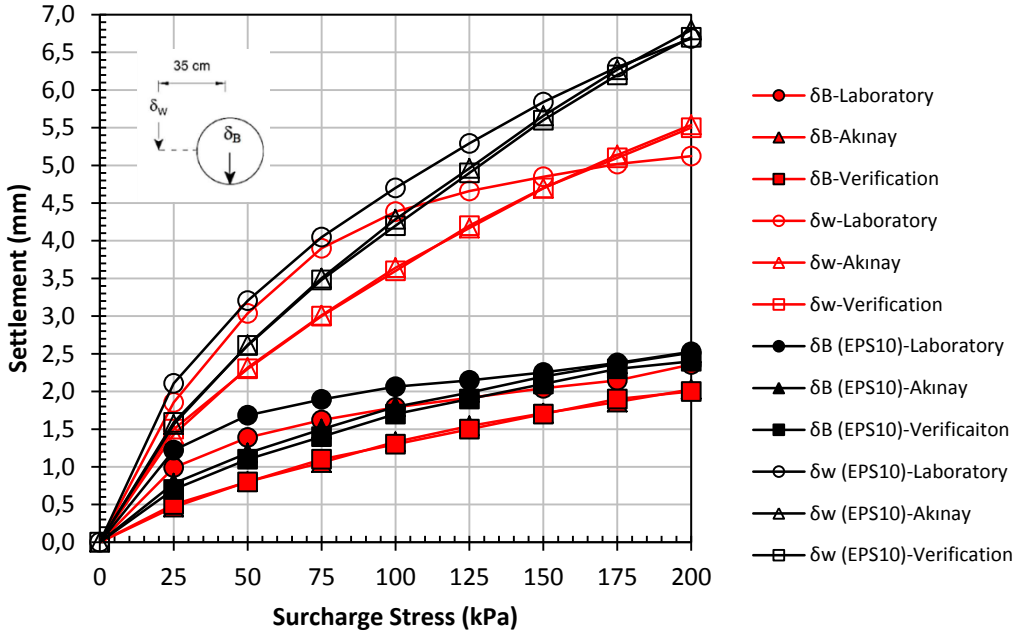

Figure 4.7. Comparison of settlements with EPS-10 (bilinear elastic parameters) in Test-1 Configuration

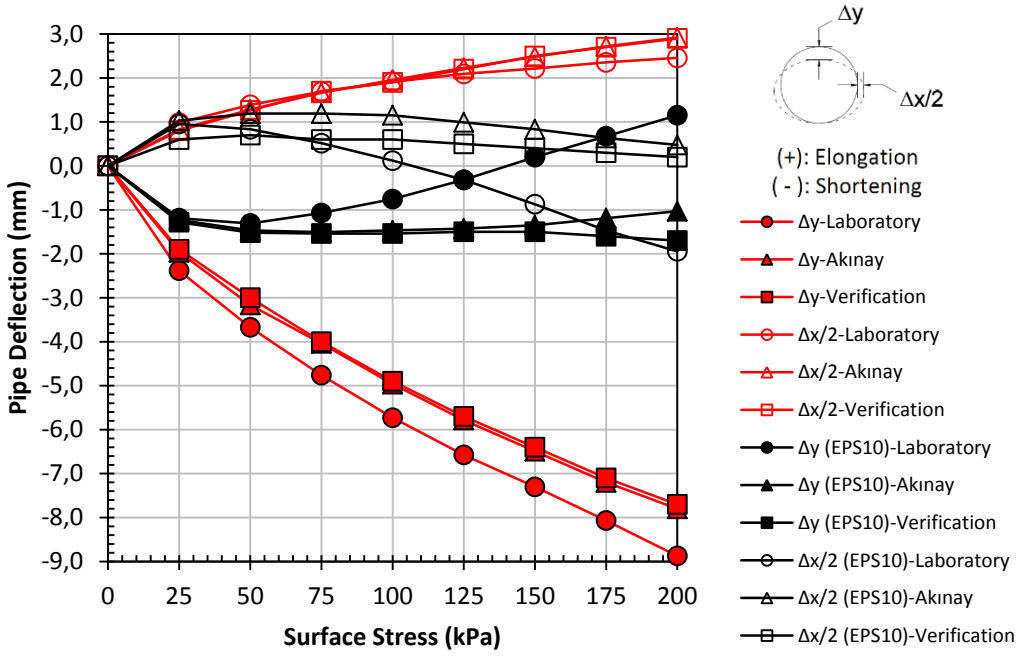

Figure 4.8. Comparison of deflections with EPS-10 (bilinear elastic parameters) in Test-1 Configuration

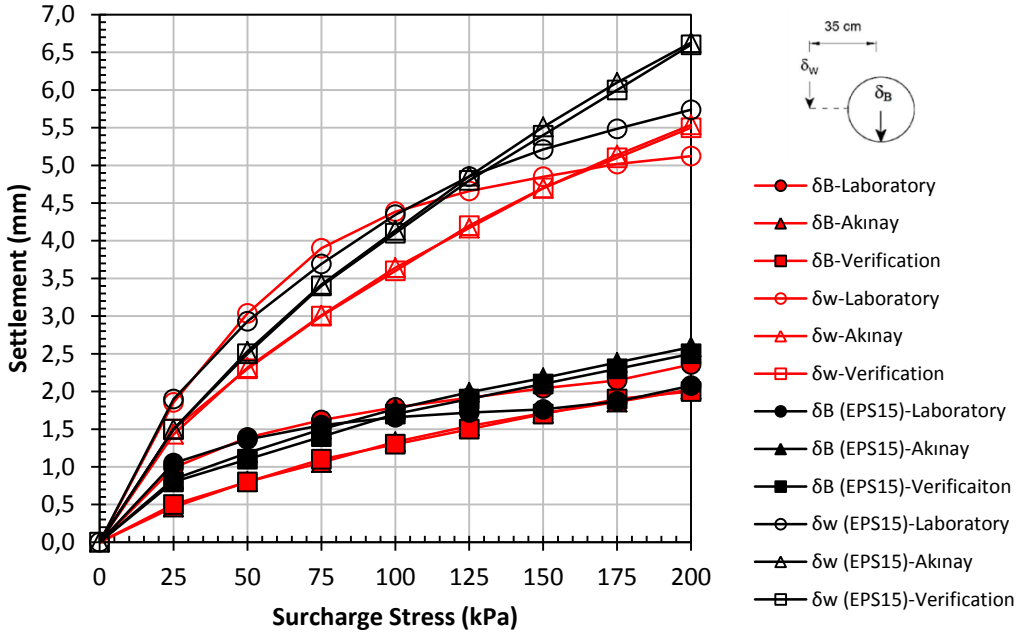

Figure 4.9. Comparison of settlements with EPS-15 (bilinear elastic parameters) in Test-1 Configuration

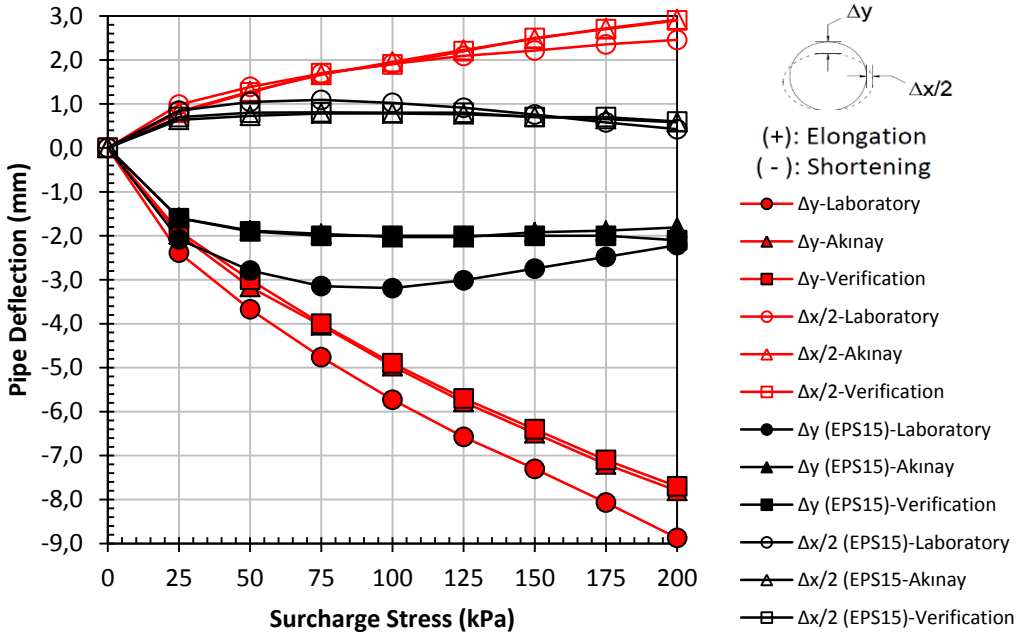

Figure 4.10. Comparison of deflections with EPS-15 (bilinear elastic parameters) in Test-1 Configuration

According to comparison of settlements and deflections presented in Figure 4.7, Figure 4.8, Figure 4.9 and Figure 4.10, numerical model (PLAXIS 2D) established in the scope of this study successfully model the settlement behavior of test sand and deflection behavior of HDPE pipe improved with EPS-10 and EPS-15 geofoam. Numerical model of Akınay and verification model give almost same results which means model are in a good conformity.

4.2.2 Trilinear Elastic Material Parameter

Although Akınay (2017) uses the initial tangent modulus values corresponding to axial strain values he obtained from his laboratory experiments, in the design stage, the laboratory test result is often not in the hands of the designer. Therefore, instead of reading corresponding initial tangent modulus from strain – stress curve obtained from unconfined compression test in the laboratory, one can easily prepare a numerical model with linear elastic material parameters obtained from literature. One of the aims of this study is to verify the numerical model with laboratory data by using linear elastic material parameters obtained from the literature as input and to show the usability of numeric models in advanced design stages. For this reason, in this part of the study, it is aimed to reveal the consistency (verification) of numerical models made by using the idealized trilinear elastic material parameters that can be found easily in the literature for EPS geofoam. Accordingly, the stress-strain curves obtained as a result of the unconfined compression test results given by Akınay (2017) for EPS-10 and EPS-15 geofoam were idealized in 3 parts and linear elastic material parameters were determined. Trilinear elastic material parameters are given in chapter “3.1.2.3 EPS Geofoam (page:53)" and summarized in Table 3.8 and Table 3.9 for EPS-10 & EPS-15 and EPS-20, respectively.

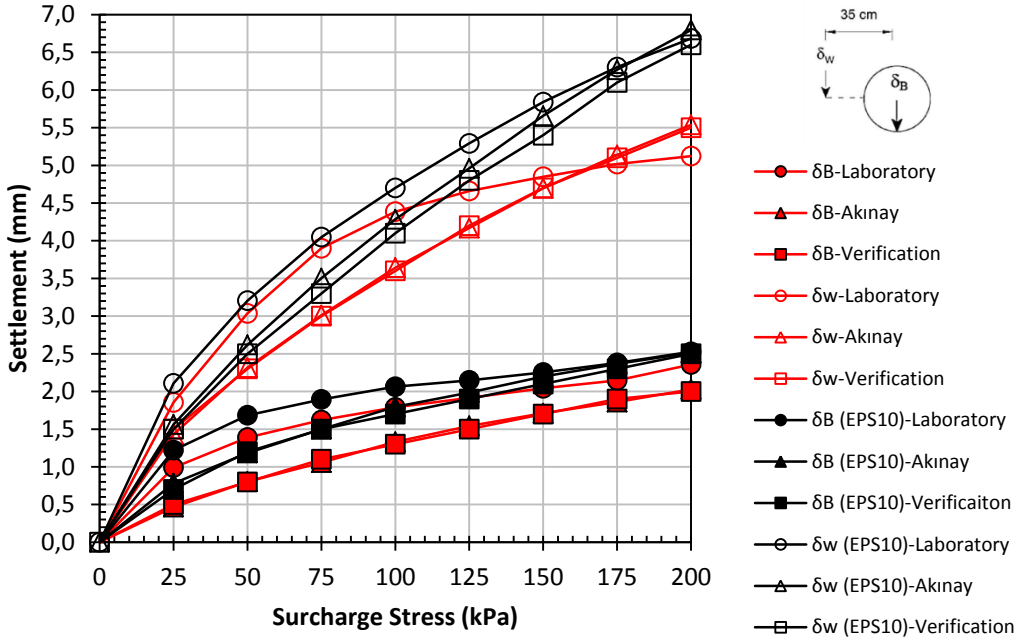

Figure 4.11. Comparison of settlements with EPS-10 (trilinear elastic parameters) in Test-1 Configuration

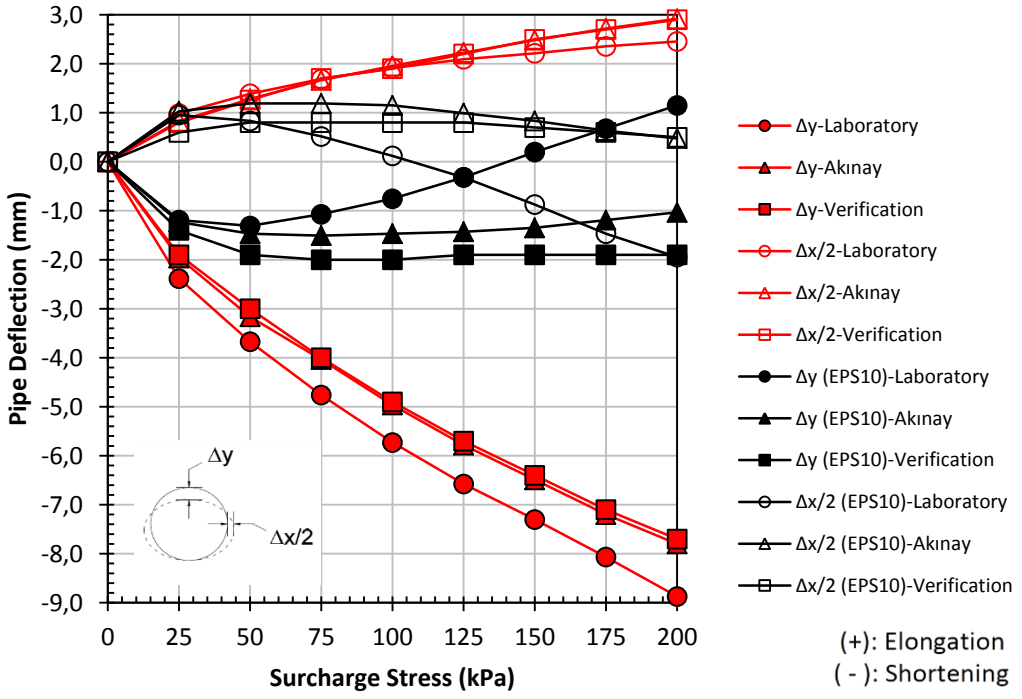

Figure 4.12. Comparison of deflections with EPS-10 (trilinear elastic parameters) in Test-1 Configuration

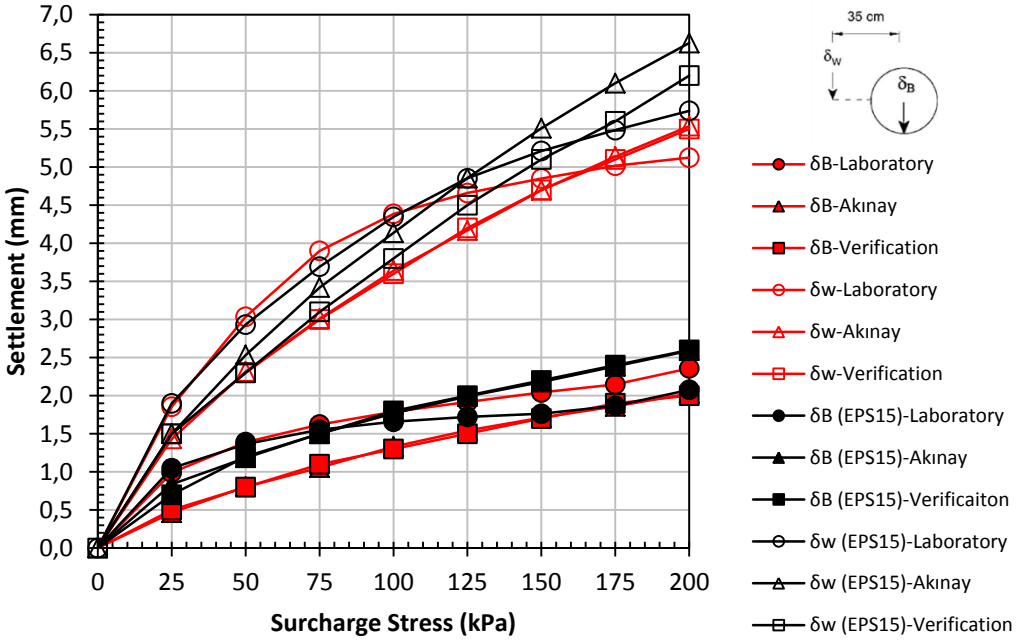

Figure 4.13. Comparison of settlements with EPS-15 (trilinear elastic parameters) in Test-1 Configuration

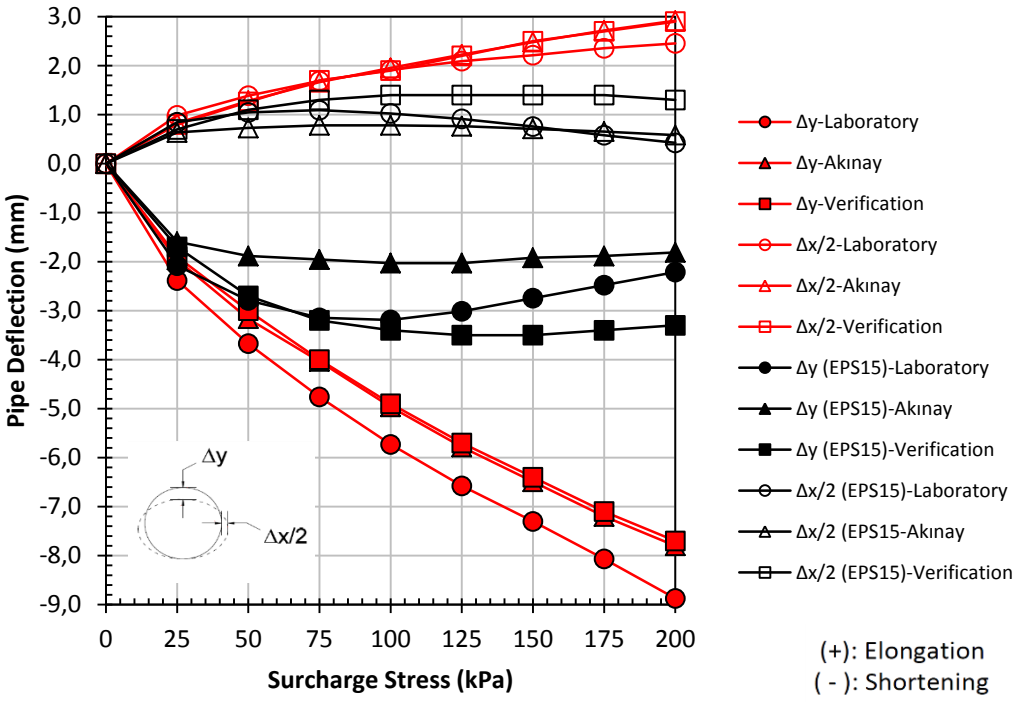

Figure 4.14. Comparison of deflections with EPS-15 (trilinear elastic parameters) in Test-1 Configuration

The numeric analysis results made by using the trilinear elastic parameters are presented in Figure 4.11, Figure 4.12, Figure 4.13 and Figure 4.14, together with the laboratory test results and the results obtained from the numerical model of Akınay in order to verification. It should be remembered that, Akınay ignores the deformation on EPS geofoam takes place during filling of test tank with sand and takes into account only deformations after surface loading started. However, in numerical models where trilinear material parameters are used, axial strain values formed on EPS geofoam material due to gravity loading during the placement of the test sand in the test tank were not ignored.

According to comparison of settlements and deflections presented in Figure 4.11, Figure 4.12, Figure 4.13 and Figure 4.14, numerical model (PLAXIS 2D) established in the scope of this study successfully models the settlement behavior of test sand and deflection behavior of HDPE pipe improved with EPS-10 and EPS-15 geofoam with trilinear elastic material parameters.

In the case of placing EPS-10 geofoam at the crown of the pipe, if the curves of settlement are to be compared; while wedge settlements (δ_W) are detected more closely with bilinear elastic material parameters, no significant difference is observed for base settlements (δ_B) between bilinear and trilinear material parameters. If the pipe deformation curves are compared for the cases where bilinear and trilinear elastic materials are used, numerical model with trilinear elastic material parameter captures the horizontal pipe deflection ($\Delta x/2$) behavior better. In the case of vertical deformation (Δy), numerical model with bilinear elastic material parameter is better. Already, the bilinear parameters are obtained by determining the initial tangent modulus values corresponding to the axial strain values occurring in the geofoam material located at the base of the pipe in laboratory tests (all configurations except test-1; Figure 4.1), which is expected to be better.

In the case of pacing EPS-15 geofoam at the crown of the pipe, if the curves of settlement are to be compared; while wedge settlements (δ_W) are detected more

closely with bilinear elastic material parameters, numerical model with trilinear elastic material parameters captures the base settlements (δ_B) better with respect to case of using bilinear elastic material parameter. Likewise, numerical model with trilinear elastic material parameter captures the vertical and horizontal pipe deflection (Δy and $\Delta x/2$, respectively) behavior better up to surface loading of 100 kPa however for the surface loading of 175 - 200 kPa bilinear elastic material parameters obtains closer values.

As a result, under low applied surface load (up to 100 kPa), models with trilinear elastic parameters give more accurate results generally by considering pipe deflections. For the base settlement which is important than wedge settlements, models with trilinear elastic material parameters captures settlement behavior more closely. Because of its ease of obtaining, giving more closer (up to 100 kPa) and conservative (100 – 200 kPa) results, it was decided to perform parametric analysis with numerical models in which trilinear elastic material parameters were used.

CHAPTER 5

PARAMETRIC STUDY AND FINDINGS

In this chapter, the behavior of deformable HDPE pipe under uniformly distributed surcharge pressure was examined by using verified numerical model in order to investigate effect of EPS geofoam location, effect of thickness, effect of density and effect of width where EPS geofoam material is used as a soft inclusion on the pipe in order to create a compressible layer. Material parameters for EPS geofoam were explained in detail in previous chapters together with geometrical properties of numerical model. The validity of the prepared numerical model has been demonstrated by comparing the results of the laboratory experiments made by Akınay (2017) in the previous section.

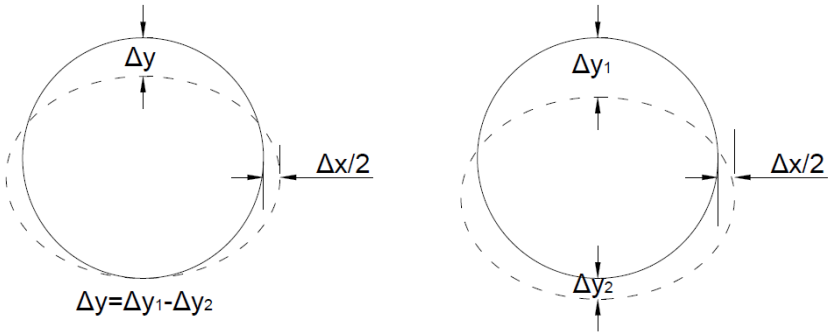

a) Idealized notation b) Actual notation

Figure 5.1. Notation for pipe deflections

In the analysis, vertical and horizontal pipe deflections (in mm) were notated as Δy and Δx/2, respectively. Analysis combinations were distinguished with following notation;

cX_EPSXX_tX_wXX,X_ΔX

Where;

cX denotes location of EPS geofoam (in cm)

- X can be 0 (at crown), 5 (above 5 cm from pipe crown) and 10 (above 10 cm from pipe crown)

EPSXX denotes density of EPS geofoam in (kg/m^3)

- XX can be 10, 15 and 20

tX denotes thickness of EPS geofoam (in cm)

- X can be 2, 5, 7 and 10

wXX,X denotes width of EPS geofoam (in cm)

- XX,X can be 30, 37.5 and 45 (should be remembered that due to symmetry half geometry was modeled)

c10_EPS10_t2_w37,5

denotes that EPS-10 geofoam with thickness of 2 cm and width of 37.5 cm located 10 cm above the HDPE pipe crown.

5.1 Without EPS Geofoam

In order to observe the improvement by the existence of EPS geofoam in any thickness, any width and any density above the deformable pipe a condition, called reference test, without EPS geofoam above pipe was analyzed. Result of reference analysis is given in Figure 5.2

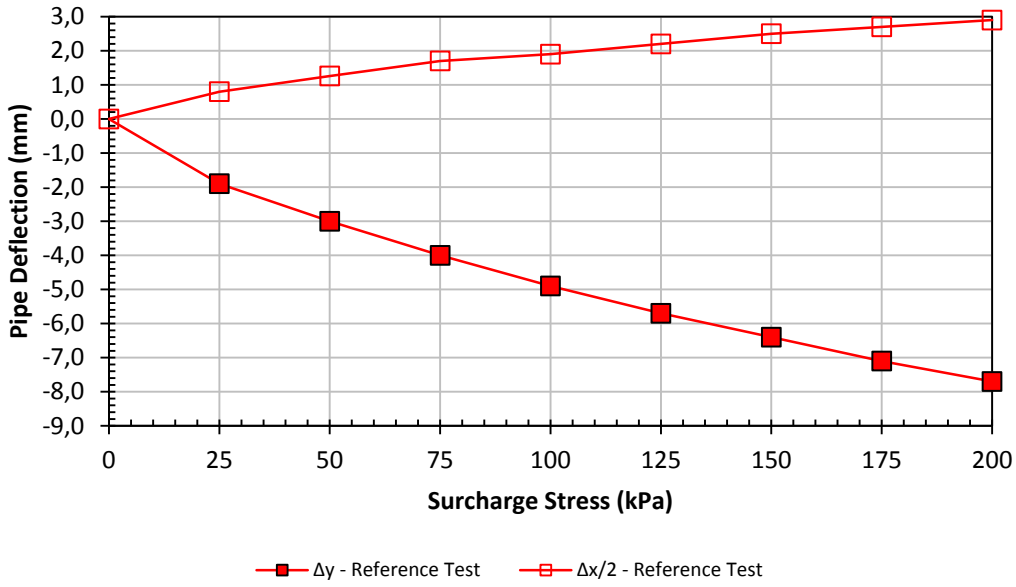

Figure 5.2. Result of the reference test

5.2 Effect of the EPS Geofoam Location

In order to observe the effect of location, the combinations where 2, 5, 7 and 10 cm thick EPS geofoams were placed on the pipe crown, 5 cm above and 10 cm above, respectively, were examined. In these analyzes, the geofoam width was kept constant at 37.5 cm. In order to examine the effect of location on all densities, EPS-10, EPS-15 and EPS-20 geofoams were used in the study.

5.2.1 Thickness=2 cm and Width=37.5 cm

The effect of location for EPS-10, EPS-15 and EPS-20 geofoams were given as Figure 5.3, Figure 5.4 and Figure 5.5, respectively. From these figures it can be concluded that for all densities, 2 cm thick EPS geofoam placed at pipe crown and 5 cm above the pipe crown gives almost same result. In the case where EPS geofoam placed 10 cm above pipe crown (c10), pipe deflections are slightly more than that of combinations which EPS geofoam placed at pipe crown (c0) and 5 cm above pipe crown (c5). However, considerable amount of improvement was

achieved in all combinations. It can be concluded that as the density of EPS increases, the amount of improvement decreases. When 2 cm thick of EPS geofoam used as soft inclusion, it can be said that location has no significant effect on pipe deformation behavior.

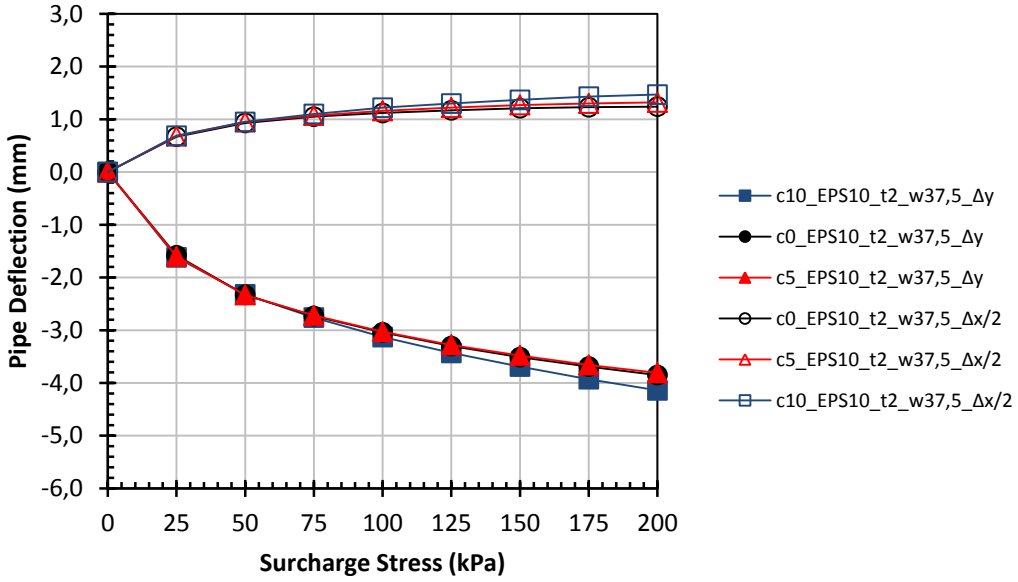

Figure 5.3. Effect of EPS-10 location while thickness=2 cm and width=37.5 cm

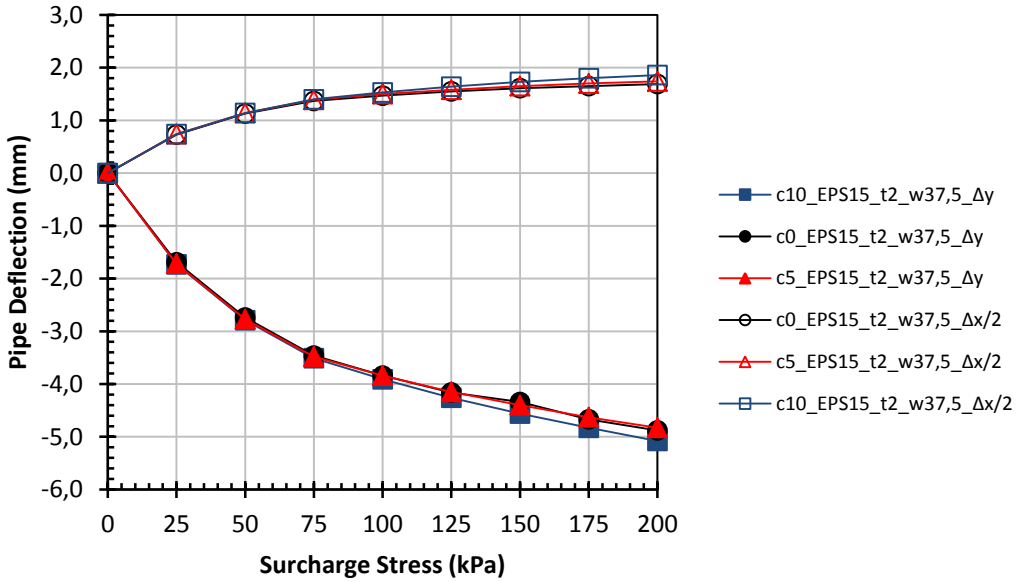

Figure 5.4. Effect of EPS-15 location while thickness=2 cm and width=37.5 cm

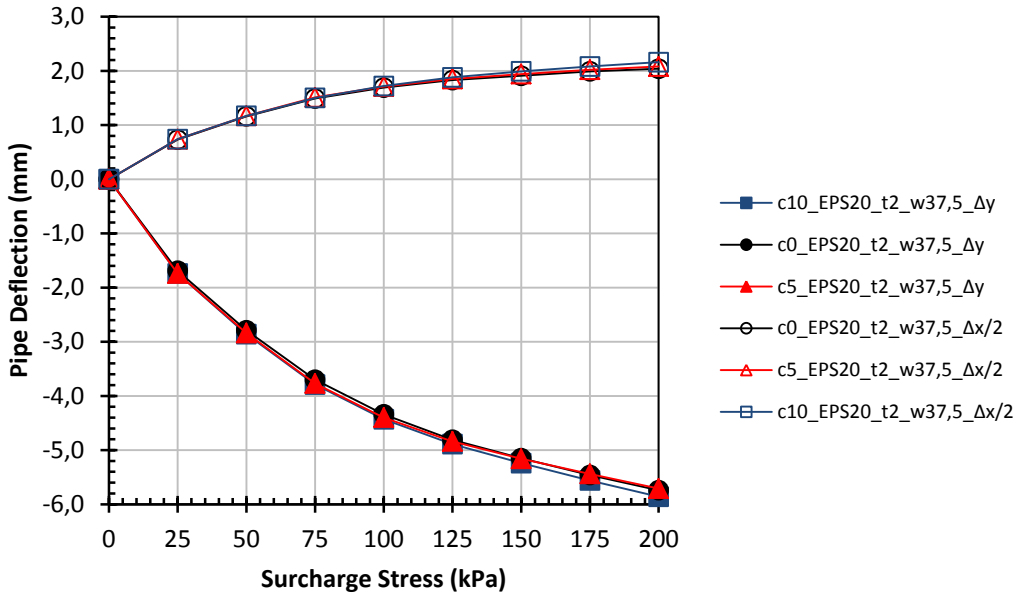

Figure 5.5. Effect of EPS-20 location while thickness=2 cm and width=37.5 cm

5.2.2 Thickness=5 cm and Width=37.5 cm

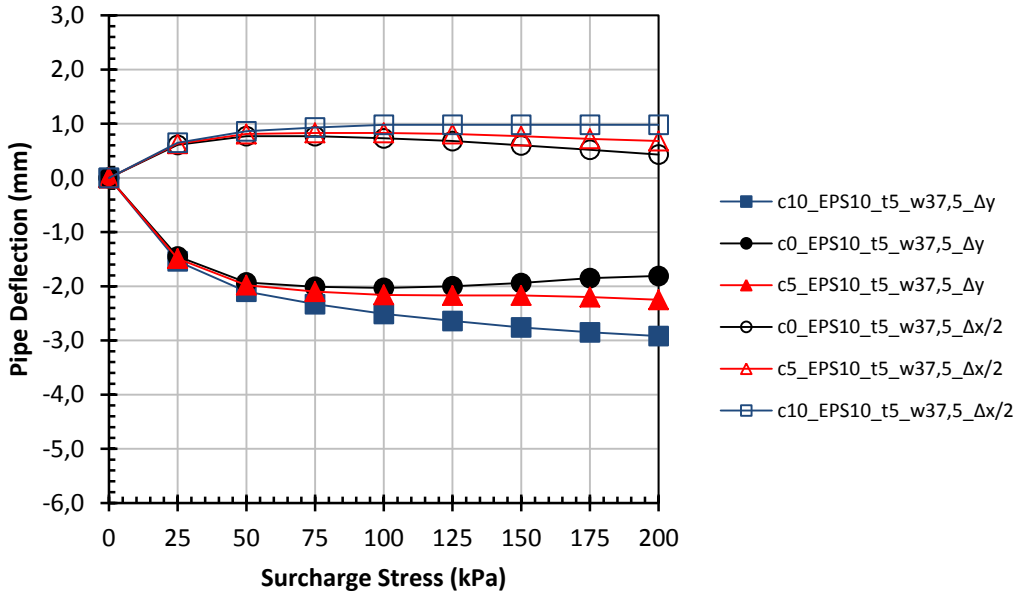

Figure 5.6. Effect of EPS-10 location while thickness=5 cm and width=37.5 cm

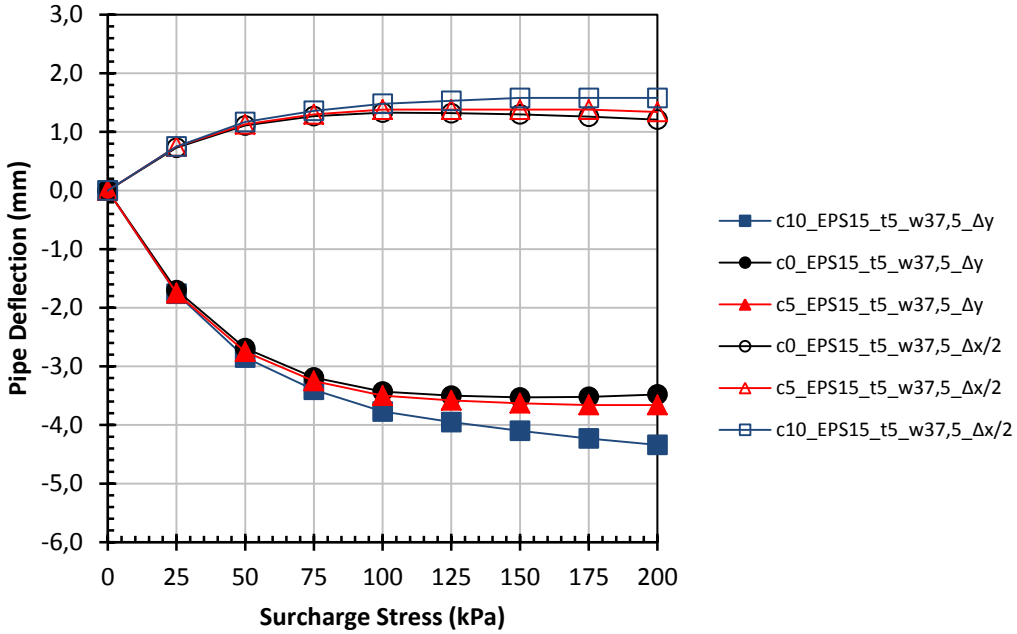

Figure 5.7. Effect of EPS-15 location while thickness=5 cm and width=37.5 cm

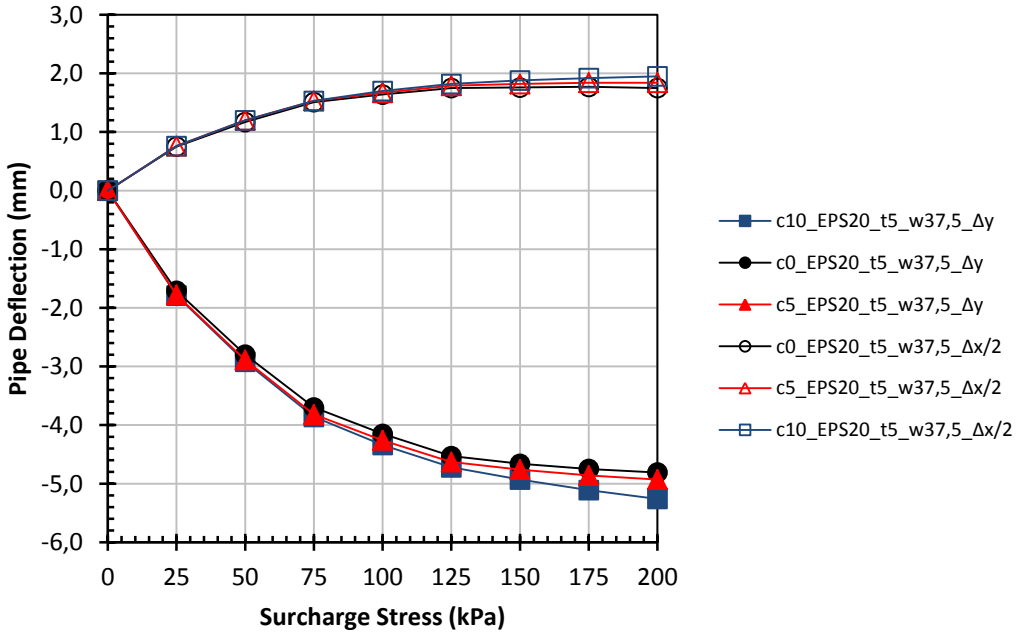

Figure 5.8. Effect of EPS-20 location while thickness=5 cm and width=37.5 cm

For the thickness of 5 cm, the effect of location for EPS-10, EPS-15 and EPS-20 geofoam was given as Figure 5.6, Figure 5.7 and Figure 5.8, respectively. In the case of using EPS geofoam with a thickness of 5 cm, the combination where EPS geofoam is placed on the pipe crown (c0) has given the best performance in all analyzes. Likewise, the performance of placing EPS geofoam 5 cm above the pipe crown (c5) is better than placing EPS geofoam 10 cm above the pipe crown for all densities. As the EPS density increases, effect of location loses its importance.

5.2.3 Thickness=7 cm and Width=37.5 cm

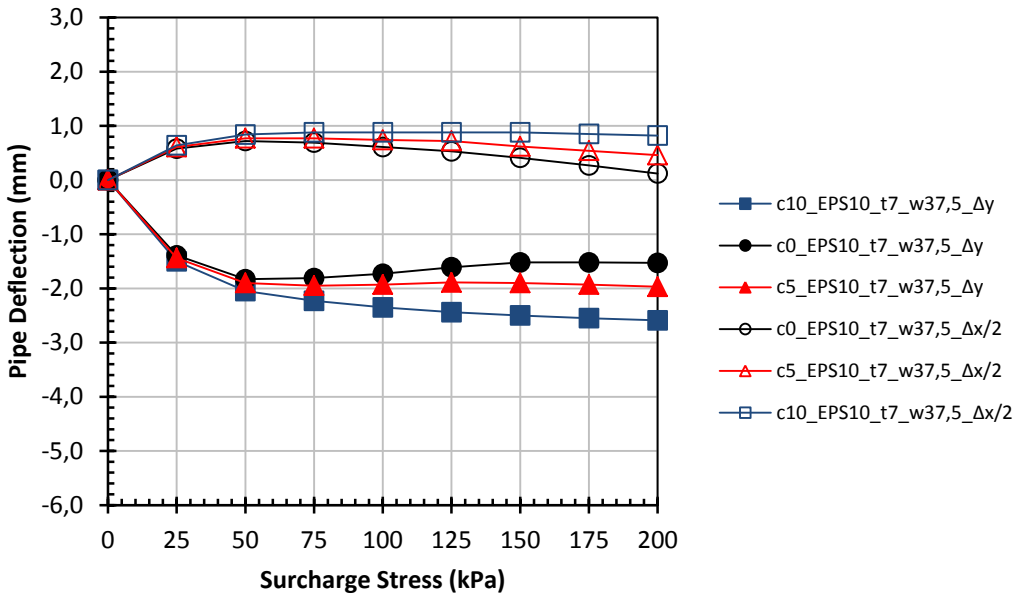

Figure 5.9. Effect of EPS-10 location while thickness=7 cm and width=37.5 cm

For the thickness of 7 cm, the effect of location for EPS-10, EPS-15 and EPS-20 geofoam was given as Figure 5.9, Figure 5.10 and Figure 5.11, respectively. As it was in the case of thickness=5 cm, in the case of using EPS geofoam with a thickness of 7 cm, the combination where EPS geofoam is placed on the pipe crown (c0) has given the best performance in all analyzes. Likewise, the performance of placing EPS geofoam 5 cm above the pipe crown (c5) is better than

placing EPS geofoam 10 cm above the pipe crown for all densities. As the EPS density increases, effect of location loses its importance.

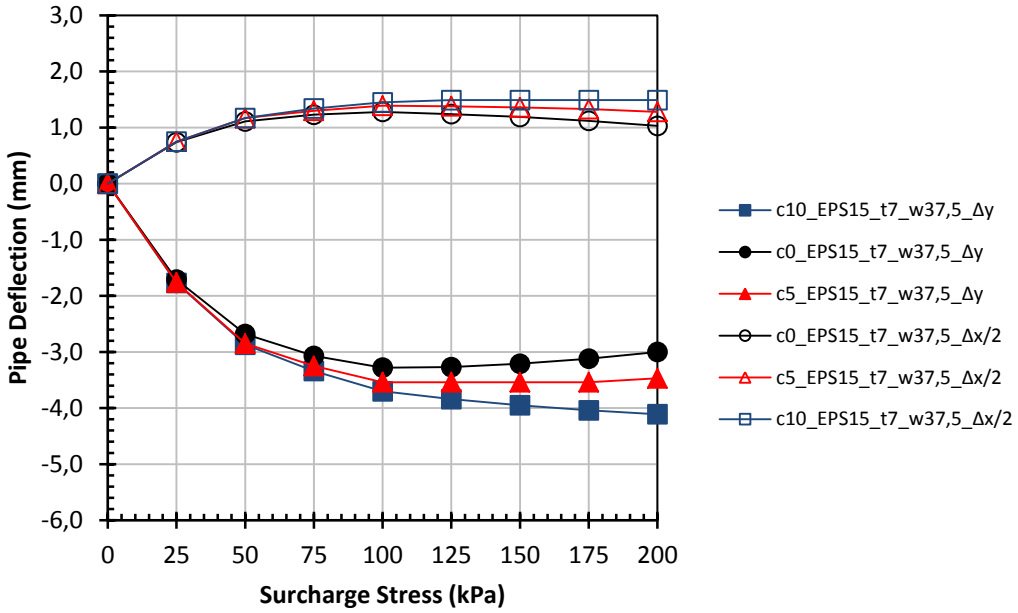

Figure 5.10. Effect of EPS-15 location while thickness=7 cm and width=37.5 cm

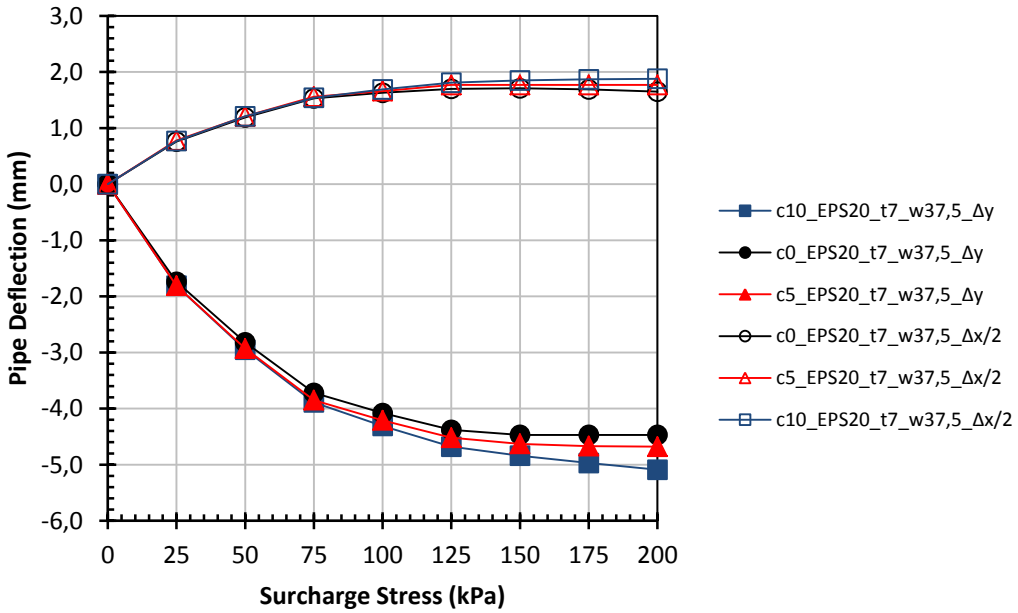

Figure 5.11. Effect of EPS-20 location while thickness=7 cm and width=37.5 cm

5.2.4 Thickness=10 cm and Width=37.5 cm

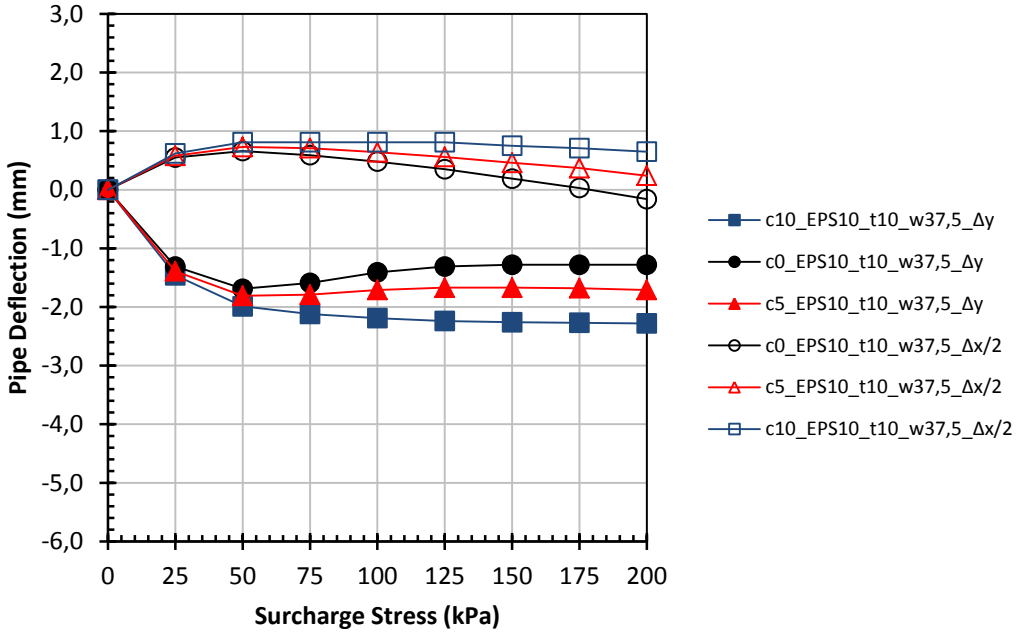

Figure 5.12. Effect of EPS-10 location while thickness=10 cm and width=37.5 cm

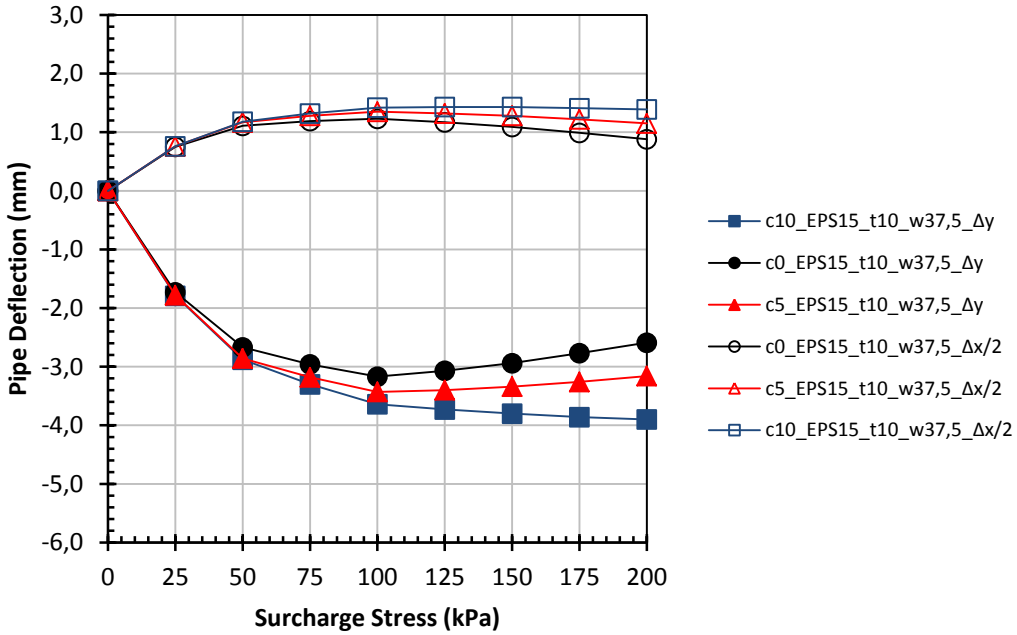

Figure 5.13. Effect of EPS-15 location while thickness=10 cm and width=37.5 cm

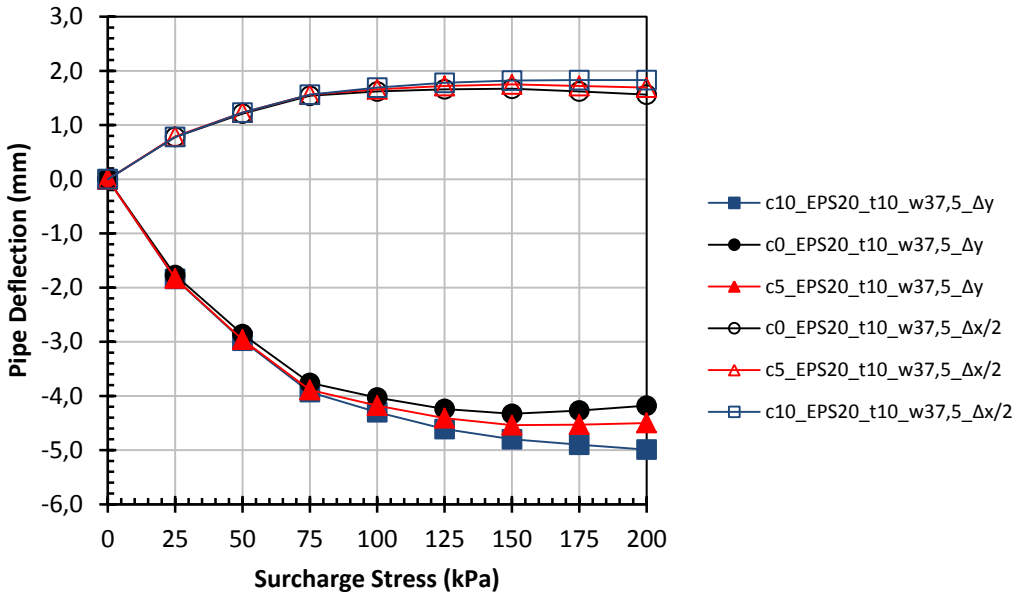

Figure 5.14. Effect of EPS-20 location while thickness=10 cm and width=37.5 cm

For the thickness of 10 cm, the effect of location for EPS-10, EPS-15 and EPS-20 geofoam was given as Figure 5.12, Figure 5.13 and Figure 5.14, respectively. As it was in the cases of thickness=5 cm and thickness=7 cm, in the case of using EPS geofoam with a thickness of 10 cm, the combination where EPS geofoam is placed on the pipe crown (c0) has given the best performance in all analyzes. Likewise, the performance of placing EPS geofoam 5 cm above the pipe crown (c5) is better than placing EPS geofoam 10 cm above the pipe crown for all densities. However, effect of location on improvement performance is more distinctive in this case. As usual, when the EPS density increases, effect of location loses its importance. Nevertheless, effect of location was visibly significant in all densities.

Effect of EPS geofoam location was investigated for densities of EPS-10, EPS-15 and EPS-20 together with thickness of 2 cm, 5 cm, 7 cm and 10 cm and the results were presented above. From Figure 5.3 to Figure 5.14, there is no doubt that, placing EPS geofoam at the crown is better than any other options like 5 cm above and 10 cm above the pipe.

In order to comprehend effect of location, results of analyses which thicker EPS geofoam placed 10 cm above the pipe were compared with 5 cm thick EPS geofoam placed at crown of the pipe in Figure 5.15

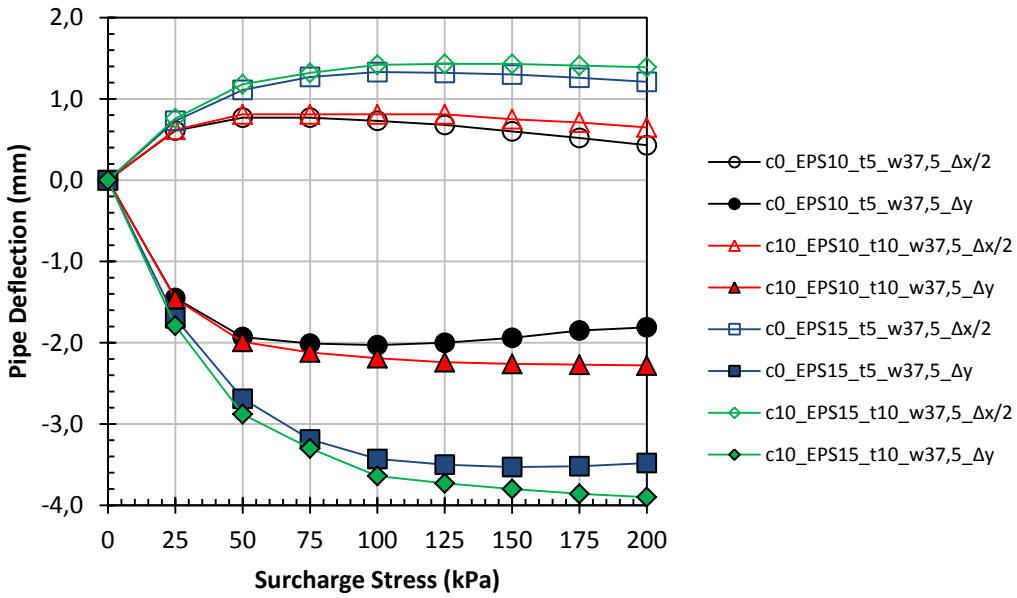

Figure 5.15. Comparison of EPS location for EPS-10 and EPS-15

As can be seen from Figure 5.15, 5 cm thick EPS geofoam placed on pipe crown shows better performance than that of 10 cm thick EPS geofoam placed 10 cm above the pipe crown. This phenomenon is valid for all densities but only EPS-10 and EPS-15 were shown on figure.

Therefore, if the subject is improving the shallowly buried flexible pipe, compressible zone which is EPS for this study, must be placed right above the pipe crown for better performance. For this reason, only the combinations where the EPS geofoam is placed on pipe crown (c0) will be considered in the following analyses.

5.3 Effect of the EPS Geofoam Thickness

In order to examine the effect of thickness, combinations of 2 cm, 5 cm, 7 cm and 10 cm thick EPS geofoams were placed on the pipe crown (c0). In order to observe the effect of EPS density and EPS width on thickness, geofoams of all width and all densities were used.

5.3.1 EPS Density=10 kg/m^3

The effect of thickness for width=30 cm, 37.5 cm and 45 cm was given as Figure 5.16, Figure 5.17 and Figure 5.18, respectively. From these figures, it is clear that as the geofoam thickness increases, the amount of improvement increases. Although the surcharge stress increased, the increase in horizontal and vertical deflections stopped at a surcharge stress of 50-75 kPa in all combinations except for 2 cm thick geofoam. This states that, arching was fully mobilized in all combinations except 2 cm. Nevertheless, a significant improvement was achieved even when 2 cm thick EPS-10 geofoam was placed in the crown of the pipe.

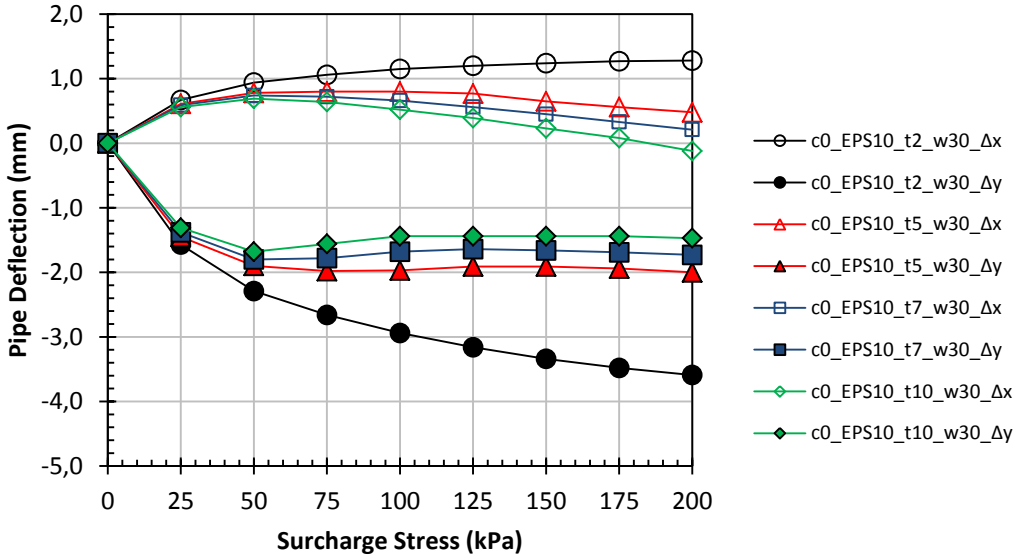

Figure 5.16. Effect of EPS-10 thickness while width=30.0 cm

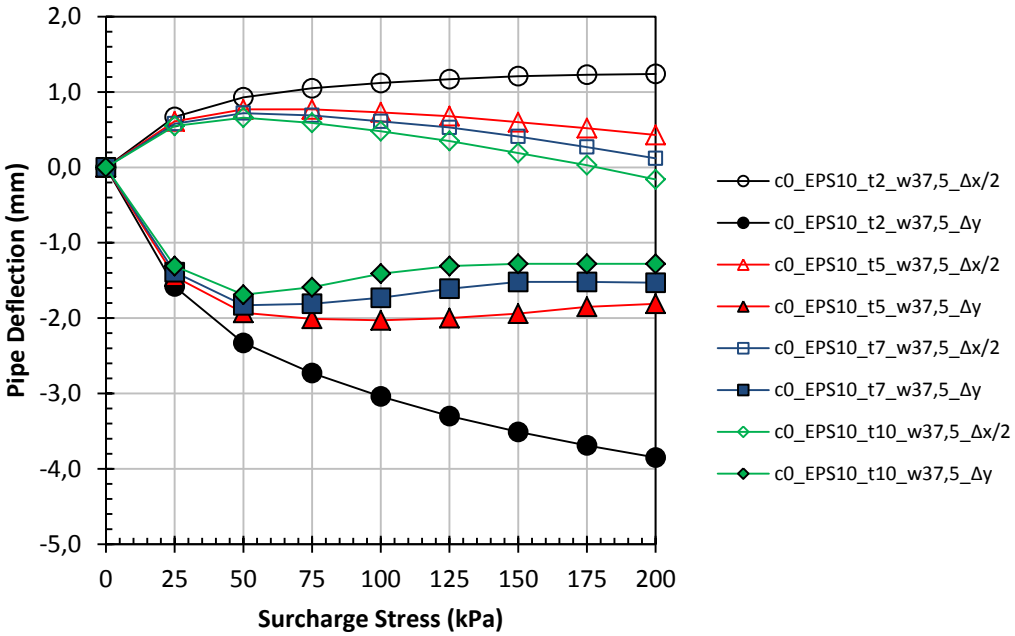

Figure 5.17. Effect of EPS-10 thickness while width=37.5 cm

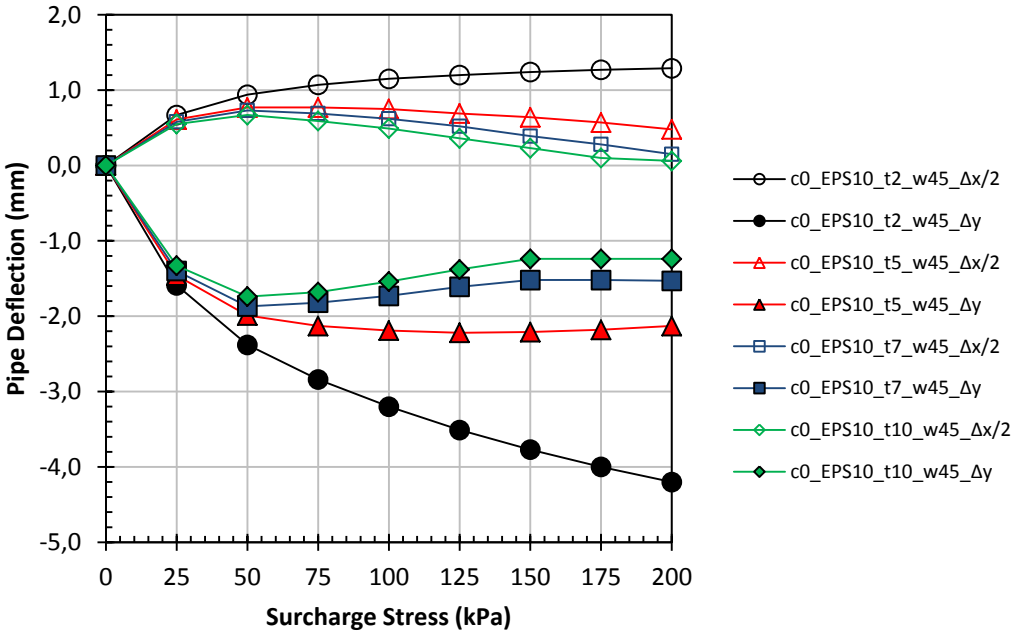

Figure 5.18. Effect of EPS-10 thickness while width=45 cm

5.3.2 EPS Density=15 kg/m^3

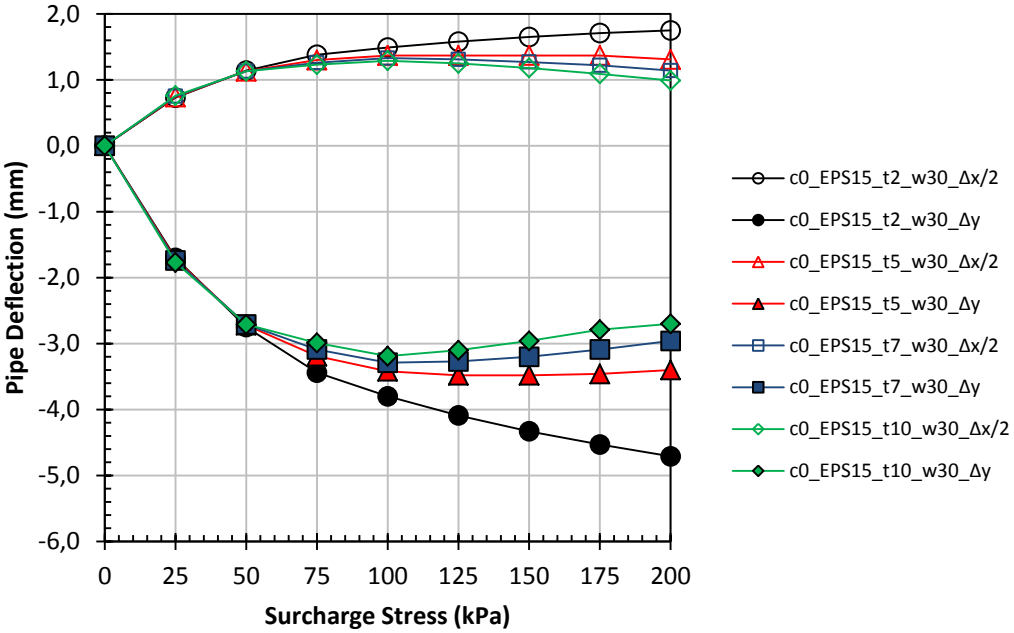

Figure 5.19. Effect of EPS-15 thickness while width=30 cm

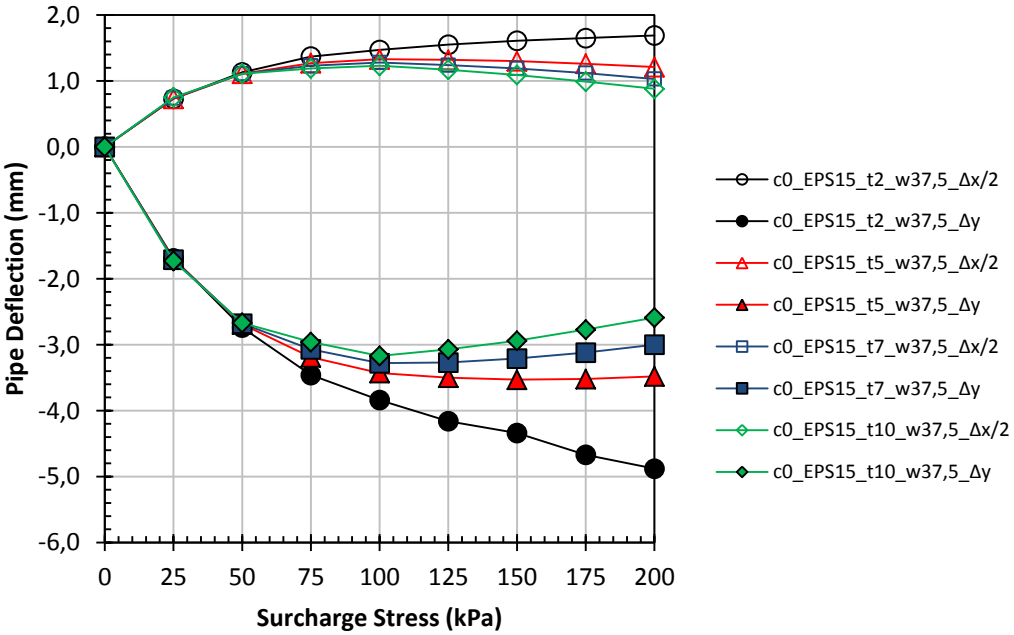

Figure 5.20. Effect of EPS-15 thickness while width=37.5 cm

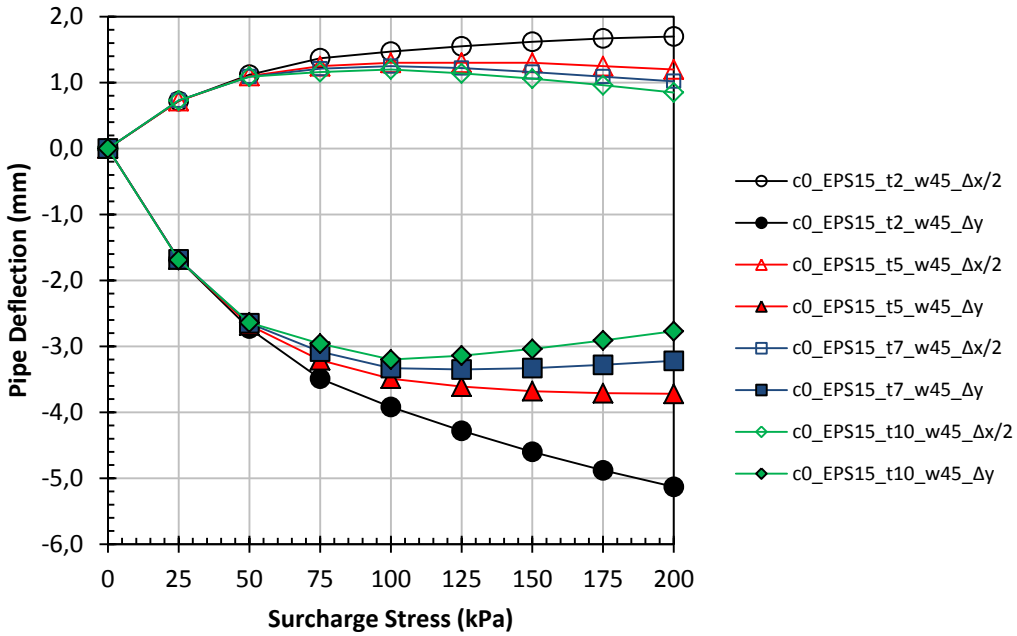

Figure 5.21. Effect of EPS-15 thickness while width=45 cm

In the case of using EPS-15, the effect of thickness for width = 30 cm, 37.5 cm and 45 cm was given as Figure 5.19, Figure 5.20 and Figure 5.21, respectively. As in the case of EPS-10, in the case of using EPS-15, pipe deformations decreased as EPS thickness increased. Although the surcharge stress increased, the increase in horizontal and vertical deflections remained almost same at a surcharge stress of 100-125 kPa in all combinations except for 2 cm thick geofoam. It yields that mobilization of full arching takes place at relatively higher stresses. In the case of using 2 cm thick EPS geofoam, pipe deflections increased with increasing surcharge stress. Nevertheless, a significant improvement was achieved even when 2 cm thick EPS-15 geofoam material was placed in the crown of the pipe.

5.3.3 EPS Density=20 kg/m^3

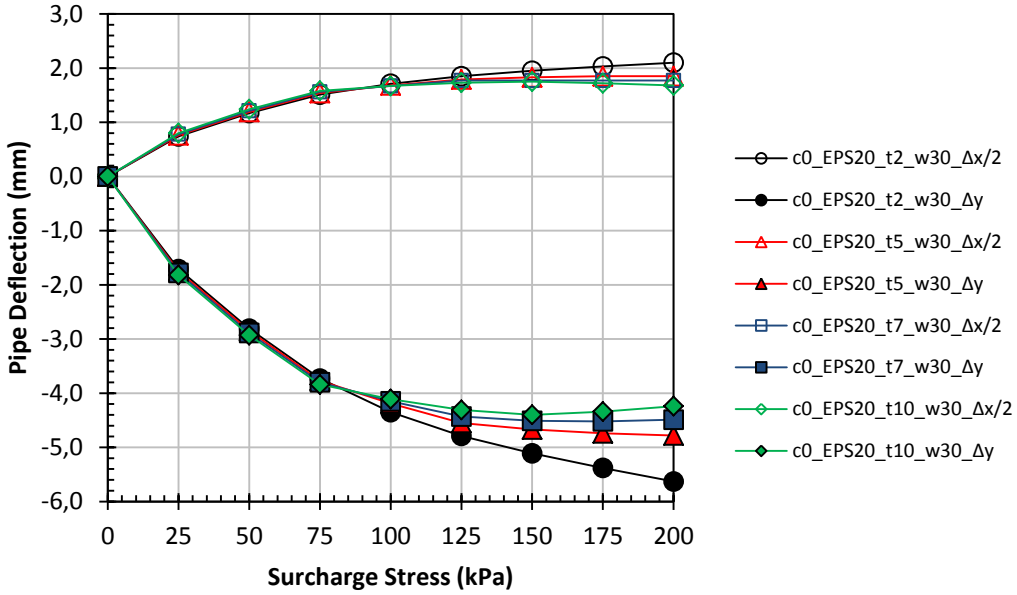

Figure 5.22. Effect of EPS-20 thickness while width=30 cm

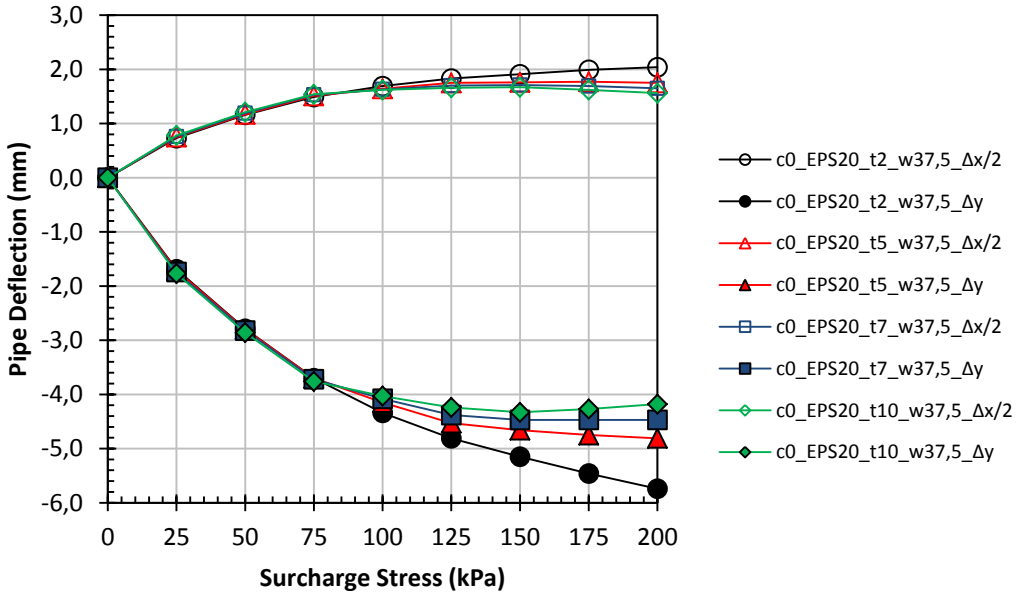

Figure 5.23. Effect of EPS-20 thickness while width=37.5 cm

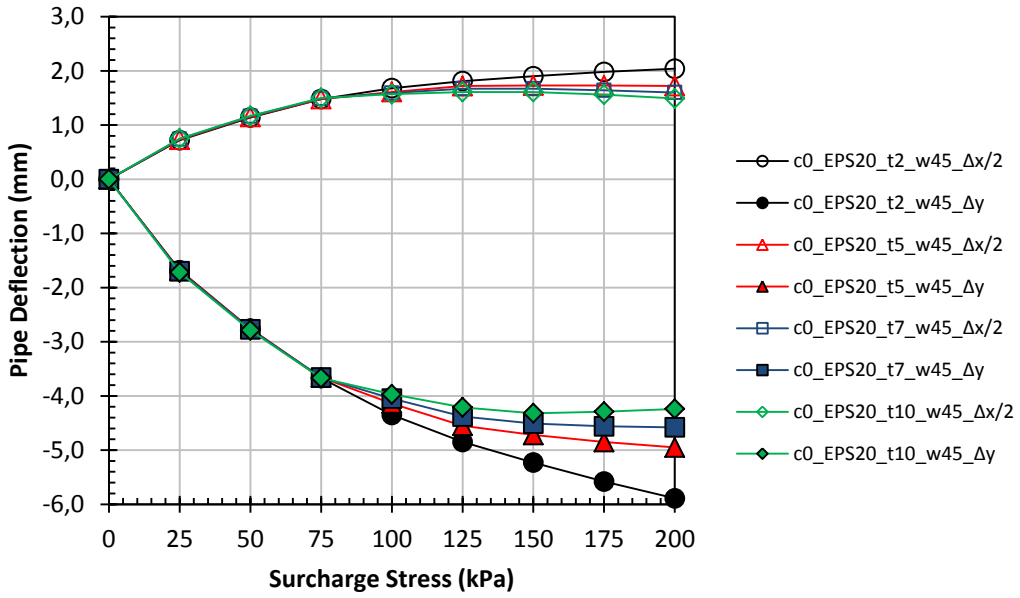

Figure 5.24. Effect of EPS-20 thickness while width=45 cm

In the case of using EPS-20, the effect of thickness for width = 30 cm, 37.5 cm and 45 cm was given as Figure 5.22, Figure 5.23 and Figure 5.24, respectively. As in the case of EPS-10 and EPS-15, in the case of using EPS-20, pipe deformations decreased as EPS thickness increased for all widths.

From aforementioned findings, there is no doubt that, increase in the EPS thickness decreases the pipe deflections for all widths and densities. As the density of EPS increases, the amount of improvement achieved with increasing thickness decreases.

Another important finding is that 2 cm thick EPS geofoam is not enough to develop the arching fully. For all densities and widths, 5 cm EPS geofoam is enough to mobilize the arching fully. The benefit of EPS thickness has been best traced in the softest EPS case. In the case of placing 10 cm thick EPS-10 at pipe crown, the deflection behavior of the deformable pipe tends to revert to the its initial state as the surcharge stress increases.

5.4 Effect of the EPS Geofoam Density

In order to examine the effect of density, parametric numerical analyses were conducted for all widths and thicknesses. In the graphs, all variables kept constant except density so that for every combination, effect of density could be investigated.

5.4.1 Width=30 cm

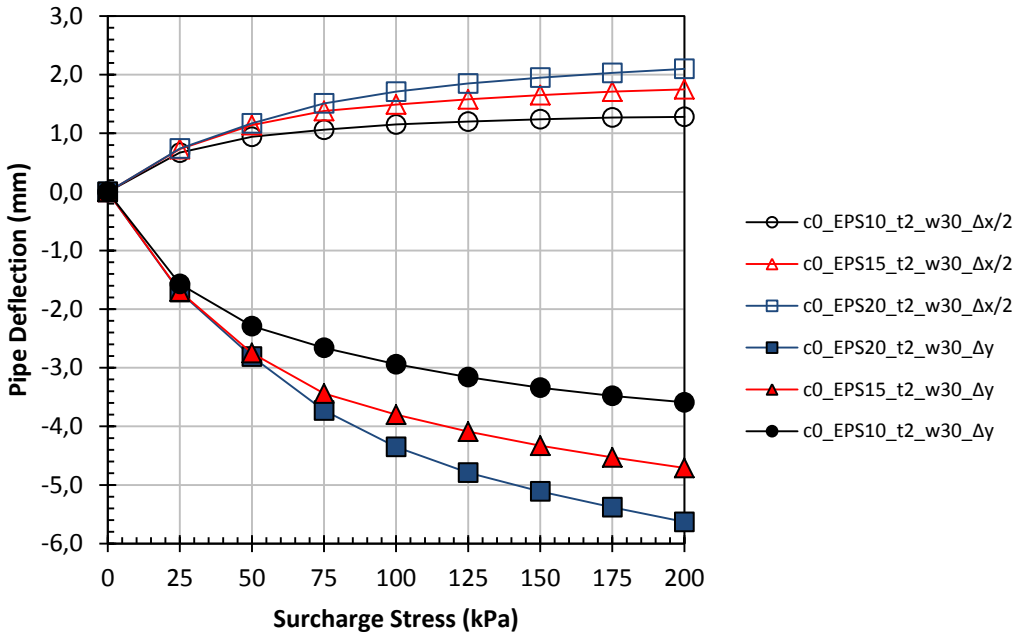

Figure 5.25. Effect of EPS density while width=30 cm & thickness=2 cm

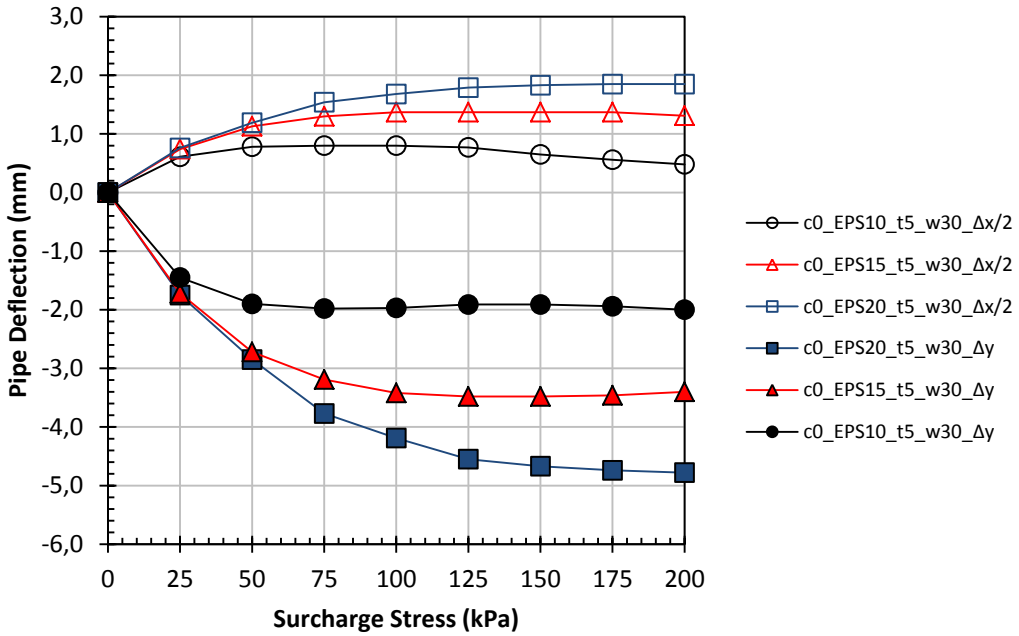

Figure 5.26. Effect of EPS density while width=30 cm & thickness=5 cm

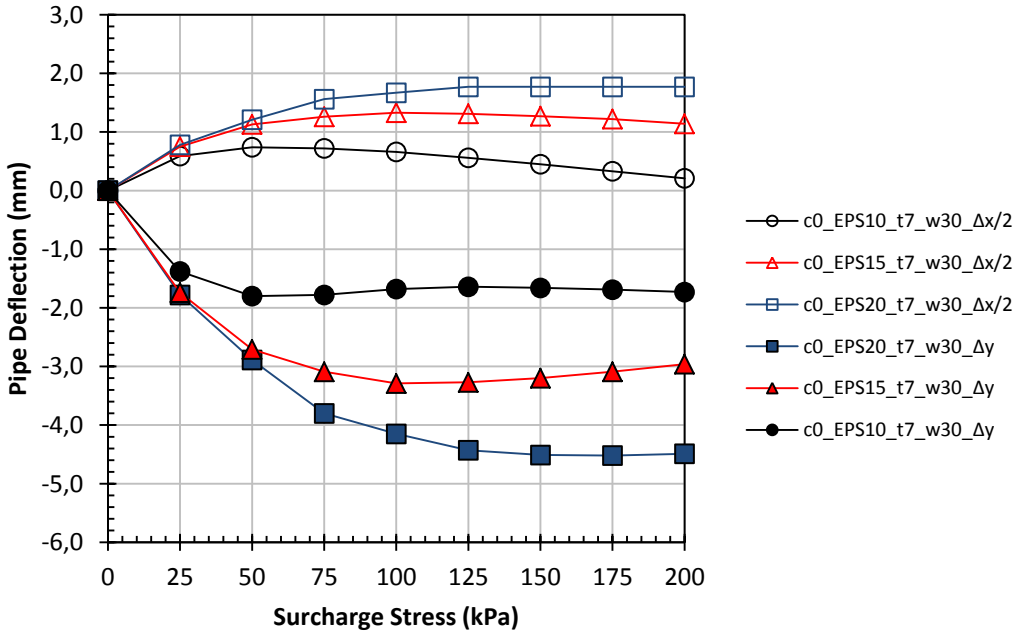

Figure 5.27. Effect of EPS density while width=30 cm & thickness=7 cm

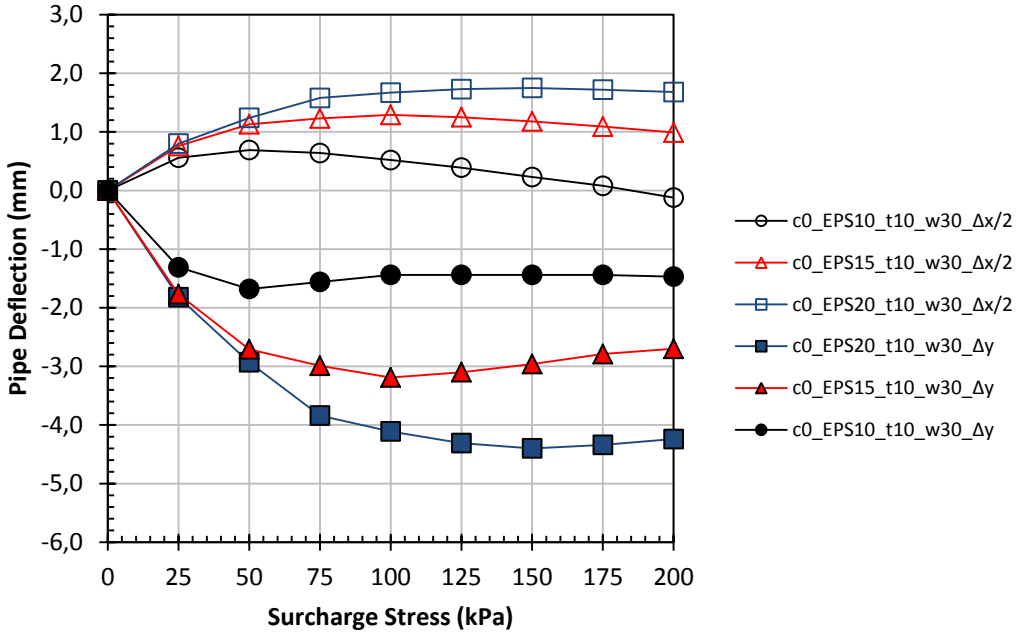

Figure 5.28. Effect of EPS density while width=30 cm & thickness=10 cm

5.4.2 Width=37.5 cm

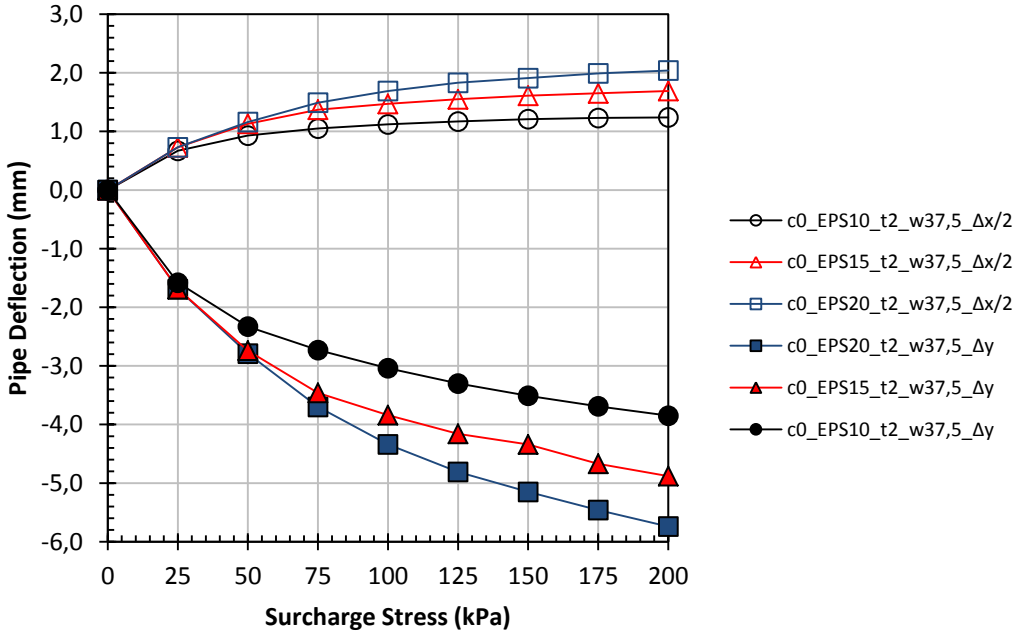

Figure 5.29. Effect of EPS density while width=37.5 cm & thickness=2 cm

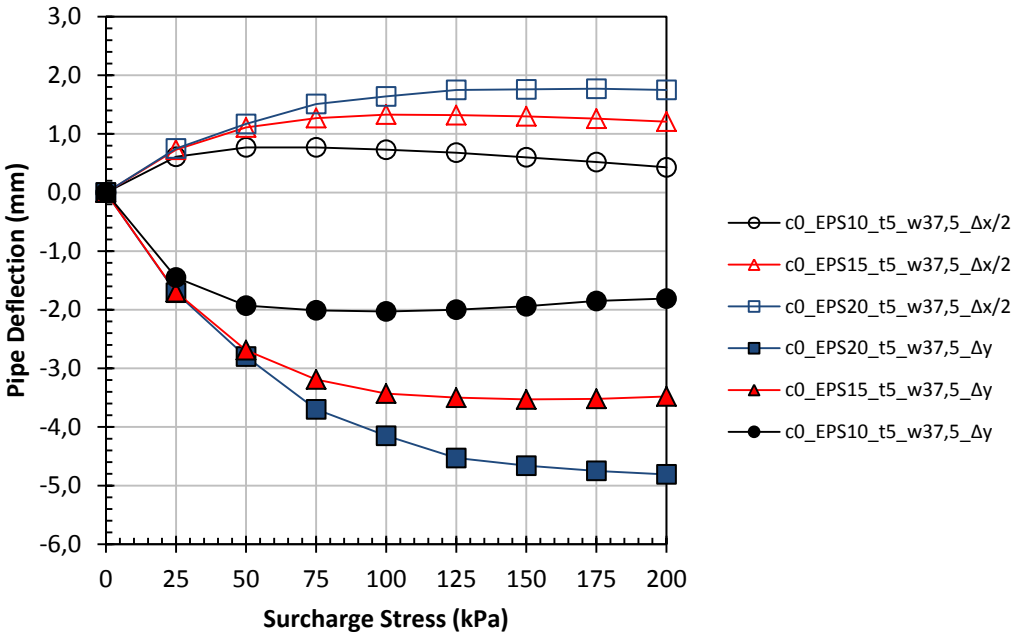

Figure 5.30. Effect of EPS density while width=37.5 cm & thickness=5 cm

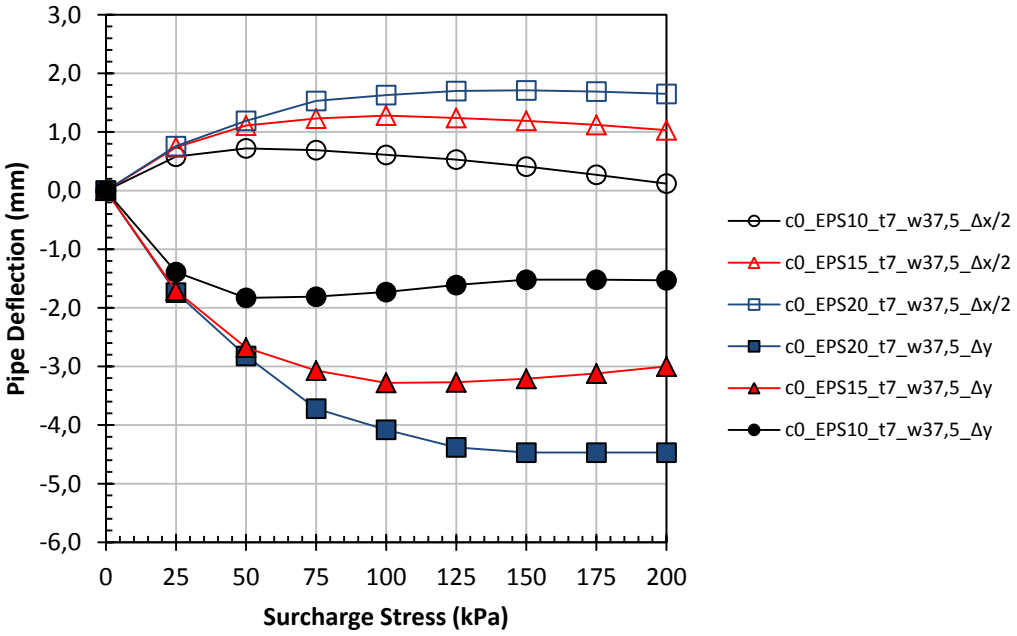

Figure 5.31. Effect of EPS density while width=37.5 cm & thickness=7 cm

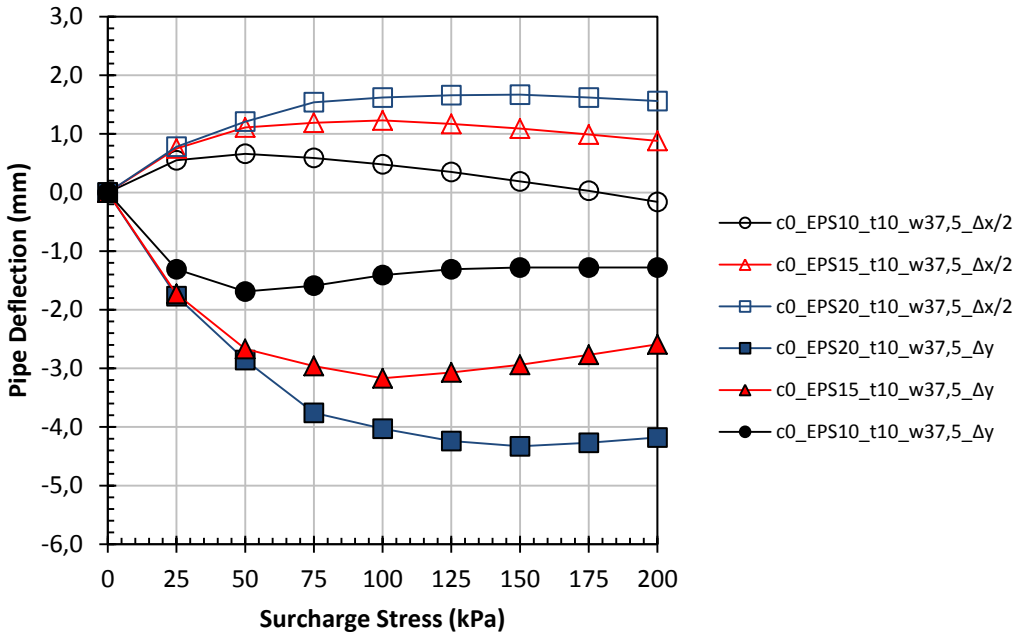

Figure 5.32. Effect of EPS density while width=37.5 cm & thickness=10 cm

5.4.3 Width=45 cm

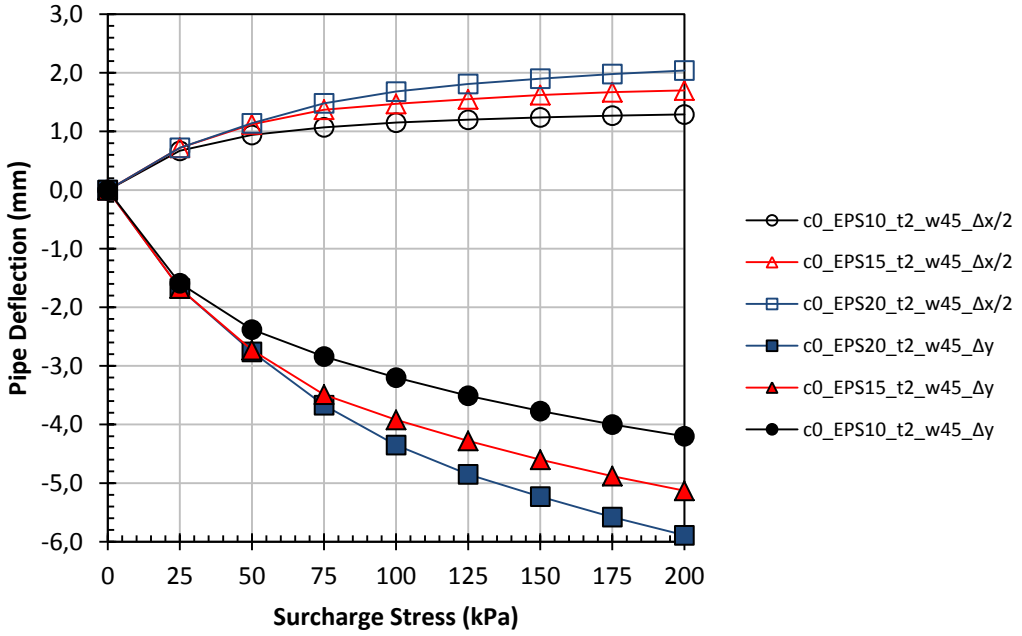

Figure 5.33. Effect of EPS density while width=45 cm & thickness=2 cm

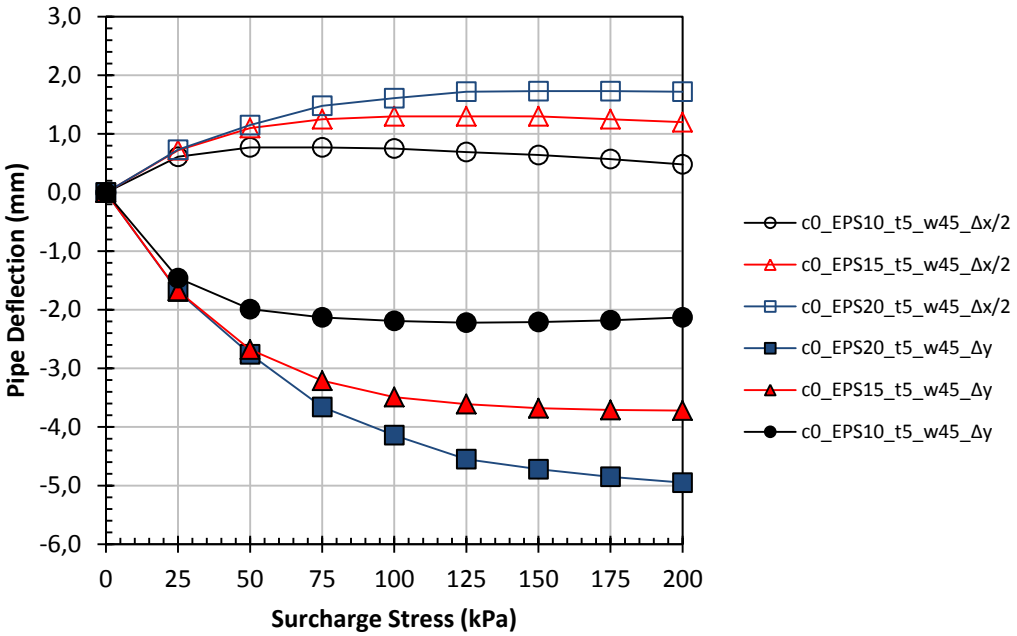

Figure 5.34. Effect of EPS density while width=45 cm & thickness=5 cm

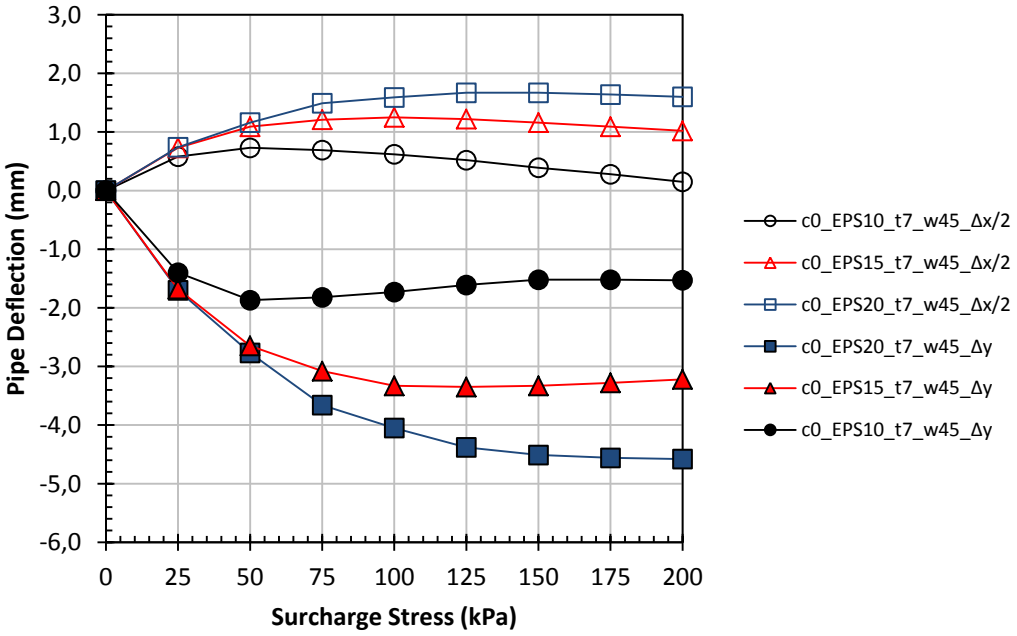

Figure 5.35. Effect of EPS density while width=45 cm & thickness=7 cm

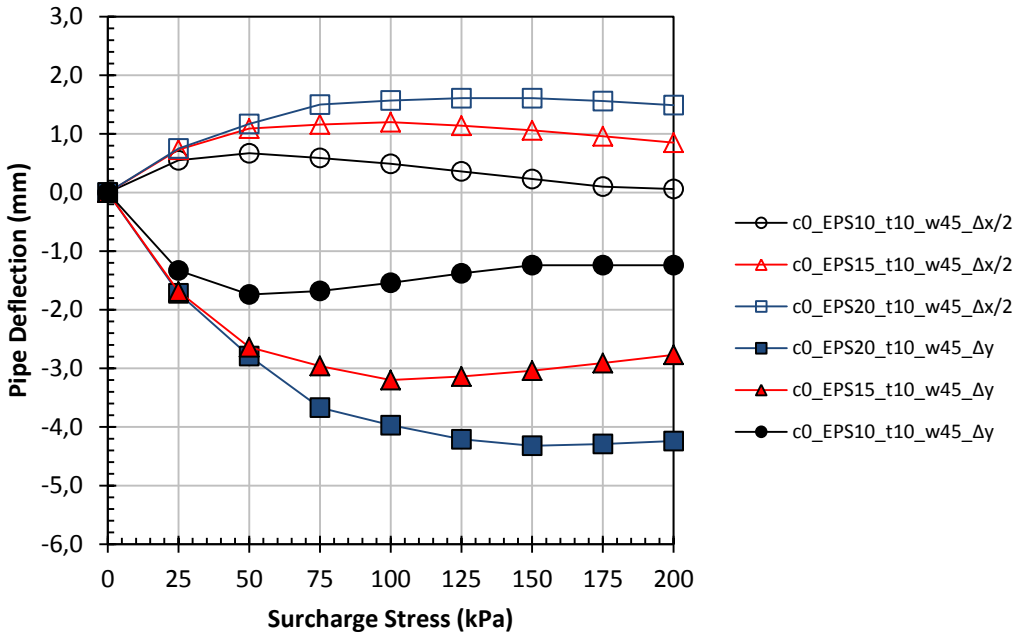

Figure 5.36. Effect of EPS density while width=45 cm & thickness=10 cm

The effect of density in the cases of width=30, 37.5 and 45 cm was shown on Figure 5.25 - Figure 5.36 for thicknesses of 2 cm, 5 cm, 7 cm and 10 cm. In all combinations presented above, while density of EPS geofoam increases, pipe deflections were also increased. Therefore, it can be concluded that the more compressible EPS geofoam shows better performance.

Another conclusion for all densities, 2 cm thick EPS geofoam is not enough to develop full arching mobilization. While EPS density increases, required stress for fully arching mobilization increases. For EPS-10, full arching developed at 50 kPa for all thicknesses except 2 cm. For EPS-15, full arching developed between stresses of 100 – 200 kPa for all thicknesses except 2 cm. However, for EPS-20, full mobilization of arching could only be possible between surcharge stresses of 175 – 200 kPa for only thicknesses of 7 cm and 10 cm. In the case of using EPS-20 with thicknesses of 2 cm and 5 cm, full arching mobilization was not observed.

5.5 Effect of the EPS Geofoam Width

As it was clearly demonstrated in the previous sections of the study, the highest performance was achieved at the lowest EPS density. The necessity of placing EPS geofoam on just above the pipe crown, instead of 5 cm or 10 cm away, was specified at first. However, for EPS geofoam depending on the surcharge stress, there might be strain values that should not be exceeded in practice. In addition, Söylemez (2017) shows that creating a compressible zone above the flexible pipe when EPS geofoam yields is not beneficial for pipe deflections, but is harmful. Therefore, although the best performance is shown by EPS-10, it may be necessary to use EPS-15 or EPS-20 depending on the effective stress increase at the location of EPS geofoam

In the meantime, it is explained that the arching effect is completely mobilized in case of using EPS geofoam with 5 cm (for EPS-10 and EPS-15) and 7 cm (for EPS-20) thickness at least. Likewise, it may be necessary to use EPS geofoam thicker than 5 cm (or 7 cm) in order to reduce the axial strain value on the EPS geofoam or to achieve the targeted improvement performance. For this reason, all densities and all thicknesses are taken into consideration while examining the width effect.

5.5.1 EPS Density=10 kg/m^3

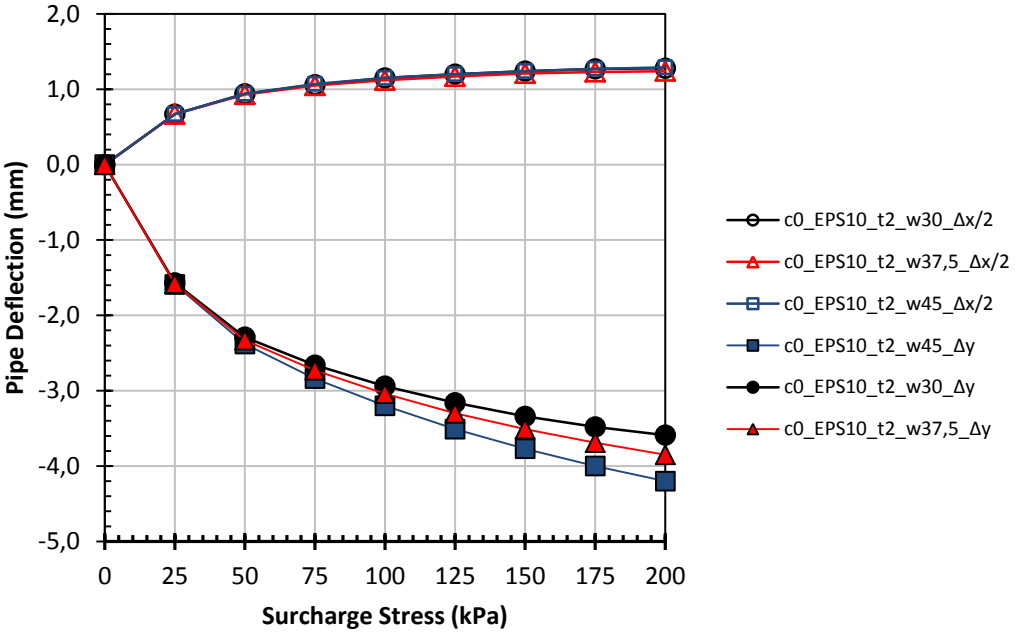

Figure 5.37. Effect of EPS width while density=10 kg/m^3 & thickness=2 cm

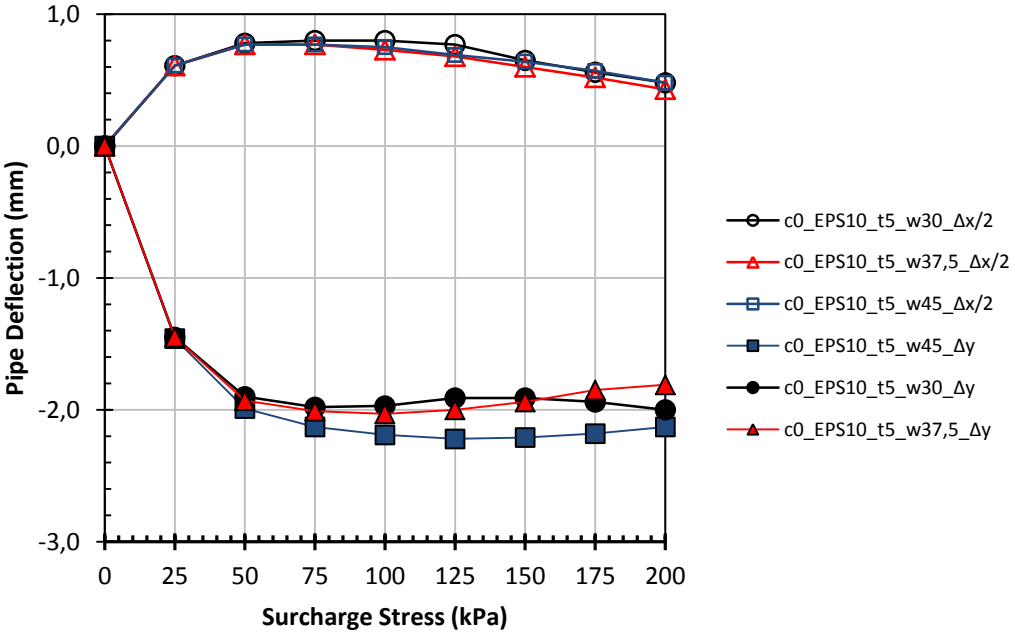

Figure 5.38. Effect of EPS width while density=10 kg/m^3 & thickness=5 cm

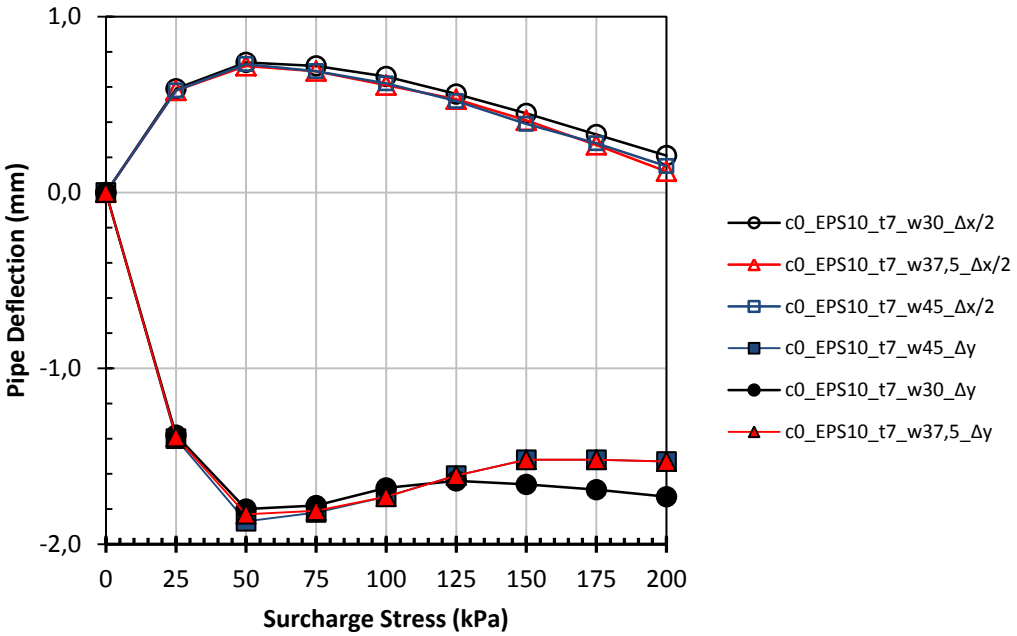

Figure 5.39. Effect of EPS width while density=10 kg/m^3 & thickness=7 cm

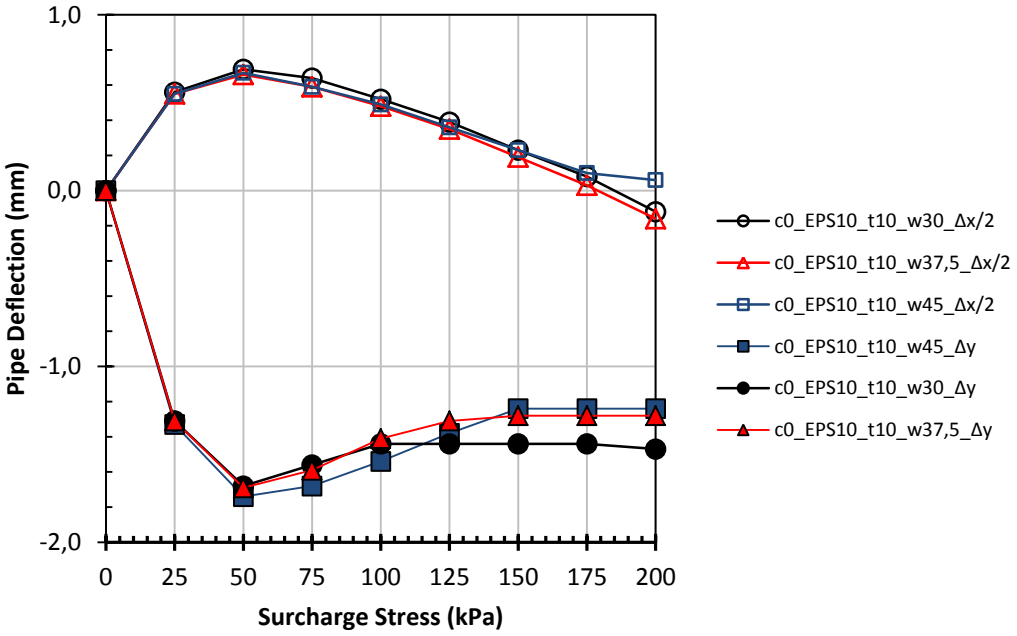

Figure 5.40. Effect of EPS width while density=10 kg/m^3 & thickness=10 cm

5.5.2 EPS Density=15 kg/m^3

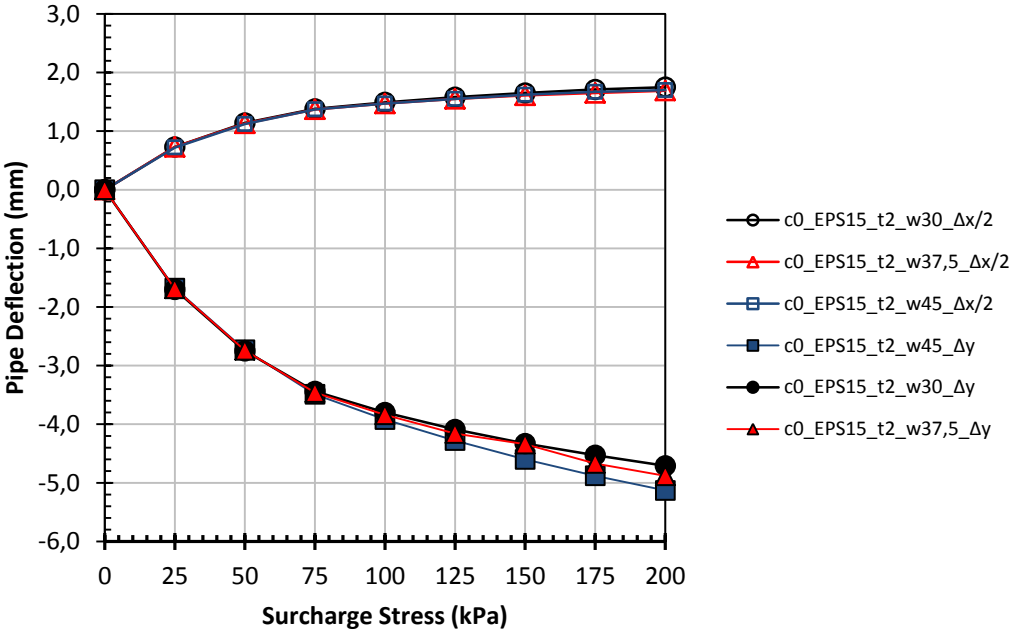

Figure 5.41. Effect of EPS width while density=15 kg/m^3 & thickness=2 cm

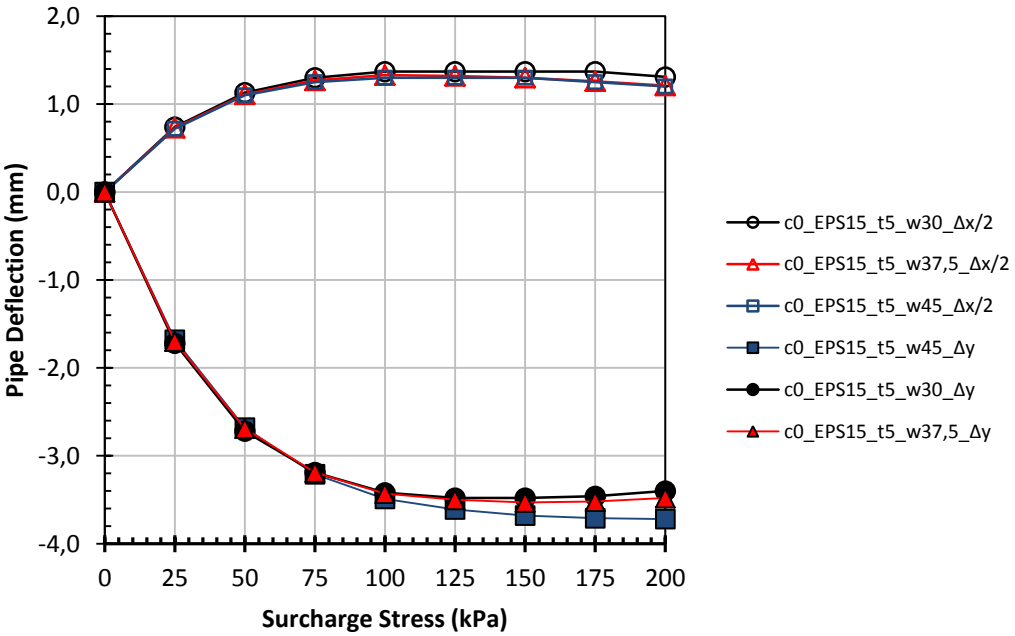

Figure 5.42. Effect of EPS width while density=15 kg/m^3 & thickness=5 cm

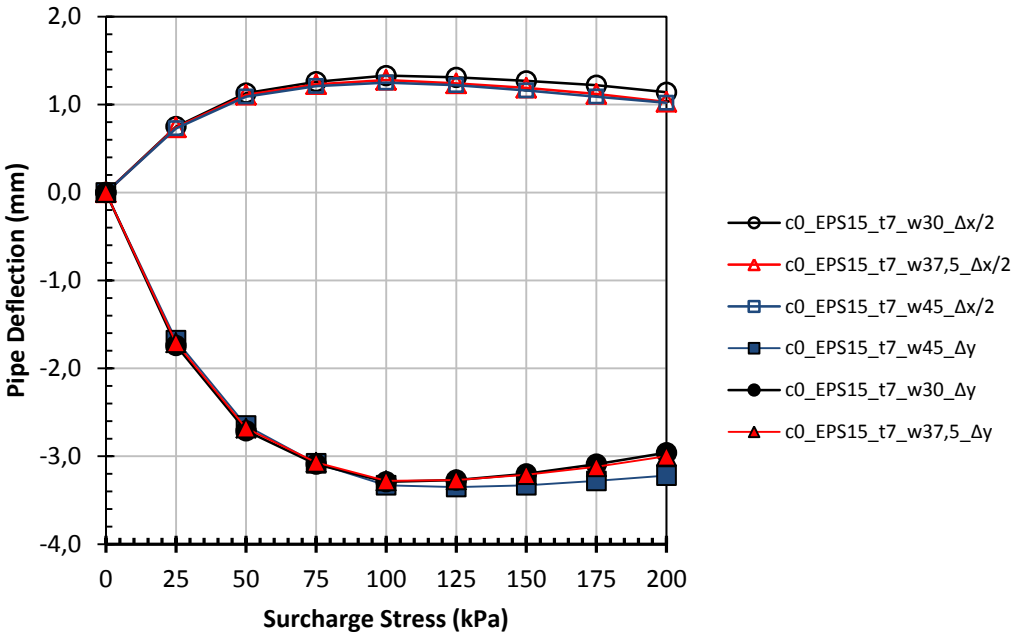

Figure 5.43. Effect of EPS width while density=15 kg/m^3 & thickness=7 cm

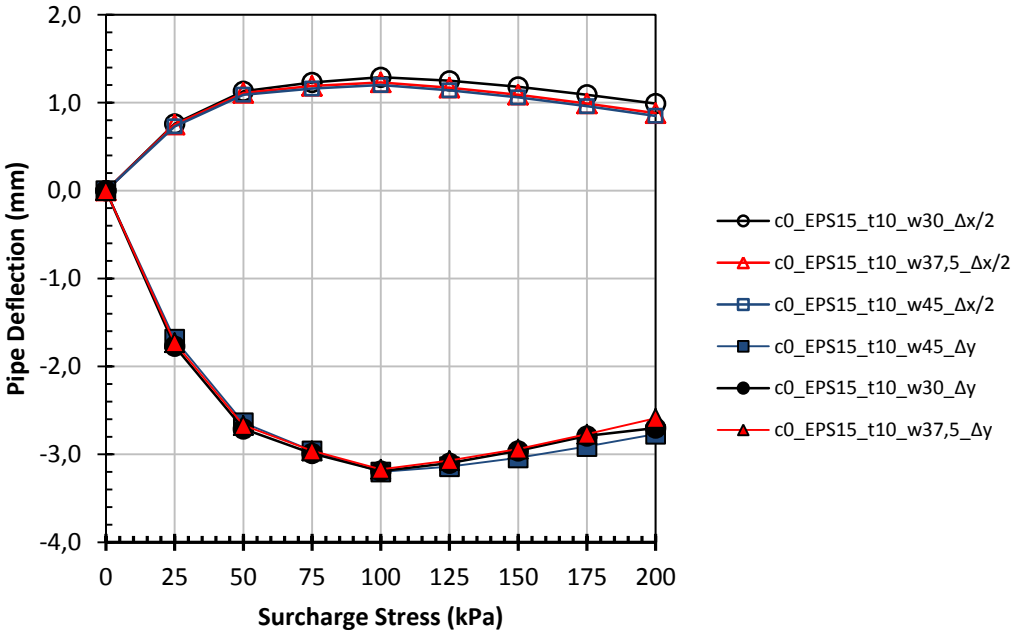

Figure 5.44. Effect of EPS width while density=15 kg/m^3 & thickness=10 cm

5.5.3 EPS Density=20 kg/m^3

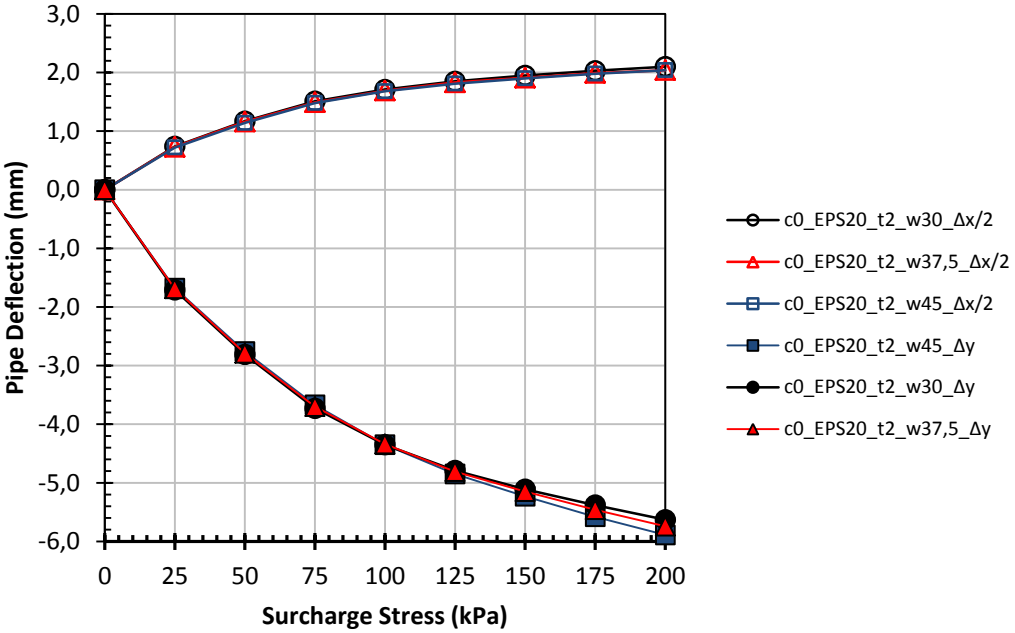

Figure 5.45. Effect of EPS width while density=20 kg/m^3 & thickness=2 cm

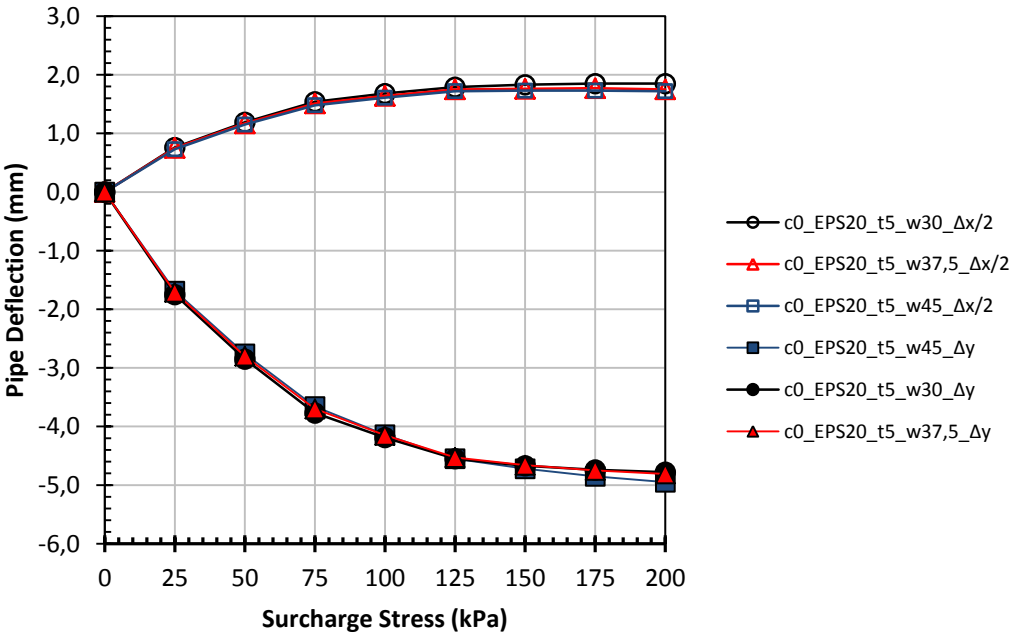

Figure 5.46. Effect of EPS width while density=20 kg/m^3 & thickness=5 cm

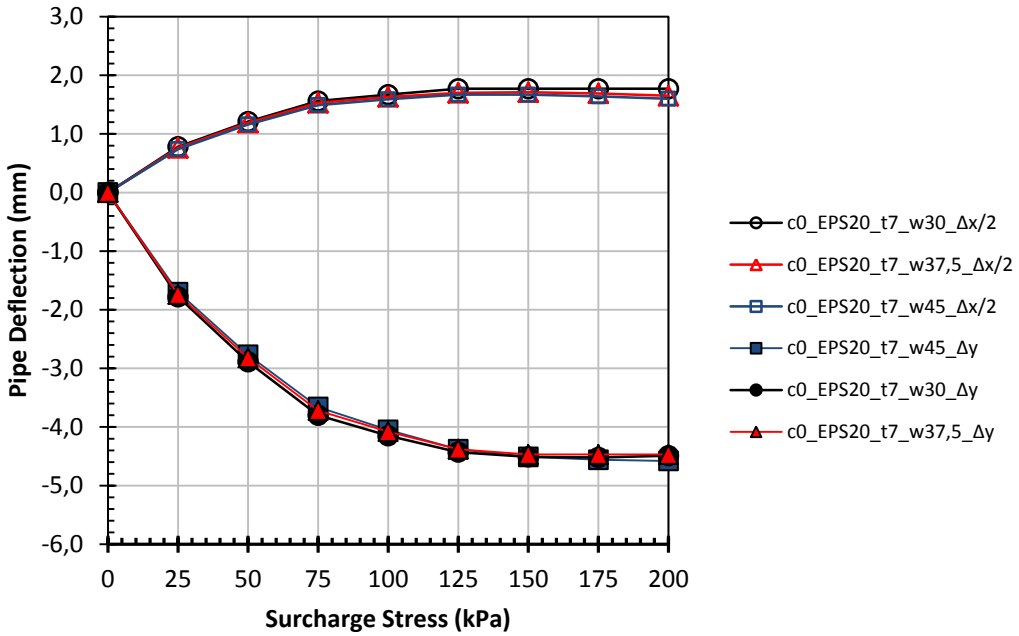

Figure 5.47. Effect of EPS width while density=20 kg/m^3 & thickness=7 cm

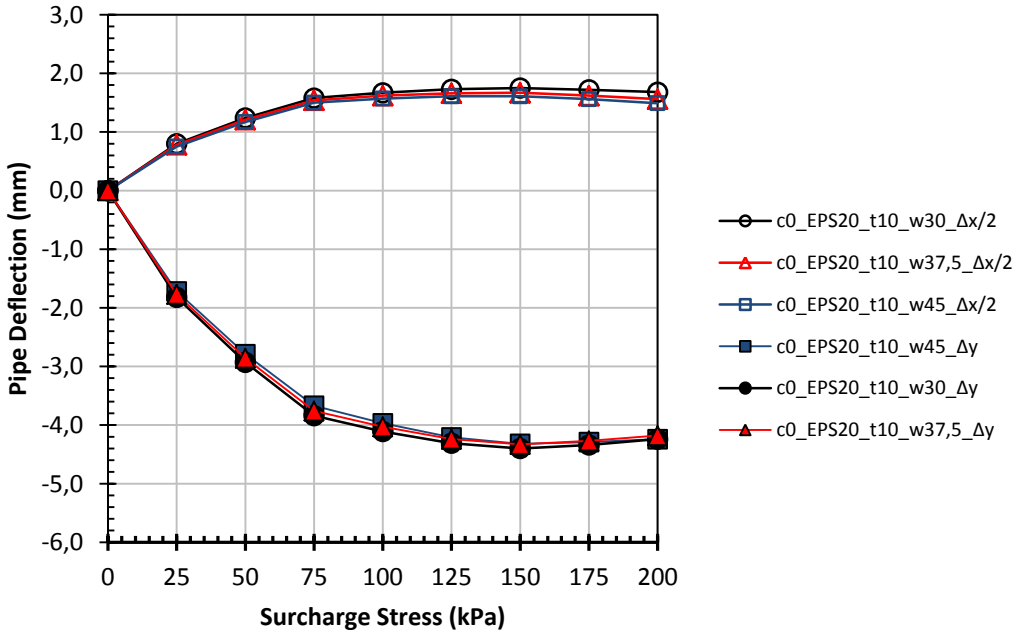

Figure 5.48. Effect of EPS width while density=20 kg/m^3 & thickness=10 cm

With respect to figures (between Figure 5.37 - Figure 5.48) shown above, the effect of width has no significant importance on improvement performance. Evaluation of the figures was made for demonstration purposes for EPS-10 combinations below.

- When 2 cm thick EPS-10 geofoam is placed just above the pipe crown, W30 and W45 give the same performance in terms of horizontal displacement, while W37.5 performs slightly better with insignificant difference. The W30 performed best in terms of vertical displacement.
- Numerically, W37.5 gives the best result in terms of horizontal displacement when 5 cm thick EPS-10 geofoam is placed just above the pipe crown. In terms of vertical displacement, up to 150 kPa, W30 shows the best performance, after 150 kPa, W37.5 performed better.
- In the case where 7 and 10 cm thick EPS-10 geofoam is placed just above the pipe crown, it gives the best result in terms of horizontal displacement of W37.5, but the difference is very small. In terms of vertical displacement, the W30 gives the best performance up to approximately 100 kPa, while at higher load levels W37.5 and W45 performs better than W30.

Likewise, W30 shows the best overall performance for EPS-15, while for EPS-20 the difference among widths is negligible. The one another conclusion that can be drawn regarding EPS width is that as the ratio of geofoam's deformation modulus to be used gets closer to the modulus of the ground, the geofoam width effect disappears.

Lastly, for the case of using wider EPS geofoam than one pipe diameter, it can be concluded that effect of EPS width does not affect the deformation behavior of flexible pipe too much. Therefore, for the design purposes, it is strictly recommended to investigate effect of width on pipe performance with related material parameters.

5.6 Effect of Two Layers and Spacing

From previous discussions, it was concluded that increase in the thickness of the EPS geofoam increases the improvement on the shallowly buried flexible pipe deformations. At this point, the idea of using EPS geofoam material with the same thickness in two layers and the question to what extent this idea will affect the pipe deformation arises. In order to reveal the answers to these questions, the cases where EPS geofoams of 2 cm and 3 cm thickness, represents the total of 5 cm of geofoam thickness, and 5 cm thickness of geofoams, represents the total of 10 cm of EPS geofoam, were placed on pipes in different configurations.

As described in the previous sections of the study, EPS-10 and W30 geofoam were used in this part of the study since the effect of geofoam width on improvement performance is not distinguishable and the highest performance is obtained in EPS-10 geofoam.

In the analysis, vertical and horizontal pipe deflections (in mm) for single EPS geofoam layer were notated as Δy and $\Delta x/2$, respectively as explained before (Figure 5.1).

cX_tX_ΔX

Where;

cX denotes location of EPS geofoam layer (in cm)

- X can be 0 (at crown), 5 (above 5 cm from pipe crown) and 10 (above 10 cm from pipe crown)

tX denotes thickness of EPS geofoam (in cm)

- X can be 5 and 10

c0_t5_ΔX/2

denotes that EPS geofoam with thickness of 5 cm is located at the crown of the HDPE pipe crown.

For the case of multiple EPS geofoam layer, analysis combinations were distinguished with following notation;

$$cX\_tX+tX\_(S=X)\_\Delta X$$

Where;

cX denotes location of the first EPS geofoam layer (in cm)

- X can be 0 (at crown), 2 (above 2 cm from pipe crown) and 5 (above 5 cm from pipe crown)

tX+tX denotes thickness of EPS geofoam (in cm) in the order of proximity to the pipe crown

- X can be 2, 3 and 5

(S=X) denotes the spacing between two consecutive EPS geofoam layers (in cm)

- X can be 2, 3 and 5

$$c2\_t3+t2\_(S=5)\_\Delta Y$$

denotes that 3 cm thickness of EPS geofoam located 2 cm above the pipe crown and 2 cm thickness of EPS geofoam located 5 cm above the first EPS geofoam layer.

5.6.1 EPS Thickness of 5 cm

Effect of placing two layers EPS geofoam, in total thickness of 5 cm, above the pipe crown in different spacing and also effect of spacing between two consecutive EPS geofoam were investigated under this title. Figure 5.49 shows the placement of two layers EPS geofoam combinations for total thickness of 5 cm.

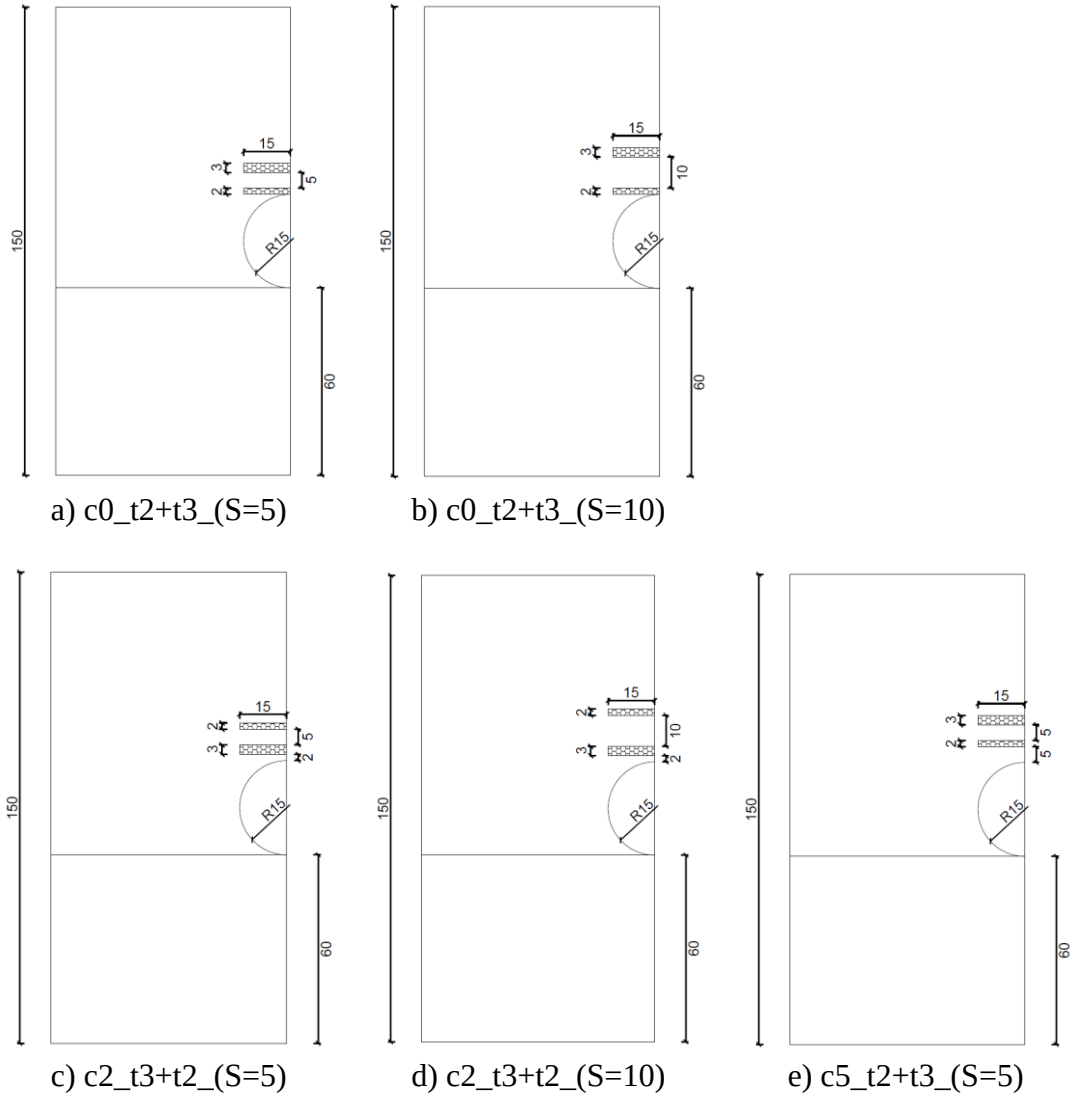

a) c0_t2+t3_(S=5) b) c0_t2+t3_(S=10)

c) c2_t3+t2_(S=5) d) c2_t3+t2_(S=10) e) c5_t2+t3_(S=5)

Figure 5.49. Two layers EPS combinations for total thickness of 5 cm

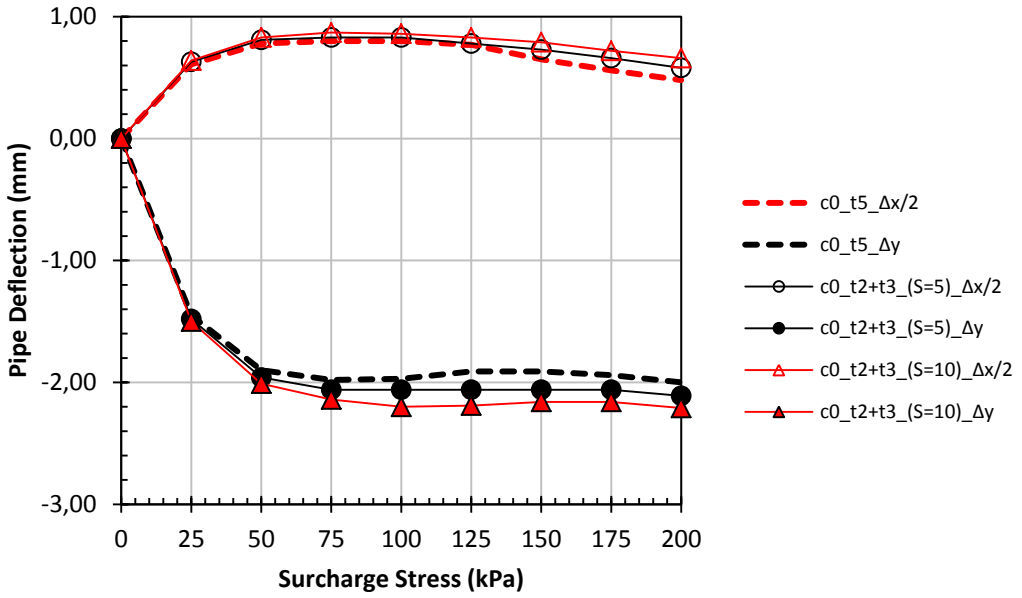

Figure 5.50. Two layers comparison of EPS geofoam for 5 cm thick in total (first layer at crown)

From Figure 5.50, it can be concluded that placing 5 cm EPS geofoam at the pipe crown shows better performance than placing 2 cm EPS geofoam at the pipe crown and 3 cm EPS geofoam 5 and 10 cm above the first layer. Also when the spacing between two consecutive EPS geofoam smaller, better improvement obtained in the pipe deflections. Likewise, Figure 5.51 and Figure 5.52 shows that placing a single 5 cm thick EPS geofoam shows better performance than any other combinations of placing a total thickness of 5 cm EPS geofoam above the HDPE pipe at any location. Another conclusion can be drawn as better improvement performance can be obtained when more EPS geofoam, volumetrically, is placed close to the pipe crown.

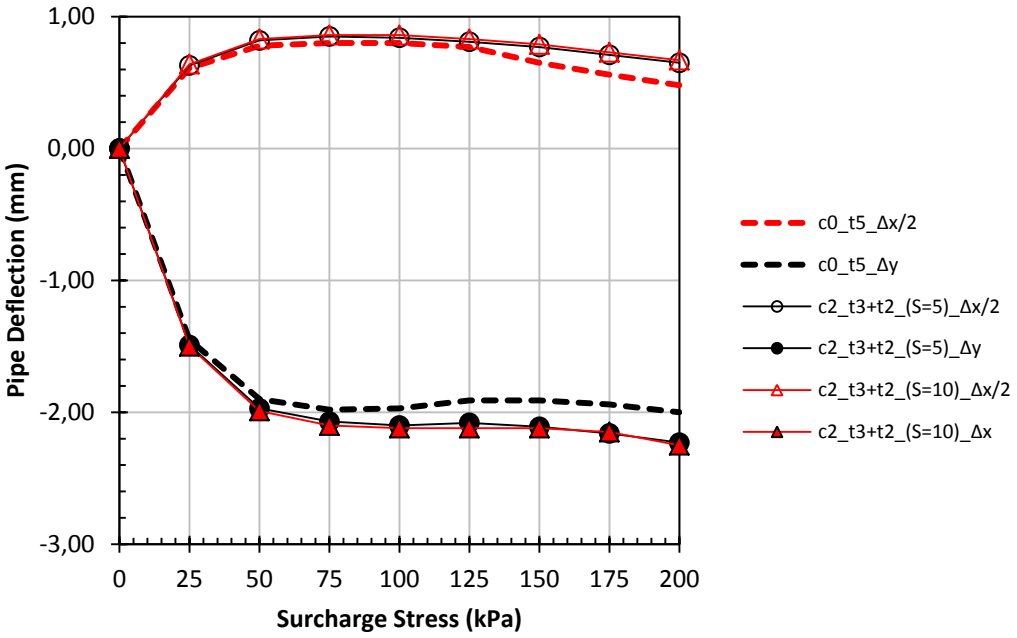

Figure 5.51. Two layers comparison of EPS geofoam for 5 cm thick in total (first layer at 2 cm above the crown)

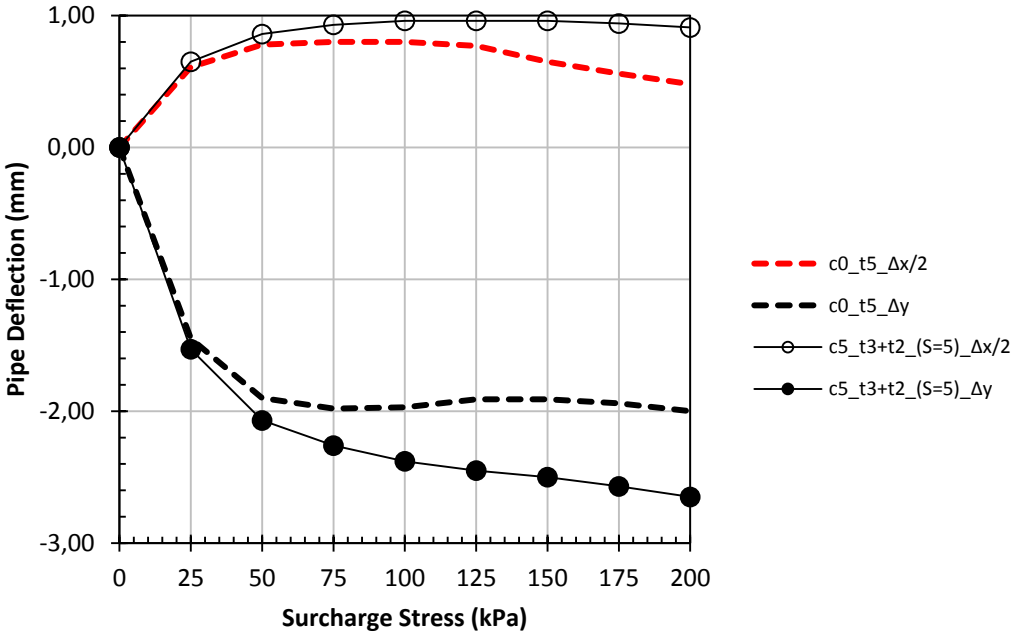

Figure 5.52. Two layers comparison of EPS geofoam for 5 cm thick in total (first layer at 5 cm above the crown)

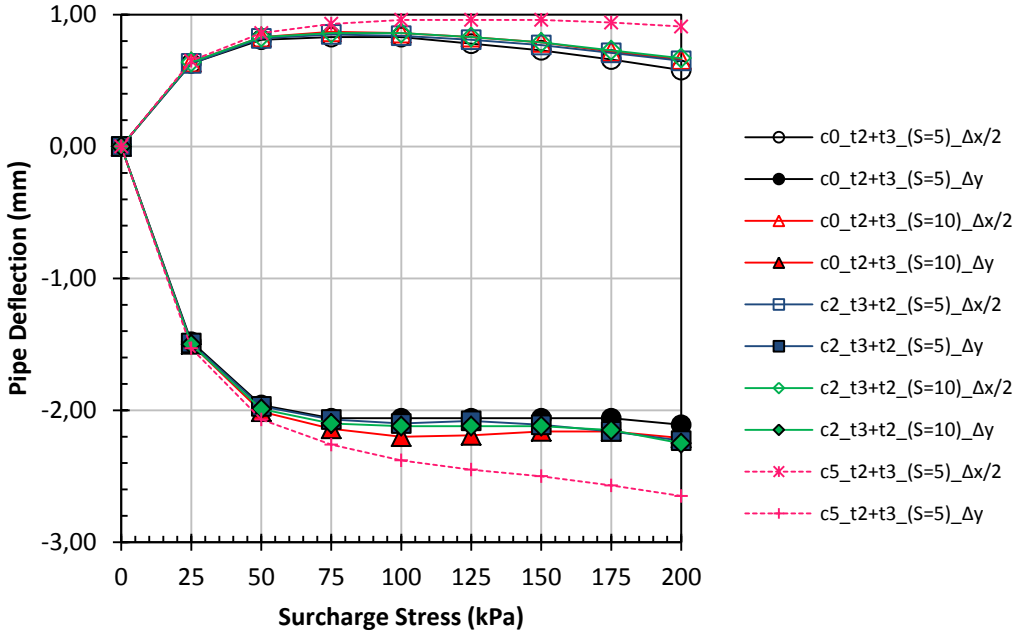

Figure 5.53. Two layers comparison of EPS geofoam for 5 cm thick in total for all combinations

One important and expected result, which is placing 3 cm thick EPS geofoam 2 cm above the pipe crown plus 2 cm thick EPS geofoam 10 cm above the first layer (c2_t3+t2_(S=10) – green diamond) shows better performance than placing 2 cm thick EPS geofoam at pipe crown plus 3 cm thick EPS geofoam 10 cm above the first layer (c0_t2+t3_(S=10) – red triangle), can be observed in Figure 5.53. This yields a conclusion that thicker EPS geofoam located close to pipe crown shows better performance than thinner EPS geofoam located at the right pipe crown.

All in all, when the EPS geofoam thickness is the same, placing multiple layer of EPS geofoam did not improve the pipe behavior better than single EPS geofoam layer. Since placement of single layer is easier than that of multiple layers, single layer EPS geofoam should be preferred.

5.6.2 EPS Thickness of 10 cm

Effect of placing two layers of EPS geofoam, in total thickness of 10 cm, above the pipe crown in different spacing and also effect of spacing between two consecutive EPS geofoam were investigated under this title. Figure 5.55 shows the placement of two layers of EPS geofoam combinations.

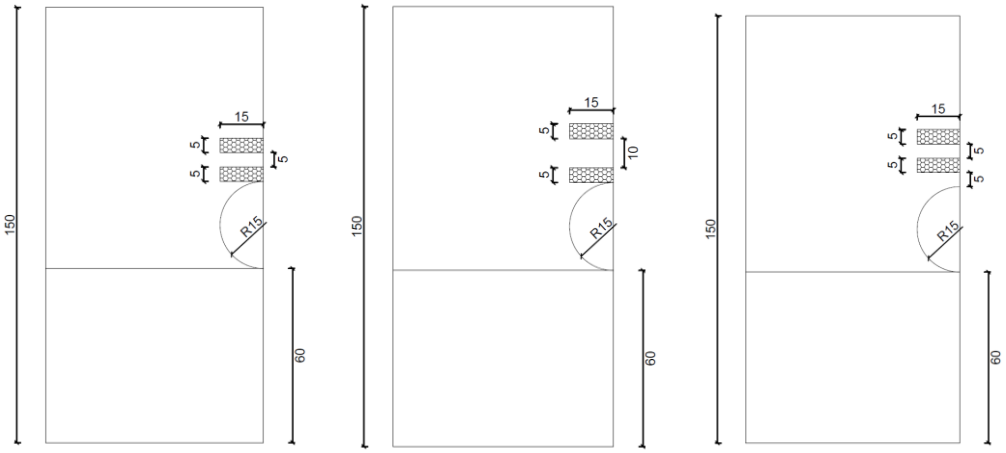

a) c0_t5+t5_(S=5) b) c0_t5+t5_(S=10) c) c5_t5+t5_(S=5)

Figure 5.54. Two layers EPS combinations for total thickness of 10 cm

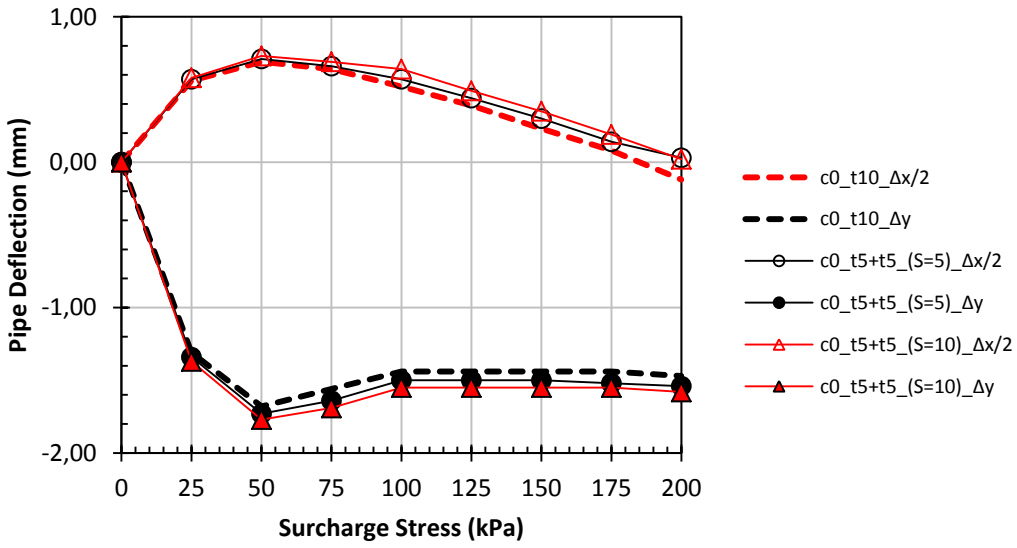

Figure 5.55. Two layers comparison of EPS geofoam for 10 cm thick in total (first layer at crown)

As can be understood from Figure 5.55, placing multiple layer geofoams with the same thickness did not provide any additional benefit. In fact, since compressible zone is farther from pipe crown, placing multiple layer of EPS geofoam decreases the improvement performance with respect to single layer geofoam with the same thickness in total. The same conclusion can be drawn for the situations that first layer of geofoam placed at pipe crown or 5 cm above the pipe crown. When compressible zone is close to pipe crown, better improvement can be achieved (Figure 5.56).

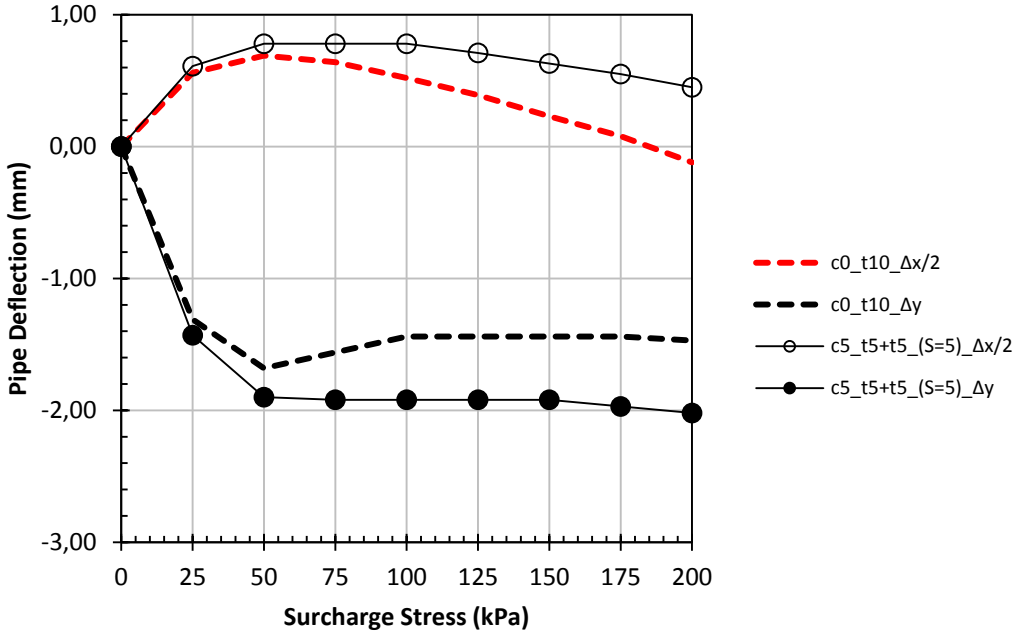

Figure 5.56. Two layers comparison of EPS geofoam for 10 cm thick in total (first layer at 5 cm above the crown)

By confirming previous results (Figure 5.57), placing 5 cm thick single EPS geofoam (c0_t5 – black and red dashed line) at the pipe crown shows almost same improvement performance with the case of placing 5 cm thick EPS geofoam at 5 cm above the pipe crown plus 5 cm thick EPS geofoam 5 cm above the first layer (c5_t5+t5_(S=5) – blue rectangle). Although amount of compressible zone is twice, placing it farther from pipe crown did not provide additional improvement with respect to single layer geofoam placed at the pipe crown.

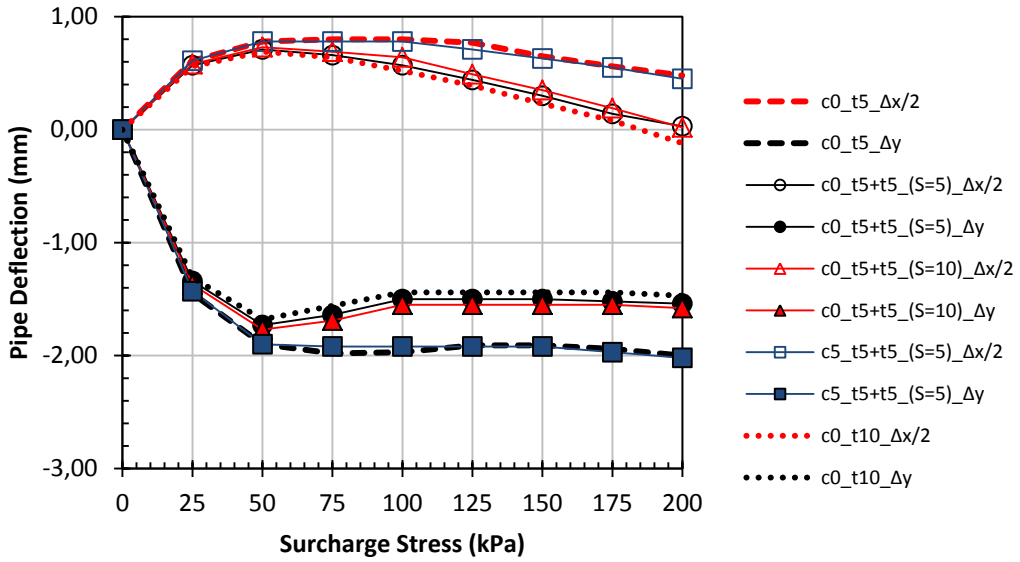

Figure 5.57. Two layers comparison of EPS geofoam for 10 cm thick in total for all combinations

One additional and important reminding at this point should be made that for the shallowly buried flexible pipes, when the multiple EPS geofoam layers placed near to surface, there is a possibility that EPS geofoam can yield earlier and at this case, resultant deformations have observed higher than even without geofoam case (Söylemez, 2017).

As a result, there is no additional improvement on pipe deflections observed in the case of using multiple layer EPS geofoam in any spacing between pipe crown and first layer, and also between two consecutive EPS geofoam layers. In fact, using single layer EPS geofoam with the same total thickness provides better improvement.

5.7 Evaluations of the Parametric Study

As a parametric study, effect of EPS location, density, thickness and width have been investigated together with effect of using two layers EPS via finite element method by using PLAXIS 2D.

In order to examine the efficiency and come up with a recommendation of EPS configuration, vertical improvement ratios (eqn. 5.1) are plotted for various EPS thicknesses under three different surcharge stresses in order to represent typical embankment loads (Figure 5.58 - Figure 5.60). As can be seen in these figures, as the thickness of EPS increases the improvement ratio increases. It can be seen that from 2 cm thick EPS to 5 cm thick EPS, there is a significant increase in the improvement ratio. However after a certain thickness value, the benefit is not too dramatic (i.e. the rate of increase of improvement ratio with EPS thickness decreases). As the thickness (therefore the cost of the EPS) increases from 5 cm to 10 cm, although required EPS volume is doubled, obtained relative improvement with respect to 5 cm thick EPS is around 7-11%, 5-9% and 2-7% for EPS-10, EPS-15 and EPS-20, respectively. Therefore by considering cost / performance 5 cm (D/6) thick EPS can be considered as optimum thickness.

$$Improvement\ (\%) = \frac{\Delta_{y,unimproved} - \Delta_{y,improved}}{\Delta_{y,unimproved}} \qquad (5.1)$$

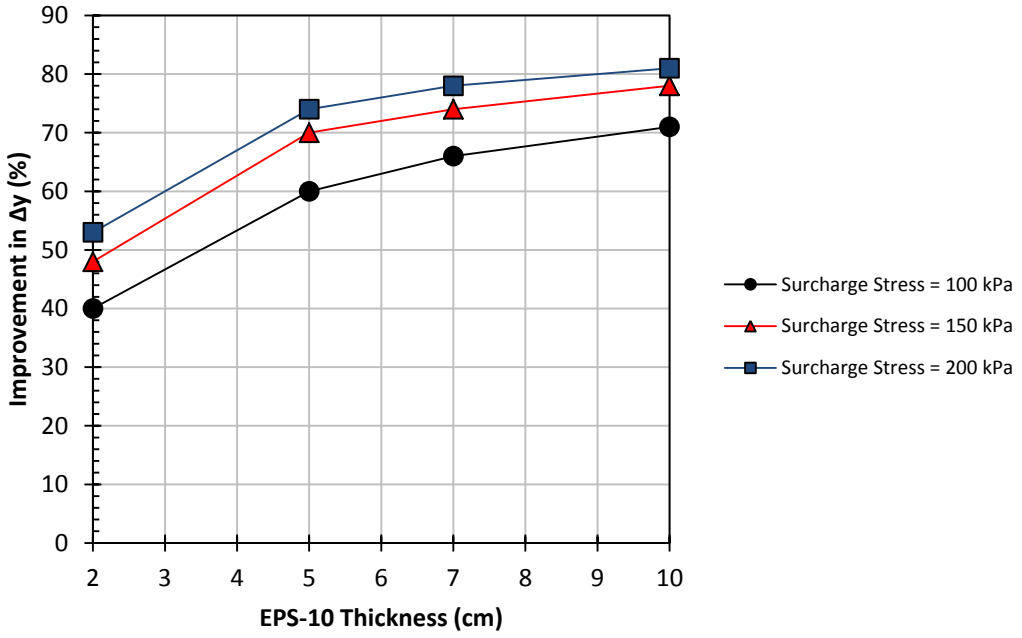

Figure 5.58. Vertical improvement ratio (%) vs. EPS-10 thickness

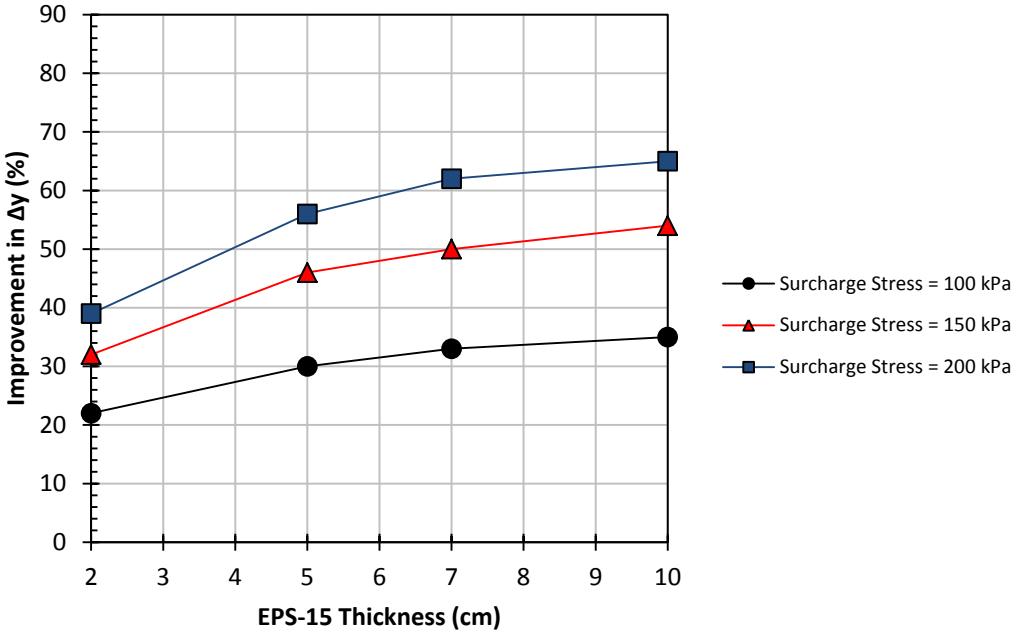

Figure 5.59. Vertical improvement ratio (%) vs. EPS-15 thickness

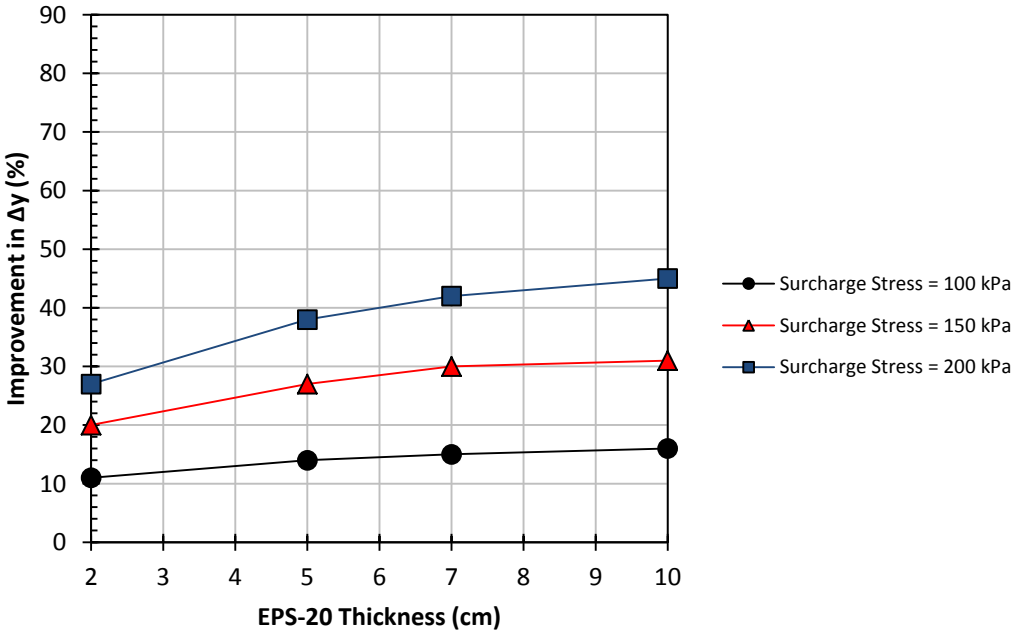

Figure 5.60. Vertical improvement ratio (%) vs. EPS-20 thickness

Although it is clear from figures related with effect of EPS width (Figure 5.37-Figure 5.48) presented in this study, in order to underline effect of EPS width in the scale of improvement ratio, additional figures are presented as Figure 5.61 - Figure 5.63, where EPS thickness is 5 cm. From these figures, it can be concluded that as the EPS width increases from 15 cm (equal to half the pipe diameter) to 30 cm which is equal to one pipe diameter, improvement performance also increases with the varying slope depending on the ratio of stiffness of the EPS to stiffness of the soil. However, beyond a certain point (one pipe diameter) for all densities it is obvious that, for the recommended thickness of 5 cm, increase in the EPS width does not provide additional improvement (yet increasing the width of EPS too much reduces the improvement ratio). Therefore, EPS width 30 cm which is equal to one pipe diameter (width=1xD) is recommended.

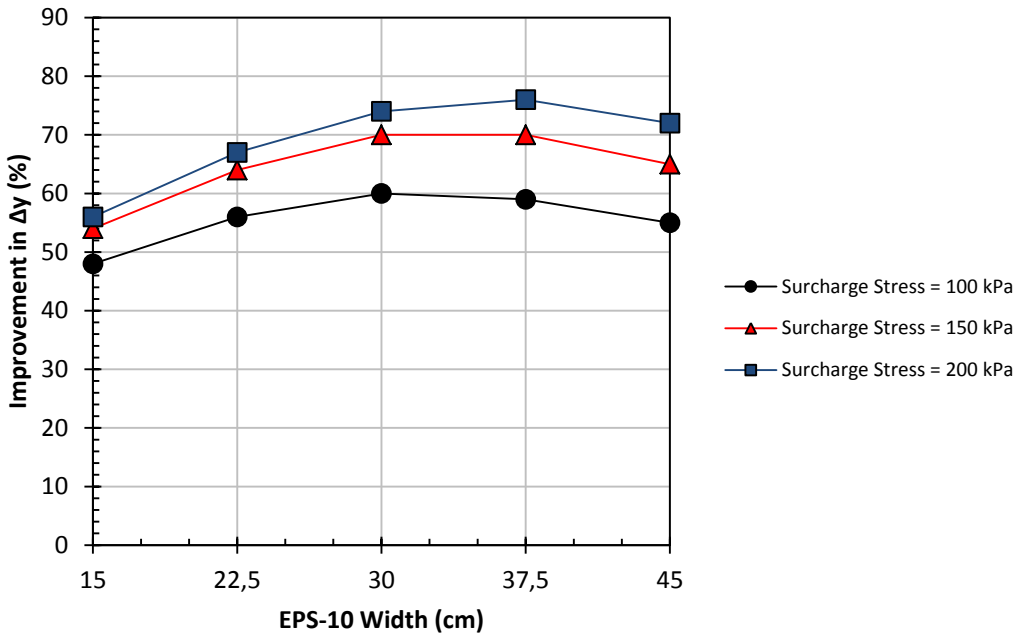

Figure 5.61. Vertical improvement ratio (%) vs. EPS-10 width

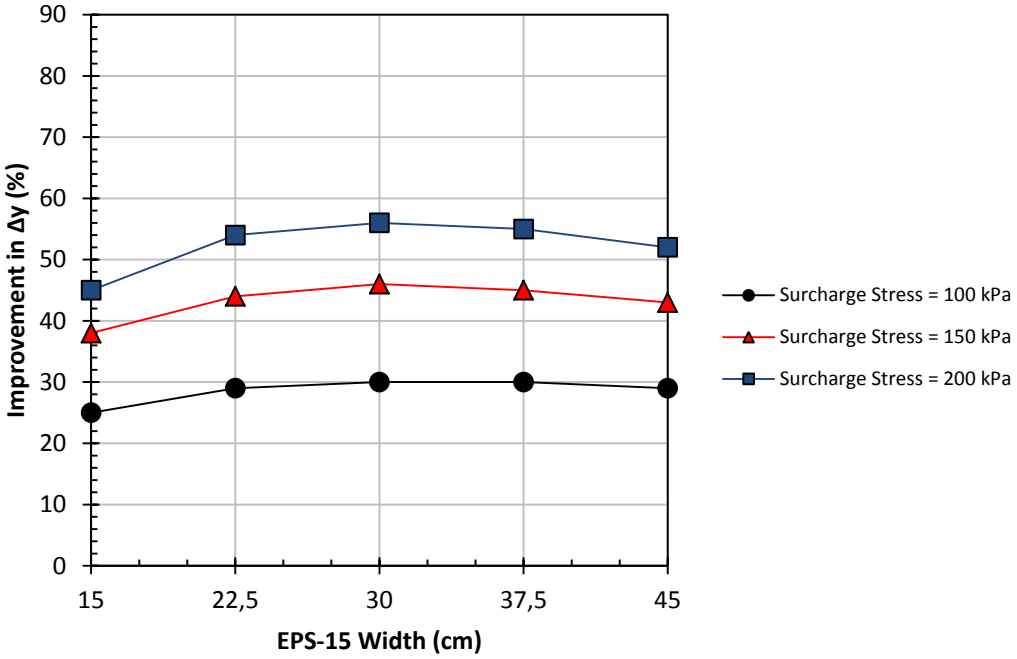

Figure 5.62. Vertical improvement ratio (%) vs. EPS-15 width

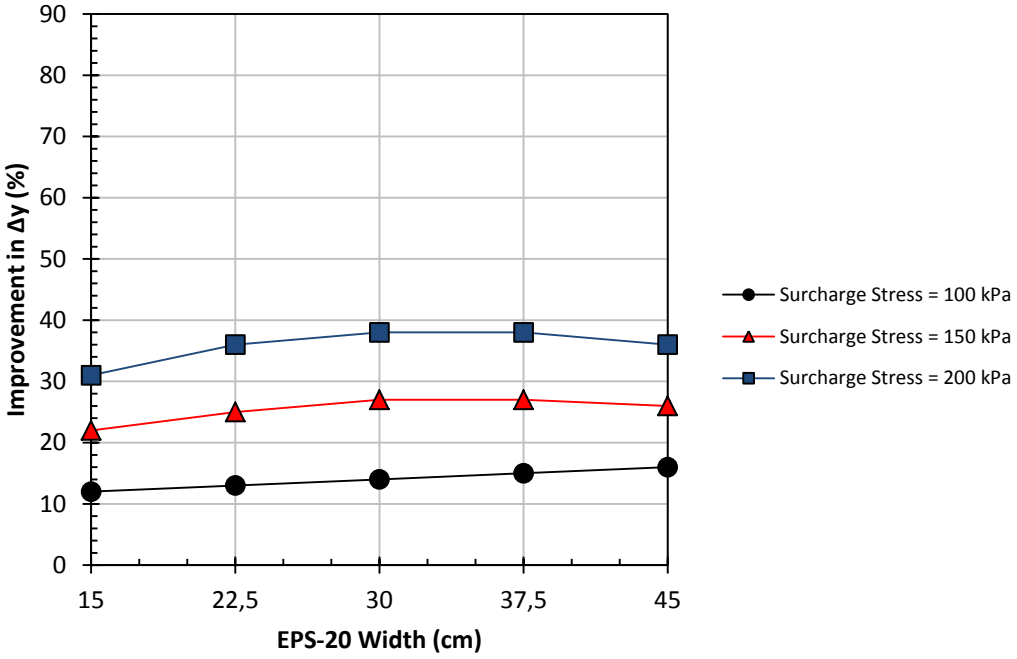

Figure 5.63. Vertical improvement ratio (%) vs. EPS-20 width

After parametric study, the followings can be concluded (considering the pipe burial depth, the pipe and soil types and loading conditions used in this study);

- It is suggested to place the EPS directly above the pipe crown with zero vertical distance from pipe crown.
- EPS width has negligible effect if, the width of the EPS is larger than one pipe diameter, on the behavior of pipe deflection. Therefore, EPS width equal to 1 x pipe diameter (1xD) is suggested to be used.
- EPS thickness should be at least 5 cm (D/6) to mobilize the positive arching fully.
- Softer (more compressible) EPS should be used (EPS-10 in this study).

From aforementioned conclusions, 5 cm thick EPS-10 located at the pipe crown with a width of one pipe diameter is recommended by considering cost / performance criteria. Comparison of the analyses results of reference test (without EPS) and recommended EPS configuration is given in Figure 5.64 together with the FEM outputs. FEM outputs of reference test and recommended EPS configuration are given in Appendix-D and Appendix-E, respectively.

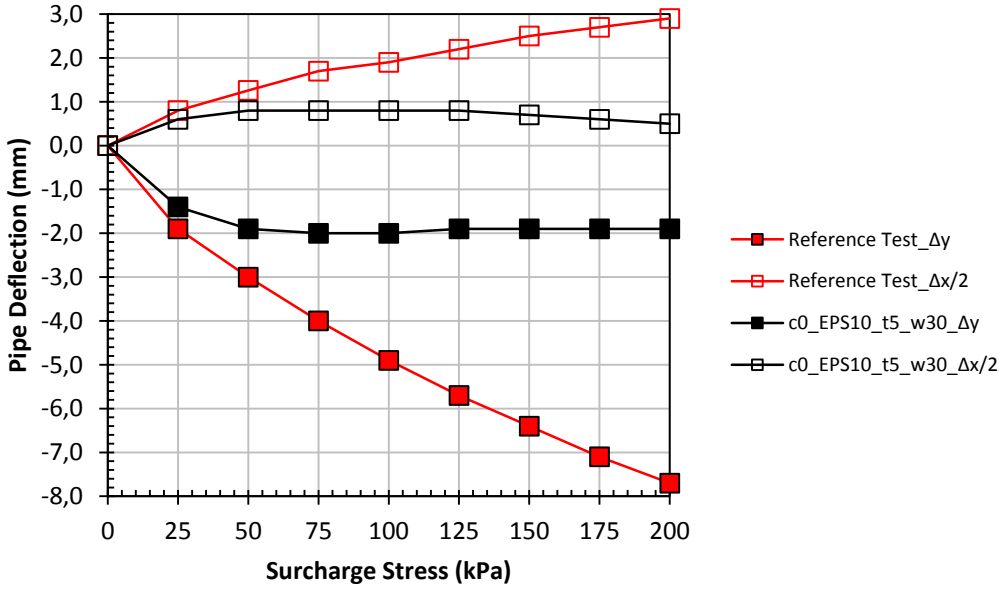

Figure 5.64. Comparison of the reference test (without EPS) and recommended EPS configuration

CHAPTER 6

CONCLUSIONS

In this thesis study, a very comprehensive literature review has been done on improvement of buried structures like pipes and culverts. In the light of the data obtained from the literature review, it was seen that there are very few studies on the protection of shallowly buried flexible pipes with compressible material inclusion and almost all of these studies are laboratory experiments. Recent studies on flexible pipes recommend implementation of embedded trench installation and also very limited number of study recommends, roughly, imperfect trench installation.

It has been observed that there is a need for more detailed study on the optimization of compressible zone geometry in order to protect shallowly buried flexible pipes by imperfect trench method. For this purpose, in the scope of this study, numerical model created by PLAXIS 2D was verified with the laboratory test results. Following that more than 120 finite element analyses have been conducted for the purpose of parametric study. Results of the parametric study were shown in detail both in graphically and tabular form.

EPS geofoam was used as compressible inclusion by considering increasing trend in using EPS in the construction industry together with its benefits compared to other compressible materials used in the previous studies. In numerical program, EPS was modeled as linear elastic soil model since only deformation properties of EPS was investigated under the scope of this study. Unconfined compression (UC) test results conducted on EPS material were directly used in the study and depending on stress-strain relation, material parameters were updated for all corresponding loadings (surcharge stresses) through study by manually.

6.1 Discussions of the Results

This study was conducted for the case where a 30 cm diameter flexible pipe was buried at a depth of two (2xD) diameters, and the results are valid for similar conditions. In order to demonstrate the validity of the results, the values suggested as a result of this study were compared with the recommended values in the literature. Thus, the validity of the results was compared with studies performed under similar conditions but with different diameters and burial depths.

6.1.1 Effect of the Location

The cases where 2, 5, 7 and 10 cm thick EPS-10, EPS-15 and EPS-20 geofoams were placed on the pipe crown, 5 cm above the pipe crown and 10 cm above the pipe crown, respectively, were examined in numerical analysis in order to examine the effect of the location of the EPS on deformation behavior of flexible pipe.

- It was observed that placing EPS close to the pipe crown gives the best improvement performance for all densities and all thicknesses.
- When the EPS thickness increases the effect of location is more distinctive.
- When the density of EPS decreases, the effect of the location is more distinctive.
- 5 cm thick EPS layer placed at pipe crown has showed better performance than 10 cm thick EPS placed at the 10 cm above the pipe crown (Figure 5.15) although thicker EPS should have shown better performance.

In the literature, for the flexible pipes, effect of EPS geofoam location was also investigated by Söylemez (2017) under circular loadings and placing EPS at 0.25xD above the pipe crown is recommended. For the rigid concrete pipes, NPRA (2010) recommends to place EPS 0.2xD above the pipe crown. Unlike other studies, the deformation behavior of a flexible pipe under uniformly distributed load was investigated in this study and the situation where EPS was placed on the pipe crown was determined to be the most advantageous.

6.1.2 Effect of the EPS Thickness

The effect of the EPS thickness has been investigated by comparing 2, 5, 7 and 10 cm thick of EPS layers placed at pipe crown with varying widths of 30 cm, 37.5 cm and 45 cm for all densities (EPS-10, EPS-15 and EPS-20).

- There is no doubt that, increase in the EPS thickness also increases the improvement performance for all densities and widths.
- It was observed that 2 cm thick EPS is not enough to develop positive arching fully. Pipe deflections increase parallel to the increasing load for the case of using 2 cm thick EPS for all widths and densities. However, significant amount of improvement was observed yet.
- 5 cm thick EPS was able to mobilize full positive arching for all densities and widths. Therefore, in the design EPS thickness of at least 5 cm (D/6) should be selected.
- According to Figure 5.58, Figure 5.59 and Figure 5.60 there is a dramatic increase in the improvement ratio while EPS thickness is increases from 2 cm to 5 cm. However, when EPS thickness increases from 5 cm to 10 cm, although amount of EPS is double, gained improvement ratio for the vertical deflections of pipe is varying between 2-11% depending on the surcharge stress and EPS density.

In the literature, for the flexible pipes, Söylemez (2017) and Akınay (2017) have recommended EPS thickness of 0.1xD and 0.17xD for the flexible pipes having diameter of 20 cm and 30 cm, respectively. For the rigid culverts, Vaslestad et al. (1993) and McGuigan & Valsangkar (2010) recommend EPS thickness of 0.2 – 0.4 times of the culvert width. In the same way, Al-Naddaf et al. (2019) also recommends to use EPS thickness as 0.2 times of the culvert width. For these studies since pipe type (rigid or flexible) and loading conditions differ, result may also differ from recommended EPS thickness in this study. Also, since flexible pipes can deflect itself too (in addition to the deflection in the EPS), it also contributes to the development of the positive soil arching and thus for the flexible

pipes required EPS thickness should be less than that of recommended for rigid structures. As a conclusion, EPS thickness of D/6 is recommended as compatible with the results of laboratory studies of Söylemez (2017) and Akınay (2017) for flexible pipes.

6.1.3 Effect of the EPS Density

In order to investigate the effect of the density EPS-10, EPS-15 and EPS-20 were used in the parametric analyses for all widths (30 cm, 37.5 cm and 45 cm) and thicknesses (2 cm, 5 cm, 7 cm and 10 cm).

- In all analyses, improvement performance increases as the density decreases.
- For the case of using EPS-10 and EPS-15, fully mobilization of the positive arching was obtained at surcharge stresses of 50-75 kPa and 100-175 kPa, respectively for all thicknesses except 2 cm.
- For the case of using EPS-20, fully mobilization of positive arching could only be achieved with the EPS thicknesses of 7 cm and 10 cm under the surcharge stresses of 175 – 200 kPa. For the 2 cm and 5 cm EPS thicknesses pipe deflections were increased with the increasing stresses.
- Nevertheless, considerable amount of improvement was achieved even the use of EPS-20.
- In the design, it is strictly recommended to select appropriate EPS density since compressive strength of EPS increases with increasing density so that EPS will not fail, especially for shallowly buried cases, under applied surcharge through service life. Study of Söylemez (2017) states that if the EPS geofoam fails under applied load, obtained improvement is completely lost and pipe deflections are even worse than no-geofoam case.

Effect of EPS density on the flexible pipes were investigated by Söylemez (2017) and Akınay (2017) via laboratory tests and researchers reported that lower density

geofoam provided better improvement. For the rigid structures, it was reported by McGuigan & Valsangkar (2010), Meguid et al. (2017) and Al-Naddaf et al. (2019) that higher stiffness EPS has increased the pressure on the culvert. Therefore, it is recommended to use low density (softer inclusion) EPS as possible.

6.1.4 Effect of the EPS Width

Effect of EPS width (equally from one pipe diameter to one and a half pipe diameter) was investigated for all densities (EPS-10, EPS-15 and EPS-20) and all thicknesses (2 cm, 5 cm, 7 cm and 10 cm). Then, for the recommended thickness which is 5 cm (D/6), additional analyses, where EPS widths are 0.5xD and 0.75xD, were also carried out.

- For the EPS widths from one pipe diameter to one and a half pipe diameter, it was observed that EPS width has negligible effect on the behavior of flexible pipe. Over and above, widening the EPS width too much has negative effect on the vertical deflection of the pipe.
- For the EPS widths narrower than a pipe diameter, improvement performance decreases as the EPS width get narrower. It was observed that normal stress, axial force and bending moment acting on the pipe wall increases (so that pipe deflections) as the width of the EPS decreases from one pipe diameter (1xD) to the half of the pipe diameter (0.5xD).
- When stiffness of the EPS come close to the stiffness of soil, effect of width vanishes and all widths gives almost similar results (i.e. for the case of using EPS-20, improvement performances were almost same for all thicknesses and widths).

In the literature, for the rigid structures (culverts and pipes), Kim and Yoo (2005), Sun et al. (2005), NPRA (2010), Kim et al. (2010) and Witthoeft and Kim (2016) pointed out that there is no significant improvement if the width of the EPS is wider than one and a half times of the pipe diameter (1.5xD). For the flexible pipes,

Akınay (2017) recommended to use EPS width equal to one pipe diameter (1xD) based on full scale laboratory tests. Additionally, Söylemez (2017) stated that EPS width equal to two times of the pipe diameter (2xD) does not provide considerable amount of improvement under circular loading conditions with respect to EPS width of one times the pipe diameter. In line with the findings of the literature about flexible pipes and contrary to the rigid structures, EPS width which is equal to the one pipe diameter is recommended after this study.

6.1.5 Effect of Two Layers and Spacing

Effect of multiple layer EPS and also distance between two consecutive EPS layer were also investigated in two parts. In the first part, a comparison have been made between 5 cm thick single EPS layer placed at the pipe crown and multiple EPS layers placed at various positions in various thicknesses in total of 5 cm. All the same, the same comparison have been made between 10 cm thick single EPS layer placed at pipe crown and multiple layers of EPS placed at various location above the pipe in total of 10 cm.

- For the case of placing same thickness of EPS, there is no additional improvement have been observed in the case of placing in two layers in fact placing in multiple layer has negative effect on improvement performance.
- When the distance between two consecutive EPS layer increases, improvement performance decreases.
- 5 cm thick single EPS-10 placed at pipe crown has showed almost same improvement performance with 5 cm EPS layer placed 5 cm above the pipe crown plus additional 5 cm EPS placed 5 cm above the first EPS layer. In total, although 10 cm EPS was used in multiple layer, effect on the improvement was almost same with 5 cm single EPS which emphasizes the effect of location.
- For design purposes, instead of using multiple layers of EPS, single EPS close as possible as to pipe crown is recommended.

For flexible pipe, Söylemez (2017) concluded that placing two layers of EPS has shown no better improvement in terms of soil deflection with respect to same thickness (in total) single EPS. For rigid pipe, Kim et al. (2010) also stated that using two layers of EPS has shown no additional improvement regarding vertical pressure on pipe. Witthoeft and Kim (2016) conducted numerical study and concluded that in the case of using multiple layers of EPS, upper EPS should be placed below the plane of equal settlement so that additional settlement and positive arching could occur. In addition, Söylemez (2017) pointed out that effect of distance between two consecutive EPS layer has negligible effect on pipe deflection for the case of using circular loading plate. However, after this study, for the case of uniformly distributed loading, it was concluded that increase in the distance between two consecutive EPS layer also increases the pipe deflection (Figure 5.51 - Figure 5.57).

One of the conclusion after this thesis study is that the deflection behavior of shallowly buried flexible pipes protected by imperfect trench installation via EPS geofoam can be modeled with the help of the PLAXIS 2D, proven and widely accepted FEM numerical analysis program, by using material parameters obtained from simple laboratory experiments (UC) conducted on EPS samples or common literature.

To the best knowledge of the author, this study is the only and the first study that uses numerical model (FEM) verified with laboratory test results and uses exact material parameters obtained from laboratory experiments for EPS without back-calculation. For this reason, this study demonstrates that with the appropriate constitutive model for EPS, soil and pipe together with the initial and boundary conditions, behavior of shallowly buried flexible pipe improved with EPS can successfully be modeled via PLAXIS 2D with numerical modeling techniques and can be used in the design.

6.2 Limitations of the Study and Future Recommendations

- Since parametric study starts with verification of existing laboratory test results, therefore, in this study single pipe diameter with constant material parameters and constant soil parameters were used. In order to overcome this limitation, the same or similar test setup can be installed and similar experiments can be conducted with varying pipe diameters, burying depths, soil and material parameters.
- Material parameters for EPS updated for each surcharge stress by manually which takes longer time and prone to error. Instead, in a robust way, a soil model that can represent stress-strain behavior of EPS can be programmed and embedded in numerical program.
- Verification and parametric study presented in this study can be verified also using 3D finite element programs.

REFERENCES

AbdelSalam, S. S., Azzam, S. A., & Abdel-Awad, A. S. (2015). Laboratory characterization and numerical modeling of EPS geofoam. *International Conference on Advances in Structural and Geotechnical Engineering*.

Akınay, E. (2017). *Investigating the effects of the use of compressible bedding on the behavior of buried flexible pipes (In Turkish)*. Yıldız Technical University (Ph. D. Dissertation).

Al-Naddaf, M., Han, J., Xu, C., & Rahmaninezhad, S. M. (2019). Effect of geofoam on vertical stress distribution on buried structures subjected to static and cyclic footing loads. *Journal of Pipeline Systems Engineering and Practice*, *10*(1). https://doi.org/10.1061/(ASCE)PS.1949-1204.0000355

American Lifelines Alliance. (2005). Guidelines for the design of buried steel pipe. *American Socoiety of Civil Engineers*, *2001*(July 2001).

Anil, Ö., Erdem, R. T., & Kantar, E. (2015). Improving the impact behavior of pipes using geofoam layer for protection. *International Journal of Pressure Vessels and Piping*, *132–133*. https://doi.org/10.1016/j.ijpvp.2015.05.007

ASCE. (2009). *Buried Flexible Steel Pipe*. American Society of Civil Engineers. https://doi.org/10.1061/9780784410585

ASTM D2487-11. (2011). Standard practice for classification of soils for engineering purposes (Unified Soil Classification System). *ASTM Standard Guide*, *D2487-11*. https://doi.org/10.1520/D2487-11.

Atmatzidis, D. K., Missirlis, E. G., & Chrysikos, D. A. (2001). An investigation of EPS geofoam behaviour in compression. *Proceedings of the EPS Geofoam, 3rd International Conference*.

Beju, Y. Z., & Mandal, J. N. (2017a). Combined use of jute geotextile-EPS geofoam to protect flexible buried pipes: Experimental and numerical studies. *International Journal of Geosynthetics and Ground Engineering*, *3*(32). https://doi.org/10.1007/s40891-017-0107-5

Beju, Y. Z., & Mandal, J. N. (2017b). Expanded polystyrene (EPS) geofoam: Preliminary characteristic evaluation. *Procedia Engineering*, *189*(May), 239–246. https://doi.org/10.1016/j.proeng.2017.05.038

Bhatia, S. K., & Kasturi, G. (1996). Comparison of PVC and HDPE geomembranes (interface friction performance). In *Research Report, Dept. of Civil and Environmental Engineering, Syracuse University*.

Birhan, A., & Negussey, D. (2014). Effects of confinement on the stress strain behavior of EPS geofoam. *Ground Improvement and Geosynthetics, Geo-Shanghai, ASCE Geotechnical Special Publication*, 536–546.

Brinkgreve, R. B. J., Kumarswamy, S., Swolfs, W. M., Zampich, L., & Manoj, N. R. (2019a). Plaxis 2D Material Models Manual. *Rotterdam, Netherlands, Balkema*.

Brinkgreve, R. B. J., Kumarswamy, S., Swolfs, W. M., Zampich, L., & Manoj, N. R. (2019b). Plaxis 2D Reference Manual. *Rotterdam, Netherlands, Balkema*.

Chun, B. S., Lim, H. S., Sagong, M., & Kim, K. (2004). Development of a hyperbolic constitutive model for expanded polystyrene (EPS) geofoam under triaxial compression tests. *Geotextiles and Geomembranes*, *22*(4), 223–237. https://doi.org/10.1016/j.geotexmem.2004.03.005

CPPA. (2006). Recommanded installation practices for corrugated polyethylene pipe and fittings. *Corrugated Polyethylene Pipe Association*.

Edgar, T. V., Puckett, J. A., & D'Spain, R. B. (1989). Effects of geotextiles on lateral pressure and deformation in highway embankments. *Geotextiles and Geomembranes*, *8*(4). https://doi.org/10.1016/0266-1144(89)90012-5

EDO. (1992). Expanded polystyrene construction method. *EPS Construction Method Development Organization (in Japanese)*, 310.

Han, J. (2015). *Principles and practice of ground improvement*. Wiley. https://doi.org/10.13140/RG.2.1.4155.7366

Hazarika, H. (2006). Stress-strain modeling of EPS geofoam for large-strain applications. *Geotextiles and Geomembranes*, *24*(2), 79–90. https://doi.org/10.1016/j.geotexmem.2005.11.003

Horvath, J. S. (1997). The compressible inclusion function of EPS geofoam. *Geotextiles and Geomembranes*, *15*(3), 77–120. https://doi.org/10.1016/s0266-1144(97)00008-3

Jaky, J. (1944). The coefficient of earth pressure at rest. *Journal of the Society of Hungarian Architects and Engineers*, *7*, 355–358.

Janson, L.-E., & Molin, J. (1981). Design and installation of underground plastic sewer pipes. *International Conference on Underground Plastic Pipe*, 79–88.

Järvenkylä, J. J. (1989). Thin-walled thermoplastic pipes. *Construction and Building Materials*, *3*(4), 191–200. https://doi.org/10.1016/0950-0618(89)90013-5

Jean, P. A., & Long, N. T. (1990). Creation of arching (pneusol and other techniques). *Geotechnical Instrumentation in Practice*, 663–670.

Kang, J. (2007). *Soil-structure interaction and imperfect trench installations as applied to deeply buried conduits*. Auburn University (Ph.D. Dissertation).

Kang, J. (2019). Finite element analysis for deeply buried concrete pipes in proposed imperfect trench installations with expanded polystyrene (EPS) foams. *Engineering Structures*, *189*(April 2018), 286–295. https://doi.org/10.1016/j.engstruct.2019.03.083

Kang, J., Im, H., & Park, J. S. (2020). The effect of load reduction on underground concrete arch structures in embedded trench installations. *Tunnelling and Underground Space Technology*, *98*(December 2019), 103240. https://doi.org/10.1016/j.tust.2019.103240

Kang, J., Parker, F., Kang, Y. J., & Yoo, C. H. (2008b). Effects of frictional forces acting on sidewalls of buried box culverts. *International Journal for Numerical and Analytical Methods in Geomechanics*, *32*(3), 289–306. https://doi.org/10.1002/nag.628

Kang, J., Parker, F., & Yoo, C. H. (2007a). Soil-structure interaction and imperfect trench installations for deeply buried corrugated polyvinyl chloride pipes. *Transportation Research Record: Journal of the Transportation Research Board*, *2028*(1), 192–202. https://doi.org/10.3141/2028-21

Kang, J., Parker, F., & Yoo, C. H. (2007b). Soil-structure interaction and imperfect trench installations for deeply buried concrete pipes. *Journal of Geotechnical and Geoenvironmental Engineering*, *133*(3), 277–285. https://doi.org/10.1061/(ASCE)1090-0241(2007)133:3(277)

Kang, J., Parker, F., & Yoo, C. H. (2008a). Soil–structure interaction for deeply buried corrugated steel pipes Part II: Imperfect trench installation. *Engineering Structures*, *30*(3), 588–594. https://doi.org/10.1016/j.engstruct.2007.04.006

Katona, M. G., & Vittes, P. D. (1982). Soil-structure analysis and evaluation of buried box-culvert designs. *Transportation Research Record*, *878*.

Kim, H., Choi, B., & Kim, J. (2010). Reduction of earth pressure on buried pipes by EPS Geofoam inclusions. *Geotechnical Testing Journal*, *33*(4), 304–313. https://doi.org/10.1520/GTJ102315

Kim, K., & Yoo, C. H. (2005). Design loading on deeply buried box culverts. *Journal of Geotechnical and Geoenvironmental Engineering*, *131*(1), 20–27. https://doi.org/10.1061/(ASCE)1090-0241(2005)131:1(20)

Kılıç, H., & Akınay, E. (2019). Effects of using eps geofoam as compressible inclusion on hdpe pipe behavior. *Journal of Pipeline Systems Engineering and Practice*, *10*(2), 1–15. https://doi.org/10.1061/(ASCE)PS.1949-1204.0000368

Krizek, R. J., Parmelee, R. A., Kay, J. N., & Elnaggar, H. A. (1971). Structural analysis and design of pipe culverts. In *NCHRP Report* (Issue 116).

Larsen, N., & Hendrickson, J. G. (1962). A practical method for constructing rigid conduits under high fill. *Proceedings of the 41st Annual Meeting of the Highway Research Board*, 273–280.

Ma, Q., Ku, Z., & Xiao, H. (2019). Model tests of earth pressure on buried rigid pipes and flexible pipes underneath expanded polystyrene (EPS). *Advances in Civil Engineering*, *2019*. https://doi.org/10.1155/2019/9156129

Mahgoub, A., & El Naggar, H. (2019). Using TDA as an engineered stress-reduction fill over preexisting buried pipes. *Journal of Pipeline Systems Engineering and Practice*, *10*(1), 1–15. https://doi.org/10.1061/(ASCE)PS.1949- 1204.0000362

Marston, A. (1922). Second progress report to the joint concrete culvert pipe committee. *Iowa Engineering Experiment Station*.

Marston, A., & Anderson, A. O. (1913). The theory of loads on pipes in ditches and tests of cement and clay drain tile and sewer pipe. *Bulletin 31, Iowa Engineering Experiment Station*.

Martin, J. P., Koerner, R. M., & Whitty, J. E. (1984). Experimental friction evaluation of slippage between geomembranes, geotextiles and soils. *Proceedings of the International Conference on Geomembranes*, 191–196.

McAffee, R. P., & Valsangkar, A. J. (2004). Geotechnical properties of compressible materials used for induced trench construction. *Journal of Testing and Evaluation*, *32*(2), 143–152. https://doi.org/10.1520/jte11924

McAffee, R. P., & Valsangkar, A. J. (2005). Performance of an induced trench installation. *Transportation Research Record: Journal of the Transportation Research Board*, *1936*(1), 230–237. https://doi.org/10.1177/0361198105193600126

McAffee, R. P., & Valsangkar, A. J. (2008). Field performance, centrifuge testing, and numerical modelling of an induced trench installation. *Canadian Geotechnical Journal*, *45*(1), 85–101. https://doi.org/10.1139/T07-086

Mcgrath, T. J. (1999). Calculating loads on buried culverts based on pipe hoop stiffness. *Transportation Research Record: Journal of the Transportation Research Board*, *1656*(1), 73–79. https://doi.org/10.3141/1656-10

Mcguigan, B. L., & Valsangkar, A. J. (2011). Earth pressures on twin positive projecting and induced trench box culverts under high. *Canadian Geotechnical Journal*, *48*(2), 173–185. https://doi.org/10.1139/T10-058

McGuigan, B. L., & Valsangkar, A. J. (2010). Centrifuge testing and numerical analysis of box culverts installed in induced trenches. *Canadian Geotechnical Journal*, *47*(2), 147–163. https://doi.org/10.1139/T09-085

Meguid, M. A., & Ahmed, M. R. (2020). Earth pressure distribution on buried pipes installed with geofoam inclusion and subjected to cyclic loading. *International Journal of Geosynthetics and Ground Engineering*, *6*(1), 1–8. https://doi.org/10.1007/s40891-020-0187-5

Meguid, M. A., Ahmed, M. R., Hussein, M. G., & Omeman, Z. (2017). Earth pressure distribution on a rigid box covered with U-shaped geofoam wrap. *International Journal of Geosynthetics and Ground Engineering*, *3*(2), 1–14. https://doi.org/10.1007/s40891-017-0088-4

Miki, G. (1996). Ten year history of EPS method in japan and its future challenges. *International Symposium on EPS Construction Method*, 394–411.

Moghaddas Tafreshi, S. N., Tavakoli Mehrjardi, G., & Dawson, A. R. (2012). Buried pipes in rubber-soil backfilled trenches under cyclic loading. *Journal of Geotechnical and Geoenvironmental Engineering*, *138*(11), 1346–1356. https://doi.org/10.1061/(ASCE)GT.1943-5606.0000710

Moser, A. P., & Folkman, S. (2008). *Buried pipe design* (3rd ed.). McGraw - Hill.

NCHRP. (1999). *HDPE pipe: Recommended material specifications and design requirements, Rep. No. 429*.

Negussey, D. (1997). Properties and applications of geofoam. *Society of the Plastics Industry*.

Negussey, D., Anasthas, N., & Srirajan, S. (2001). Interface friction properties of eps geofoam. *Proceedings of the EPS Geofoam, 3rd International Conference*, 1–13.

Negussey, D., Wijewickreme, W. K. D., & Vaid, Y. P. (1989). Geomembrane interface friction. *Canadian Geotechnical Journal*, *26*(1), 165–169. https://doi.org/10.1139/t89-018

Neto, J. O. A., & Bueno, B. S. (2012). Laboratory research on EPS blocks used in geotechnical engineering. *Soils and Rocks*, *35*(2), 169–180.

Ni, P., Qin, X., & Yi, Y. (2018). Numerical study of earth pressures on rigid pipes with tire-derived aggregate inclusions. *Geosynthetics International*, *25*(5), 494–506. https://doi.org/10.1680/jgein.18.00013

NPRA. (2010). Håndbok 016: Geoteknikk i vegbygging (in Norwegian). *Norwegian Public Roads Administration*.

O'Rourke, T. D., Druschel, S. J., & Netravali, A. N. (1990). Shear strength characteristics of sand-polymer interfaces. *Journal of Geotechnical Engineering*, *116*(3), 451–469. https://doi.org/10.1061/(ASCE)0733-9410(1990)116:3(451)

Okabayashi, K., Ohtani, W., Akiyama, K., & Kawamura, M. (1994). Centrifugal model test for reducing the earth pressure on the culvert by using the flexible material. *Proceedings of the Fourth International Offshore and Polar Engineering Conference*, *1*, 620–624.

Padade, A. H., & Mandal, J. N. (2012). Behavior of expanded polystyrene (EPS) geofoam under triaxial loading conditions. *Electronic Journal of Geotechnical Engineering*, *17 S*, 2543–2553.

Parker, B. A., McAffee, R. P., & Valsangkar, A. J. (2008). Field performance and analysis of 3-m-diameter induced trench culvert under a 19.4-m soil cover. *Transportation Research Record*, *2045*, 68–76. https://doi.org/10.3141/2045-08

Rogers, C. D. F., Fleming, P. R., Loeppky, M. W. J., & Faragher, E. (1995). Structural performance of profile-wall drainage pipe-stiffness requirements contrasted with results of laboratory and field tests. *Transportation Research Record, 1514*, 83–92.

Rude, L. C. (1978). *A Study of the Imperfect Ditch Method for Rigid Culverts*. University of Virginia (Phd Dissertation).

Santos, R. R. V., Kang, J., & Park, J. S. (2020). Effects of embedded trench installations using expanded polystyrene geofoam applied to buried corrugated steel arch structures. *Tunnelling and Underground Space Technology*, *98*(February), 103323. https://doi.org/10.1016/j.tust.2020.103323

Sargand, S. M., Hazen, G. A., White, K., & Moran, A. (2001). Time-dependent deflection of thermoplastic pipes under deep burial. *Transportation Research Record, 1770*, 236–242. https://doi.org/10.3141/1770-30

Sargand, S. M., Masada, T., & Schehl, D. J. (2001). Soil pressure measured at various fill heights above deeply buried thermoplastic pipe. *Transportation Research Record, 1770*, 227–235. https://doi.org/10.3141/1770-29

Saxena, S. K., & Wong, Y. . (1984). Friction characteristics of a geomembrane. *Proceedings of the International Conference on Geomembranes*, 187–190.

Schluter, J. C., & Shade, J. W. (1999). Flexibility factor or pipe stiffness: Significant stiffness considerations. *Transportation Research Record: Journal of the Transportation Research Board*, *1656*(1), 45–50. https://doi.org/10.3141/1656-06

Söylemez, B. (2017). *Laboratory experiments on improvement of buried flexible pipes by using geofoam*. Middle East Technical University (Master Thesis).

Spangler, M. G. (1941). The structural design of flexible pipe culverts. *Bulletin 153, Iowa Engineering Experiment Station*.

Spangler, M. G. (1958). A practical application of the imperfect ditch method of construction. *Proceedings of the Thirty-Seventh Annual Meeting of the Highway Research Board*, 271–277.

Stark, T. D., Arellano, D., Horvath, J. S., & Leshchinsky, D. (2004). Geofoam applications in the design and construction of highway embankments. *National Cooperative Highway Research Program*, *65*(24-11(01)). https://doi.org/10.17226/21944

Sun, L., Hopkins, T., & Beckham, T. (2005). Stress reduction by ultra-lightweight geofoam for high fill culvert: Numerical analysis. *Geotechnical Applications for Transportation Infrastructure*, 146–154. https://doi.org/http://dx.doi.org/10.1061/9780784408216

Terzaghi, K. (1943). *Theoretical Soil Mechanics*. John Wiley & Sons, Inc. https://doi.org/10.1002/9780470172766

Tognon, A. R., Rowe, R. K., & Brachman, R. W. I. (1999). Evaluation of side wall friction for a buried pipe testing facility. *Geotextiles and Geomembranes*, *17*, 193–212.

TS EN ISO 9969. (2009). *Thermoplastic pipes - determination of ring stiffness*.

Uni-Bell. (2013). *Handbook of PVC pipe design and construction* (5th ed.). Industrial Press Inc.

UTest. (2020). *Concrete pipe testing machine*. http://www.utest.com.tr/en/23633/Concrete-Pipe-Testing-Machine

Vaid, Y. P., & Rinne, N. (1995). Geomembrane coefficients of interface friction. *Geosynthetics International*, *2*(1), 309–325. https://doi.org/10.1680/gein.2.0012

Vaslestad, J., Johansen, T. H., & Holm, W. (1993). Load reduction on rigid culverts beneath high fills: long-term behavior. *Transportation Research Record, 1415*, 58–68.

Vaslestad, J., Sayd, M. S., Johansen, T., & Wiman, L. (2011). Load reduction and arching on buried rigid culverts using EPS Geofoam. Design method and instrumented field tests. *Proceedings of EPS 2011*.

Williams, N. D., & Houlihan, M. F. (1987). Evaluation of interface friction properties between geosynthetics and soils. *Proceedings of Geosynthetics '87*, 616–627.

Witthoeft, A. F., & Kim, H. (2016). Numerical investigation of earth pressure reduction on buried pipes using EPS geofoam compressible inclusions. *Geosynthetics International*, *23*(4), 287–300. https://doi.org/10.1680/jgein.15.00054

Wong, H., & Leo, C. J. (2006). A simple elastoplastic hardening constitutive model for EPS geofoam. *Geotextiles and Geomembranes*, *24*(5), 299–310. https://doi.org/10.1016/j.geotexmem.2006.03.007

Xenaki, V. C., & Athanasopoulos, G. A. (2001). Experimental investigation of the interaction mechanism at the EPS geofoam-sand interface by direct shear testing. *Geosynthetics International*, *8*(6), 471–499. https://doi.org/10.1680/gein.8.0204

APPENDICES

A. RESULTS OF ANALYSES FOR EPS AT PIPE CROWN

Table A.1 EPS-10 at pipe crown

Surcharge Stress (kPa)	EPS-10																					
	Thickness=2 cm						Thickness=5 cm						Thickness=7 cm						Thickness=10 cm			
	Width=30 cm		Width=37.5 cm		Width=45 cm		Width=30 cm		Width=37.5 cm		Width=45 cm		Width=30 cm		Width=37.5 cm		Width=45 cm		Width=30 cm		Width=37.5 cm		Width=45 cm	
	Δx (mm)	Δy (mm)	Δx (mm)	Δy (mm)	Δx (mm)	Δy (mm)	Δx (mm)	Δy (mm)	Δx (mm)	Δy (mm)	Δx (mm)	Δy (mm)	Δx (mm)	Δy (mm)	Δx (mm)	Δy (mm)	Δx (mm)	Δy (mm)	Δx (mm)	Δy (mm)	Δx (mm)	Δy (mm)	Δx (mm)	Δy (mm)
0	0.00	0.00	0.00	0.00	0.00	0.00	0.00	0.00	0.00	0.00	0.00	0.00	0.00	0.00	0.00	0.00	0.00	0.00	0.00	0.00	0.00	0.00	0.00	0.00
25	0.67	-1.57	0.67	-1.58	0.67	-1.59	0.61	-1.45	0.61	-1.45	0.61	-1.46	0.59	-1.38	0.58	-1.39	0.58	-1.40	0.56	-1.31	0.55	-1.31	0.55	-1.33
50	0.94	-2.29	0.93	-2.33	0.94	-2.38	0.78	-1.90	0.77	-1.93	0.77	-1.99	0.74	-1.80	0.72	-1.83	0.73	-1.87	0.69	-1.68	0.66	-1.69	0.67	-1.74
75	1.06	-2.66	1.05	-2.73	1.07	-2.84	0.80	-1.98	0.77	-2.01	0.77	-2.13	0.72	-1.78	0.69	-1.81	0.69	-1.82	0.64	-1.56	0.59	-1.59	0.59	-1.68
100	1.15	-2.94	1.12	-3.04	1.15	-3.20	0.80	-1.97	0.73	-2.03	0.75	-2.19	0.66	-1.68	0.61	-1.73	0.62	-1.73	0.52	-1.44	0.48	-1.41	0.49	-1.54
125	1.20	-3.16	1.17	-3.30	1.20	-3.51	0.77	-1.91	0.68	-2.00	0.69	-2.22	0.56	-1.64	0.53	-1.61	0.52	-1.61	0.39	-1.44	0.35	-1.31	0.36	-1.38
150	1.24	-3.34	1.21	-3.51	1.24	-3.77	0.65	-1.91	0.60	-1.94	0.64	-2.21	0.45	-1.66	0.41	-1.52	0.39	-1.52	0.23	-1.44	0.19	-1.28	0.23	-1.24
175	1.27	-3.48	1.23	-3.69	1.27	-4.00	0.56	-1.94	0.52	-1.85	0.57	-2.18	0.33	-1.69	0.27	-1.52	0.28	-1.52	0.08	-1.44	0.03	-1.28	0.10	-1.24
200	1.28	-3.59	1.24	-3.85	1.29	-4.20	0.48	-2.00	0.43	-1.81	0.48	-2.13	0.21	-1.73	0.12	-1.53	0.15	-1.53	-0.12	-1.47	-0.16	-1.28	0.06	-1.24

Table A.2 EPS-15 at pipe crown

Surcharge Stress (kPa)	EPS-15																							
	Thickness=2 cm						Thickness=5 cm						Thickness=7 cm						Thickness=10 cm					
	Width=30 cm		Width=37.5 cm		Width=45 cm		Width=30 cm		Width=37.5 cm		Width=45 cm		Width=30 cm		Width=37.5 cm		Width=45 cm		Width=30 cm		Width=37.5 cm		Width=45 cm	
	Δx (mm)	Δy (mm)	Δx (mm)	Δy (mm)	Δx (mm)	Δy (mm)	Δx (mm)	Δy (mm)	Δx (mm)	Δy (mm)	Δx (mm)	Δy (mm)	Δx (mm)	Δy (mm)	Δx (mm)	Δy (mm)	Δx (mm)	Δy (mm)	Δx (mm)	Δy (mm)	Δx (mm)	Δy (mm)	Δx (mm)	Δy (mm)
0	0.00	0.00	0.00	0.00	0.00	0.00	0.00	0.00	0.00	0.00	0.00	0.00	0.00	0.00	0.00	0.00	0.00	0.00	0.00	0.00	0.00	0.00	0.00	0.00
25	0.73	-1.70	0.73	-1.69	0.72	-1.68	0.74	-1.72	0.73	-1.70	0.72	-1.68	0.75	-1.74	0.74	-1.71	0.73	-1.68	0.76	-1.77	0.75	-1.73	0.73	-1.69
50	1.14	-2.75	1.13	-2.74	1.12	-2.73	1.13	-2.72	1.11	-2.69	1.10	-2.68	1.13	-2.71	1.11	-2.68	1.09	-2.65	1.13	-2.71	1.11	-2.67	1.09	-2.64
75	1.38	-3.44	1.37	-3.46	1.37	-3.49	1.30	-3.19	1.27	-3.19	1.25	-3.21	1.26	-3.09	1.23	-3.07	1.21	-3.08	1.23	-2.99	1.19	-2.96	1.16	-2.96
100	1.49	-3.80	1.47	-3.84	1.47	-3.92	1.37	-3.42	1.33	-3.43	1.30	-3.49	1.33	-3.29	1.28	-3.28	1.25	-3.33	1.29	-3.19	1.23	-3.17	1.20	-3.20
125	1.58	-4.09	1.55	-4.16	1.55	-4.28	1.37	-3.48	1.32	-3.50	1.30	-3.61	1.31	-3.27	1.24	-3.27	1.22	-3.35	1.25	-3.10	1.17	-3.07	1.14	-3.14
150	1.65	-4.33	1.61	-4.34	1.62	-4.60	1.37	-3.48	1.30	-3.53	1.30	-3.68	1.27	-3.20	1.19	-3.21	1.16	-3.33	1.18	-2.96	1.09	-2.94	1.06	-3.04
175	1.71	-4.53	1.65	-4.67	1.67	-4.88	1.37	-3.46	1.26	-3.52	1.25	-3.71	1.22	-3.09	1.12	-3.12	1.09	-3.28	1.09	-2.79	0.99	-2.77	0.96	-2.91
200	1.75	-4.71	1.69	-4.88	1.70	-5.13	1.31	-3.40	1.21	-3.48	1.20	-3.72	1.14	-2.96	1.03	-3.00	1.02	-3.22	0.99	-2.70	0.88	-2.59	0.85	-2.77

Table A.3 EPS-20 at pipe crown

Surcharge Stress (kPa)	EPS-20																							
	Thickness=2 cm						Thickness=5 cm						Thickness=7 cm						Thickness=10 cm					
	Width=30 cm		Width=37.5 cm		Width=45 cm		Width=30 cm		Width=37.5 cm		Width=45 cm		Width=30 cm		Width=37.5 cm		Width=45 cm		Width=30 cm		Width=37.5 cm		Width=45 cm	
	Δx (mm)	Δy (mm)	Δx (mm)	Δy (mm)	Δx (mm)	Δy (mm)	Δx (mm)	Δy (mm)	Δx (mm)	Δy (mm)	Δx (mm)	Δy (mm)	Δx (mm)	Δy (mm)	Δx (mm)	Δy (mm)	Δx (mm)	Δy (mm)	Δx (mm)	Δy (mm)	Δx (mm)	Δy (mm)	Δx (mm)	Δy (mm)
0	0.00	0.00	0.00	0.00	0.00	0.00	0.00	0.00	0.00	0.00	0.00	0.00	0.00	0.00	0.00	0.00	0.00	0.00	0.00	0.00	0.00	0.00	0.00	0.00
25	0.74	-1.71	0.73	-1.69	0.72	-1.68	0.76	-1.75	0.75	-1.71	0.73	-1.69	0.78	-1.78	0.76	-1.74	0.74	-1.70	0.80	-1.82	0.78	-1.77	0.75	-1.72
50	1.17	-2.81	1.16	-2.79	1.14	-2.76	1.19	-2.85	1.17	-2.80	1.15	-2.76	1.21	-2.89	1.19	-2.82	1.16	-2.77	1.24	-2.93	1.21	-2.86	1.17	-2.79
75	1.51	-3.73	1.49	-3.70	1.48	-3.67	1.54	-3.77	1.51	-3.70	1.48	-3.66	1.56	-3.80	1.53	-3.72	1.49	-3.66	1.58	-3.84	1.54	-3.76	1.50	-3.67
100	1.71	-4.35	1.69	-4.34	1.68	-4.35	1.68	-4.19	1.64	-4.15	1.61	-4.14	1.67	-4.15	1.63	-4.08	1.59	-4.05	1.67	-4.11	1.62	-4.03	1.57	-3.97
125	1.85	-4.79	1.83	-4.81	1.81	-4.85	1.79	-4.55	1.75	-4.53	1.72	-4.55	1.77	-4.43	1.70	-4.38	1.67	-4.38	1.73	-4.31	1.66	-4.24	1.61	-4.21
150	1.95	-5.11	1.91	-5.15	1.90	-5.23	1.83	-4.67	1.76	-4.66	1.73	-4.72	1.77	-4.51	1.71	-4.47	1.67	-4.51	1.75	-4.40	1.67	-4.33	1.61	-4.32
175	2.03	-5.38	1.99	-5.46	1.98	-5.58	1.85	-4.74	1.77	-4.75	1.73	-4.85	1.77	-4.52	1.69	-4.47	1.64	-4.56	1.72	-4.34	1.62	-4.27	1.56	-4.29
200	2.10	-5.63	2.04	-5.74	2.04	-5.89	1.85	-4.78	1.75	-4.81	1.72	-4.95	1.77	-4.49	1.65	-4.47	1.60	-4.58	1.68	-4.24	1.56	-4.18	1.49	-4.24

B. RESULTS OF ANALYSES FOR EPS AT 5 CM ABOVE THE PIPE CROWN

Table B.1 EPS-10 at 5 cm above the pipe crown

Surcharge Stress (kPa)	EPS-10																					
	Thickness=2 cm						Thickness=5 cm						Thickness=7 cm						Thickness=10 cm			
	Width=30 cm		Width=37.5 cm		Width=45 cm		Width=30 cm		Width=37.5 cm		Width=45 cm		Width=30 cm		Width=37.5 cm		Width=45 cm		Width=30 cm		Width=37.5 cm		Width=45 cm	
	Δx (mm)	Δy (mm)	Δx (mm)	Δy (mm)	Δx (mm)	Δy (mm)	Δx (mm)	Δy (mm)	Δx (mm)	Δy (mm)	Δx (mm)	Δy (mm)	Δx (mm)	Δy (mm)	Δx (mm)	Δy (mm)	Δx (mm)	Δy (mm)	Δx (mm)	Δy (mm)	Δx (mm)	Δy (mm)	Δx (mm)	Δy (mm)
0	0.00	0.00	0.00	0.00	0.00	0.00	0.00	0.00	0.00	0.00	0.00	0.00	0.00	0.00	0.00	0.00	0.00	0.00	0.00	0.00	0.00	0.00	0.00	0.00
25	0.68	-1.60	0.68	-1.60	0.68	-1.61	0.64	-1.50	0.63	-1.49	0.63	-1.50	0.62	-1.46	0.61	-1.44	0.60	-1.44	0.60	-1.40	0.58	-1.39	0.58	-1.38
50	0.96	-2.33	0.95	-2.33	0.95	-2.37	0.84	-2.01	0.81	-1.98	0.79	-2.00	0.81	-1.95	0.77	-1.90	0.76	-1.92	0.76	-1.86	0.73	-1.81	0.71	-1.81
75	1.11	-2.72	1.07	-2.72	1.07	-2.79	0.90	-2.17	0.83	-2.10	0.81	-2.13	0.83	-2.04	0.77	-1.95	0.74	-1.95	0.77	-1.89	0.71	-1.79	0.66	-1.78
100	1.21	-3.00	1.16	-3.03	1.15	-3.12	0.92	-2.27	0.83	-2.16	0.79	-2.19	0.83	-2.07	0.74	-1.93	0.69	-1.94	0.73	-1.86	0.64	-1.71	0.59	-1.70
125	1.29	-3.29	1.22	-3.28	1.21	-3.40	0.92	-2.31	0.81	-2.17	0.76	-2.22	0.80	-2.08	0.72	-1.89	0.63	-1.90	0.67	-1.84	0.56	-1.67	0.51	-1.60
150	1.35	-3.50	1.27	-3.48	1.25	-3.63	0.90	-2.37	0.77	-2.17	0.72	-2.22	0.75	-2.11	0.62	-1.90	0.62	-1.83	0.59	-1.86	0.46	-1.67	0.42	-1.58
175	1.40	-3.68	1.30	-3.66	1.28	-3.83	0.87	-2.44	0.72	-2.20	0.67	-2.22	0.69	-2.16	0.54	-1.93	0.49	-1.85	0.50	-1.89	0.37	-1.68		
200	1.44	-3.84	1.32	-3.81	1.30	-4.00	0.83	-2.52	0.68	-2.25	0.61	-2.18	0.63	-2.22	0.46	-1.97	0.42	-1.86	0.39	-1.94	0.24	-1.71		

Table B.2 EPS-15 at 5 cm above the pipe crown

Surcharge Stress (kPa)	EPS-15																							
	Thickness=2 cm						Thickness=5 cm						Thickness=7 cm						Thickness=10 cm					
	Width=30 cm		Width=37.5 cm		Width=45 cm		Width=30 cm		Width=37.5 cm		Width=45 cm		Width=30 cm		Width=37.5 cm		Width=45 cm		Width=30 cm		Width=37.5 cm		Width=45 cm	
	Δx (mm)	Δy (mm)	Δx (mm)	Δy (mm)	Δx (mm)	Δy (mm)	Δx (mm)	Δy (mm)	Δx (mm)	Δy (mm)	Δx (mm)	Δy (mm)	Δx (mm)	Δy (mm)	Δx (mm)	Δy (mm)	Δx (mm)	Δy (mm)	Δx (mm)	Δy (mm)	Δx (mm)	Δy (mm)	Δx (mm)	Δy (mm)
0	0.00	0.00	0.00	0.00	0.00	0.00	0.00	0.00	0.00	0.00	0.00	0.00	0.00	0.00	0.00	0.00	0.00	0.00	0.00	0.00	0.00	0.00	0.00	0.00
25	0.74	-1.73	0.74	-1.72	0.73	-1.71	0.75	-1.77	0.75	-1.75	0.74	-1.73	0.76	-1.79	0.75	-1.76	0.74	-1.74	0.76	-1.80	0.76	-1.78	0.75	-1.75
50	1.14	-2.79	1.14	-2.77	1.13	-2.76	1.15	-2.78	1.13	-2.75	1.12	-3.73	1.18	-2.88	1.17	-2.85	1.16	-2.81	1.19	-2.89	1.17	-2.86	1.16	-2.82
75	1.40	-3.48	1.39	-3.48	1.37	-3.50	1.33	-3.29	1.30	-3.25	1.28	-3.25	1.34	-3.31	1.30	-3.25	1.28	-3.23	1.31	-3.26	1.28	-3.18	1.25	-3.14
100	1.53	-3.85	1.50	-3.84	1.48	-3.89	1.43	-3.56	1.38	-3.50	1.34	-3.50	1.44	-3.62	1.39	-3.54	1.32	-3.47	1.41	-3.54	1.35	-3.43	1.31	-3.39
125	1.63	-4.16	1.58	-4.15	1.56	-4.21	1.50	-3.69	1.38	-3.58	1.34	-3.59	1.47	-3.69	1.38	-3.54	1.32	-3.48	1.41	-3.56	1.32	-3.40	1.26	-3.35
150	1.72	-4.42	1.65	-4.40	1.62	-4.50	1.50	-3.77	1.38	-3.63	1.32	-3.64	1.47	-3.73	1.36	-3.54	1.28	-3.47	1.40	-3.55	1.28	-3.34	1.20	-3.28
175	1.78	-4.65	1.70	-4.63	1.67	-4.75	1.50	-3.83	1.38	-3.66	1.30	-3.68	1.47	-3.73	1.33	-3.54	1.22	-3.43	1.37	-3.51	1.22	-3.26	1.13	-3.20
200	1.84	-4.85	1.74	-4.83	1.71	-4.97	1.50	-3.87	1.34	-3.66	1.26	-3.69	1.44	-3.73	1.28	-3.47	1.16	-3.39	1.32	-3.45	1.15	-3.16	1.05	-3.10

Table B.3 EPS-20 at 5 cm above the pipe crown

Surcharge Stress (kPa)	EPS-20																							
	Thickness=2 cm						Thickness=5 cm						Thickness=7 cm						Thickness=10 cm					
	Width=30 cm		Width=37.5 cm		Width=45 cm		Width=30 cm		Width=37.5 cm		Width=45 cm		Width=30 cm		Width=37.5 cm		Width=45 cm		Width=30 cm		Width=37.5 cm		Width=45 cm	
	Δx (mm)	Δy (mm)	Δx (mm)	Δy (mm)	Δx (mm)	Δy (mm)	Δx (mm)	Δy (mm)	Δx (mm)	Δy (mm)	Δx (mm)	Δy (mm)	Δx (mm)	Δy (mm)	Δx (mm)	Δy (mm)	Δx (mm)	Δy (mm)	Δx (mm)	Δy (mm)	Δx (mm)	Δy (mm)	Δx (mm)	Δy (mm)
0	0.00	0.00	0.00	0.00	0.00	0.00	0.00	0.00	0.00	0.00	0.00	0.00	0.00	0.00	0.00	0.00	0.00	0.00	0.00	0.00	0.00	0.00	0.00	0.00
25	0.75	-1.75	0.74	-1.74	0.73	-1.72	0.77	-1.81	0.76	-1.78	0.75	-1.75	0.78	-1.83	0.78	-1.81	0.76	-1.77	0.79	-1.87	0.79	-1.83	0.77	-1.79
50	1.18	-2.87	1.17	-2.84	1.16	-2.82	1.21	-2.94	1.20	-2.89	1.18	-2.85	1.22	-2.97	1.21	-2.93	1.19	-2.87	1.24	-3.01	1.23	-2.96	1.20	-2.89
75	1.52	-3.80	1.51	-3.77	1.49	-3.74	1.56	-3.87	1.53	-3.82	1.52	-3.77	1.57	-3.91	1.56	-3.85	1.53	-3.78	1.57	-3.95	1.56	-3.89	1.53	-3.81
100	1.73	-4.42	1.71	-4.40	1.70	-4.39	1.70	-4.32	1.67	-4.26	1.65	-4.22	1.70	-4.29	1.66	-4.21	1.63	-4.16	1.69	-4.28	1.66	-4.18	1.61	-4.10
125	1.88	-4.86	1.85	-4.84	1.83	-4.85	1.83	-4.71	1.79	-4.63	1.75	-4.58	1.81	-4.62	1.77	-4.52	1.71	-4.47	1.78	-4.55	1.72	-4.41	1.67	-4.33
150	1.98	-5.18	1.94	-5.16	1.92	-5.20	1.89	-4.87	1.82	-4.76	1.75	-4.71	1.88	-4.76	1.77	-4.63	1.70	-4.54	1.83	-4.71	1.75	-4.54	1.66	-4.41
175	2.08	-5.46	2.02	-5.44	1.99	-5.51	1.93	-5.00	1.84	-4.86	1.75	-4.81	1.88	-4.84	1.77	-4.67	1.68	-4.57	1.84	-4.75	1.72	-4.53	1.62	-4.39
200	2.16	-5.73	2.08	-5.71	2.05	-5.80	1.96	-5.10	1.84	-4.93	1.75	-4.89	1.88	-4.90	1.77	-4.68	1.65	-4.59	1.83	-4.76	1.69	-4.50	1.57	-4.36

C. RESULTS OF ANALYSES FOR EPS AT 10 CM ABOVE THE PIPE CROWN

Table C.1 EPS-10 at 10 cm above the pipe crown

Surcharge Stress (kPa)	EPS-10																							
	Thickness=2 cm						Thickness=5 cm						Thickness=7 cm						Thickness=10 cm					
	Width=30 cm		Width=37.5 cm		Width=45 cm		Width=30 cm		Width=37.5 cm		Width=45 cm		Width=30 cm		Width=37.5 cm		Width=45 cm		Width=30 cm		Width=37.5 cm		Width=45 cm	
	Δx (mm)	Δy (mm)	Δx (mm)	Δy (mm)	Δx (mm)	Δy (mm)	Δx (mm)	Δy (mm)	Δx (mm)	Δy (mm)	Δx (mm)	Δy (mm)	Δx (mm)	Δy (mm)	Δx (mm)	Δy (mm)	Δx (mm)	Δy (mm)	Δx (mm)	Δy (mm)	Δx (mm)	Δy (mm)	Δx (mm)	Δy (mm)
0	0.00	0.00	0.00	0.00	0.00	0.00	0.00	0.00	0.00	0.00	0.00	0.00	0.00	0.00	0.00	0.00	0.00	0.00	0.00	0.00	0.00	0.00	0.00	0.00
25	0.69	-1.63	0.69	-1.62	0.68	-1.62	0.66	-1.56	0.65	-1.54	0.65	-1.53	0.65	-1.53	0.64	-1.50	0.63	-1.49	0.63	-1.49	0.62	-1.46	0.61	-1.44
50	0.98	-2.37	0.95	-2.32	0.94	-2.32	0.90	-2.18	0.86	-2.10	0.84	-2.07	0.87	-2.13	0.84	-2.05	0.81	-2.01	0.84	-2.06	0.81	-1.99	0.78	-1.94
75	1.15	-2.85	1.10	-2.76	1.08	-2.76	1.00	-2.49	0.93	-2.33	0.86	-2.27	0.95	-2.38	0.88	-2.23	0.81	-2.14	0.90	-2.27	0.81	-2.12	0.77	-2.02
100	1.28	-3.25	1.22	-3.13	1.18	-3.11	1.06	-2.71	0.98	-2.51	0.90	-2.41	1.00	-2.56	0.88	-2.35	0.81	-2.23	0.90	-2.39	0.81	-2.19	0.74	-2.06
125	1.39	-3.59	1.30	-3.43	1.25	-3.41	1.11	-2.90	0.98	-2.64	0.90	-2.52	1.00	-2.69	0.88	-2.44	0.81	-2.29	0.90	-2.47	0.81	-2.24	0.70	-2.08
150	1.48	-3.89	1.37	-3.69	1.31	-3.67	1.15	-3.04	0.98	-2.76	0.90	-2.61	1.00	-2.79	0.88	-2.50	0.78	-2.33	0.90	-2.52	0.75	-2.26	0.66	-2.10
175	1.55	-4.16	1.43	-3.93	1.36	-3.89	1.15	-3.17	0.98	-2.85	0.90	-2.68	1.00	-2.86	0.85	-2.55	0.75	-2.39	0.85	-2.53	0.71	-2.27	0.61	-2.11
200	1.61	-4.40	1.47	-4.14	1.39	-4.09	1.15	-3.27	0.98	-2.92	0.86	-2.75	1.00	-2.91	0.82	-2.59	0.72	-2.45	0.81	-2.54	0.65	-2.28	0.55	-2.14

Table C.2 EPS-15 at 10 cm above the pipe crown

Surcharge Stress (kPa)	EPS-15																							
	Thickness=2 cm						Thickness=5 cm						Thickness=7 cm						Thickness=10 cm					
	Width=30 cm		Width=37.5 cm		Width=45 cm		Width=30 cm		Width=37.5 cm		Width=45 cm		Width=30 cm		Width=37.5 cm		Width=45 cm		Width=30 cm		Width=37.5 cm		Width=45 cm	
	Δx (mm)	Δy (mm)	Δx (mm)	Δy (mm)	Δx (mm)	Δy (mm)	Δx (mm)	Δy (mm)	Δx (mm)	Δy (mm)	Δx (mm)	Δy (mm)	Δx (mm)	Δy (mm)	Δx (mm)	Δy (mm)	Δx (mm)	Δy (mm)	Δx (mm)	Δy (mm)	Δx (mm)	Δy (mm)	Δx (mm)	Δy (mm)
0	0.00	0.00	0.00	0.00	0.00	0.00	0.00	0.00	0.00	0.00	0.00	0.00	0.00	0.00	0.00	0.00	0.00	0.00	0.00	0.00	0.00	0.00	0.00	0.00
25	0.74	-1.73	0.74	-1.73	0.73	-1.72	0.75	-1.77	0.75	-1.76	0.74	-1.74	0.76	-1.78	0.75	-1.77	0.75	-1.75	0.76	-1.79	0.76	-1.79	0.76	-1.77
50	1.14	-2.80	1.14	-2.79	1.14	-2.78	1.16	-2.87	1.17	-2.85	1.16	-2.83	1.18	-2.88	1.17	-2.87	1.17	-2.84	1.18	-2.89	1.18	-2.88	1.17	-2.86
75	1.41	-3.53	1.40	-3.51	1.40	-3.51	1.38	-3.46	1.36	-3.40	1.34	-3.37	1.37	-3.42	1.34	-3.34	1.31	-3.30	1.35	-3.38	1.32	-3.30	1.29	-3.24
100	1.57	-3.98	1.53	-3.91	1.51	-3.90	1.53	-3.88	1.48	-3.77	1.44	-3.71	1.51	-3.85	1.45	-3.70	1.41	-3.63	1.48	-3.77	1.42	-3.64	1.37	-3.54
125	1.70	-4.37	1.64	-4.26	1.60	-4.24	1.61	-4.14	1.53	-3.95	1.48	-3.85	1.57	-4.05	1.49	-3.84	1.41	-3.72	1.53	-3.98	1.43	-3.73	1.36	-3.59
150	1.80	-4.71	1.73	-4.56	1.68	-4.54	1.67	-4.35	1.58	-4.10	1.48	-3.97	1.61	-4.22	1.49	-3.95	1.41	-3.79	1.57	-4.12	1.43	-3.80	1.33	-3.62
175	1.90	-5.02	1.80	-4.83	1.74	-4.80	1.71	-4.54	1.58	-4.23	1.48	-4.07	1.64	-4.37	1.49	-4.04	1.41	-3.84	1.57	-4.23	1.41	-3.86	1.30	-3.63
200	1.97	-5.30	1.86	-5.08	1.79	-5.04	1.75	-4.70	1.58	-4.34	1.48	-4.15	1.66	-4.49	1.49	-4.11	1.36	-3.88	1.57	-4.31	1.39	-3.90	1.26	-3.65

Table C.3 EPS-20 at 10 cm above the pipe crown

Surcharge Stress (kPa)	EPS-20																							
	Thickness=2 cm						Thickness=5 cm						Thickness=7 cm						Thickness=10 cm					
	Width=30 cm		Width=37.5 cm		Width=45 cm		Width=30 cm		Width=37.5 cm		Width=45 cm		Width=30 cm		Width=37.5 cm		Width=45 cm		Width=30 cm		Width=37.5 cm		Width=45 cm	
	Δx (mm)	Δy (mm)	Δx (mm)	Δy (mm)	Δx (mm)	Δy (mm)	Δx (mm)	Δy (mm)	Δx (mm)	Δy (mm)	Δx (mm)	Δy (mm)	Δx (mm)	Δy (mm)	Δx (mm)	Δy (mm)	Δx (mm)	Δy (mm)	Δx (mm)	Δy (mm)	Δx (mm)	Δy (mm)	Δx (mm)	Δy (mm)
0	0.00	0.00	0.00	0.00	0.00	0.00	0.00	0.00	0.00	0.00	0.00	0.00	0.00	0.00	0.00	0.00	0.00	0.00	0.00	0.00	0.00	0.00	0.00	0.00
25	0.75	-1.75	0.74	-1.74	0.74	-1.74	0.76	-1.80	0.76	-1.79	0.76	-1.77	0.77	-1.82	0.77	-1.81	0.77	-1.79	0.78	-1.84	0.78	-1.84	0.78	-1.81
50	1.18	-2.87	1.17	-2.86	1.17	-2.84	1.20	-2.94	1.20	-2.92	1.19	-2.89	1.21	-2.97	1.21	-2.95	1.20	-2.91	1.23	-3.00	1.23	-2.98	1.22	-2.94
75	1.51	-3.81	1.50	-3.79	1.50	-3.77	1.53	-3.88	1.53	-3.86	1.52	-3.82	1.55	-3.92	1.54	-3.89	1.53	-3.84	1.56	-3.95	1.56	-3.93	1.55	-3.88
100	1.73	-4.46	1.72	-4.43	1.71	-4.42	1.72	-4.41	1.70	-4.34	1.68	-4.29	1.72	-4.40	1.69	-4.31	1.66	-4.24	1.71	-4.39	1.69	-4.30	1.66	-4.22
125	1.91	-4.95	1.88	-4.89	1.86	-4.88	1.87	-4.84	1.82	-4.72	1.79	-4.66	1.86	-4.81	1.81	-4.68	1.76	-4.59	1.83	-4.76	1.78	-4.61	1.73	-4.50
150	2.04	-5.34	1.99	-5.24	1.96	-5.23	1.95	-5.11	1.88	-4.93	1.82	-4.83	1.93	-5.07	1.85	-4.84	1.78	-4.71	1.91	-5.03	1.82	-4.80	1.75	-4.65
175	2.15	-5.69	2.08	-5.56	2.04	-5.55	2.02	-5.34	1.92	-5.11	1.85	-4.98	1.99	-5.27	1.87	-4.97	1.78	-4.81	1.95	-5.20	1.83	-4.90	1.74	-4.71
200	2.24	-6.02	2.16	-5.86	2.11	-5.84	2.07	-5.55	1.95	-5.26	1.86	-5.11	2.03	-5.45	1.88	-5.09	1.78	-4.89	1.98	-5.35	1.83	-4.99	1.72	-4.75

D. FEM OUTPUTS FOR THE REFERENCE TEST (WITHOUT EPS)

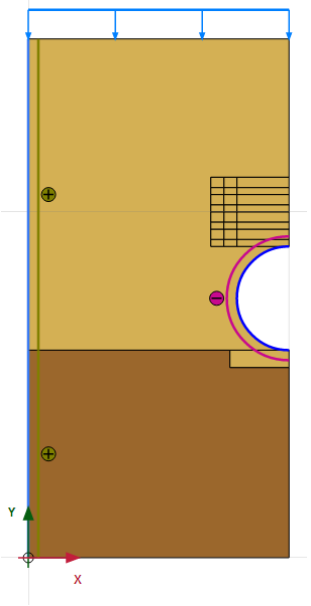

Figure D.1. General overview of the reference test

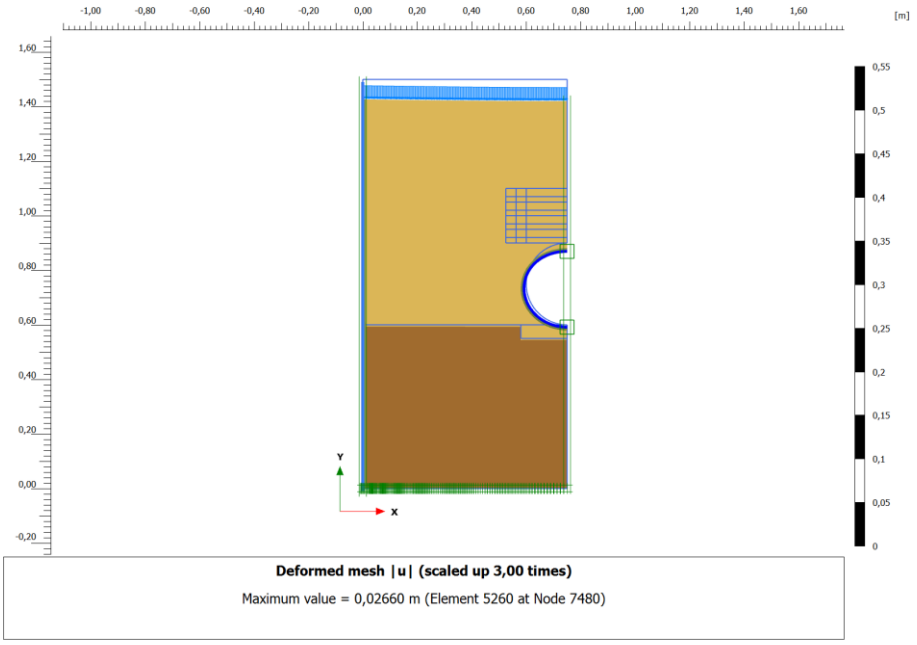

Figure D.2. Deformed mesh of reference test at 200 kPa

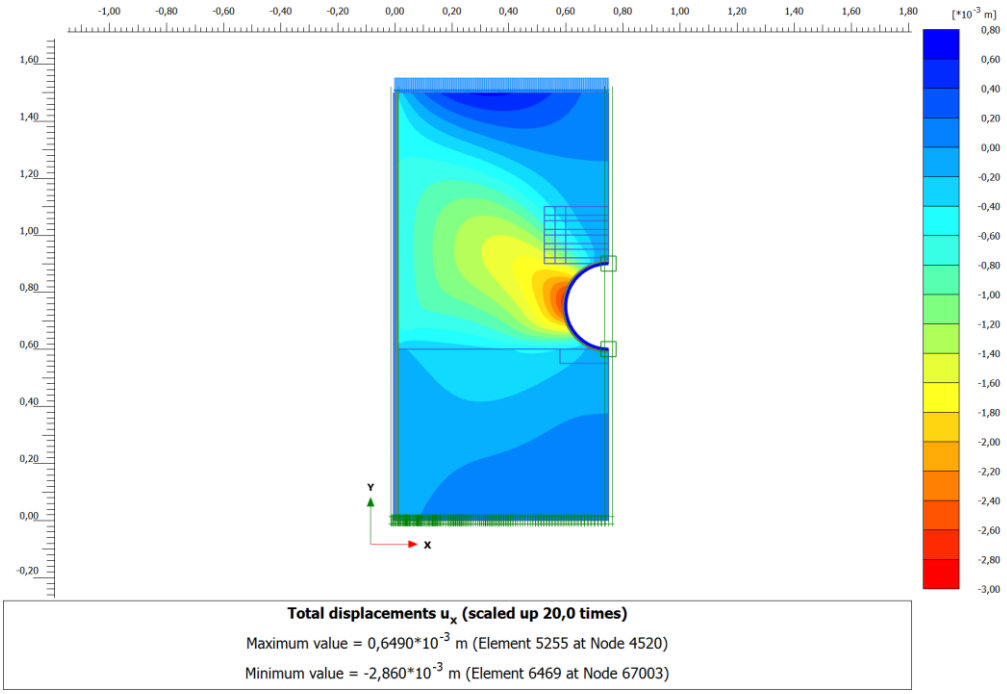

Figure D.3. Horizontal displacements (u_x) at 200 kPa

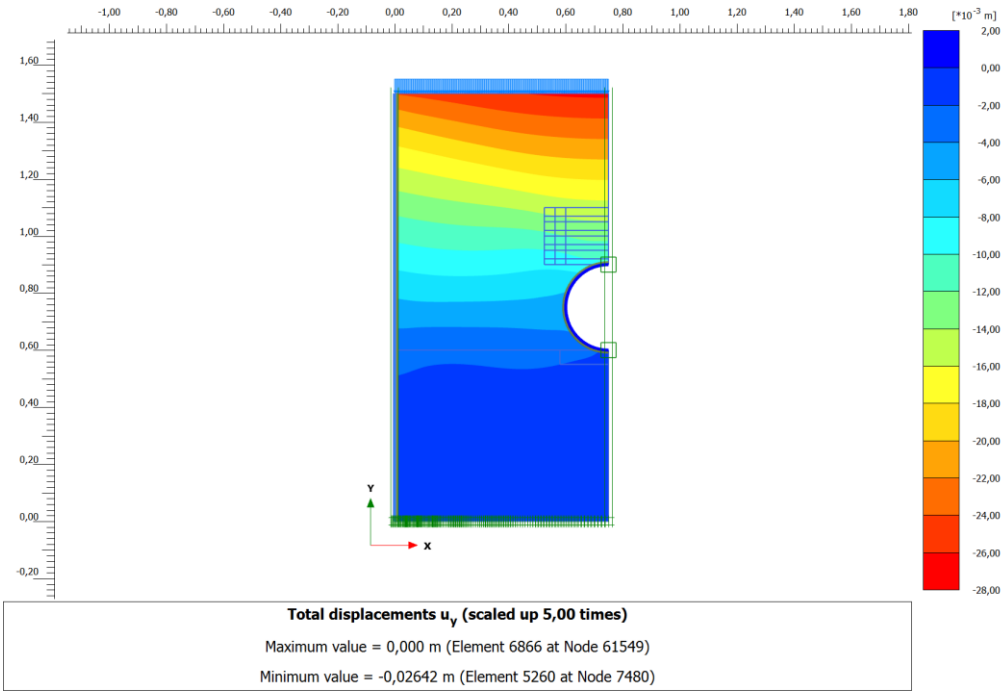

Figure D.4. Vertical displacements (u_y) at 200 kPa

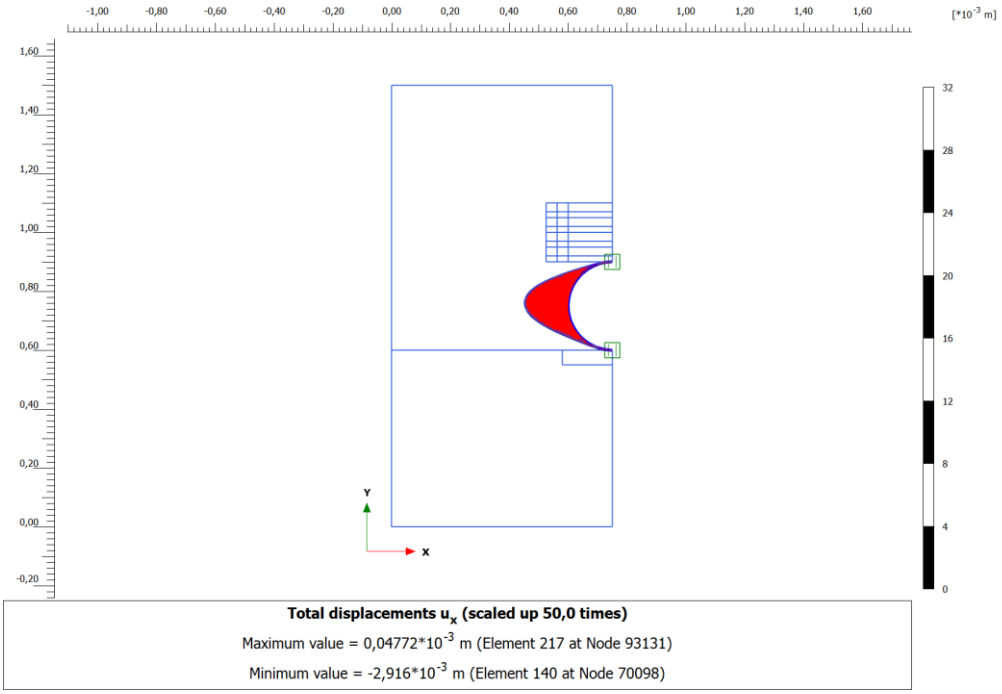

Figure D.5. Horizontal displacements of pipe (u_x) at 200 kPa

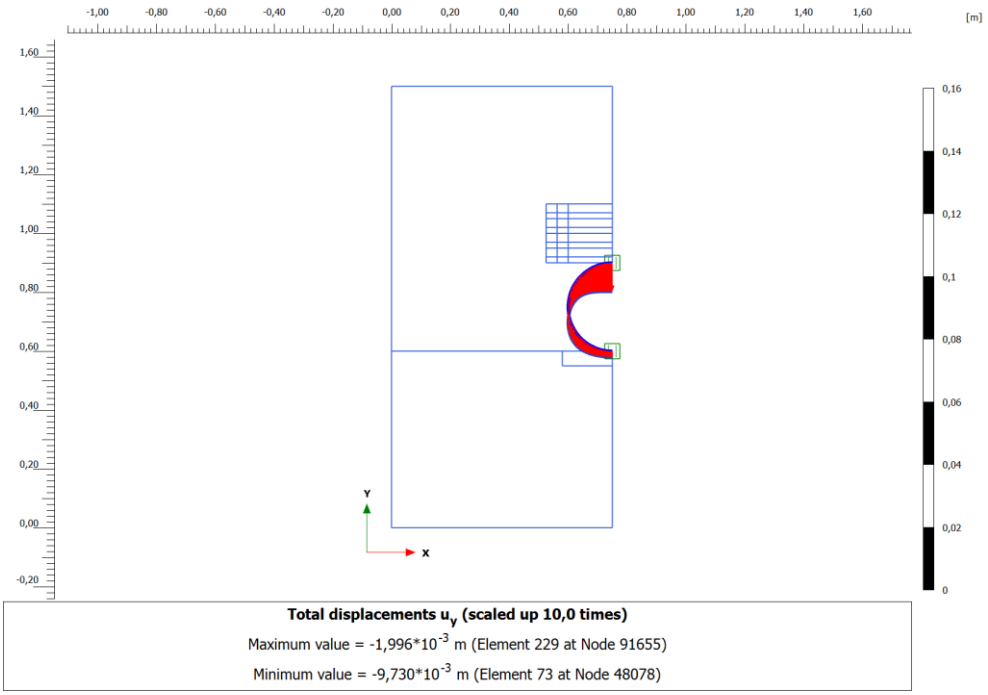

Figure D.6. Vertical displacements of pipe (u_y) at 200 kPa

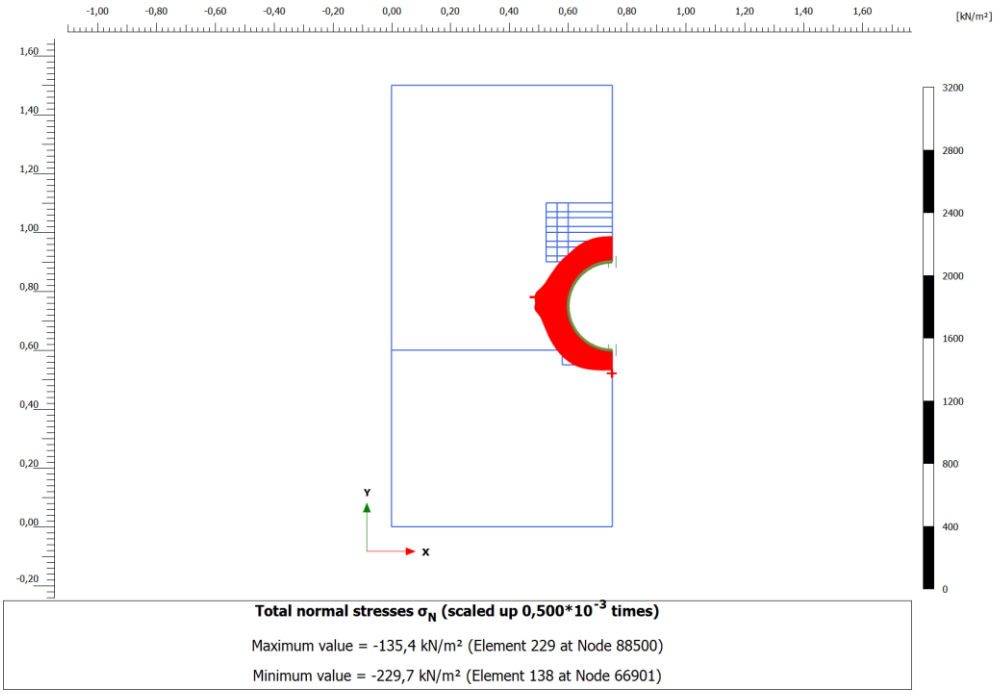

Figure D.7. Total normal stresses acting on perimeter of pipe (σ_N) at 200 kPa

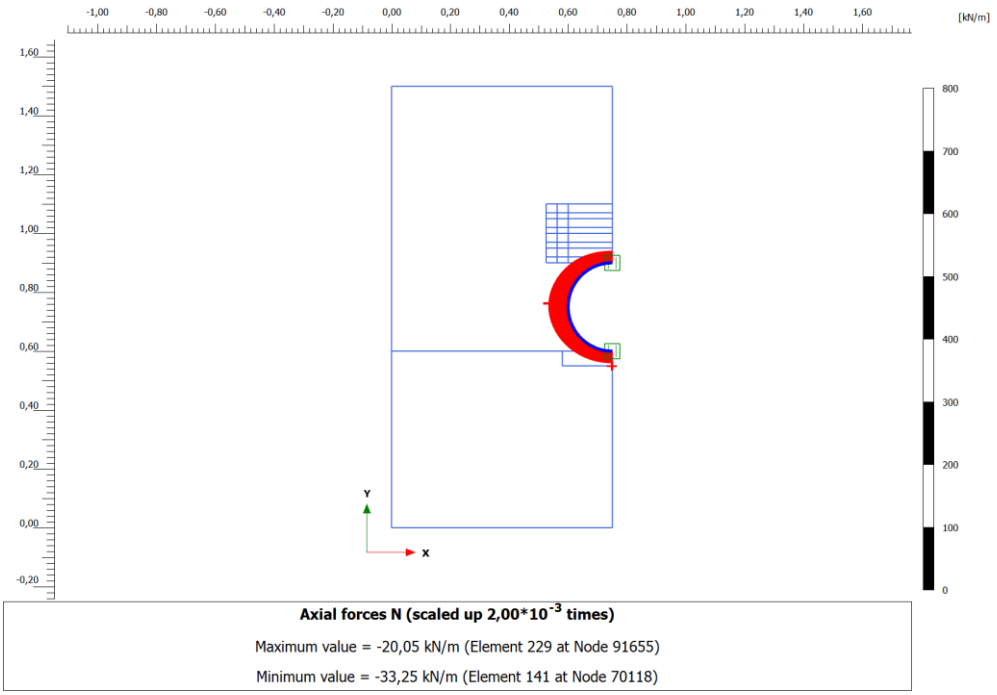

Figure D.8. Axial forces at pipe wall (N) at 200 kPa

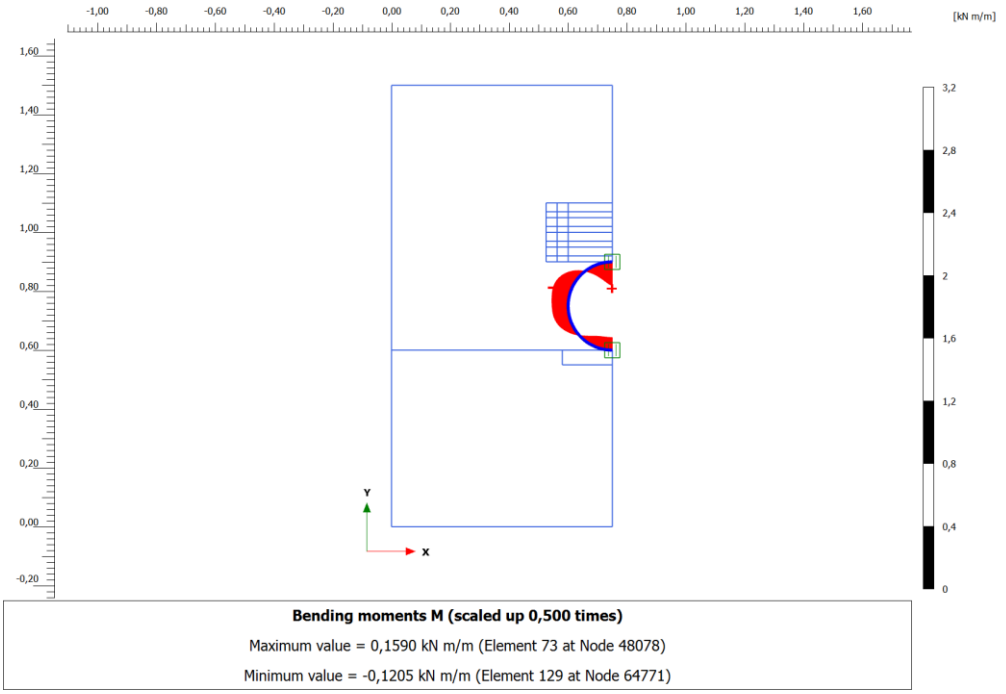

Figure D.9. Bending moments at pipe wall (M) at 200 kPa

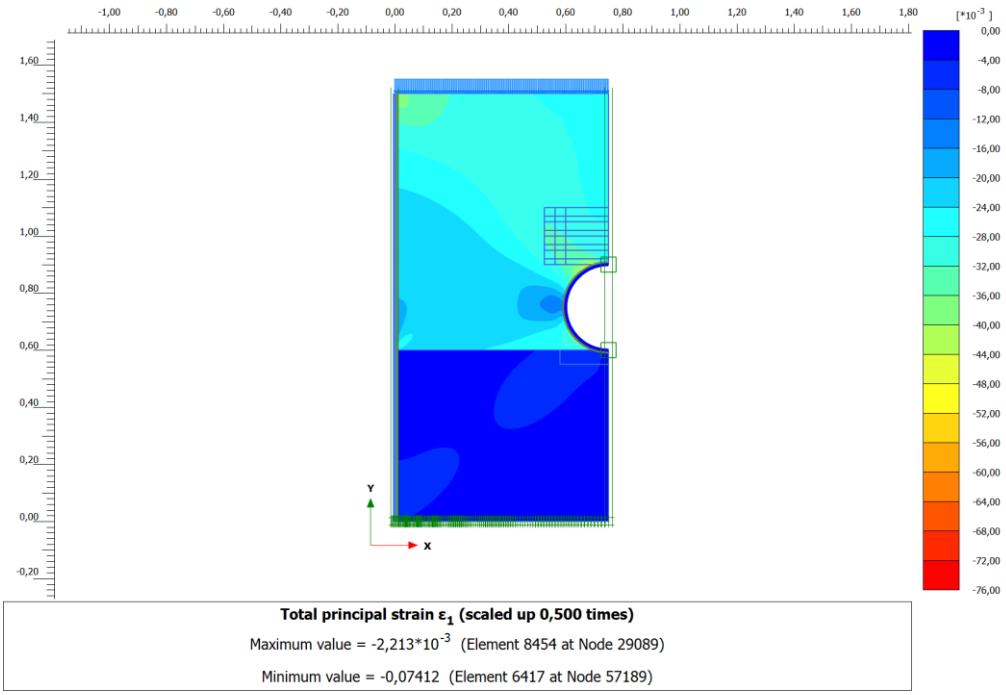

Figure D.10. Principal strain (ε_1) at 200 kPa

E. FEM OUTPUTS FOR THE RECOMMENDED EPS-10 CONFIGURATION

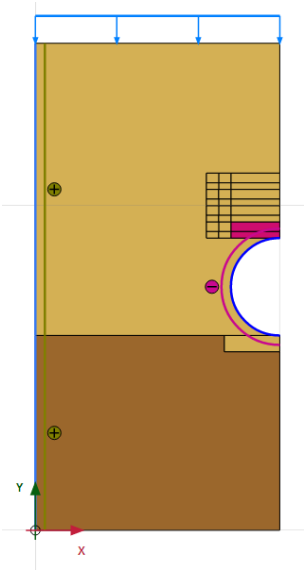

Figure E.1. General overview of recommended EPS configuration (c0_EPS10_t5_w30)

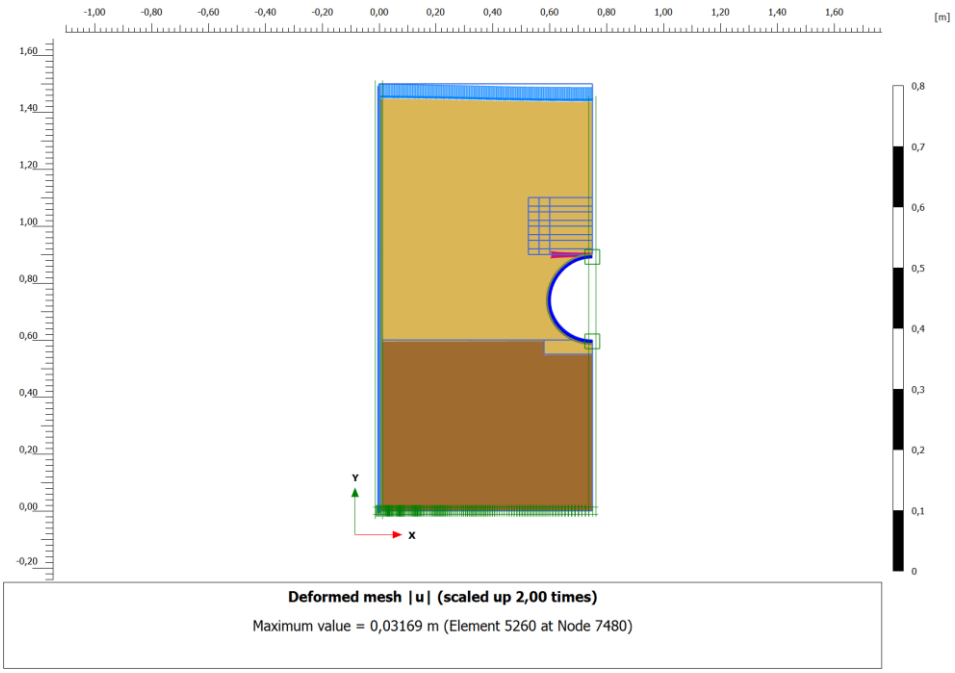

Figure E.2. Deformed mesh of recommended configuration at 200 kPa

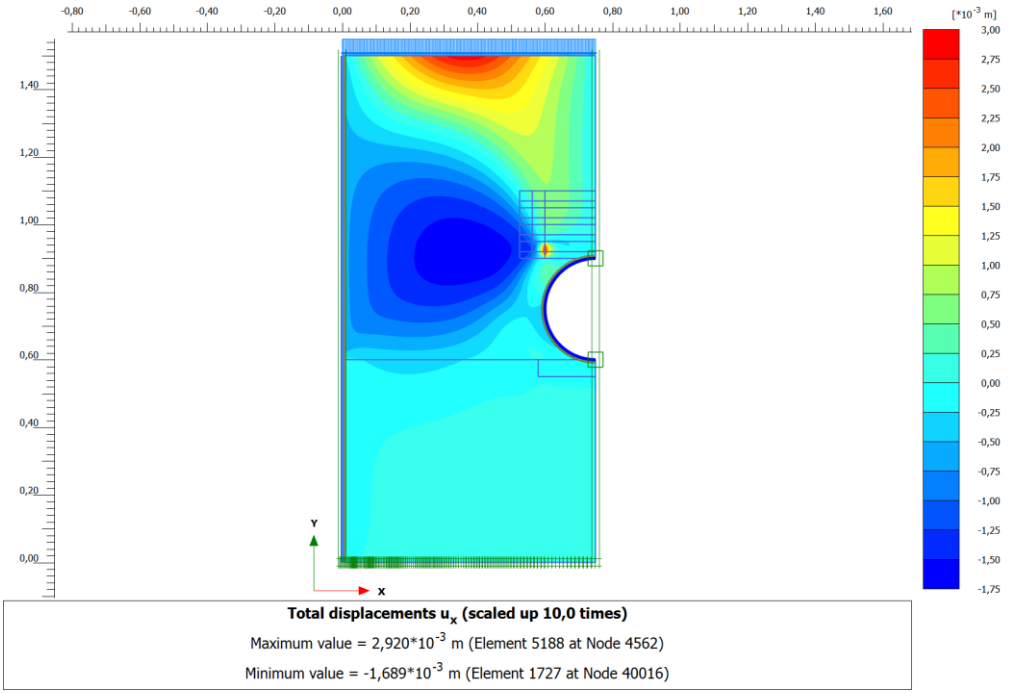

Figure E.3. Horizontal displacements (u_x) after improved with EPS-10

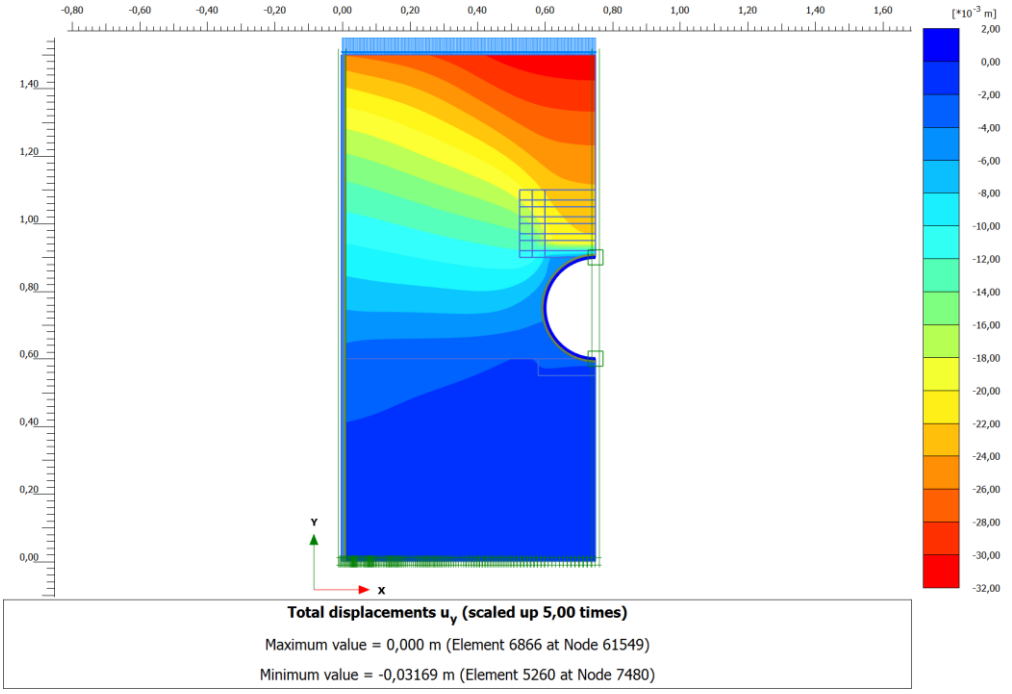

Figure E.4. Vertical displacements (u_y) after improved with EPS-10

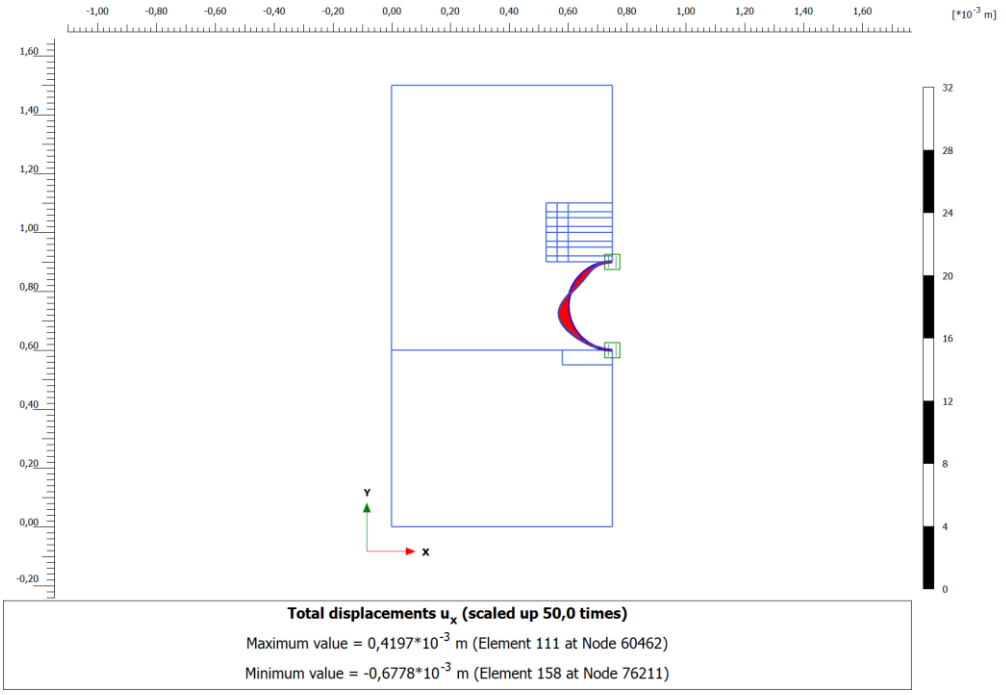

Figure E.5. Horizontal displacements of pipe (u_x) after improved with EPS-10

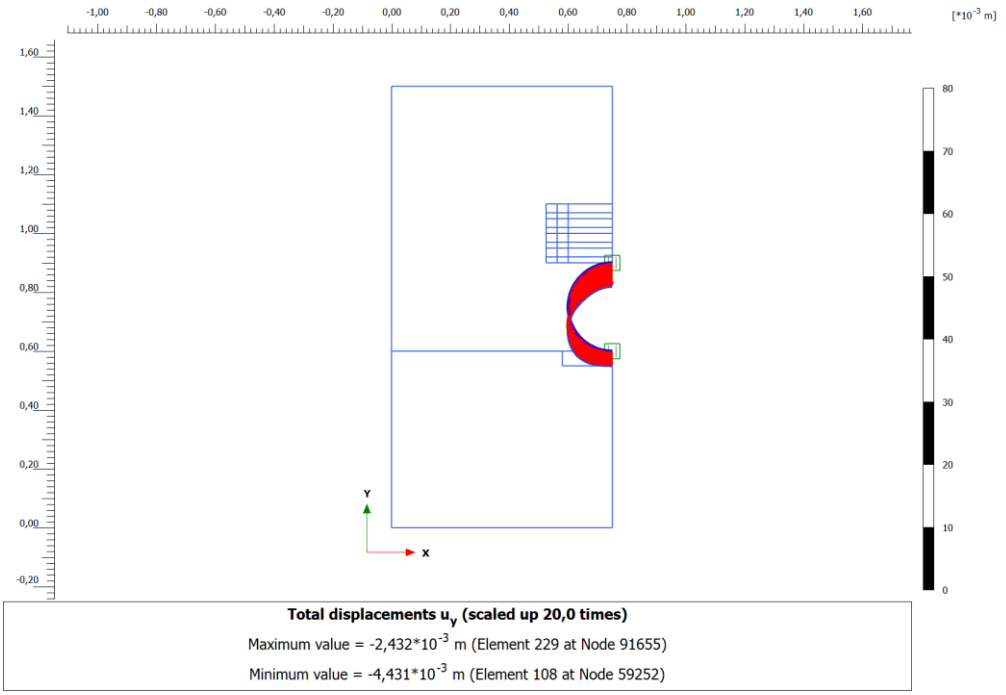

Figure E.6. Vertical displacements of pipe (u_y) after improved with EPS-10

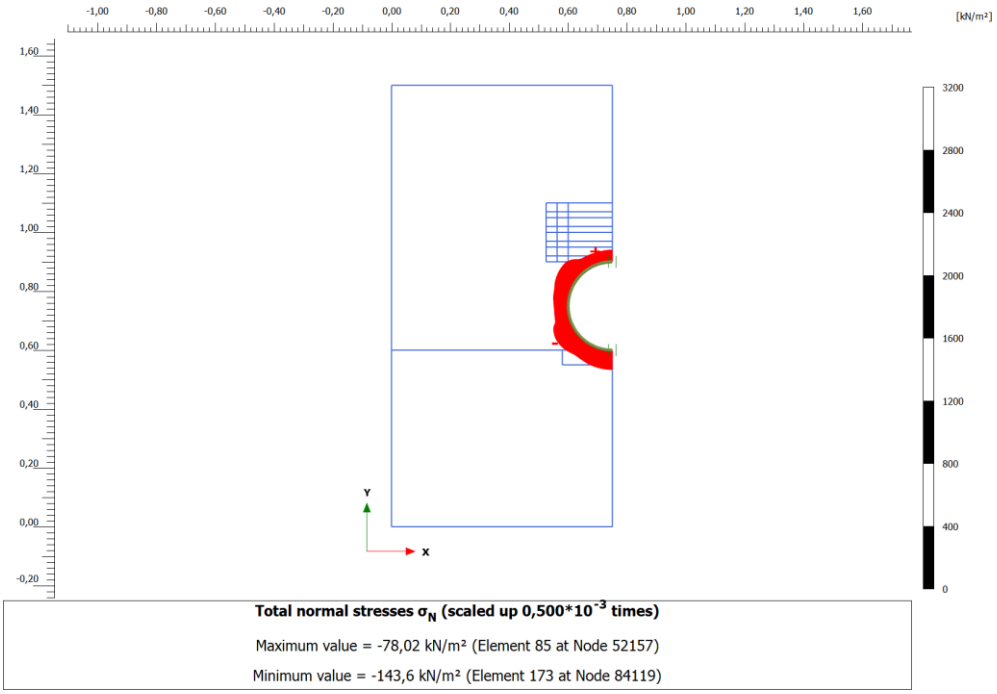

Figure E.7. Total normal stresses acting on perimeter of pipe (σ_N) at 200 kPa after improved with EPS-10

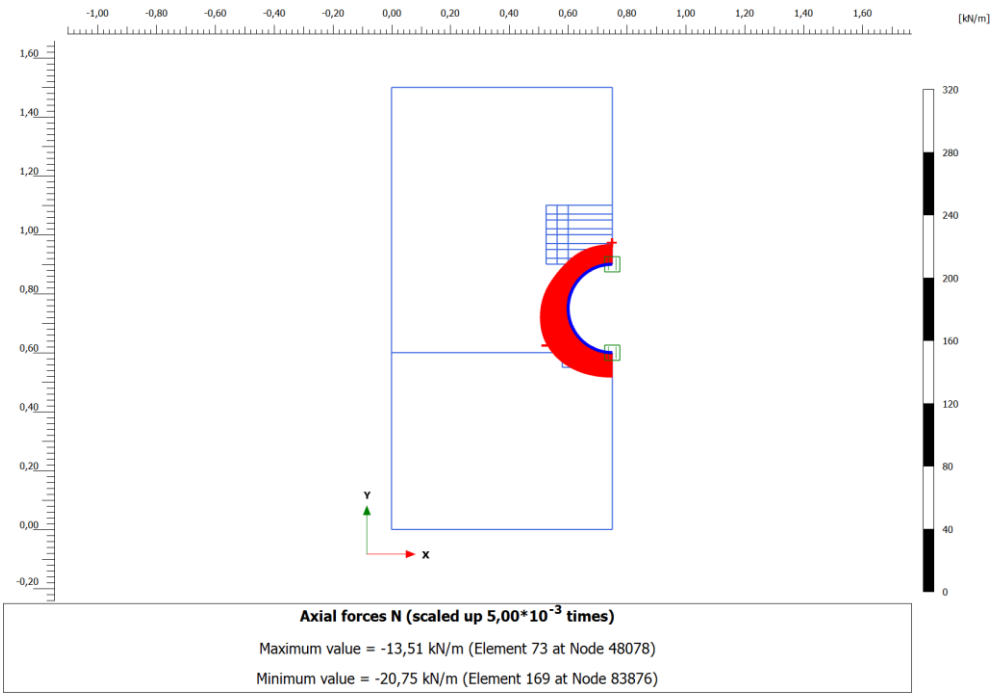

Figure E.8. Axial forces at pipe wall (N) at 200 kPa after improved with EPS-10

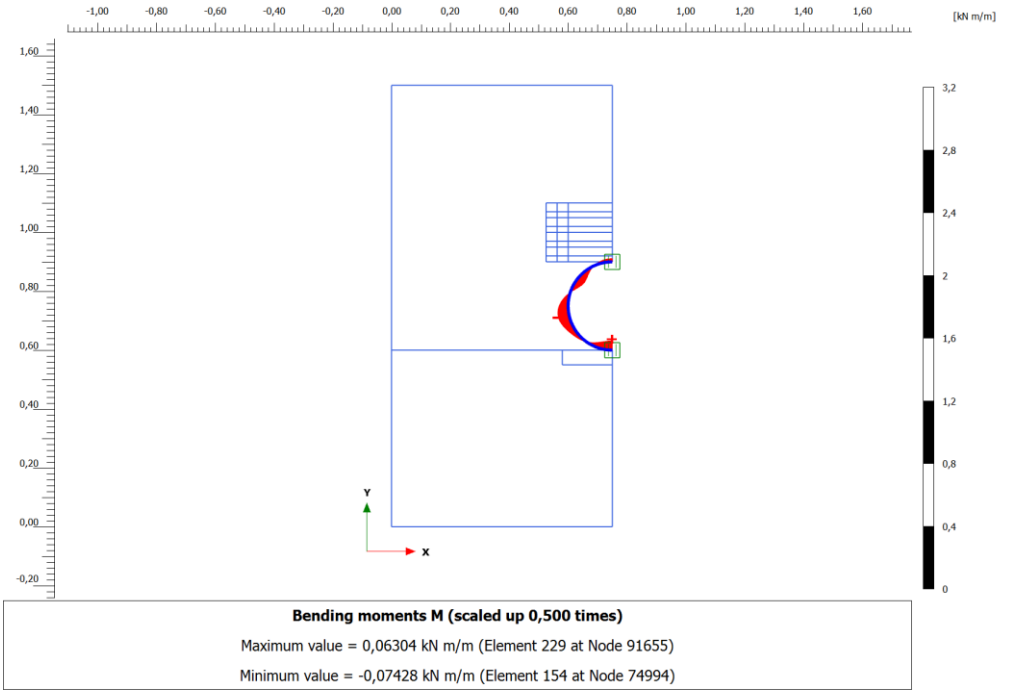

Figure E.9. Bending moments at pipe wall (M) at 200 kPa after improved with EPS-10

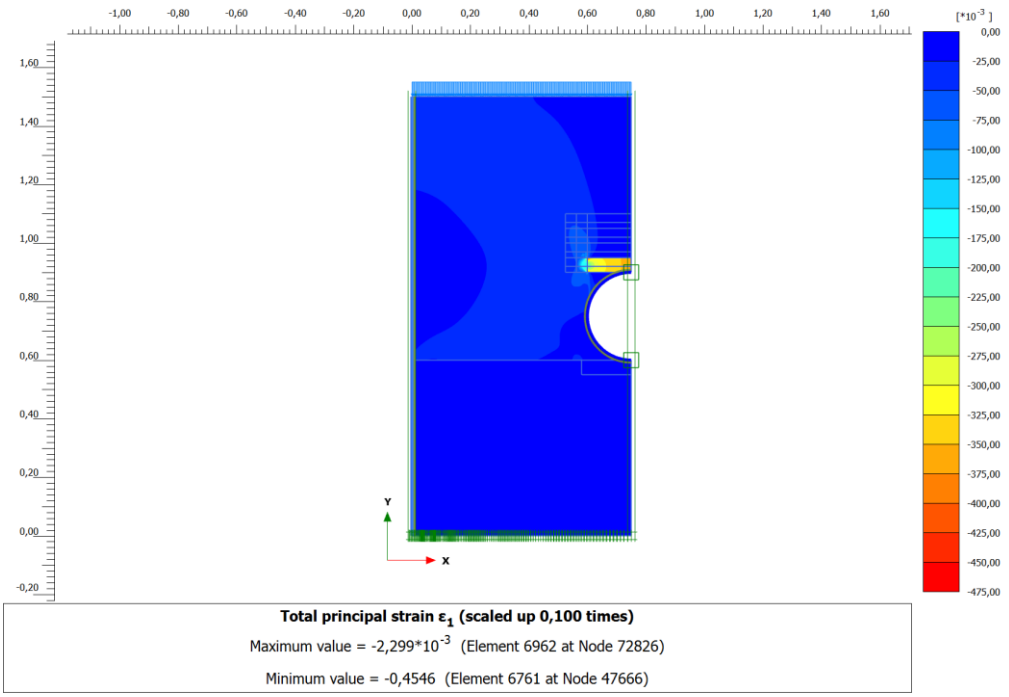

Figure E.10. Principal strain (ε_1) at 200 kPa after improved with EPS-10